Regulation of Cell Polarity and Double Fertilization in *Arabidopsis thaliana*

Dissertation zur Erlangung des
Doktorgrades der Naturwissenschaften (Dr. rer. nat.)
der Fakultät für Biologie und Vorklinische Medizin
der Universität Regensburg

vorgelegt von

Frank Vogler

aus

Altdorf bei Nürnberg

im Jahr

2015

Das Promotionsgesuch wurde eingereicht am:
27.04.2015

Die Arbeit wurde angeleitet von:
DR. STEFANIE SPRUNCK

Unterschrift:

Für Dani und Feli

Table of Contents

Table of Figures

Abbreviations

Abbreviations indicating gene and protein names are explained in the text at the first time of appearance and abbreviatinos used in Figures are explained in the respective captions.

3AT	1,2,4-Triazole
aa	Amino acid(s)
AD	Activation Domain
ANOVA	Analysis Of Variance
ATP	Adonsine Triphosphate
ATPase	Adonsine Triphosphatase
BF	Brightfield
BFA	Brefeldin A
bHLH	Basic Helix-Loop-Helix
bp	Base pair(s)
BP	Band Pass
BR	Brassinosteroid
CCD	Charge Coupled Device
cDNA	Complementary DNA
CHX	Cycloheximide
CLSM	Confocal Laser Scanning Microscopy
cm	Centimeter(s)
Col-0	Columbia-0
CRIB	Cdc42/Rac Interactive Binding
Ct	Cycle threshold
cyto	Cytosolic
DAPI	4',6-Diamidino-2-Phenylindole
DB	DNA-Binding Domain
DEPC	Diethylpyrocarbonate
DIC	Differential Interference Contrast
DMSO	Dimethyl Sulfoxide
DNA	Desoxyribonucleic Acid
DOC	Sodium Deoxycholate
DTT	Dithiothreitol
ECM	Extracellular Matrix
EDTA	Ethylenediaminetetraacetic Acid
(e)GFP	(Enhanced) Green Fluorescent Protein
EMCCD	Electron-Multiplying CCD
EMT	Epithelial-Mesenchymal Transition
epiBL	Epibrassinolide
ER	Endoplasmatic Reticulum
EST	Expressed Sequence Tag
F-actin	Filamentous actin
FL	Fluorescence
FRET	Förster Resonance Energy Transfer
g	Gramm(s)
GA3	Gibberellic Acid
GABA	Gamma-Aminobutyric Acid
gDNA	Genomic DNA
GDP	Guanosine Diphosphate
GPI	Glycosylphosphatidylinositol
GTP	Guanosine Triphosphate
GTPase	Guanosine Triphosphatase
GUS	β-Glucuronidase
h	Hour(s)
hap	Hours after pollination
HRP	Horseradish Peroxidase
HyD	Hybrid Detector
IAA	Indoleacetic Acid
IQR	Interquartile Range
kDa	Kilo Dalton
kg	Kilogramm(s)
L	Liter(s)
LatB	Latrunculin B
LC	Liquid Chromatography
LED	Light-Emitting Diode
LUT	Look Up Table
m	Meter(s)
M	Molar
MAP	Mitogen Activated Protein
MAPK	MAP Kinase
MAPKK	MAP Kinase Kinase
MES	2-(N-Morpholino)ethanesulfonic Acid
mg	Milligramm(s)
MGU	Male Germ Unit
µg	Microgramm(s)
µL	Microliter(s)

µm	Micrometer(s)
µM	Micromolar
min	Minute(s)
miRNA	MicroRNA
mL	Milliliter(s)
mM	Millimolar
mm	Millimeter
(m)RFP	(Monomeric) Red Fluorescent Protein
mRNA	Messenger Ribonucleic Acid
MS	Mass Spectrometry
MS medium	Murashige and Skoog medium
MW	Molecular Weight
MYB	Myeloblastosis
NA	Numerical Aperture
NAA	1-Naphthaleneacetic Acid
NLS	Nuclear Localization Signal
nm	Nanometer(s)
nM	Nanomolar
nt	Nucleotide(s)
PAGE	Polyacrylamide Gel Electrophoresis
PAT	Phosphinotricin-Acetyltransferase
PBS	Phosphate Buffered Saline
PCR	Polymerase Chain Reaction
PGM	Pollen Germination Medium
PMSF	Phenylmethanesulfonyl Fluoride
PMT	Photomultiplier Tube
PT	Pollen Tube
PVDF	Polyvinylidene Fluoride
Rf	Retardation factor
RNA	Ribonucleic Acid
RNAi	RNA interference
ROI	Region Of Interest
ROS	Reactive Oxygen Species
RT-PCR	Reverse Transcriptase PCR
S	Svedberg
s	Second(s)
SDS	Sodium Dodecylsulfate
SE	Standard Error
SI	Self Incompatibility
SV	Secretory Vesicles
TCA	Trichloracetic Acid
T-DNA	Transfer DNA
TGN	Trans-Golgi Network
TIRF	Total Internal Reflection Fluorescence
TOF	Time Of Flight
Tris	Tris(hydroxymethyl)-aminomethane
TRITC	Tetramethylrhodamine Isothiocyanate
UHR-Q-TOF	Ultra-High Resolution Quadrupole-Time Of Flight
UTR	Untranslated Region
UV	Ultra Violett
v/v	Volume/volume
WS4	Wassilewskija-4
WT	Wild-Type
w/v	Weight/volume
X-Gluc	5-Bromo-4-chloro-3-indolyl-beta-D-glucuronic Acid
YFP	Yellow Fluorescent Protein

CHAPTER 1 General Introduction

1.1 The Phenomenon of Cell Polarity

Cell polarity is generally defined as the asymmetric distribution of organelles, molecules such as proteins, lipids or nucleic acids, or ions within a cell (Cove, 2000; Ebnet, 2015). Cell polarity is a fundamental feature of almost all cells (Thompson, 2013), no matter if they are prokaryotic or eukaryotic and whether they belong to unicellular or multicellular organisms. Cell polarity is the intrinsic property to embrace different shapes (Csikász-Nagy et al., 2013) and has already been described by Thomas H. Morgan and Jaques Loeb as a fundamental and universal biological phenomenon (Morgan, 1905; Loeb, 1906). A prerequisite for cell polarity is the presence of poles that are distinct and opposite, e.g. an anterior and posterior pole, with an asymmetrical and ordered distribution of structures along a center axis (Wolpert, 2013). This feature allows at any point to draw an arrow pointing to one of these poles.

In some cell types like animal neurons with axons and dendrites, cell polarity is morphologically very obvious, whereas in others such as plant root tip cells, polarity is conferred by the asymmetric distribution of efflux carriers. Cell polarity can also appear only temporarily in some points of an organisms' life cycle, as it is for example during budding in baker's yeast.

The first entry of 'Cell Polarity' in the title of a publication in the PubMed database ranges back to 1926 (Csikász-Nagy et al., 2013). This first publication dealt about fibroblast polarity in rabbits (Bunting and Eads, 1926). Strikingly, the next entry dates back to 1939 and in this publication cell polarity in grass root hairs was described (Sinnott and Bloch, 1939). As **Figure 1.1** shows, by the 1980's research on cell polarity drastically increased. This is likely related to pioneering work in developmental, cell and molecular biology, as for example carried out by the Noble Prize laureates Edward B. Lewis, Christiane Nüsslein-Volhard and Eric F. Wieschaus, who discovered cell polarity genes like *gooseberry*, *hedgehog*, *patch* and *armadillo* in *Drosophila* (Nüsslein-Volhard and Wieschaus, 1980; Riggleman et al., 1989; Pfeifer and Wieschaus, 1990).

A very recent hypothesis even put the phenomenon of cell polarization in context with the evolution of the eukaryotic cell by endosymbiosis and stresses a rethinking of its origin by mere engulfment of eubacteria by archeae (Axelrod and Bergmann, 2014). According to their hypothesis, Buzz and David Baum suggested that archeae could have formed multiple cytoplasmic protrusions that surrounded symbiotic eubacteria. Thereby this primary extracellular compartment would have increased and became the cytoplasm, and the archeal cell body would have been reduced to the nucleus of the eukaryotic cell. Cytoplasmic membrane protrusions could have fused to bring the eubacteria into the cell. Also the endoplasmic reticulum (ER) could have originated from fused membrane protrusions. Polar distribution of mRNAs into individual compartments of this highly compartmentalized cell would have been a natural consequence and could have formed the basis for cell polarity (Axelrod and Bergmann, 2014).

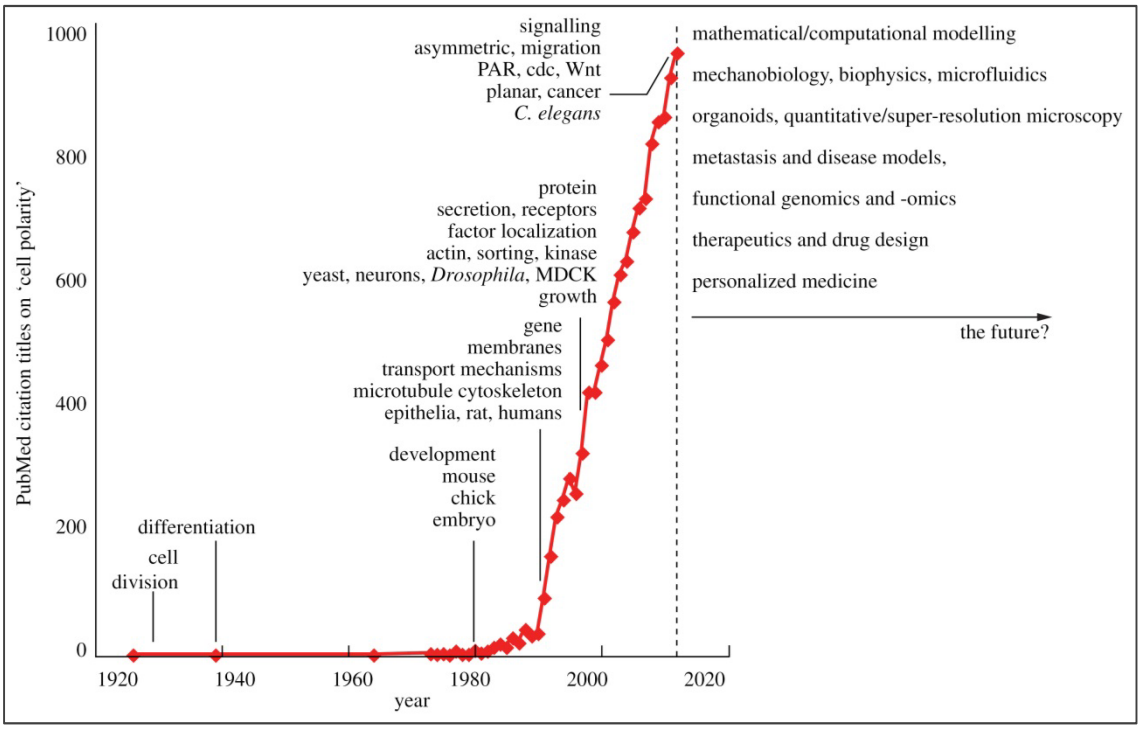

Figure 1.1 | Cell polarity – whence and whither?

Yearly number of publications in the PubMed database with titles harboring the search term 'Cell Polarity' from 1926 to 2013. Prominent key words for each decade are indicated, as well as possible future trends. Figure adopted from Csikász-Nagy et al. (2013).

Despite being a general phenomenon of almost all cells, cell polarity or its defects play a crucial role in human diseases. For example the loss of apical-basal cell polarity in epithelial cells, also known as epithelial-mesenchymal transition (EMT), is related to metastatic tumor growth and tumor recurrence, which are among the most observed causes of death in breast cancer (Alvarez et al., 2013; Macara and McCaffrey, 2013). Also polar hyphal growth of the human pathogenic fungus *Candida albicans* initiated upon the contact with serum, is directly linked to human diseases like candidiasis or candidaemia (Sudbery, 2011; Arkowitz and Bassilana, 2014).

Human nutrition is directly or indirectly related to the yield of crop plants such as maize, wheat, or rice. However, many processes during plant fertilization and seed formation rely on cell polarity. These processes are described below in detail. Thus, the understanding and control of cell polarity represents not only an interesting question from a research perspective, but also is tightly linked to human welfare.

1.2 Fundamental Principles of Cell Polarity

Although cell polarity can be found among all cells ranging from bacteria to higher eukaryotes and controls diverse biological processes, the underlying mechanisms are highly similar which allows to abstract fundamental principles.

1.2.1 Cell polarity requires the spatiotemporal regulation of small GTPases

Most often, these small GTPases are members of the Ras-GTPase superfamily and only contain one G domain. The G domain is subdivided into four to five conserved fingerprint motifs, G1 to G5 (Vetter and Wittinghofer, 2001; Wittinghofer and Vetter, 2011). The G1 motif (also called P-loop) binds the α- and β-phosphates of GTP and GDP, and the G2 and G3 motif (also called switch regions I and II) bind the γ-phosphate of GTP. The G4 and, if present, the G5 motifs are responsible for binding the guanine ring. Thereby the GTPase can cycle between an active, GTP-bound form and an inactive, GDP-bound form. As these GTPase have high nucleotide binding affinities but only low intrinsic hydrolysis activities, the interaction with regulatory proteins is crucial for GTPase function with downstream effectors. GUANINE NUCLEOTIDE EXCHANGE FACTORS (GEFs), GTPASE ACTIVATING PROTEINS (GAPs) and GUANINE NUCLEOTIDE DISSOCIATION INHIBITORS (GDIs) are effective GTPase regulators (**Figure 1.2**). GEFs facilitate the exchange of GDP by GTP and thus function as activators, while GAPs facilitate the GTP hydrolysis to GDP and thereby function as inactivators (Vetter and Wittinghofer, 2001; Wittinghofer and Vetter, 2011). GDIs impede the release of GDP from the GTPases, inhibit GTPase activity and extract the GTPases from plasma membranes into the cytosol.

In bacteria, only recently it has been shown that the two small GTPases SofG and MglA play an important role in cell polarity and motility in *Myxococcus xanthus* (Leonardy et al., 2010; Patryn et al., 2010; Zhang et al., 2010; Bulyha et al., 2013). The response regulator RomR, which is regulated by the Frz chemosensory system, interacts with MglA-GTP and recruits it to both poles of the rod-shaped bacterium (Keilberg and Søgaard-Andersen, 2014). Its cognate GAP MglaB selectively inactivates MglA, so that the future leading pole is characterized by MglA-GTP and a higher local concentration of RomR. The lagging pole in contrast is marked by a high MglB concentration and a low concentration of RomR. Asymmetrically localized MglA and its interplay with the GTPase SofG serve in the correct polar localization of the ATPases PilT and PilB to the leading and to the lagging pole respectively. PilB and PilT function in type-IV-pilus (T4P) dependent motility by providing energy for T4P retraction and extension.

In eukaryotes, Rho (for RAS HOMOLOGY) GTPases of the Ras superfamily play a crucial role in cell polarity. Whereas fungi and animals have developed diverse Rho GTPase families, such as Rho, Rac or Cdc42, in plants only one, called ROP (RHO OF PLANTS), with a high similarity to human Rac GTPases can be found (Craddock et al., 2012; Hall, 2012). The probably best understood eukaryotic small GTPase in terms of polarity establishment and signaling is the CELL DIVI-

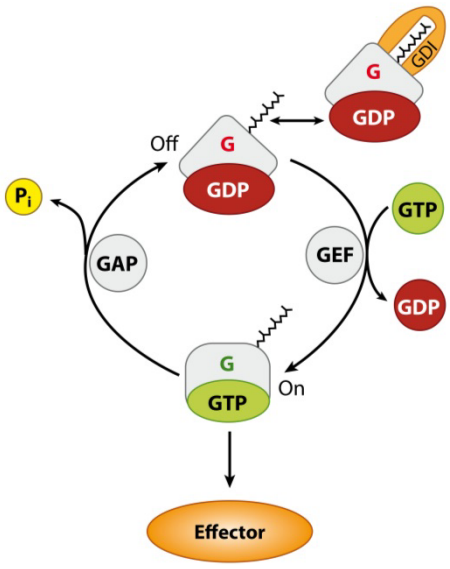

Figure 1.2 | The functional cycle of G proteins.

Small GTPases from the Ras superfamily bind lipids at their C-terminus and show partial membrane association. Regulation occurs by interaction with guanine nucleotide exchange factors (GEFs), GTPase activating proteins (GAPs), and guanine nucleotide dissociation inhibitors (GDIs), which activate (GEF) or inactivate (GAPs, GDIs) GTPases by facilitating the exchange of guanine nucleotides, the hydrolase activity or the release from membranes. Figure adopted from Wittinghofer and Vetter (2011).

SION CYCLE protein Cdc42 from the budding yeast, *Saccharomyces cerevisiae*. Its function is highly conserved, and mammalian *Cdc42* genes are at least partially able to rescue yeast c*dc42* deletions (Shinjo et al., 1990). Loss-of-function mutants for Cdc42 in yeast are unable to establish cell polarity and stay symmetrical (Thompson, 2013). Its C-terminal CAAX motif can bind geranyl-geranyl molecules, which partially anchors Cdc42 to the plasma membrane. Upon interaction with its GEF Cdc24 or its GAPs Bem2, Bem3, Rga1 or Rga2, Cdc42 is activated or inactivated respectively (Howell and Lew, 2012; Bi and Park, 2012). The polar localization of its GEF Cdc24 plays an essential role in cell polarity establishment and maintenance. Also the GAPs are localized polar and their inhibition by phosphorylation furthermore contributes to the temporal Cdc42 activation. Another polarity regulator is the RHO GDI Rdi1 that effectively extracts Cdc42 from membranes and thus facilitates its rapid cycling between the plasma membrane and the cytoplasm. The spatiotemporal regulation of Cdc42 is an important trigger for downstream cell polarization. Upstream, Cdc42 is controlled by the action of the GTPase Bud1/Rsr1, its GAP Bud2 and its GEF Bud5. Transmembrane glycoproteins such as Bud8, Bud9 and Bud10/Axl2 serve as polar localized landmarks in axial or bipolar budding and finally determine the site of Cdc42-mediated cell polarity (Howell and Lew, 2012; Bi and Park, 2012).

1.2.2 The dynamic reorganization of the cytoskeleton is important for cell polarity

Both, in eukaryotes and in prokaryotes, the small GTPase-regulated organization of the cytoskeleton formed by actin or actin-like proteins is necessary for cell polarity. In the bacterium *Caulobacter crescentus*, the BACTOFILIN cytoskeleton proteins BacA and BacB specifically localize to the site of the cell where a thin protrusion, the stalk, is localized. The polar localization of BacA and BacB serves as a landmark for the recruitment of the stalk-building cell wall biosynthesis enzyme PbpC (Kühn et al., 2010; Hughes et al., 2013). In *M. xanthus* it has been shown that by disturbing the assembly of the actin-like cytoskeleton protein MreB, the polar localization of

the small GTPase MglA is perturbed and motility is inhibited (Mauriello et al., 2010). The small GTPase SofG has been shown to interact with the cytoskeleton protein BACTOFILIN BacP that forms two polar patches at both sites of the rod (Bulyha et al., 2013). However, SofG is specifically recruited to the BacP patch at the leading pole of the cell and together with MglA promotes T4P-dependent motility.

The yeast Cdc42 GTPase interacts with two formins, Bni1 and Bnr1 that mediate actin nucleation and thus initiate the filament formation (Bi and Park, 2012). Cells in which these formins are deleted are synthetically lethal and show strong polarity defects. If the actin filament is disrupted by treatment with the drug Latrunculin A, also the polarized localization of the GTPase Bud1/Rsr1 is abolished (Kozubowski et al., 2008), highlighting the important role of actin organization in cell polarity establishment.

1.2.3 Polar secretion and rapid turnover by exo- and endocytosis determines cell polarity

The polar distribution of new cell wall and plasma membrane material in cells that elongate at one site such as budding yeast, animal neurons or plant pollen tubes and root hairs is essential for polar growth that is initiated by small GTPase-mediated actin transport. In yeast, actin cables polarized by the Cdc42-activated formin Bni1, guide vesicles via a myosin-V-dependent transport to the site of bud formation (Bi and Park, 2012). Bound to the vesicle membrane, additional Cdc42 is transported to the bud site, thereby supporting the positive feedback loop of cell polarization. Once vesicles reach at their target membrane, protein complexes such as the hetero-octameric exocyst complex act in membrane tethering. Finally membrane fusion occurs via a SNARE (SOLUBLE N-ETHYLMALEIMIDE-SENSITIVE FACTOR ATTACHMENT PROTEIN RECEPTOR) mediated process. The evolutionary conserved exocyst complex composes of the Sec proteins 3, 5, 6, 8, 10 and 15, identified as their mutants show defects in secretion, and the Exo70 and Exo84 proteins (Heider and Munson, 2012). Whereas in yeast and animals all of these proteins are encoded by single-copy genes (Heider and Munson, 2012), in plants often more copies are found (Žárský et al., 2009; Cvrčková et al., 2012). Especially the Exo70 family has a high number of members indicating functional diversification among these proteins in plants. The exocyst complex is supposed to form dynamically in each round of exocytosis (Bi and Park, 2012). In *Drosophila* epithelia, the transmembrane protein CRUMBS (Crb) is secreted polar to the apical membrane via the exocyst machinery in a Rab GTPase dependent manner (Thompson, 2013). Simultaneously, endocytosis of Crb via the AP2/Clathrin machinery at basolateral membranes is required for cell polarity establishment and maintenance. Dynamic rapid exo- and endocytosis and cycling of components between the plasma membrane and the cytoplasm are further important determinants of cell polarity in eukaryotes. FRAP experiments have shown that Cdc42 undergoes fast cycling between both localizations, the plasma membrane and the cytoplasm (Wedlich-Soldner et al., 2004). This cycling is thought to be important for restricting the local Cdc42 acti-

vation and inactivation (Bi and Park, 2012). In plants, rapid actin-dependent endocytic cycling has been demonstrated for the polar localized auxin plant growth hormone efflux carrier PIN FOMED 1 (PIN1) (Kleine-Vehn and Friml, 2008).

In the *M. xanthus* bacterium, polar slime secretion is a prerequisite for adventurous (A) motility in gliding. If the slime is not secreted asymmetrically, A motility is abolished (Yu and Kaiser, 2007). Deletion of the polar localized small GTPase MglA or its GEF MglB in *M. xanthus* (Keilberg and Søgaard-Andersen, 2014), results in a loss of polar slime secretion and consequently in the loss of A motility (Yu and Kaiser, 2007).

1.2.4 Posttranslational protein modification by phosphorylation regulates cell polarity

The aquatic bacterium *Caulobacter crescentus* is polar organized. After division it produces a motile swarmer cell and a sessile stalked cell (Sommer and Newton, 1991; Ganguly et al., 2012). Prior to division, the cell division gene and response regulator DivK rapidly shuttles between both poles in a phosphorylation dependent manner (**Figure 1.3 A**). At the stalked pole, DivK is phosphorylated by the DivJ kinase and moves to the swarmer pole. There, the PleC phosphatase dephosphorylates DivK which then shuttles back to the stalked pole of the cell. Furthermore there is a gradient of the phosphorylated response regulator CtrA towards the swarmer pole. This gradient is generated by CckA phosphatases located at the stalked, and CckA kinases located at the swarmer pole (Tsokos and Laub, 2012). Consequently, after division the swarmer cell has a high fraction of dephosphorylated DivK and phosphorylated CtrA, and the stalked cell a high fraction of phosphorylated DivK and dephosphorylated CtrA.

The Par proteins play an essential role in cell polarity establishment in animals (Thompson, 2013). At the apical pole of *D. melanogaster* follicle cells, Par3 is localized in a complex with Cdc42, Par6 and the ATYPICAL PROTEIN KINASE C aPKC, whereas at the basolateral domains the kinase Par1 is located (**Figure 1.3 B**). Par1 phosphorylates Par3 and thereby restricts its localization to the apical plasma membrane. Conversely, Par1 is restricted to the basolateral plasma membrane by aPKC-Par6 complex mediated phosphorylation (Ganguly et al., 2012). Polarity in some *Arabidopsis thaliana* plant cells is achieved by the polar localization of PINs (**Figure 1.3 C**), the auxin plant hormone efflux carriers (Dettmer and Friml, 2011). The main driving force for polarity maintenance is PIN phosphorylation and dephosphorylation and endocytic recycling (Geldner, 2008). The serine-threonine AGC kinase PINOID (PID) is responsible for PIN phosphorylation and the PROTEIN PHOSPHATASE 2A (PP2A) for dephosphorylation. The endosomal PIN recycling process is controlled by ADENOSYL RIBOSYLATION FACTOR GUANOSINE EXCHANGE FACTORS (ARF-GEFs) and the Rab5-GTPase ARA7 (Dhonukshe et al., 2008). First, PIN proteins are secreted to the membranes in a non-polar manner and phosphorylation and recycling regulates subsequent PIN polarization. Predominantly, phosphorylated PINs show a preference for apical and dephosphorylated PINs for basal membranes (Ganguly et al., 2012). PIN

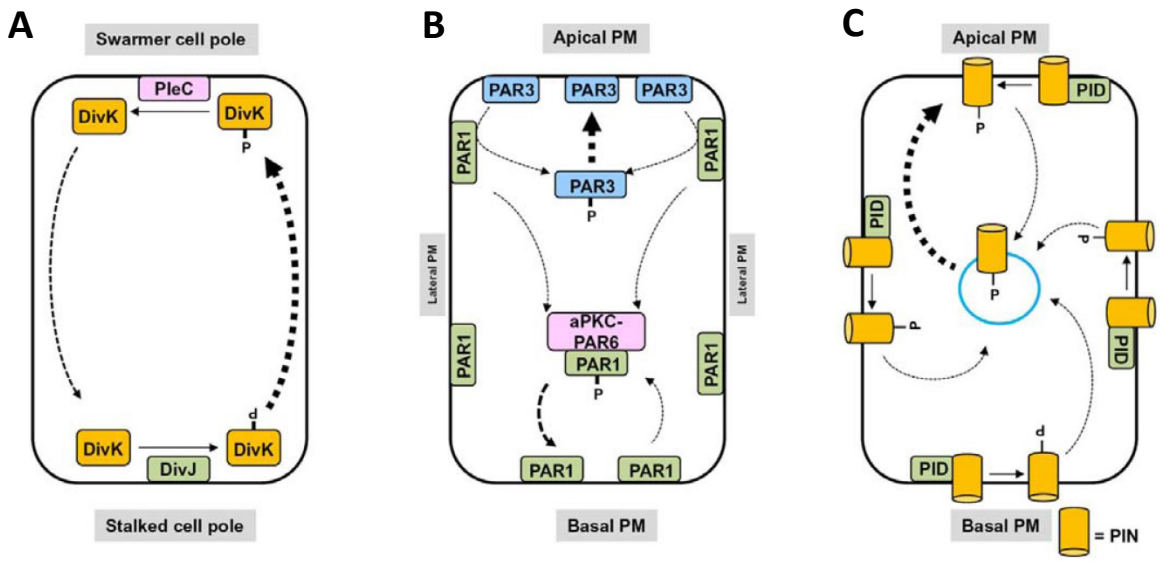

Figure 1.3 | Cell polarity regulation by phosphorylation.

Cell polarity regulation by phosphorylation-mediated polar protein trafficking in **(A)** bacteria, **(B)** mammals and **(C)** plants. (A) in the bacterium *Caulobcater crescentus*, DivK is phosphorylate by DivJ at the stalked cell pole and localizes to the swarmer cell pole. There, DivK is dephosphorylated by PleC and thus redirected to the stalked cell pole. (B) in mouse epithelial cells, phosphorylation regulates polar localization of the Par proteins. Par1 is localized basolateral and Par3 apical. Par3 is phosphorylated by Par1 and its localization is phosphorylation-dependent. Also the basolateral localization of Par1 is phosphorylation dependent and regulated by the aPKC-Par6 complex. (C) in *Arabidopsis thaliana*, PID-mediated phosphorylation of PIN specifically targets it to the apical membrane. Figure modified from Ganguly et al. (2012).

polarization is thus dependent on the level of activity of the antagonistic processes of phosphorylation and dephosphorylation (Kleine-Vehn and Friml, 2008).

1.2.5 Cell polarity underlies the principles of positive feedback loops and mutual antagonisms

Especially recent mathematical modeling approaches have revealed the importance of feedback loops that action in a cooperative, non-linear fashion to establish a single local spot for cell polarization (Thompson, 2013). Two partially redundant and interlinked feedback loops are thought to function in cell polarization in yeast. In a fast process, an autocatalytic cluster of Cdc42 in complex with its GEF Cdc24, the scaffold protein Bem1 and the kinase Cla4 is able to generate a positive feedback loop that leads to Cdc42 polarization by self-recruiting (Altschuler et al., 2008; Johnson et al., 2012; Bi and Park, 2012). Another feedback loop is generated after cytoskeleton polarity establishment by the actin-dependent Cdc42 polarization. This second slower feedback loop stabilizes the polarization process initiated by the first autocatalytic clustering (Slaughter et al., 2009). Besides the requirement of positive feedback loops, the importance of mutual antagonism between polarity components has been demonstrated by mathematic modeling of *Caenorhabditis elegans* zygotes (Goehring et al., 2011) and *Drosophila melanogaster* follicle cells (Fletcher et al., 2012). At the anterior pole of the *C. elegans* zygote, Par3 forms a complex

with the PDZ-domain protein Par6, the serine/threonine kinase aPKC and Cdc42. The kinase Par1, the RING domain protein Par2 and the LETHAL GIANT LARVAE (LGL) protein form a complex at the posterior pole (Thompson, 2013). By mutual antagonistic phosphorylation of Par3 by Par1 and of Par1 by aPKC, the respective polarity components are removed from the plasma membrane, thereby keeping the anterior-posterior restricted distribution in equilibrium (Goehring et al., 2011; Thompson et al., 2013). The same polarity components are required to generate an apical-basolateral cell polarity in *D. melanogaster* epithelia cells. Here it was also shown that mutual antagonistic regulation by phosphorylation of apical-localized BAZOOKA (the homologue to Par3 from *C. elegans*) by Par1 and basolateral-localized Lgl by aPKC is important to generate and sustain cell polarity (Fletcher et al., 2012; Thompson et al., 2013). Plant leaf epidermal pavement cells exhibit a jigsaw piece-like morphology with spots of local outgrowth, the lobes and spots with suppressed outgrowth, the indentations (**Figure 1.4**). The regulation of polarized local outgrowth and local outgrowth suppression is achieved by the mutual antagonisms between the small GTPases ROP2 and ROP6 in an auxin and PIN1 mediated positive feedback loop in *Arabidopsis* (Xu et al., 2010).

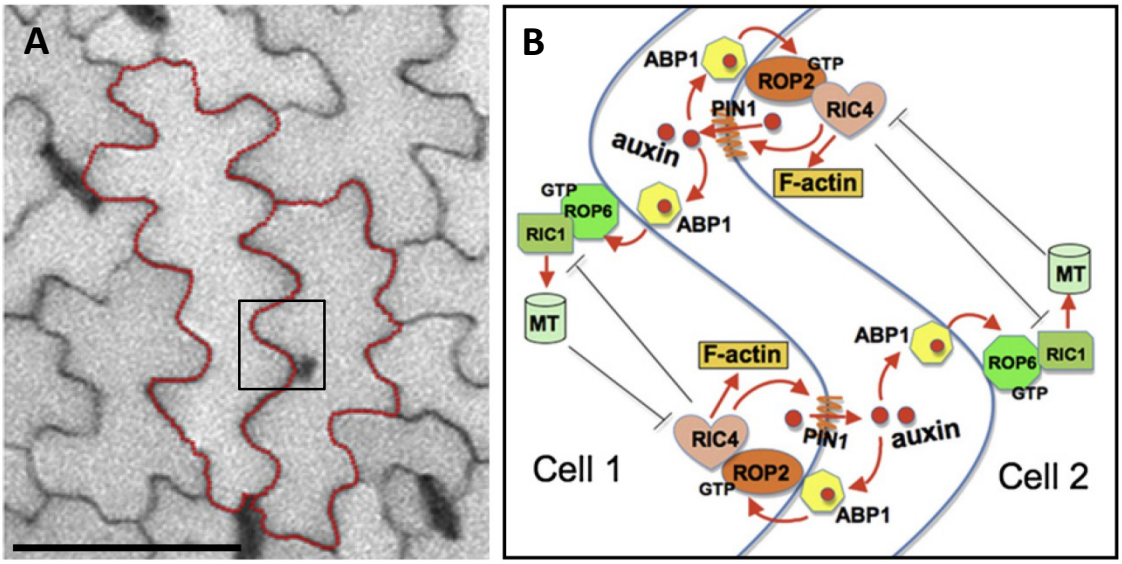

Figure 1.4 | Polarity control in leaf epidermal cells.

(A) Overview image of the *Arabidopsis thaliana* leaf epidermis showing single jig-saw piece-like pavement cells highlighted by red outlines. **(B)** Interdigitated growth of leaf epidermis pavement cells in *Arabidopsis thaliana* is regulated by feedback loops and auxin signaling and is inter- and intracellular coordinated. Central roles play the small GTPases ROP2 and ROP6 which control lobe and indent formation respectively in complementary pathways. ROP2 acts in a self-activating local feedback loop together with PIN1 and auxin and regulates actin cytoskeleton organization via RIC4. Localized extracellular auxin regulates the antagonizing ROP6 pathway and microtubule formation via RIC1 in adjacent cells. ROP2 functions in a positive feedback loop and both, the ROP2 and ROP6 pathways act mutually antagonizing. Scale bar = 25 µm in (A). Figure modified from Xu et al. (2010).

1.2.6 Cell polarization is triggered by external cues or induced spontaneously

Both, spontaneous or external-triggered polarization events are fundamental properties of polarized cells (McCaffrey and Macara, 2012). For example, the opportunistic human pathogenic fungus *Candida albicans* can grow in its predominantly unpolar yeast form that only during budding shows spontaneous cell polarization (**Figure 1.5**). Stimuli that represent stresses such as nutrient starvation, temperature variation or hypoxia, or the sensing of serum, trigger the switch to its highly polarized and oriented hyphal growth form (Arkowitz and Bassilana, 2014). Some cells are mainly polarized only upon external cues. The eggs of the worm *C. elegans* initially show a high degree of symmetry. The entry of the sperm during fertilization leads to symmetry breaking and triggers the polarization of the zygote (Thompson, 2013). Thereby the position of the sperm centrosome marks the new posterior pole. Also the zygote of the brown alga *Fucus distichus* is mainly polarized by external cues after fertilization (Cove, 2000). There, the first cell division leads to the formation of a rhizoid cell and a cell that differentiates to the later thallus. If the zygote is exposed to a light gradient, the rhizoid cell will always emerge from the shaded side. On a subcellular level, this position is marked by the occurrence of an F-actin assembly at the site of rhizoid outgrowth (Cove, 2000).

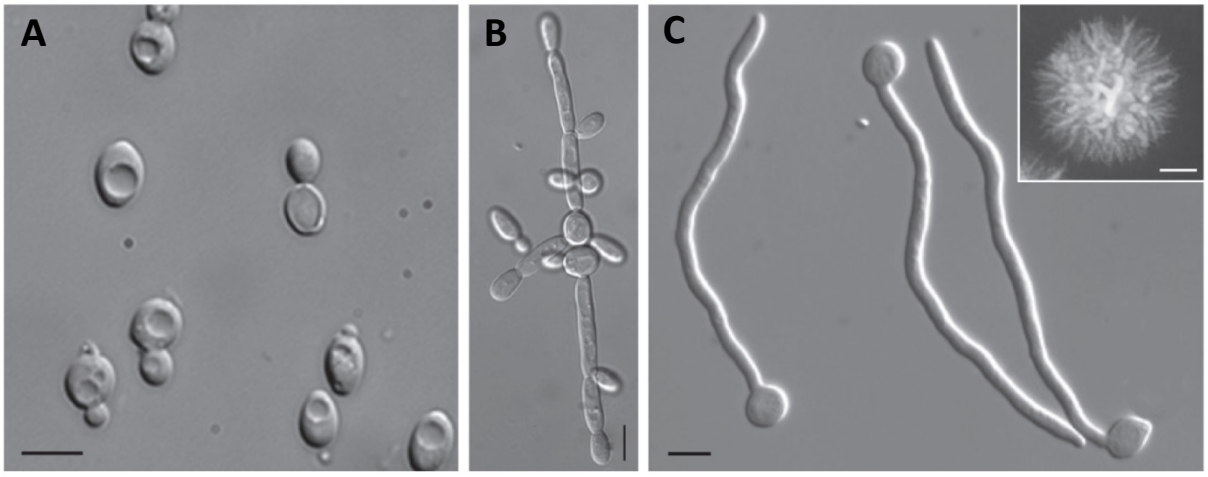

Figure 1.5 | Different growth forms of the human pathogen *Candida albicans.*

Morphology of the fungal pathogen *Candida albicans* in its yeast **(A)**, pseudohyphal **(B)** and hyphal **(C)** forms. The inset in (C) shows a hyphal colony grown for 5 days on Spider medium. Bars = 5 µm in (A) to (C) and 1 mm in inset of (C). Note the high morphological similarity of growing hyphae (C) and germinating pollen tubes (**Figure 2.1**). Figure adopted from Sudbery (2011).

1.3 Cell Polarity in Flowering Plants

Cell polarity is a fundamental necessity for the organization of the entire plant body. At every point in the life cycle of a flowering plant, cell polarity is required to control development, growth and morphogenesis (Yang, 2008). Comparable to other organisms, plants exhibit a broad range of polar organized cell types. On one side of the spectrum are cells such as root tip cells which show only a low level of morphological polarity. But as mentioned above, they exhibit a high level of molecular polar organization marked by the distribution of PIN auxin efflux carriers. On the other side, morphologically highly polarized cell types can be found, such as, for example trichomes. They are formed by the leaf epidermis and exhibit a complex 3-dimensional architecture. With respect to the rigid cell wall that surrounds the mature plant cell and limits its extension capability, polarized cell division plays an important role in plant body construction and development. Also different to animal systems, tightly cell wall-encapsulated plant cells are not able to migrate within a tissue (Dettmer and Friml, 2011). Thereby cell polarization by means of asymmetric cell division becomes an important developmental phenomenon.

Notably, already the first cell division in a flowering plants' life cycle is highly asymmetric and results in the formation of two cells that undergo completely different cell fates (**Figure 1.6**). In *Arabidopsis*, after gamete fusion in the process of double fertilization (see section 1.5), the zygote undergoes polarized elongation (Lau et al., 2012). A large vacuole is located at the micropylar pole, whereas the nucleus is positioned at the chalazal pole (Zhang and Laux, 2011). The first cell division occurs transversely to the future embryo axis and result in a small apical cell and a large basal cell. All cells derived from the apical cell differentiate into cells of the embryo. The large ba-

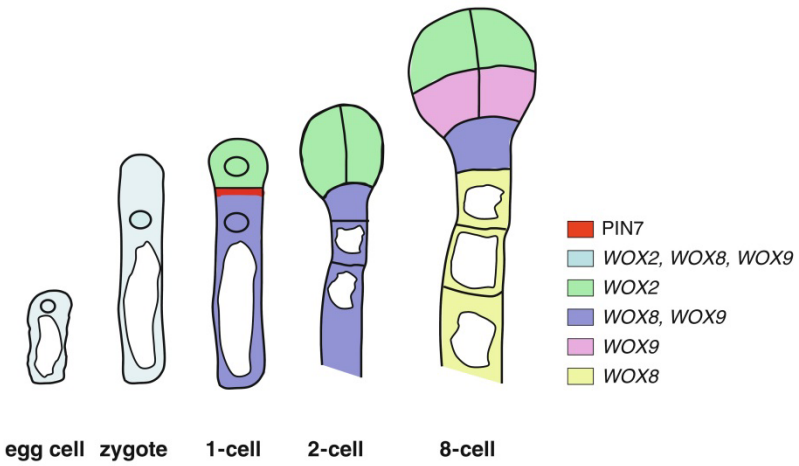

Figure 1.6 | Zygote and early embryo development in *Arabidopsis thaliana*.

Schematic drawing showing the polarized egg cell and zygote as well as apical-basal axis formation during early embryo development. In the egg cell and elongated zygote, large vacuoles reside at the basal (micropylar), and nuclei at the apical (chalazal) poles of the cell. The zygote undergoes an asymmetric cell division and forms a small apical cell (ac) and a large basal cell (bc). The cells derived from divisions of the apical cell together with the uppermost cell of the dividing basal cell (hypophysis, hy) form become embryonic cells, whereas the remaining daughter cells of the basal cell form the suspensor. Polar localization of PIN7 in the basal cell and cell-type specific expression of *WOX* genes is indicated by the color code. Figure modified from Zhang and Laux, (2011).

sal cell will give rise to a cell file of which the uppermost, the hypophysis, contributes to the root meristem of the embryo. The remaining cells differentiate into the embryo-supplying suspensor. On the molecular level, asymmetric cell division of the zygote is dependent on polarized auxin transport. As judged from the *DR5rev:GFP* reporter activity, auxin accumulates in the small apical cell (Friml et al., 2003). This accumulation is regulated by the PINFROMED 7 (PIN7) auxin efflux carriers that are localized polar in the apical membrane of the basal cell and pump auxin into the small apical cell and thus regulate its development. PIN protein expression and auxin homeostasis is furthermore regulated by the WUSCHEL HOMEOBOX (WOX) proteins. In the egg cell, *WOX2* and *WOX8* are both expressed, whereas after asymmetric cell division, *WOX2* is present only in the apical, and *WOX8* only in the basal cell (Haecker et al., 2004). Zygote elongation and asymmetric cell division is regulated by the MAPKK kinase YODA (YDA). Notably, in the *yda-1* mutant, the zygote divides almost symmetrically (Lukowitz et al., 2004). Upstream of *YDA* acts the *SHORT SUSPENSOR (SSP)* interleukin-1 receptor-associated kinase / Pelle-like kinase, and its loss phenocopies the *yda* mutant (Bayer et al., 2009). Interestingly, only the *SSP* allele that is derived from the paternal sperm cell line functions in embryo patterning as shown by crossing experiments. In a model of *SSP* function it is hypothesized that the polar delivery of the *SSP* mRNA by the sperm cell fusion with the egg cell triggers zygote elongation and asymmetric cell division via the YDA/MAPK pathway (Bayer et al., 2009). This situation of zygote polarity establishment controlled by sperm cell entry is reminiscent of the polarization that occurs in the *C. elegans* egg described above. Although far away from being entirely understood, polarity establishment in the *Arabidopsis* zygote represents an outstanding example of the close relation between polarity, cell fate determination and developmental regulation.

But already before double fertilization and zygote formation, cell polarity plays an important role in cell fate determination in the female gametophyte. Already the synergid, egg and central cells display a polar organization (Sprunck and Groß-Hardt, 2011). In the synergid and the central cell the nucleus is oriented towards the micropylar pole, whereas a large vacuole is located at the chalazal pole. In contrast, the egg cell is orientated the other way round: a large vacuole is located at the micropylar and the nucleus at the chalazal pole. Mutant analyzes suggest that polar nucleus localization is tightly linked to cell fate of the female gametophytic cells. In female gametophyte mutants such as *ATROPOS, CLOTHO, EOSTRE* or *LACHESIS*, nuclei of synergid cells are often mislocated at the chalazal pole, which ultimately results in the expression of egg cell genes (Groß-Hardt et al., 2007; Pagnussat et al., 2007; Moll et al., 2008). These examples demonstrate the tight interconnectivity between cell polarity and cell fate determination.

On a macroscopic scale, cell polarity is more obvious for leaf epidermis pavement cells or for trichomes, compared to the cells of the female gametophyte. As shown in **Figure 1.4**, pavement cells form many highly polarized structures of lobes and indentations that join together with the indentations and lobes of the neighboring cells, like the pieces of a jigsaw puzzle. As described above, in pavement cells the spatially controlled auxin-mediated interplay between local feedback-

regulated ROP signaling and cytoskeleton organization controls lobe and indentation formation, and thus cell polarity (Xu et al., 2010).

Trichomes are leaf hairs that are formed by single epidermis cells in duty to protect the plant against herbivore attacks, water loss by transpiration, or UV irradiation. Therefore, trichomes are present on most aerial parts of the *Arabidopsis* plant (Marks, 1997; Pattanaik et al., 2014). On a genetic level, trichome development is regulated by a network including the TRANSPARENT TESTA GLABRA 1 (TTG1) WD40 repeat protein, the functionally redundant GLABRA 3 (GL3) and ENHANCER OF GLABRA 3 (EGL3) bHLH transcriptions factors, and the MYB transcription factors GLABRA 1 (GL1) and MYB23 (Oppenheimer et al., 1991; Walker et al., 1999; Payne et al., 2000; Zhang et al., 2003; Kirik et al., 2005). Trichome outgrowth and proper trichome morphogenesis establishment is regulated by the GLABRA 2 (GL2) homeodomain, and the TRANSPARENT TESTA GLABRA 2 (TTG2) WRKY, (Rerie et al., 1994; Johnson et al., 2002) as well as by the MYB82 transcription factors (Liang et al., 2014). Normally, trichomes in *Arabidopsis* develop three to four branches (Marks, 1997). However, the knock-out of the RPN1A subunit of the 26S proteasome results in a higher number of trichome branches, likely by interfering with gibberellic acid and cytokinin signaling pathways (Yu et al., 2015). Also, small endogenous non-coding microRNAs (miRNAs) play a role in trichome development regulation by modulating the expression of SQUAMOSA PROMOTER BINDING PROTEIN LIKE (SPL) genes (Yu et al., 2010). The expression of a mimicry target of miR156 results in a reduction of trichome density, whereas the constitutive expression of miR156 leads to ectopic trichome development. Thus, a complex network of transcriptional regulation, protein level regulation and hormone signaling is required to control cell polarity in trichome development. Although we have a quite elaborate picture of genetic root hair developmental control, the underlying cell biological events are only poorly characterized (Kulich et al., 2015). Only very recently it was shown that the exocyst vesicle tethering complex subunit Exo70H4 plays an important role in UV irradiation-induced secondary cell wall formation in trichomes (Kulich et al., 2015).

However, detailed cell biological and molecular studies on cell polarity and polar cell growth in flowering plants have mainly been conducted on pollen tubes and root hairs where we have a quite elaborated, but still incomplete picture of the underlying mechanisms (for review see: Kost, 2008; Yang, 2008; Chebli et al., 2013; Guan et al., 2013; Rounds and Benzanilla, 2013; Ketelaar, 2013; Cai et al., 2015). The molecular basis of cell polarity establishment and polar tip growth of pollen tubes and root hairs in *Arabidopsis* represent the focus of the subsequent section.

1.4 *Cell Polarization and Polar Tip Growth of Pollen Tubes and Root Hairs*

In plant polar growth research, flowering plant pollen tubes and root hairs have developed to the cell types of choice as they represent protrusions of single cells that grow rapidly and highly polarized (Yang, 2008). The outgrowth of pollen tubes and root hairs occurs from only one single

point of the cell and the expansion of the protuberance takes place only at an annular region shortly below the very apex of the tip-growing tube. Thus, the growth of pollen tubes and root hairs can be described as heterotropic monotropic annular tip growth (Geitmann, 2009, 2010).

In both cell types the highly polarized growth is related to a specialization in their biological function. Root hairs are formed in the root differentiation zone and mainly serve in anchorage and nutrient uptake as well as in plant-microbe interactions by enormously increasing the root surface and the root diameter (Grierson et al., 2014). On the other hand, the pollen tube of flowering plants represents the mature three-cellular male gametophyte (McCormick, 2004). During microsporogenesis, diploid pollen mother cells undergo meiosis which results in the generation of haploid microspores. The microspore undergoes a first mitosis to form the bicellular pollen grain, consisting of a large vegetative and a small generative cell. In a second mitosis, the generative cell divides into the two sperm cells. The two sperm cells are enclosed by the cytoplasm and surrounded by the plasma membrane of the vegetative cell. One of the sperm cells forms a plasma membrane projection that is physically connected to the nucleus of the vegetative cell. Together the two sperm cells and the vegetative nucleus form the so called male germ unit (MGU) (McCue et al., 2011). After landing on the stigma, the large vegetative cell forms the tip-growing pollen tube that has the function to transport the two sperm cells to the female gametophyte to confer double fertilization, the fusion of one sperm cell with the haploid egg cell, and the fusion of one sperm cell with the diploid central cell nucleus (**Figure 1.7**).

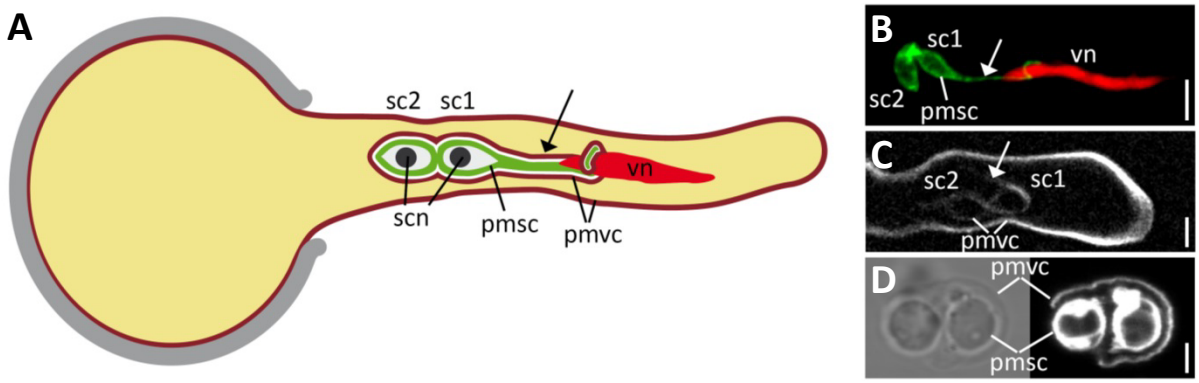

Figure 1.7 | The pollen tube and the male germ unit of *Arabidopsis thaliana*.

A) Scheme of a growing *Arabidopsis* pollen tube and the male germ unit (MGU) which comprises two physically connected sperm cells (sc1 and sc2). The plasma membrane of the distal sperm cell (pmsc) forms a projection (arrow) to the vegetative nucleus of the tube cell (vn). Both sperm cells are enclosed by the membrane of the vegetative cell (pmvc, dark red). Sperm cell nuclei (scn) are in black. **(B)** Confocal laser-scanning micrograph of a growing pollen tube with GFP-labelled sperm cell membranes (pmsc) and a red fluorescent vegetative nucleus (vn). **(C)** Spinning-disc confocal micrograph of a pollen tube expressing a fluorescent membrane protein that labels the membrane of the vegetative cell (pmvc) which also encloses the two sperm cells. **(D)** Sperm cells released from a pollen tube in vitro. The membrane-selective styryl dye FM4-64 labels the sperm cell membranes (pmsc) and the membrane of the vegetative cell (pmvc), which ruptured during pollen tube burst. Note that objects shown in **(A)** are not to scale. Scale bars = 5 µm in (B) and (C) and 2 µm in (D). Figure modified from Sprunck et al. (2014).

After microsporogenesis, mature tricellular pollen grains are partially dehydrated and metabolically inactivated until they get in contact with the receptive stigma of a flower after pollination (Edlund et al., 2004). During this contact phase, a water 'bridge' between the pollen exine and the cell wall of the papilla cell is established, the so called 'foot' (Wolters-Arts et al., 1998).

1.4.1 Pollen activation

After rehydration in a process called pollen activation, the pollen grain undergoes symmetry breaking and polarization, which finally leads to the formation of the pollen tube (Raghavan, 2003). So far we have only little knowledge about the cell biological and molecular basis of symmetry breaking and growth-site selection in pollen grains. In a recent study it was demonstrated by using cell wall component specific staining techniques, electron microscopy and mutant analysis, that in *Arabidopsis* pollen prior to germination, a structure termed germination plaque consisting of cellulose, callose and partly de-esterfied pectin is formed at the site of pollen tube emergence (Hoedemaekers et al., 2014). The *BURSTING POLLEN (BUP)* gene encodes a Golgi-located glycosyltransferase responsible for the proper organization of the germination plaque and the tip of the growing pollen tubes. Furthermore, after pollen hydration and approximately 6 minutes before germination, a cytosolic Ca^{2+} gradient is established towards the future germination site (Iwano et al., 2004). Fluorescence microscopy revealed that in *Pyrus communis* and *Narcissus pseudonarcissus* pollen the actin cytoskeleton is polarized towards the germination site (Tiwari and Polito, 1988; Heslop-Harrison and Heslop-Harrison, 1992). It seems very likely that, comparable to the role of the small GTPase Cdc42 during symmetry breaking in yeast, in the pollen grain the small GTPase ROP1 plays a central role in polarization (Yang and Lavagi, 2012). The ROP INTERACTIVE PARTNER 1 (RIP1/ICR1) was identified as molecular interactor of ROP1 by yeast two-hybrid screening. Its location switches from the nucleus to the future germination site before pollen tube emergence (Li et al., 2008). By recruiting ROP1 to the plasma membrane, it is thought that RIP1/ICR1 is involved in the positive feedback regulation of ROP1 localization to the site of pollen polarization. Very recently it was shown that the cytoplasmic ROP-interactive CRIB motif-containing protein RIC1 is localized to the plasma membrane at the pollen tube emergence site during germination and at the tip of growing pollen tubes (Zhou et al., 2015). RIC1 regulates F-actin dynamics and thus pollen tube growth by directly binding to and severing of F-actin in a Ca^{2+}-dependent manner. ROP1 was already shown to interact with two other RICs, namely RIC3 and RIC4 and thereby to activate two counteracting downstream pathways (Gu et al., 2005). RIC4 promotes the assembly of F-actin, whereas RIC3 promotes the Ca^{2+}-mediated disassembly of F-actin at the pollen tube tip (Gu et al., 2005; Lee et al., 2008).

We have shown that prior to pollen germination, vesicles marked with the ARMADILLO REPEAT ONLY 1 (ARO1) protein, an important player in polar elongation of growing pollen tubes (Gebert et al., 2008), accumulate at the pollen tube germination site shortly before outgrowth (Vogler et al., 2015, ***Chapter 2***). However, this accumulation does not represent a constant in-

crease, but rather some short and peaked maxima 12 to 3 minutes before pollen tube formation. We could also show that about 15 minutes before pollen tube formation, F-actin reorganization events take place. Especially at the flanks and the opposite pole of the germination site, massive cortical actin arrays appear, possibly forming a mechanical counter bearing for the future protrusion formation and F-actin polarization.

1.4.2 Stages of root hair and pollen tube growth

Due to large genetic screening approaches (e.g. Schiefelbein and Sommerville, 1990; Parker et al., 2000) we currently have a much better understanding of cell polarization events that take place shortly after protrusion formation in root hairs than in pollen tubes (**Figure 1.8**). This imbalance of knowledge is mainly caused by two facts. First, as they grow slower (Ketelaar et al., 2008), root hairs are much easier to investigate on a mechanistic level than pollen tubes. Second, pollen tubes are haploid and involved in sexual reproduction. Therefore already weak recessive mutations can lead to male sterility and thus hamper the screening for genetic interactions of higher order mutants. Root hair development underlies several genetically distinct steps (Schiefelbein and Sommerville, 1990; Parker et al., 2000). First, a local swelling, the so called bulge is formed by the trichoblast (i.e. the root hair forming cell) protoplast. This roundish swelling then enlarges and at a certain point transitions into an elongating structure. In the last step, the root hair finally grows by polar tip growth. For each of these steps, characteristic mutants could have been identified (summarized in Bibikova and Gilroy, 2003; Grierson et al., 2014).

Using morphological modeling and quantitative live-cell imaging, we could show that also pollen tube growth can be subdivided into comparable distinct steps, thereby providing a methodological and knowledge framework for large-scale genetic screening approaches (Vogler et al., 2015, *Chapter 2*).

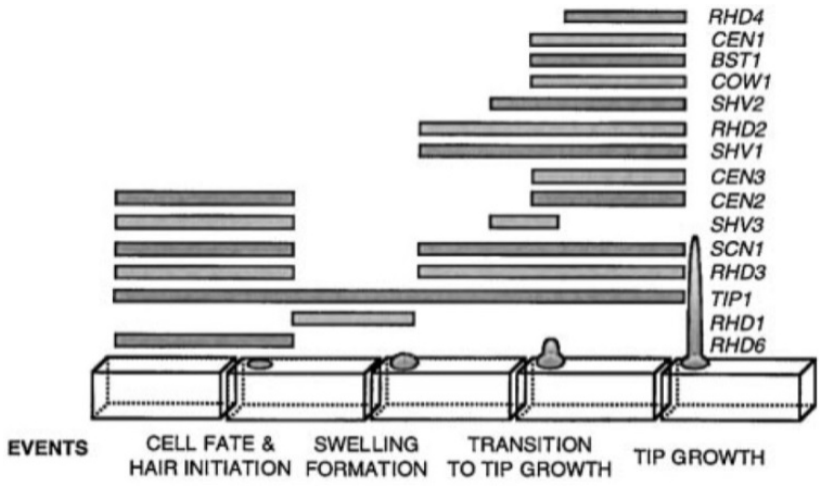

Figure 1.8 | Wild-type root hair development.

Characteristic events during the development of root hairs in *Arabidopsis*. Genes important for certain steps of root hair development are indicated on the right. Figure modified from Parker et al. (2000).

1.4.3 Molecular mechanisms of tip growth

Besides similarities in mechanisms of protrusion formation, a large body of publications has revealed significant similarities between cell biological and molecular mechanisms underlying polar tip growth of flowering plant pollen tubes and root hairs (e.g. Šamaj et al., 2006; Campanoni and Blatt, 2007; Kost, 2008). Both exhibit an inverted cone shaped vesicle-rich zone at the very apex that, due to the lack of large light-scattering organelles, is named the 'clear zone' (Hepler and Winship, 2015). In both cell types vesicles move at the flanks towards the apex and return in the center back to the shank in a so called 'reverse fountain' streaming pattern (Cheung and Wu, 2008; Chebli et al., 2013). The actin cytoskeleton is highly polarized in longitudinal bundles in both cell types (Hepler et al., 2001) and both show a steep tip-focused Ca^{2+} gradient that tightly interplays with reactive oxygen species (ROS) and ROP/RIC signaling, local pH changes, actin dynamics, and phospholipid signaling (Cárdenas et al., 2008; Cárdenas, 2009). In both cell types the polar localization and tip-restricted action of a small ROP GTPase is regulating the tubular shape and the elongation process. In pollen tubes, ROP1 is the central molecular polarity switch (Li et al., 1999), whereas in root hairs ROP2 fulfills this function (Jones et al., 2002). A recent comparative microarray transcriptomics approach has revealed that root hairs and pollen tubes cluster closely together in regard of their expression profiles (Becker et al., 2014). Given the significant mechanistic and transcription profile similarities, it is not surprising that gene knock-outs can cause polarity defects in both cell types. Thus, the loss of the ankyrin and DHHC-CRD domain containing *TIP GROWTH DEFECT 1 (TIP1)* protein, the exocyst subunit *Exo70A1*, the ARF GAP *RPA* or the *PHOSPHATIDYLINOSTITOL MONOPHOSPHATE-5-KINASE 4* (*PIP5K4*) results in both, aberrant pollen tubes and root hairs (Schiefelbein et al., 1993; Song et al., 2006; Synek et al., 2006; Ischebeck et al., 2008; Sousa et al., 2008; Wada et al., 2015). In other cases genes important for polar tip growth in one cell type can have close homologs that serve an identical function in the other cell type. For example the Rab GTPase RabA4b is localized polar in root hairs and RabA4d in pollen tubes (Preuss et al., 2004; Szumlanski and Nielsen, 2009) and the AGC kinases AGC1.5 and AGC1.7 are important for directional growth of pollen tubes, whereas AGC1.6/RSH3 (for ROOT HAIR SPECIFIC 3) is acting specifically in root hairs (Won et al., 2009; Zhang and McCormick, 2009).

We have shown that in *Arabidopsis* two close homologs of *ARMADILLO REPEAT ONLY 1* (*ARO1)* are involved in the polar elongation of root hairs (Vogler et al., submitted, ***Chapter 3***). ARO proteins are conserved plant specific Armadillo Repeat Motif (ARM) proteins (Gebert et al., 2008). The *Arabidopsis* ARO protein family comprises four members among which ARO1, ARO2 and ARO3 exhibit relatively high similarities, whereas ARO4 is the most distant related family member (Gebert et al., 2008; Vogler et al., submitted). In contrast to *ARO1* that is expressed exclusively in gametophytes, *ARO2-ARO4* are expressed in almost all sporophytic parts of the plant but are excluded from pollen tubes (Gebert et al., 2008). The double homozygous knock-out of *ARO2* and *ARO3* leads to mutant root hairs with a phenotype comparable to that of *ARO1-*

deficient pollen tubes. The ectopic expression of ARO2 or ARO3 in *aro1-3*/+ mutant pollen, as well as vice versa the ectopic expression of ARO1 in *aro2 aro3* double mutant root hairs is able to restore wild-type morphologies, thereby proofing functional conservation and redundancy among ARO proteins. To our knowledge this represents the first report of functional complementation of pollen tube and root hair growth by both, ectopic expression of a gametophyte specific gene in mutant root hairs and ectopic expression of sporophyte specific genes in mutant pollen tubes. ARO functional redundancy even more emphasizes the close similarity between pollen tubes and root hairs.

1.4.4 External factors regulating pollen tube growth

Polar pollen tube growth depends on the concerted interplay between signaling components, cytoskeleton organization and polarized membrane trafficking, to which the ARO proteins functionally contribute. However, external components and cues are necessary to induce pollen germination and to support polar growth. In vitro germination of *Arabidopsis* pollen has been shown to be dependent on the presence and concentration of sucrose and Ca^{2+}, K^{+} and borate ions in the germination medium, as well as on the pH, temperature and the water availability (Brewbaker and Kwach, 1963; Li et al., 1999; Boavida and McCormick, 2007; Bou Daher et al., 2009; Yetisen et al., 2011). Organic molecules such as the polyamine spermidine, and flavonols like kaempferol also promote in vitro pollen germination in *Arabidopsis, Petunia* and *Nicotiana tabacum* (Mo et al., 1992; Ylstra et al., 1992; Taylor and Grotewold, 2005; Rodriguez-Enriquez et al., 2013). In pollen of *Torenia fournieri* and *N. tabacum*, germination was supported by the addition of plant hormones like the auxin analog indoleacetic acid (IAA) or gibberellic acid (GA3) (Chen and Zhao, 2008; Wu et al., 2008). However, adverse, no, or only weak promoting effects on in vitro pollen germination were shown for the plant hormones abscissic acid, ethylen and zeatin (Sfakiotakis et al., 1972; Wu et al., 2008).

For in vitro pollen germination, experimentally the most demanding is *Arabidopsis* pollen, due to high variances as a result of pollen quality (Boavida and McCormick, 2007; Rodriguez-Enriquez, 2013). By adding the brassinosteroid phytohormone epibrassinolide (epiBL) to germination media we were able to significantly enhance and stabilize *Arabidopsis* in vitro pollen germination in a dose-dependent manner (Vogler et al., 2014, ***Chapter 4***). Besides promoting pollen germination by nine fold, epiBL also significantly enhances in vitro *Arabidopsis* pollen tube elongation rates by almost five fold.

In vitro pollen tube growth rates are not only elevated by the plant hormones IAA, GA3 and epiBL (Wu et al., 2008) but furthermore by organic molecules such as gamma-aminobutyric acid (GABA) (Palanivelu et al., 2003), myo-inositol (Schneider et al., 2006), N-methanesulfinyl-azadecalins (Qin et al., 2011), by peptides such as the STYLE INTERACTOR FOR LEPRKS (STIL) (Wengier et al., 2010) or by proteins such as the stigma specific small cysteine-rich STIG1 proteins from *Nicotiana tabacum* or *Lycopersicon esculentum* (Goldmann et al., 1994; Tang et al.,

2004). All these growth-promoting substances were isolated from female flower tissues. For numerous species it was demonstrated that pollen tubes germinate with higher efficiency and grow significantly faster in vivo compared to in vitro (Hewitt et al., 1985; Johnson and Preuss, 2002; Lord and Russel, 2002; Quin et al., 2011). This observation is mainly attributed to the release of growth-promoting substances by the pistil in order to enhance reproductive success during double fertilization.

1.5 *Double Fertilization*

Double fertilization represents a hallmark of angiosperms and was discovered already in 1898 by Nawashin and in 1899 by Guignard (Nawashin, 1898; Guignard, 1899). Besides the embryo that gives rise to the next plant generation, a second, supernumerary embryo derived from a second fertilization event developed into an embryo-nourishing tissue, the endosperm (Friedman, 1998, 2001). The biological significance of double fertilization lies in the rapid and cost-effective seed production which has lead to the enormous evolutionary success of flowering plants nowadays. As reproductive success is closely linked to seed production, and as our daily nutrition is directly or indirectly depending on flowering plant yield, effective double fertilization also represents an important agronomical trait. Especially the genetically biparental embryo-nourishing endosperm, high in energy-rich compounds and therefore of high cost for the mother plant, importantly contributes to the human diet.

In flowering plants, immotile sperm cells are effectively transported by the pollen tube to the female gametophytic cells even under dry conditions (Hamamura et al., 2012; Dresselhaus and Franklin-Tong, 2013). Whereas in lower plants such as algae, mosses, or ferns water is essential for reproduction to allow motile sperm cells to target the female gametes, flowering plants have almost completely detached reproduction from the availability of exogenous water.

1.5.1 *Pollen-stigma interactions*

After its deposition on the papilla cells of a receptive stigma, pollen starts to rehydrate and becomes activated. Depending on the species, pollen deposition can be carried out passively by the wind, like in the grasses, or by pollinators such as insects. Whether or not a pollen grain is able to germinate on the papillae also depends on pollen-pistil interactions (Dresselhaus and Franklin-Tong, 2013). The Brassicaceae-type and Papaveracea-type self-incompatibilities (SIs) are genetically controlled by single polymorphic S-loci (Takayama and Isogai, 2005). Already after pollen deposition, the first checkpoint for intraspecific SI takes place, and in case that pollen and stigma share an identical S-haplotype, pollen is rejected at the hydration level. In *Brassica rapa* papillar cells, two highly polymorphic genes are specifically expressed, the *S RECEPTOR KINASE* (*SRK*) and the *S LOCUS GLYCOPROTEIN* (*SLG*) genes, and together they control stigma function in SI (Takasaki et al., 2000). The small cysteine-rich protein S LOCUS PROTEIN 11 SP11/SCR is

localized to the pollen coat and represents the male determinant for SI (Shiba et al., 2001). In case of self-recognition between pollen and papilla cell, a rejection-pathway is activated via the ARMADILLO REPEAT-CONTAINING 1 (ARC1) protein that functions as an E3 ubiquitin ligase (Gu et al., 1998). In *Brassica napus*, ARC1 interacts with Exo70A1, a component of the octameric exocyst complex that is known to be important for polarized secretion (Synek et al., 2006). The interaction between armadillo repeat (ARM) and Exo70 family protein members might function as a general regulation for polarized secretion, as we also identified an interaction between the ARM repeat protein ARO3 and the exocyst subunit protein Exo70E2 in polar growing root hairs (Vogler et al., submitted, ***Chapter 3***).

In case of successful hydration, pollen is activated upon contacting the papilla cells. External water, Ca^{2+}, GABA and small molecules such as D-serine provide cues and gradients for polarity establishment and directional pollen tube growth (reviewed in Bleckmann et al., 2014). The external water gradient in turn is regulated by lipids and directs the water flow along the 'foot' and thus guides pollen tube growth (Wolters-Arts et al., 1998). In *Arabidopsis* and *Brassica rapa*, in both, the activated pollen grain and the papilla cell, internal Ca^{2+}-gradients towards the contact site are established (Iwano et al., 2004; Iwano et al., 2014). Ca^{2+} furthermore plays an important role during pollen activation, as it is exported from the papilla cell to the pollen grain at the contact site, likely via the CA^{2+}-ATPASE 13 (ACA13) that upon contact is polar localized at the papilla cell plasma membrane and in the endomembrane system (Iwano et al., 2014). The paramount role of extracellular Ca^{2+} ions for pollen germination and of intracellular Ca^{2+} ions to orchestrate polarity signaling has already been described in numerous examples (Brewbaker and Kwach, 1963; Bou Daher et al., 2009; Yang, 2008; Guan et al., 2013; Chen and Friml, 2014).

1.5.2 Pollen tube growth along the transmitting tract

After pollen germination on the stigma, the polar tip-growing pollen tubes grow along the papilla cells and enter the extracellular matrix (ECM) of the stylus (**Figure 1.9**). The tip-localized vesicle-rich clear zone of pollen tubes is highly active in secretion (Hepler and Winship, 2015). The secretion of arabinogalactan and extension-like proteins, as well as of cell wall modifiying enzymes such as pectin methylesterase inhibitors and polygalacturonases likely modifies the ECM and facilitates penetration of the stylus (reviewed in Bleckmann et al., 2014). The *Arabidopsis* style is only very short in relation to the entire pistil and is closed, in contrast to the hollow style in for example lily (Crawford and Yanofsky, 2008).

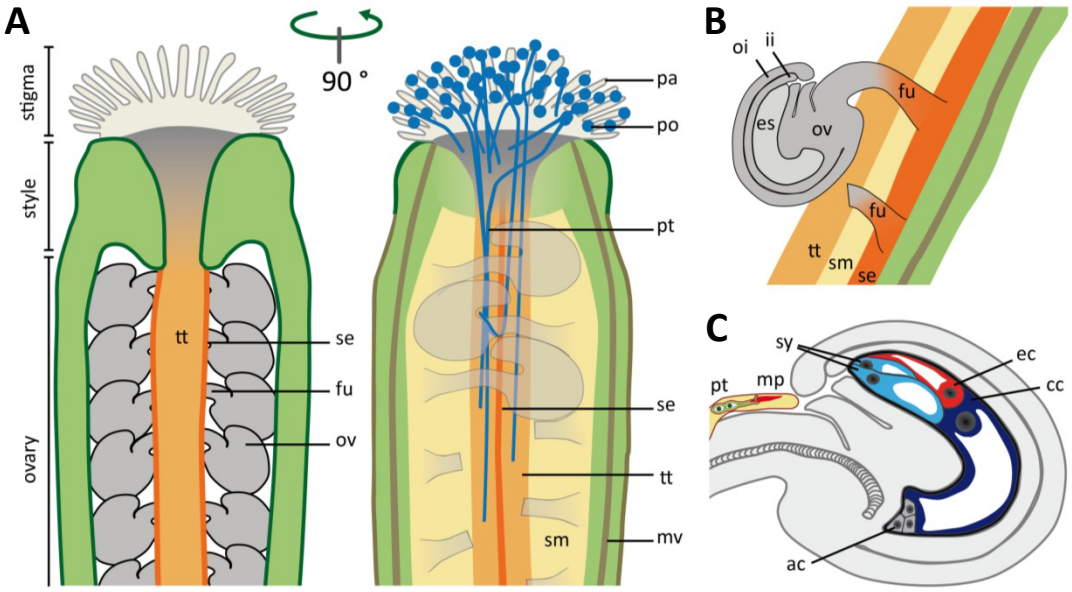

Figure 1.9 | Organization of the *Arabidopsis* pistil and ovule.

(A) Schematic representation of the *Arabidopsis* pistil. Pollen (po) germinates on papillar cells (pa) of the stigma and pollen tubes (pt) elongate through the style, transmitting tract (tt), septum epidermis (se) along the funiculus (fu) to the ovary (ov). **(B)** The ovule is connected to the septum (sm) by the funiculus and harbors the female gametophyte, the so called embryo sac (es) that is surrounded by an outer and an inner integument (oi, ii). **(C)** At the funicular end, the integuments form a small opening, the micropyle (mp) by which pollen tubes enter during fertilization. The embryo sac is comprised of two synergid cells (sy), one egg (ec) and central cell (cc) and three antipodal cells (ac). Figure modified from Sprunck et al., 2014 and Vogler et al., 2014.

Pollen tubes grown through the style enter the transmitting tract, a specialized and in *Arabidopsis* intercellular-rich tissue that serves as a highway for pollen tube growth by means of its morphology and by secretion of growth-influencing substances (Lennon et al., 1998; Crawford and Yanofsky, 2008). Thus, the transmitting tract plays an important role in regulating double fertilization. Mutants defective in proper transmitting tract organization exhibit reduced fertility and reduced in vivo pollen tube growth rates (Crawford et al., 2007; Smith et al., 2013). In the Solanaceae-type SI, rejection of self-pollen occurs in the transmitting tract and is mediated by the S-RNase genes (reviewed in Takayama and Isogai, 2005). S-RNases are incorporated into the growing pollen tubes and only in case of non-matching haplotypes degraded by an E3-ubiquitin ligase complex. In self-pollen, this leads to a non-degradation of S-RNases and thus to a degradation of RNAs which in turn leads to pollen tube growth cessation. Furthermore, the transmitting tract serves as an interspecific fertilization barrier as shown for tobacco (Smith et al., 2013). However mainly, the transmitting tract functions by pollen tube growth promotion. In lily and tobacco, the small secreted cell wall peptide chemocyanin and the TRANSMITTING TRACT SPECIFIC (TTS) arabinogalactan proteins have shown pollen tube growth-enhancing activities (Cheung et al., 1995; Wu et al., 1995; Kim et al., 2003). Interestingly, the TTS proteins are not glycosylated equally along the transmitting tract, but show a gradient of increasing glycosylation that could direct pollen tube growth (Wu et al., 1995). The lipid transfer protein SCA (for STIGMA/STYLE

CYSTEINE-RICH ADHESION) is secreted from the transmitting tract and supports pollen tube growth (Chae and Lord, 2011). Generally, in the transmitting tract a high number of genes encoding secreted proteins or proteins that modify the ECM are expressed in *Arabidopsis* (Tung et al., 2005). For example the small CLE45 peptide was shown to stimulate pollen tube growth and its expression is induced in heat-stressed *Arabidopsis* transmitting tracts (Endo et al., 2013). Ca^{2+} ions could also play a role in promoting pollen tube growth in the transmitting tract. In lily, pollination induces a significant Ca^{2+}-increase in the ECM and energy-dispersive X-ray microanalysis proofed the presence of Ca^{2+} ions also in the cell wall of pollen tubes growing through the transmitting tract (Zhao et al., 2004). Furthermore the rare amino acid D-serine plays a role in pollen tube growth by activating glutamate receptors in the pollen tube apex that facilitate Ca^{2+} influx (Michard et al., 2011). Notably, in *Arabidopsis* the enzyme responsible for conversion of L-serine to D-serine, SERINE RACEMASE 1 (SR1), is highly expressed in the style, transmitting tract and ovules.

The amount of the free plant hormones IAA and GA3 was found to increase after pollination in the part of the pistil harboring the transmitting tract (Wu et al., 2008). Our work indicates that also brassinosteroids promote pollen tube growth in the transmitting tract in *Arabidopsis* (Vogler et al., 2014, ***Chapter 4***). The promotor of one of the the key enzyme in brassinosteroid-biosynthesis, the *CYTOCHROME P450 MONOOXYGENASE CYP90A1/CPD*, is highly expressed along the pollen tube track in the pistil. Furthermore, in vivo pollen tube growth is significantly reduced in a *cyp90a1/cpd* mutant.

Besides regulating pollen tube growth, there is increasing evidence that the passage through the female pistil tissues renders pollen tubes competent for fertilization. Pollen tubes that grew through the *Arabidopsis* stigma and style in a semi-in vivo fertilization setup show a much larger set of expressed genes compared to those that were grown in vitro on germination medium (Qin et al., 2009; Palanivelu and Johnson, 2010), indicating pollen tube-pistil interactions that could function in activating genes for pollen tube maturation. Growing through the pistil induces the expression of three closely related Myb transcription factors, *Myb97*, *Myb101* and *Myb120* (Leydon et al., 2013, 2014) and pollen tubes defective in these *Myb* genes fail to stop their growth once reaching the female gametophyte without being able to release sperm cells for double fertilization. Transporters, carbohydrate-active enzymes and small peptides are under control of these Myb transcription factors that likely mediate pollen tube maturation. Besides transcriptomics and mutant analysis data, another line of evidences comes from in vitro experiments that show that *Arabidopsis* and *T. fournieri* pollen tubes are able to fully respond to certain attractants only after they have passed through parts of the pistil (Higashiyama et al., 1998; Palanivelu and Preuss, 2006). In *T. fournieri,* immunostainings revealed that the pollen tube attracting small cysteine-rich LURE peptides (Okuda et al., 2009) do not bind to pollen tubes that were grown in vitro, but to pollen tubes that initially grew through an approximate 15 mm piece of the pistil, sufficient to confer fertilization competency to the pollen tubes (Okuda et al., 2013). Required for the

response to the LURE peptides is a pair of membrane-associated receptor-like cytoplasmic kinases, namely LOST IN POLLEN TUBE GUIDANCE, LIP1 and LIP2 (Liu et al., 2013). Comparably to the above mentioned *Myb* genes, their expression is induced in pollen tubes by their passage through the pistil.

1.5.3 Ovular pollen tube guidance

Ovule-derived attractants trigger the pollen tubes to exit the transmitting tract and to continue their growth along the septum epidermis towards the funiculus and the ovule containing the female gametophyte (**Figure 1.9**). In *Arabidopsis* and *T. Fournieri* it was demonstrated that pollen tubes preferentially exit the transmitting tract at the upper part of the ovary (Hulskamp et al., 1995; Higashiyama and Takeuchi, 2015). This tendency is lost in mutants that are defective in ovule and female gametophyte development, indicating the importance of the ovule for pollen tube guidance. In general, female tissue-induced pollen tube growth stimulation can be subdivided in preovular guidance, which starts at the stigma and ranges to the transmitting tract, and ovular and micropylar pollen tube guidance that occurs after pollen tubes have exited the transmitting tract. Morphologically, the entity of stigma, style, transmitting tract and funiculus is also referred to as reproductive tract, comprising all female tissues that are passed by the pollen tubes (Crawford and Yanofsky, 2008). In *Arabidopsis,* ovular guidance of pollen tubes from the septum epidermis along the funiculus to the micropyle is mediated on the female side by amino acids such as D-serine, and a gradient of GABA (reviewed in Takeuchi and Higashiyama, 2011; Bleckmann et al., 2014). On the male side, the ER-localized potassium transporters CHX21 and CHX23 (for CATION HYDROGEN EXCHANGERS) are important factors as they regulate the ability of the pollen tube to respond to ovular attractants (Lu et al., 2011). The homeostasis of K^+ ions is likely important for pollen tube orientation and involved in the regulation of the pollen tube Ca^{2+} and pH gradient (reviewed in Higashiyama and Takeuchi, 2015). Also the link between the cytoplasmic Ca^{2+} levels and D-serine via GLUTAMATE RECEPTOR-LIKE (GLR) channels has already been established (reviewed in Bleckmann et al., 2014). Given that cytoplasmic Ca^{2+} oscillations are crucial for polarity signaling and polar growth in pollen tubes (Steinhorst and Kudla, 2013), and that Ca^{2+}-levels in pollen tubes increase when growing towards the embryo sac (Iwano et al., 2012), the spatiotemporal regulation of intracellular Ca^{2+}-levels appear to be essential in ovular pollen tube attraction. The pollen tube ER-localized POLLEN DEFECTIVE IN GUIDANCE 1 (POD1) protein is also required for attraction competency and *pod1* mutant pollen tubes fail to target the female gametophyte (Li et al., 2011). As POD1 interacts with the Ca^{2+}-binding ER chaperon CALRETICULIN 3 (CRT3), this furthermore emphasizes the significance of Ca^{2+} homeostasis for proper pollen tube attraction in ovular guidance. In the plasma membrane at the tip of the growing pollen tube, the GPI-anchored COBRA-LIKE 10 (COBL10) protein is located and regulates cell wall component deposition (Li et al., 2013). Mutants defective in COBL10 show male sterility and compromised directional sensing of female attractants. Pollen

tube morphology and guidance in vivo is also altered in the above mentioned LIP receptor-like cytoplasmic kinase mutants that also predominantly localize to the tip of the pollen tube beneath the plasma membrane and which are necessary for LURE peptide guidance control (Liu et al., 2013). Abnormal ovule targeting was also observed in the actin filament-severing mutants MICROTUBULE-ASSOCIATED PROTEIN 18 (MAP18)(Zhu et al., 2013) and MICROTUBULE-DESTABILIZING PROTEIN 25 (MDP25) (Quin et al., 2014). The knock-out of two mitogen-activated protein kinases, MPK3 and MPK6 also leads to hampered ovular pollen tube attraction (Guan et al., 2014). Taken together, ovular pollen tube guidance requires female components such as D-serine and GABA to induce ovular targeting in pollen tubes via MAP kinase signaling, ionic homeostasis and actin cytoskeleton regulation.

1.5.4 Micropylar pollen tube guidance

In the last step of pollen tube guidance, pollen tubes are finally directed into the ovule at the micropyle, a small opening formed by the two ovule-enlacing integuments, until they get in contact with the synergid cells of the female gametophyte. At their micropylar end, the synergid cells harbor a specialized structure, the plasma membrane indentation-rich filiform apparatus (Drews and Koltunow, 2011).

The synergid cells are the 'hotspot' for the active secretion of ovular pollen tube attractants (reviewed in Higashiyama and Takeuchi, 2015). A master-regulator of filiform apparatus formation and attractant production is the predominantly synergid-expressed MYB-transcription factor Myb98 (Kasahara et al., 2005; Punwani et al., 2007). Not surprisingly, *myb98* mutants are not able to properly attract pollen tubes. Also small proteins play an important role in micropylar guidance. In *Arabidopsis* and *T. fournieri*, the above mentioned defensin-like cysteine-rich LURE proteins serve as micropylar pollen tube attractants (Okuda et al., 2009; Takeuchi and Higashiyama, 2012). In *Zea mays*, the EGG APPARATUS 1 (EA1) protein that is expressed only in the egg apparatus that is comprised of the synergid cells and the egg cell, mediates micropylar pollen tube attraction (Márton et al., 2005). The knock-down of EA1 results in omitted fertilization and seed production. However, pollen tube attraction is not only conveyed by the synergid cells. As mutant analysis revealed, the egg cell and the central cell also produce pollen tube attractants that mediate micropylar guidance (Chen et al., 2007; Alandete-Saez et al., 2008; Shimizu et al., 2008).

1.5.5 Pollen tube growth termination and gamete interaction

Once the pollen tubes have reached the synergid cells their growth is terminated, extensive cell-cell communication occurs and subsequently pollen tubes burst to release their sperm cell cargo for double fertilization. Pollen tube growth termination and burst is regulated by both, the synergid cell and the pollen tube. In *Arabidopsis*, pollen tube growth termination control by the

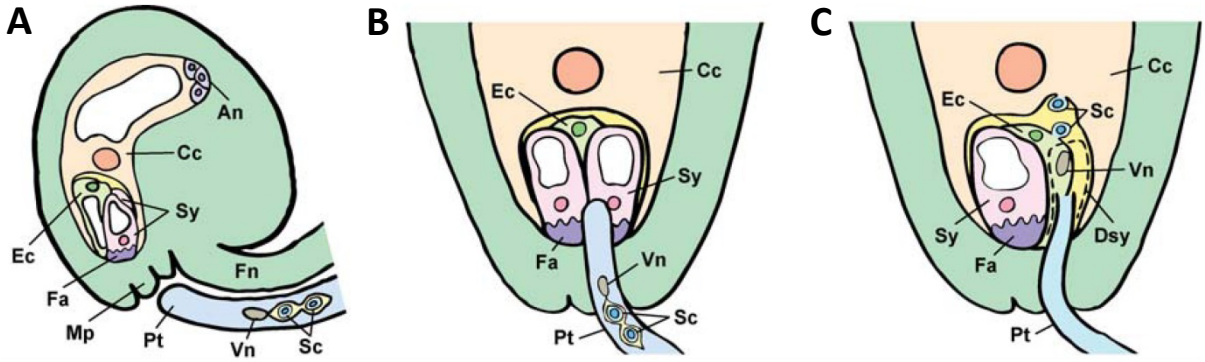

Figure 1.10 | Schematic representation of the double fertilization process in *Arabidopsis thaliana*.

(A) The pollen tube (Pt) containing the male germ unit consisting of the vegetative nucleus (Vn) and the sperm cells (Sc) is guided to the micropylar opening (Mp) of the ovule by attractants that are secreted from the synergid cells at the filiform apparatus (Fa). The female gametophyte comprises two synergid cells (Sy), one egg and central cell (Ec and Cc) and three antipodal cells (An). **(B)** After pollen tube and synergid cell-cell communication, pollen tube growth arrests and the male germ unit is discharged. **(C)** The receptive synergid degenerates (Dsy, dotted line) and the sperm cells are pushed in the cleft between the egg and central cell. One of the sperm cells fuses with the egg cell to form the zygote, and the other sperm cell fuses with the central cell to form the endosperm. Figure modified from Kawashima and Berger, 2011.

synergid cells involves the receptor-like kinase FERONIA/SIRÈNE (FER/SIR), the GPI-anchored protein LORELEI (LRE) and the Mildew Resistance Locus O family protein NORTIA (NTA). Their mutants show pollen tube overgrowth at the micropylar part of the ovule and are defective in pollen tube burst (Huck et al., 2003; Capron et al., 2008; Kessler et al., 2010). On the male side, an almost identical synergid-overgrowth phenotype is observed in a triple knock-out mutant of the pollen-expressed MYB transcription factors *Myb97, Myb101* and *Myb120* (Liang et al., 2013). Furthermore it was demonstrated that the male expressed receptor-like kinases ANXUR 1 and 2 (ANX1, ANX2) are important for preventing pollen tube burst before arrival at the synergid cells (Boisson-Dernier et al., 2009; Miyazaki et al., 2009). Interestingly, ANX1 and ANX2 are closely related to FER. Likely, ANX1 and ANX2 function by preventing pollen tubes from bursting until they receive a deactivating trigger from the synergid cells (Kessler and Grossniklaus, 2011). Pollen tube burst also seems to be regulated by Ca^{2+}, as ovules defective in the AUTOINHIBITED CA^{2+}-ATPASE 9 (ACA9) attract pollen tubes but they are not able to burst and fertilize (Schiøtt et al., 2004). In *Z. mays*, pollen tube burst is regulated by the interplay between the female gametophyte-specific expressed ZmES4 (for *ZEA MAYS* EMBRYO SAC) defensin-like cysteine-riche peptide and its target on pollen tubes, the potassium transporter KZM1 (Amien et al., 2010). Upon ZmES4 application, KZM1 is activated which leads to K^+ and likely passive water influx and thus pollen tube burst.

Before pollen tube burst and sperm cell discharge, cell-cell communication between the synergid and the pollen tube takes place. We were able to show that physical contact of the pollen tube apex induces Ca^{2+} oscillation in the synergid cells (Denninger et al., 2014, ***Chapter 5***). Intracellu-

lar Ca^{2+} levels increase in the synergid that contacts the pollen tube in close proximity to the contact site. Pollen tube burst is marked by a short Ca^{2+} increase in the degenerating synergid.

During fertilization the pollen tube bursts at its tip, the receptive synergid degenerates and the two immobile sperm cells are as a pair, likely by the explosive forces of the pollen tube rupture, pushed inside the female gametophyte. In *Arabidopsis*, the *Polygonum*-type female gametophyte (**Figure 1.7**) consist of two haploid synergid cells and one haploid egg cell, that together form the egg apparatus, of the diploid central cell, and three haploid antipodal cells (Drews and Yadegari, 2002). After positioning of the released sperm cell pair in the cleft between the egg and the central cell, one of the sperm cells fuses with the egg cell to form the diploid zygote, and the other with the central cell to form the triploid embryo-nourishing endosperm tissue (Berger et al., 2008) (**Figure 1.10**). Live-cell imaging revealed that in *Arabidopsis*, sperm cells are not predetermined and show the same capability to fuse with either the egg or the central cell (Hamamura et al., 2011).

The transmembrane protein GAMETE EXPRESSED 2 (GEX2) is necessary for the adhesion of the sperm cells to the female gametes (Mori et al., 2014). GEX2 is localized to the plasma membrane and, similar to interaction factors in mammals and algae, contains extracellular immunoglobolin-like domains (Misamore et al., 2003; Inoue et al., 2005). Sperm cells of the *GENERATIVE CELL SPECIFIC 1* / *HAPLESS 2* (*gcs/hap2*) mutant are able to adhere to the female gametes but do not proceed to fusion (Johnson et al., 2004; Mori et al., 2006). GCS1/HAP2 homologue genes are present in many eukaryotes and have proven to be required in gamete fusion also in protozoans and algae (reviewed in Wong and Johnson, 2010).

We showed that after sperm cell release and prior to gamete fusion, the egg cell starts to secrete the small cysteine-rich EGG CELL 1 (EC1) protein that in unfertilized ovules is localized to storage vesicles in the egg cell and is released during fertilization (Sprunck et al., 2012, ***Chapter 6***). In vitro, EC1 peptides are able to activate the redistribution of GCS1/HAP2 in sperm cells from the endomembrane system to the plasma membrane. A quintuple knock-down of the whole *EC1* gene family leads to reduced fertility and a significantly higher amount of unfertilized sperm cells in the female gametophyte. Also cytosolic Ca^{2+} signaling plays a role in sperm cell fusion. During the fertilization process, the egg cell shows two distinct intracellular Ca^{2+} maxima (Denninger et al., 2014, ***Chapter 5***). The first is synchronous with the central cell and occurs when the pollen tube bursts and the sperm cells are released into the embryo sac, and the second appears shortly before gamete fusion. Our data suggest that distinct intracellular Ca^{2+} ion signatures are of paramount importance as second messengers during pollen tube and synergid interaction as well as during gamete fusion. Besides EC1, no other female component required for gamete fusion in higher plants is known so far. In mammals, the TETRASPANIN (TET) membrane proteins are involved in fertilization (Primakoff and Myles, 2007). In *Arabidopsis*, TET11 and TET12 are localized to the sperm cell membranes and are highly enriched at the contact site of the sperm cells in

the sperm cell pair (Boavida et al., 2013). Interestingly, TET9 localizes to the plasma membranes of the female gametes. However, so far the function of these proteins is not known.

In the past few years our knowledge has significantly increased on how fertilization is efficiently regulated by means of blocking multiple sperm cell entry and the reuptake of pollen tube attraction in case of unsuccessful fertilization in *Arabidopsis*. Different to mammalian systems, in flowering plants the control of single gamete fusion events can take place at two steps, that is the attraction of pollen tubes and the prevention of multiple gamete fusion events. We could show that characteristic Ca^{2+} signatures follow sperm cell fusion with the egg cell (Denninger et al., 2014, ***Chapter 5***), probably providing a rapid block of polyspermy. Gamete fusion is a critical step to block multiple pollen tube attraction by the ovule, a phenomenon called polytubey (Beale et al., 2012) or polysiphonogamy (Kasahara et al., 2012). If a *gcs1/hap2* fusion-defective mutant sperm cell pair is delivered to the female gametes, further pollen tube attraction is initiated resulting in the deposition of at least one additional sperm cell pair (Beale et al., 2012; Kasahara et al., 2012). In the *gcs1/hap2* mutant ovules, after fertilization LURE peptides continue to exist, whereas in normal ovules they cease after successful fertilization (Higashiyama and Takeuchi, 2015). After the first pollen tube delivering *gcs1/hap2* sperm cells has burst and its receptive synergid has degenerated, the remaining synergid is able to reuptake the pollen tube attraction. Its intracellular Ca^{2+} signatures then resemble those of the first synergid (Ngo et al., 2014). The synergid cells therefore are essential signalers in regulating pollen tube attraction depending on the fertilization state of the female gametes. Gametophytes often are entered by multiple pollen tubes in synergid-defective mutants such as *MAGATAMA, MYB98* or *CENTRAL CELL GUIDANCE* (Shimizu and Okada, 2000; Kasahara et al., 2005; Chen et al., 2007). Interestingly, the polyspermy block is only present in the egg cell and not in the central cell as indicated by the *TETRASPORE* (*tes*) mutant (Scott et al., 2008). Pollen of the *tes* mutant produces up to four sperm cell pairs. However, whereas fusion of multiple sperm cells with the central cell was observed, leading to higher-ploidy endosperm, only single sperm cell fusion events with the egg cell and resulting diploid embryos were observed.

After successful pollen tube attraction, pollen tube burst, competent sperm cell delivery and gamete fusion, the embryo and the endosperm are formed and develop into the seed, which after dispersal marks the beginning of a new life cycle. However, the orchestrated spatiotemporal regulation of pollen polarization and germination, pollen tube tip-growth along the female tissues, pollen tube/synergid and sperm cell/egg cell communication as well as the triggered secretion of egg cell-derived proteins are essential key steps in fertilization and ultimately in the formation of the seed.

1.6 Aims of the Work

The following thesis intends to contribute to our understanding of the cell biological, genetic and molecular basis of pollen polarization and polar cell growth, of cell-cell communication events between male and female gametophytes and gametes, and of factors involved in the regulation of double fertilization.

Our knowledge on pre-germination cell polarization events in pollen is scarce, especially in *Arabidopsis*, the flagship of basic molecular plant research. In ***Chapter 2***, a methodological and knowledge framework is provided on *Arabidopsis* pollen polarization and early pollen tube formation based on quantitative live cell imaging. Morphology changes and growth kinetics of the emerging pollen tubes were assessed as well as the polarization of vesicles and the F-actin cytoskeleton. Furthermore, the precise timing of the male germ unit transport into the extending pollen tube was also quantitatively measured. The results of this chapter have been recently published in *Frontiers in Plant Science* (Vogler et al., 2015).

After pollen germination, the pollen tube elongates by polar tip growth. In our group it was discovered that the gametophyte-expressed ARMDILLO REPEAT ONLY 1 (ARO1) protein is required for pollen tube growth and male fertility (Gebert et al., 2008). However, *ARO1* belongs to a gene family with four members (*ARO1-4*) and the expression pattern and biological function of the other ARO family members was investigated in this thesis. In ***Chapter 3***, the effect of multiple *aro* knock-outs on polar tip growth of root hairs is demonstrated. Furthermore, functional redundancy and conservation among ARO proteins, their cell biological properties, as well as the identification of ARO protein interaction partners is experimentally addressed. The obtained data were submitted for publication (Vogler et al., submitted).

It is a broadly known phenomenon that pollen germination and tube growth is much more efficient in pistils compared to the in vitro situation due to female-produced growth-promoting substances. The elongation-promoting effect of the plant hormone epi-brassinolide is characterized on in vitro germinated pollen tubes in ***Chapter 4***. By using a brassinosteroid-synthesis and perception mutant we also showed that brassinosteroids stimulate pollen tube growth inside the pistil. This work was published in *Plant Reproduction* (Vogler et al., 2014).

The second messenger Ca^{2+} is a crucial component in many signaling processes. As the above mentioned synergid mutant phenotypes suggest, intensive cell-cell communication between the pollen tube and the synergid cells must take place prior to pollen tube burst and sperm cell discharge. ***Chapter 5*** describes intracellular Ca^{2+} changes in synergid and egg cells during pollen tube arrival, burst and sperm cell release, using ratiometric Förster Resonance Energy Transfer (FRET) live cell imaging. These results were published in *Nature Communications* (Denninger et al., 2014).

After pollen tube burst and sperm cell release, two gamete fusions take place mediated by male and female gametic factors. Homology searches, based on a *Triticum aestivum* egg cell tran-

scriptomics approach that was performed in our group (Sprunck et al., 2005), identified an egg cell specific cysteine-rich protein gene family in *Arabidopsis*. In ***Chapter 6***, genetic and functional analyses of the *EGG CELL 1* (*EC1*) gene family is provided, revealing that secretion of EC1 proteins by the egg cell is essential for the sperm cells to be able to rapidly fuse with the female gametes. We also investigated the effect of EC1 peptides on isolated sperm cells, indicating that sperm cells gain fusion competence by EC1 proteins. The data presented in this chapter were published in *Science* (Sprunck et al., 2012).

CHAPTER 2 *Knockin' on Pollen's Door: Live Cell Imaging of Early Polarization Events in Germinating* Arabidopsis *Pollen*

This chapter was published in *Frontiers in Plant Science* (Vogler et al., 2015) as part of the research topic 'Molecular and Cellular Plant Reproduction'. The experiments were designed by Frank Vogler and Stefanie Sprunck. F.V. performed all the molecular cloning and the generation of transgenic lines. F.V. developed the live cell imaging techniques for germinating *Arabidopsis* pollen and conducted the live cell imaging. Quantitative image analysis, all other analysis and statistical evaluations, and the morphological modeling of pollen tube growth was designed and evaluated by F.V.. TIRF microscopy with *Arabidopsis* pollen tubes was performed together with Sebastian Konrad in collaboration at the LMU Munich. All figures and movies were prepared by F.V. who also wrote the manuscript with input from and proof reading by S.K. and S.S..

2.1 *Introduction*

The pollen tube (PT) of flowering plants is formed by the pollen grain vegetative cell and represents a cell of enormous specialization, responsible for the transport of the two male gametes through the female tissues of the pistil to the ovule. It is the fastest elongating plant cell (Sanati Nezhad et al., 2014) and can reach lengths of 30 cm, with growth rates up to 1 cm/h (Mascarenhas, 1993). PT growth is monotropic by expansion at an annular region located at the tip in a process called polar tip growth (Taylor and Hepler, 1997; Geitmann, 2010).

Deeply embedded in the tissues of the pistil, in vivo PT growth is difficult to investigate with high temporal and spatial resolution and has been achieved so far only by using two-photon microscopy (Feijó and Moreno, 2004; Cheung et al., 2010). As an advantageous alternative, pollen can be germinated in vitro to study the cellular dynamics and complex signaling pathways that coordinate polar tip growth (Qin and Yang, 2011). From these studies we know that intensive exo- and endocytosis at the tip supported by regulated vesicle trafficking and cytoskeleton dynamics, as well as coordinated changes in cell wall properties are essential cellular activities of the growing pollen tube (for review see Geitmann, 2010; Guan et al., 2013). Great advances have been made during the past years in identifying key signaling molecules for the proper elongation of the pollen tube tip, such as Rho GTPases, calcium ions, and phosphoinositides (for review see Cheung and Wu, 2008; Qin and Yang, 2011; Steinhorst and Kudla, 2013). These key regulators are components of distinct signaling pathways forming a complex network that controls the cellular activities of tip-growing pollen tubes (Guan et al., 2013). However, there are still significant gaps in our knowledge of pollen tube growth regulation, especially with regard to the question

when and how symmetry breaking in the apparently unpolar pollen vegetative cell occurs, and what the molecular mechanism for selecting the growth site is.

Polar tip growth of PTs is very similar to the polar elongation of root hairs on genetic and mechanistic levels (reviewed in Šamaj et al., 2006; Campanoni and Blatt, 2007; Kost, 2008; Lee and Yang, 2008). Root hair growth is known as a multi-phasic process, consisting of cell fate determination, the formation of a root hair bulge, and the initiation of tip growth in the root hair bulge, each of which is characterized by distinct physiological and mutant phenotypes in the model plant *Arabidopsis* (Schiefelbein and Somerville, 1990; Parker et al., 2000; Schiefelbein, 2000; Bibikova and Gilroy, 2003; Müller and Schmidt, 2004). Since pollen germination and the initiation of pollen tube tip growth is rapid and much faster than root hair growth, it is technically more demanding to perform live cell imaging in order to study the cellular dynamics and the growth kinetics during pollen hydration, activation, germination and pollen tube formation. Moreover, in vitro germination rates and growth dynamics of *Arabidopsis* pollen are known to be highly variable (Johnson-Brousseau and McCormick, 2004; Boavida and McCormick, 2007), complicating its use for cellular and molecular genetic studies of pollen germination and growth. However, methodological advances in germination techniques meanwhile facilitated the experimental use of *Arabidopsis* pollen (Bou Daher et al., 2009; Rodriguez-Enriquez et al., 2013; Vogler et al., 2014), offering possibilities to establish methods for larger-scale screening and quantitative phenotyping of wild-type and mutant pollen.

To optimize high throughput time-lapse live imaging of germinating *Arabidopsis* pollen, we established an inexpensive and easy mounting technique suitable for every standard microscope, based on an improved pollen germination medium (Vogler et al., 2014). Using this setup for Spinning Disc confocal microscopy we investigated the growth kinetics and morphology changes of *Arabidopsis* PTs expressing GFP in the cytoplasm of the vegetative pollen cell. We focused on early cell polarization events during pollen activation and germination by studying the spatiotemporal localization of GFP-labeled ARMADILLO REPEAT ONLY 1 (ARO1), which is known to be essential for polar pollen tube growth (Gebert et al., 2008). ARO1-GFP accumulates in the inverted cone-shaped region of growing PT tips in a Brefeldin A and Latrunculin B sensitive manner and TIRF microscopy, applied in this study, confirmed that ARO1-GFP localizes vesicle-associated at the pollen tube tip.

We used *Arabidopsis* marker lines expressing ARO1-GFP and tagRFP-T-Lifeact in the pollen to study vesicle and filamentous actin (F-actin) dynamics before and during pollen germination. Furthermore, we used a pollen marker line with fluorescently labeled sperm cell nuclei and plasma membranes (Sprunck et al., 2012) to address the question when the two sperm cells, physically linked to the nucleus of the vegetative cell forming a male germ unit (MGU) (McCue et al., 2011; Zhou and Meier, 2014), are transported from the pollen grain into the germinated PT.

Our time-lapse live imaging of germinating *Arabidopsis* pollen tubes revealed similarities between root hair formation and pollen germination as we observed successive phases of cell polarization,

bulge formation, growth site selection and the initiation of rapid tip growth. Prior to pollen germination, we observed a characteristic polarization of vesicle-associated ARO1-GFP and tagRFP-T-Lifeact labeled F-actin in the pollen grain. After bulging, a transition phase is observed where vesicle-associated ARO1-GFP heavily accumulates at the distal end of the bulge and adopts an inverted cone-like shape before the pollen tube switches to rapid tip growth. At the same time, long F-actin cables appear, extending in parallel orientation from within the pollen grain into the pollen tube, while the volume of the vacuole, arising opposite the germination site, increases. During the phase of rapid tip growth, F-actin bundles massively accumulate at the germination site and increasing vacuolization occurs, followed by sperm cell transport into the PT.

2.2 Material and Methods

2.2.1 Plant material

Arabidopsis thaliana (accession Col-0) plants were grown under long-day conditions (16 h light, 20 °C, 70 % humidity) in growth chambers after seeds were subjected to stratification 2 days at 4 °C in the dark. Homozygous lines carrying the P_{Lat52}*:GFP* transgene were used to express cytoplasmic GFP in the vegetative PT cell (Twell et al., 1990). A C-terminal GFP fusion of the ARO1 protein under control of its endogenous promoter (Gebert et al., 2008) was used to investigate its subcellular localization in pollen and PTs. A double homozygous marker for P_{HTR10}*:HTR10-RFP* and P_{HTR10}*:TET9-GFP* line (Sprunck et al., 2012) was used to visualize sperm cell nuclei and sperm cell plasma membranes.

2.2.2 Molecular cloning and generation of transgenic lines

A double stranded DNA fragment encoding for a 17 aa actin binding domain termed Lifeact (Riedl et al., 2008) with additional 5' and 3' *Hind*III restriction sites was synthesized by proof-reading PCR on the partially overlapping template oligonucleotides 5'-GGGGCCATG-GAAGCTTTGGGACCAGCCGTAGGAATGGGTGTTGCTGATCTTATTAAGAAGTTC-GAGTCTATTTCTAAGGAGG-3' and 5'-GGGGAAGCTTATGCCATGGCTCCAGCTAC-AGGTGCTCCCGCCCCTCCTTCCTCCTTAGAAATAGACTCGAACTTCTTAA-3' with the PCR primers Lifeact-fwd (5'-GGGGCCATGGAAGCTTTGG-3') and Lifeact-rev (5'-GGG-GAAGCTTATGCCATGGC-3'). After *Hind*III digestion, the PCR product was ligated behind the fluorophore coding sequence into the modified Gateway destination vector pENTR-tagRFP-T (Denninger et al., 2014) to obtain pENTR-tagRFP-T-Lifeact. To achieve expression in pollen, 712 bp of the *ARO1* promoter with additional 5' *Sac*I and 3' *Spe*I sites were amplified from the 95P-Nos-ARO1p:ARO1-GFP plasmid (Gebert et al., 2008) with the primers pARO1-II-for (5'-TCGGGTACCGAGCTCAGATCTAAGCTG-3') and pARO1-II-rev (5'-TGTCGACGC-GGCCGCACTAGTCAGATC-3'). The *35S* promoter of the binary gateway expression vector pB2GW7 (Karimi et al., 2002) was replaced by the *ARO1* promoter via *Sac*I/*Spe*I to obtain

pB2GW7-ARO1p. Gateway LR reaction with pENTR-tagRFP-T-Lifeact and pB2GW7-ARO1p was performed according to the manufacturer's recommendations (Life Technologies) to obtain the expression vector pARO1:tagRFP-T-Lifeact that was used for Agrobacterium-mediated plant transformation by floral dip method (Clough and Bent, 1998).

2.2.3 Pollen mounting and live cell imaging

Micro-germination slides were prepared in either a single-well or a multi-well setup (**Figures S2.1** and **S2.2**). To prepare a single-well micro-germination slide, a 1-2 mm high planar plasticine layer was added on the margin of the ring of a slide with an attached glass ring (L4246, PLANO, Wetzlar, Germany). The well was filled with molten pollen germination medium (PGM) according to Vogler et al. (2014), containing 10 µM 24-epibrassinolide (epiBL, Sigma-Aldrich E-1641) and solidified with 0.5 % low melting point agarose. After solidification the center of the well was hand pollinated using single dehiscent anthers, manually removed from flowers at flower stage 13-14 (according to Smyth et al., 1990). The well was then sealed by gently pressing evenly a 24 x 24 mm No. 1.5 cover slip onto the plasticine until it slightly touched the PGM. The illustrated instruction on how to prepare a single-well micro-germination slide is shown in **Figure S2.1**.

Multi-well micro-germination slides were prepared by attaching a 12 well silicon profile (flexiPERM® micro12, SARSTEDT, Germany) to a standard microscope slide (26 x 76 mm) and filling each well with 50 - 75 µL molten PGM. After solidification, the silicon profile was removed and another 25 µL of molten PGM were added on top of each agar pad to obtain convex shapes. After a frame of plasticine was modeled around the agar pads, they were hand pollinated and then sealed by gently pressing evenly a 24 x 60 mm No. 1.5 cover slip on the plasticine frame. The scheme on how to prepare a multi-well micro-germination slide is shown in **Figure S2.2**. Immediately after pollen application, micro-germination slides were used for live-cell imaging. No obvious differences in germination or PT growth were observed between single-well or multi-well micro-germination setups. By contrast, much lower and highly variable germination rates as well as slower pollen tube growth rates were observed when PGM without 10 µM epiBL was used to prepare the micro-germination slides, while the different phases of pollen germination and tube growth described in this work were unaffected.

Microscopy was performed on a ZEISS Cell Observer Spinning Disc confocal microscope (Yokogawa CSU-X1) equipped with a motorized stage using 20x/0.8 NA dry, 40x/1.30 NA DIC oil immersion or 63x/1.40 NA DIC oil immersion objectives. GFP fluorescence was excited with a 488 nm laser line and emission was detected from 505 to 545 nm. A 561 nm laser line was used to excite tagRFP-T and emission was detected from 570 to 640 nm. Free GFP in the pollen cytoplasm and ARO1-GFP fusion protein were imaged every 3 minutes, tagRFP-T-Lifeact every 10-

15 minutes over 4-6 hours in z-stacks of 11 optical slices at each of 10-20 positions representing individual pollen spots.

2.2.4 Morphological modeling of pollen germination

We assumed two extreme morphological models describing cellular geometries of germinating PTs and simulated these models graphically with Illustrator CS4 software (Adobe). In the 'protrusion model' we proposed linear growth at the tip of a protuberance, generating a constantly elongating cylinder with a dome-shaped tip that emerges from the germination site. In the 'bulging model' a first phase of isodiametric inflation was assumed for the germinating pollen tube, followed by a second phase in which isodiametric growth switches to polar growth at a dome-shaped tip. Thus, in the 'protrusion model', a tubular object constantly emerges out of an ellipse, representing the pollen grain. To generate the 'bulging model' a circle, representing the PT, was placed below the upper margin of an ellipse, representing the pollen grain. The diameter of the circle was frame-wise and constantly increased, while keeping its position constant at the lowermost point. After 20 frames, we changed the distal region of the circle into a dome-shaped tip, which then constantly elongates in form of a cylinder like in the 'protrusion model'. In both morphological models, the width of the dome-shaped tip was set identical and did not change during elongation. Furthermore, the net increase in PT area was set identical for both models. Modeled PTs were measured in ImageJ like described for microscopic images (2.2.7).

2.2.5 Pollen staining and microscopy

For membrane staining with FM4-64, pollen of ARO1-GFP expressing plants were germinated in 35 mm petri dishes on solidified PGM as described above. Three hours after pollination a small agar piece was excised and mounted upside down on a cover slip in a droplet of 8 µM FM4-64 (Life Technologies) dissolved in liquid PGM. Images were taken with an inverted SP8 Confocal Laser Scanning Microscope (Leica Microsystems) with a 40x/1.3NA oil immersion objective and 1 airy unit pinhole opening. GFP and FM4-64 were excited simultaneously with a 488 nm laser line. GFP emission was detected from 495 to 550 nm and FM4-64 emission from 650 to 725 nm using HyD detectors. For DAPI staining pollen of plants expressing *P_{ARO1}:tagRFP-T-Lifeact* were put in a droplet of DAPI staining solution (2.5 µg/ml 4',6-diamidino-2-phenylindole (DAPI), 0.01% Tween-20, 5% DMSO, 50 mM PBS, pH 7.2). Confocal z-stacks were acquired at the Spinning Disc system described above using a 100x/1.40 NA oil immersion objective. DAPI fluorescence was excited with a 365 nm LED illumination (COLIBRI, ZEISS) and emission light was filtered by the microscope stand built-in filter cube (emission filter: 447-507 nm) and channeled through an empty Spinning Disc position to display DAPI fluorescence on the same camera as for tagRFP-T and DIC channels.

2.2.6 TIRF microscopy

For TIRF microscopy of pollen tubes, a very planar gel pad was generated by laying two microscope slides orthogonal on the edges of three adjacent slides (**Figure S2.3**). 500 µl of molten PGM containing 2 % agarose was pipetted to the middle of the lower slides and immediately covered with another slide. After solidification, the uppermost slide and all flanking slides were removed and the PGM pad was hand pollinated as described above (2.2.3). Pollinated slides were kept in a damp box for three to five hours. Prior to microscopy, a droplet of double distilled water was pipetted onto the pad and a No. 1.5H cover slip was added. TIRF illumination was generated in a Delta Vision Elite (GE, Healthcare, Applied Precision) system with an Olympus IX-71 microscope, equipped with an Insight SSI(TM) solid state illumination system and an X4 laser module. Images were taken with an Olympus UAPON 100XOTIRF 1.49 NA oil immersion objective and recorded with a CoolSnap HQ2 CCD camera (Photometrics, Tucson, USA). GFP was excited with the 488 nm laser line and emission was detected between 501-549 nm. Image exposure time and TIRF angle were adjusted according to sample fluorescence intensity and specimen location.

2.2.7 Image processing and quantitative analysis

All images were processed in ImageJ (http://rsbweb.nih.gov/ij, version 1.45). In time-lapse experiments, the frame before a pollen tube emerged from the germination site was set to zero. Z-stacks of time lapse images of pollen expressing P_{Lat52}*:GFP* were subjected to projection algorithms. Bright field images were sum slice, GFP images maximum intensity projected. Afterwards, for the GFP channel a threshold was applied to obtain binary images. The implemented WAND tool was used to determine the pollen area, which was then subtracted from all images for a given PT and subsequently the PT area was measured for each frame. The analysis of PTs was only carried out with those PTs where growth was not disturbed by any other object and which could be observed for at least 1 hour. Of all PTs the shape descriptor 'roundness' was measured, given by 4*area/(pi*(major axis)^2) of a respective PT. To compare the frame wise PT area increase shortly after germination and in later PT growth phases, the mean frame wise increase of the first 10 and the last 10 frames was calculated and compared in a Friedman's 2-way variance analysis. Z-stacks of time lapse images of pollen expressing P_{ARO1}*:ARO1-GFP* were also subjected to maximum intensity projections first. For those pollen that were monitored at least half an hour before and after the time point of germination, images were cropped in a rectangular selection containing only the pollen and emerging PT. All frames of a PT were included in a stack histogram that was used for subsequently computing gray values for setting a 70 % signal threshold to determine the PT shape (false colored in red) and a 0.5 % signal threshold (false colored in yellow) to determine the maximum intensity peaks for ARO1-GFP. Frame-wise PT area increase was measured by overlaying unbiased PT shape outlines that were obtained using the WAND tool, which was also used to determine the size of individual PT areas. ARO1-GFP max-

imum intensity peaks were quantified using a variable ROI selection and measuring its mean gray value that was subsequently multiplied by the ROI size. To compare multiple PTs in a mean value computation, ARO1-GFP maximum intensity was normalized for each PT to its maximum signal value. Z-stacks of images of pollen expressing tagRFP-T-Lifeact were maximum intensity projected and to better visualize the maximum signal intensities false colored using the 'spectrum' LUT. Calculations were performed with Excel2010 (Microsoft) and statistical analyses were computed with SPSS22 (IBM).

2.3 Results

2.3.1 Live cell imaging of pollen germination and PT growth

To facilitate time lapse live cell imaging of *Arabidopsis* pollen germination and PT growth using high NA immersion objectives, we designed a single-well and a multi-well micro-germination setup as shown in **Figure 2.1 A** and **2.1 B**. Both setups are fast and easy to prepare (see **Figures S2.1** and **S2.2**), based on inexpensive components. Pollen germination and PT growth of up to 12 genetically different plants can be simultaneously observed over many hours when using the 12-well micro-germination setup. Pollen germinates in the direct proximity to the cover slip in a film of PGM that is formed when the cover slip is gently pressed on the medium to seal the well (**Figure 2.1 C**). Pollen germination rates within this film are very high (> 80 %) and homogenous (**Figure 2.1 D, F**), with normal PT morphology (**Figure 2.1 E**). In an exemplary 10 well setup, no temporal or morphological deviations in pollen germination or PT growth were observed (**Supplemental Movie 2.1** on www.youtube.com/watch?v=M9H2XVKIE1s). This technique can be broadly used in every lab, adapted to many microscopic techniques and may be even up-scaled for the simultaneous imaging of pollen from more than 12 individuals.

2.3.2 Pollen tube growth kinetics

We evaluated a total of 66 PTs expressing cytoplasmic GFP in the PT vegetative cell that fulfilled our quality criteria for quantitative PT analyses, that is the absence of any obstacle during germination and growth and the complete recording of at least 1 hour after germination. As PTs represent 3-dimensional cylindrical objects, we did not determine pollen tube length in µm but measured the PT as area in μm^2. Automatic size measurements using the WAND tool (ImageJ) were performed with thresholded binary images of maximum intensity projections (**Figure 2.2 A**). The growth kinetics of this pollen tube is depicted as frame-wise increase in PT area and as cumulative increase in PT area over time, respectively (**Figure 2.2 B**). After germination, no marked increase in PT area can be observed during the first 21 minutes of PT growth. 24 minutes after germination, PT growth strongly increases and rises even more after 42 minutes. Comparing the growth rate determined by PT area measurements with pollen tube length as a measure of growth revealed similar growth kinetics (**Figure S2.4**). When we estimated the ratio

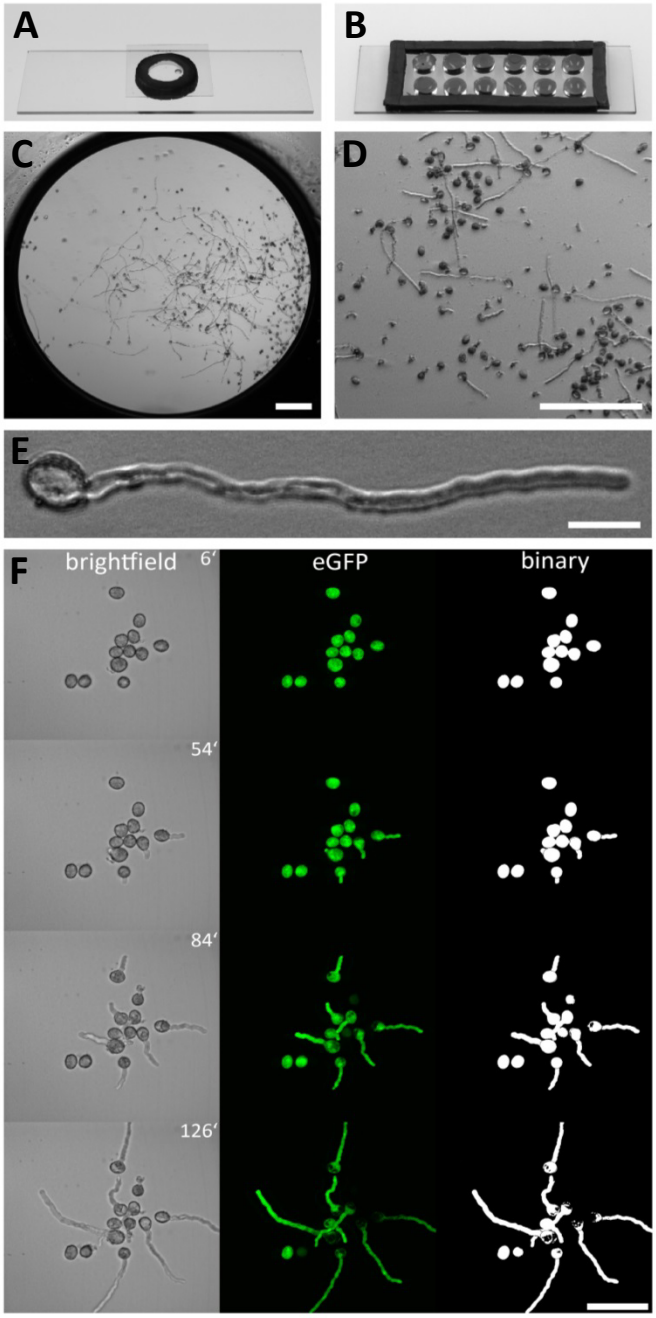

Figure 2.1 | *Arabidopsis* pollen imaging in the micro-germination setup.

Mounting pollen in a single **(A)**, or multi well **(B)**, micro-germination setup for live cell imaging. In the center of one well **(C)** PTs grow in close proximity to the cover slip **(D)**, allowing the use of high NA immersion objectives with low working-distances. Pollen germination is not affected by the mounting technique and PTs showed normal morphology **(E)**. A time series of germinating P_{Lat52}*:GFP* pollen is shown in **(F)**. Brightfield images are shown as sum slice projections and confocal fluorescence images of cytoplasmic GFP as maximum intensity projections. Binary images of GFP channel enable unbiased quantitative measurement of PT area size and morphology (F). Scale bar = 200 µm in (C), (D), 20 µm in (E) and 50 µm in (F).

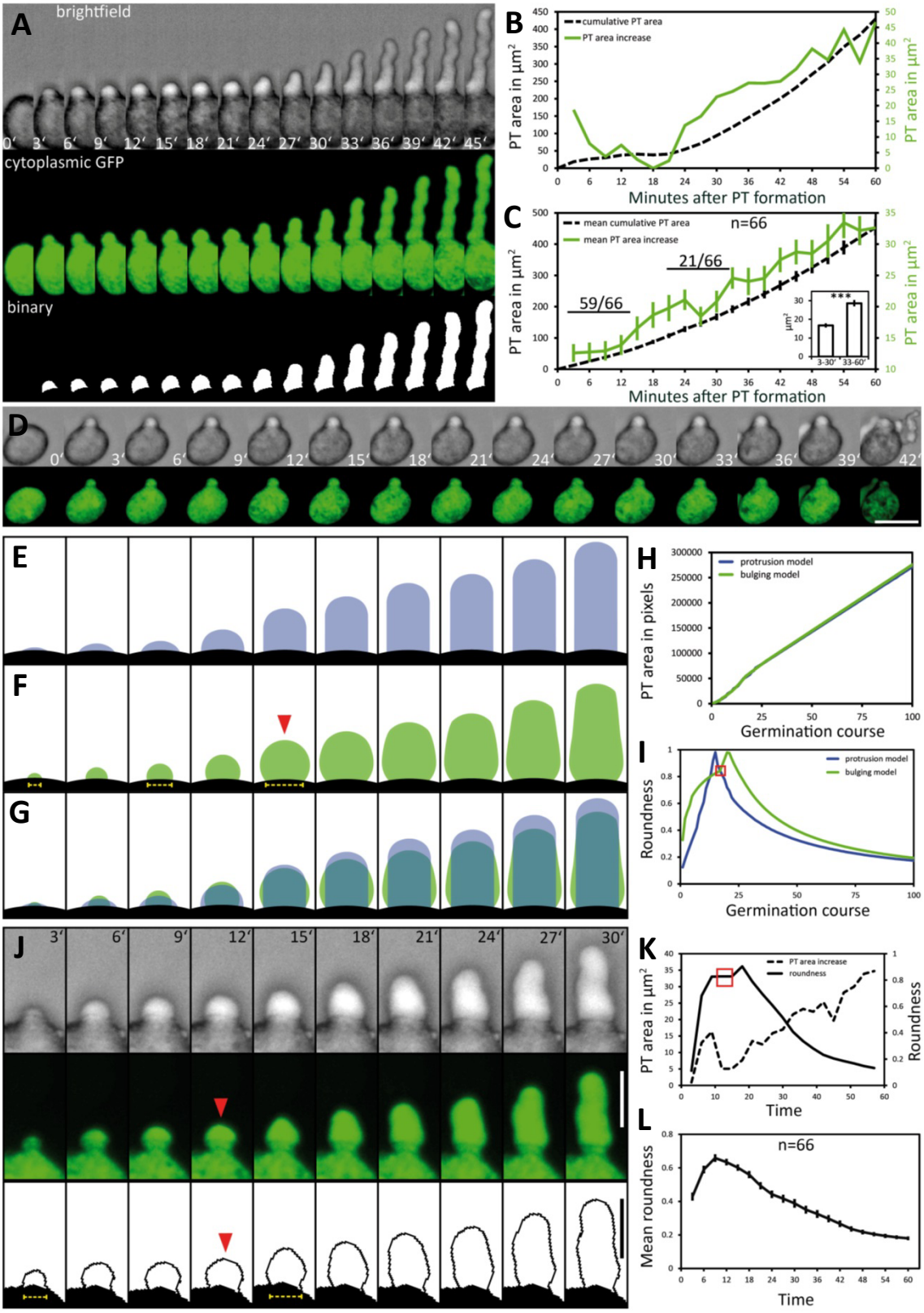

Figure 2.2 | Pollen tube growth kinetics and morphology changes.

Pollen expressing GFP in the cytoplasm of the vegetative cell (P_{Lat52}:*GFP*) was used to quantitatively assess the kinetics of PT growth and PT morphology during germination. Brightfield and fluorescence channel, together with the binary image generated from the fluorescence channel, are shown in **(A).** Time point 0′ indicates the last frame before germination. The quantification of the cumulative PT area and frame-wise increase in PT areas over time is given in **(B)**. Mean values ± 1SE of cumulative PT areas and the frame-wise in-

Figure 2.2 | *continued*

crease in PT areas of 66 evaluated PT's are shown in **(C)**. Numbers in (C) represent the frequency of an observed pattern. The mean frame-wise increase in PT areas for the first 10 frames of each pollen tube is significantly lower compared to the last 10 frames of each PT (inset of (C); asterisks indicate statistically highly significant differences, $p < 0.001$). A pollen that germinates but fails to bursts after germination is shown in **(D)**. 'Protrusion' and 'bulging' model for PT morphology changes during pollen germination and PT elongation are shown in **(E)** and **(F)**. The overlay of both morphological models is shown in **(G)**, their PT area increase over time is shown in **(H)**. The course of 'roundness' for both morphological models is shown in **(I)**. Red solid arrowhead in (F) and red square in (I) highlights the transition from unpolar bulging to polar elongation in the 'bulging model'. A representative germinating PT is shown in **(J)** and its course of PT area increase and 'roundness' is shown in **(K)**. Mean values ± 1SE of the 'roundness' of 66 PTs are given in **(L)**. Scale bar = 25 µm in (A), (B) and 12.5 µm in (J).

of PT length to PT area over time we calculated an approximated conversion factor of 0.18 μm^{-1} for transferring PT area (μm^2) in PT length (µm).

When all 66 PTs were included into the quantification of growth kinetics, a high overall PT growth rate of 400.2 μm^2/h (mean cumulative PT area) was observed (**Figure 2.2 C**). We observed no or only very low increase in the PT area during the first 12 minutes of PT formation, resembling a lag phase. To statistically test this, we compared the mean PT area increase rate for the first and the last 10 frames of PT growth (inset in **Figure 2.2 C**). In almost all cases (59 of 66), the mean PT area increase during the first 30 minutes was lower than for the last 30 minutes. Friedman's 2-way variance analysis revealed that PT growth during the first 30 minutes is highly significantly slower ($p < 0.001$) than during the last 30 minutes.

From these results we conclude that PT growth in *Arabidopsis* starts with a first, distinct phase of slow growth shortly after germination that is followed by a second phase of rapid PT growth. This is furthermore corroborated by the finding that in case of PT burst, also a short protuberance is first initiated but obviously does not pass over to the next phase of rapid elongation (**Figure 2.2 D**). A later short phase of decelerated growth could be observed in about one third (21 of 66) of all pollen tubes investigated (**Figure 2.2 B**). This lag phase occurred when PTs reached a mean size of approximately 200 μm^2 and it was more variable and less pronounced (**Figure 2.2 B**; **Figure S2.5**).

2.3.3 Changes in PT shape after pollen germination

We investigated the PT morphologies during germination and the transition to rapid tip growth in more detail and compared them with two extreme morphological models describing possible PT geometries. The 'protrusion model' assumes that a PT would emerge from the pollen grain as an elongating cylinder with a dome-shaped tip that is maintained during germination and rapid tip growth (**Figure 2.2 E**). As a result the diameter of the junction between the pollen grain and the PT, which is the site of germination, would remain rather constant in this model. By contrast the 'bulging model' assumes that the PT initially exhibits isodiametric growth, lead-

ing to a round bulge emerging at the germination site (**Figure 2.2 F**, red arrowhead). In a second phase, isodiametric growth would have to switch to polar tip growth by selecting a growth site and forming an elongating cylinder. A unique feature of the 'bulging model' is that the isodiametric inflation of the bulge will increase the diameter of the germination site over time.

The differences between the two morphological models are highlighted in **Figure 2.2 G**. For both models we determined a similar net increase in PT area and the same width of the dome-shaped tip. When we compared the increase in PT area over time it was indeed almost identical for both models (**Figure 2.2 H**). We computed the course of 'roundness' for both morphological models during germination and found the 'roundness' to increase linearly to a sharp peak in the 'protrusion model', followed by a rapid decrease when the PT continues to elongate (**Figure 2.2 I**). In the 'bulging model', by contrast, the course of roundness of a germinating PT forms a rather hyperbolic increasing curve with a broader maximum leading to an accentuated peak (**Figure 2.2 I**).

Notably, live imaging of germinating pollen revealed considerable similarities to the 'bulging model' (**Figure 2.2 J, K**). During the first 12 minutes of germination the pollen vegetative cell forms a round bulge at the germination site that exhibits isodiametric growth. Afterwards, the uniformly expanding bulge undergoes the transition into a polar growing PT (**Figure 2.2 J**; 15′ to 18′). The changes in its shape are reflected by the course of 'roundness' plotted for this PT (**Figure 2.2 K**). A hyperbolic increase with a broad maximum (red box in **Figure 2.2 K**) is characteristic for the phase of bulging. The following peak defines the transition phase, when the bulge starts to form a dome-shaped tip, followed by a switch to rapid tip growth (**Figure 2.2 K**).

We found the same tendency when we plotted the mean course of 'roundness' for all 66 PTs (**Figure 2.2 L**). Furthermore, in 37 of 66 examined pollen the increasing diameter of the germination site during bulging was clearly visible (**Figure 2.2 J**, yellow dotted line), which is in line with the unique feature predicted by the 'bulging model' (**Figure 2.2 F**, yellow dotted line).

2.3.4 ARO1-GFP is associated to vesicles

In the growing pollen tube the GFP fusion of ARMADILLO REPEAT ONLY 1 (ARO1) accumulates in the vesicle-rich 'clear zone' (**Figure 2.3 A; Supplemental Movie 2.2**). We observed partial co-localization of ARO1-GFP fluorescence with FM4-64 in the 'clear zone', but almost no co-localization in the subapical part of the PT (**Figure 2.3 A**). Spinning Disc confocal time-lapse imaging of growing PTs furthermore revealed that ARO1-GFP streams in a reverse fountain pattern (**Supplemental Movie 2.2**). The fact that ARO1-GFP accumulates in the pollen tube tip in a Brefeldin A-sensitive manner (Gebert et al., 2008) suggested that ARO1-GFP is associated to vesicles in the PT tip.

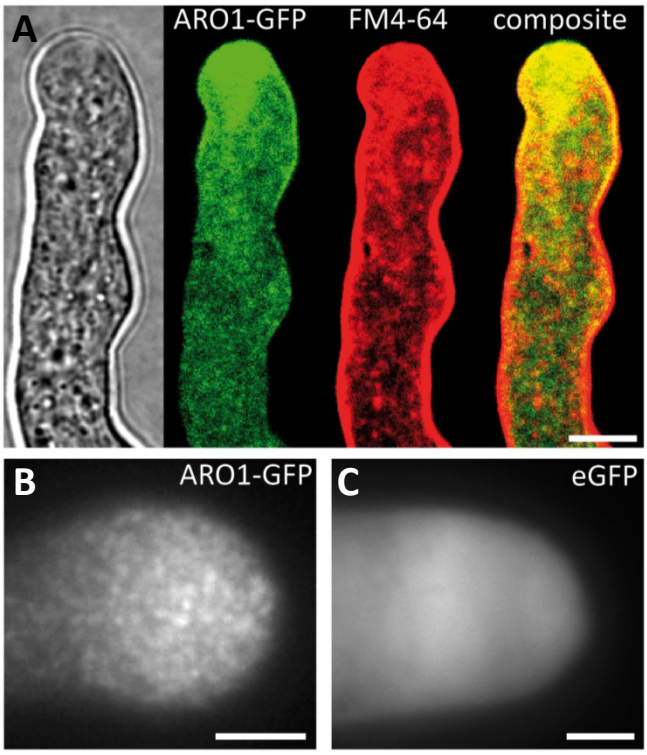

Figure 2.3 | ARO1-GFP localizes on vesicles at the pollen tube tip, accumulating in the inverted cone-shaped region.

(A) At the PT tip, ARO1-GFP predominantly accumulates in the vesicle-rich inverted cone-shaped region and partially co-localizes with FM4-64. No co-localization of ARO1-GFP and FM4-64-stained membrane compartments is detected in the subapical region of the PT. **(B)** TIRF microscopy reveals that ARO1-GFP signals appear as discrete punctate structures of approximately 0.2 µm in the PT tip. These punctate structures are not observed in PTs that express cytoplasmic GFP **(C)**. Scale bars = 5 µm.

We performed TIRF microscopy to confirm the proposed vesicle-association of ARO1-GFP. By illuminating only a thin region of the PT tip, including the cytoplasmic zone immediately beneath the PT plasma membrane, we compared the fluorescent signals of ARO1-GFP with that of free GFP. As shown in **Figure 2.3 B**, ARO1-GFP signals appeared as numerous dot-like structures with a size of approximately 200 nm in the PT tip. In contrast pollen tubes expressing cytoplasmic GFP showed a homogenous fluorescence (**Figure 2.3 C**).

2.3.5 ARO1-GFP decorated vesicles peak at the future germination site during pollen activation

We then investigated the subcellular localization and signal intensity changes of vesicle-associated ARO1-GFP before and during pollen germination using Spinning Disc microscopy (**Figure 2.4 A**; **Supplemental Movie 2.3**). The respective outlines of the frame wise increase in PT area are shown in **Figure 2.4 B**. The quantification of ARO1-GFP signal intensity in relation to the increase in PT area is given in **Figure 2.4 C**.

Notably, we observed 18 and 12 minutes before pollen germination high intensity peaks of ARO1-GFP subjacent to the future site of PT outgrowth (arrows in **Figure 2.4 A**; peaks in **Figure 2.4 C**), resembling two knocks on the door. During the following bulging phase (0 to 12 min), ARO1-GFP steadily accumulated at the distal pole of the bulge (**Figure 2.4 A, C**). High fluorescence intensities at the PT tip, shaped as inverted cone, were observed when the PT switched to rapid tip growth (24 to 60 min), with moderate downturns during short phases of

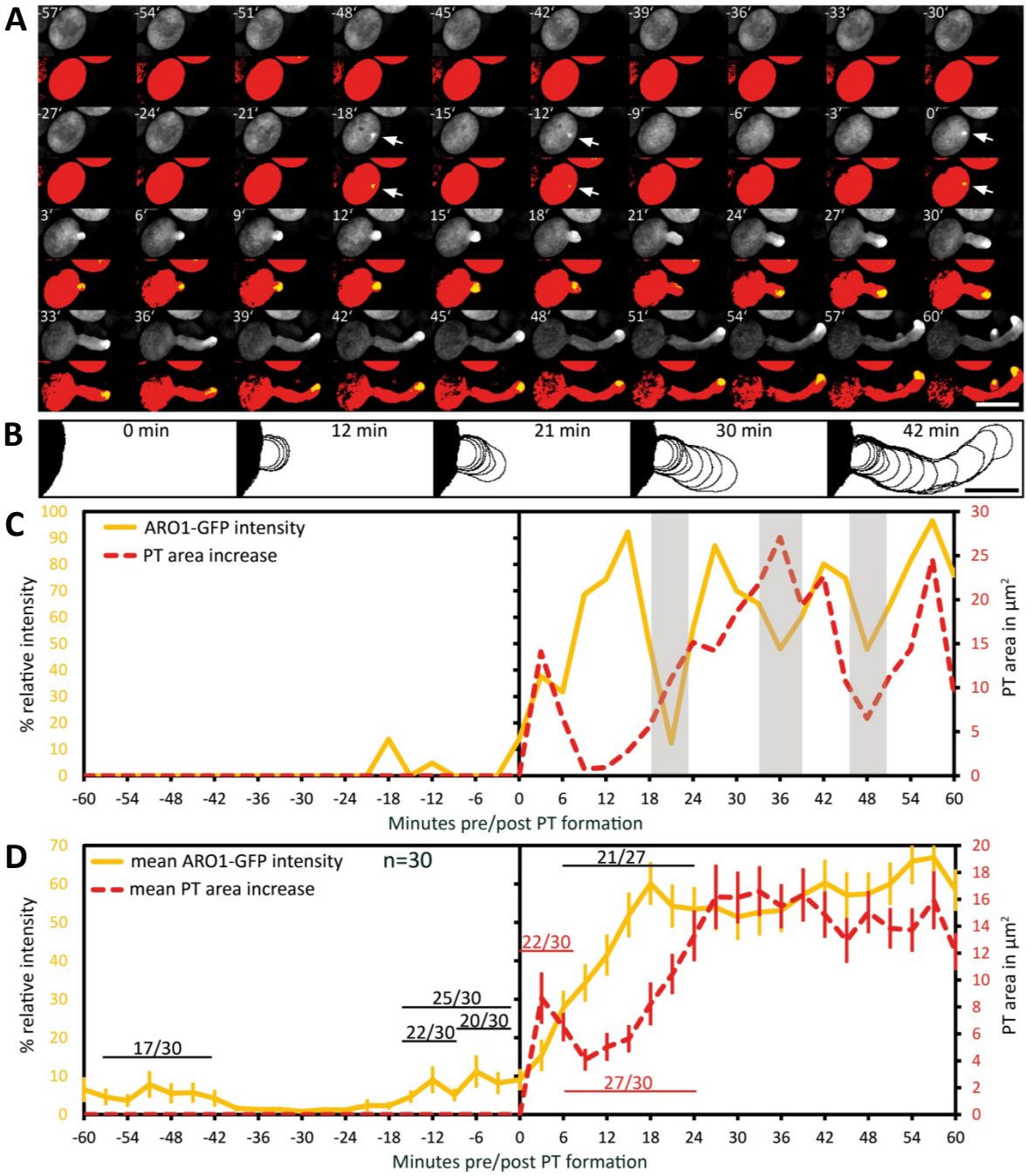

Figure 2.4 | Polarization of vesicle trafficking in activated pollen predetermines the site of pollen tube emergence.

Time series of fluorescence signal in germinating pollen expressing P_{ARO1}*:ARO1-GFP*. Maximum intensity projected fluorescence raw signal and thresholded signals of a representative PT are shown in **(A)**. GFP fluorescence is shown in yellow (0.5 % of highest intensities), and in red (70 % of highest intensities) representing the ARO1-GFP maxima and the pollen cytoplasm. Outlines of PT shape for successive frames are drawn in **(B).** The frame-wise increases in PT area over time and relative ARO1-GFP intensities for the PT in (A) are plotted in **(C)**. Grey shaded areas indicate phases of PT growth reorientation. Mean value ± 1SE of frame-wise PT area increase and normalized ARO1-GFP signal maxima for 30 PTs are given in **(D)**. Numbers in (D) represent the frequency of an observed pattern. Time point 0' indicates the last frame before germination. Arrows point to ARO1-GFP intensity maxima before germination. Scale bar = 25 µm in (A) and 10 µm in (B).

tube growth re-orientation (30 to 36 min; 45 to 48 min), which also took place during the transition to rapid tip growth (18 to 24 min).

The quantitative analysis of 30 PTs is shown in **Figure 2.4 D**. 60 to 36 minutes before germination, intensity peaks of ARO1-GFP appeared in 17 out of 30 pollen grains (**Supplemental Movie 2.3**). These intensity peaks, indicating rapid and local vesicle accumulation, were often but not always located near the future site of PT outgrowth. However, shortly before germination in 25 out of 30 pollen at least one high-intensity peak was detected subjacent to the future site of PT outgrowth (**Figure 2.4 D**). 22 of 30 pollen grains showed one peak 12 to 9 minutes before germination at the future germination site and in two thirds of observed pollen the ARO1-GFP high-intensity peak was recorded 6 to 3 minutes before germination. In 50 % of the pollen two high-intensity peaks were visible (**Supplemental Movie 2.3**), while one third of pollen showed a single peak before germination. Frequencies and statistics of ARO1-GFP intensity peaks in pollen subjacent to the future site of PT outgrowth are shown in **Figure S2.6**.

Taken together, the temporary polar accumulation of ARO1-GFP decorated vesicles in activated pollen precedes pollen germination and marks the future site of PT outgrowth. Furthermore, we observed a strong increase of ARO1-GFP signal intensity after bulging, indicating the transition to rapid PT elongation (**Figure 2.4 D**). Like observed for PTs expressing cytoplasmic GFP, almost all (27 of 30) ARO1-GFP expressing PTs showed an initial lag phase of growth after germination. During this lag phase, including bulging and transition phase, ARO1-GFP signal intensity strongly increased at the distal end of the bulge/dome-shaped tip in 21 of 27 PTs. Nine minutes after ARO1-GFP reached its maximum signal intensity at the tip of the tube, PT elongation rates reached their maxima, recognized by the rapid increase in PT area over time (**Figure 2.4 D**). By contrast, during the first 9 minutes of the bulging phase 22 of 30 bulges substantially expanded while the accumulation of ARO1-GFP decorated vesicles at the distal end of the bulge was delayed, suggesting that bulging does not depend on pronounced vesicle trafficking to the very tip of the bulge.

2.3.6 Patterns of abnormal PT growth correlate with deviating ARO1-GFP signals

Using our multi-well micro-germination setup a high number of pollen germinated and thus we were able to observe very rare events (less than 3.3 %) of abnormal PT growth, such as bulging without subsequent elongation (**Figure 2.5 A, B**), the initiation of a second PT from one grain (**Figure 2.5 C, D**) or the branching of a PT (**Figure 2.5 E, F**).

In the first case of a PT that did not switch to the phase of rapid PT elongation, a high intensity peak of ARO1-GFP signals appeared 24 minutes before germination at the future site of PT outgrowth (**Figure 2.5 A, B**). During germination a roundish PT bulge was formed showing isodiametric expansion and constant increase in ARO1-GFP fluorescence intensity with a maximum

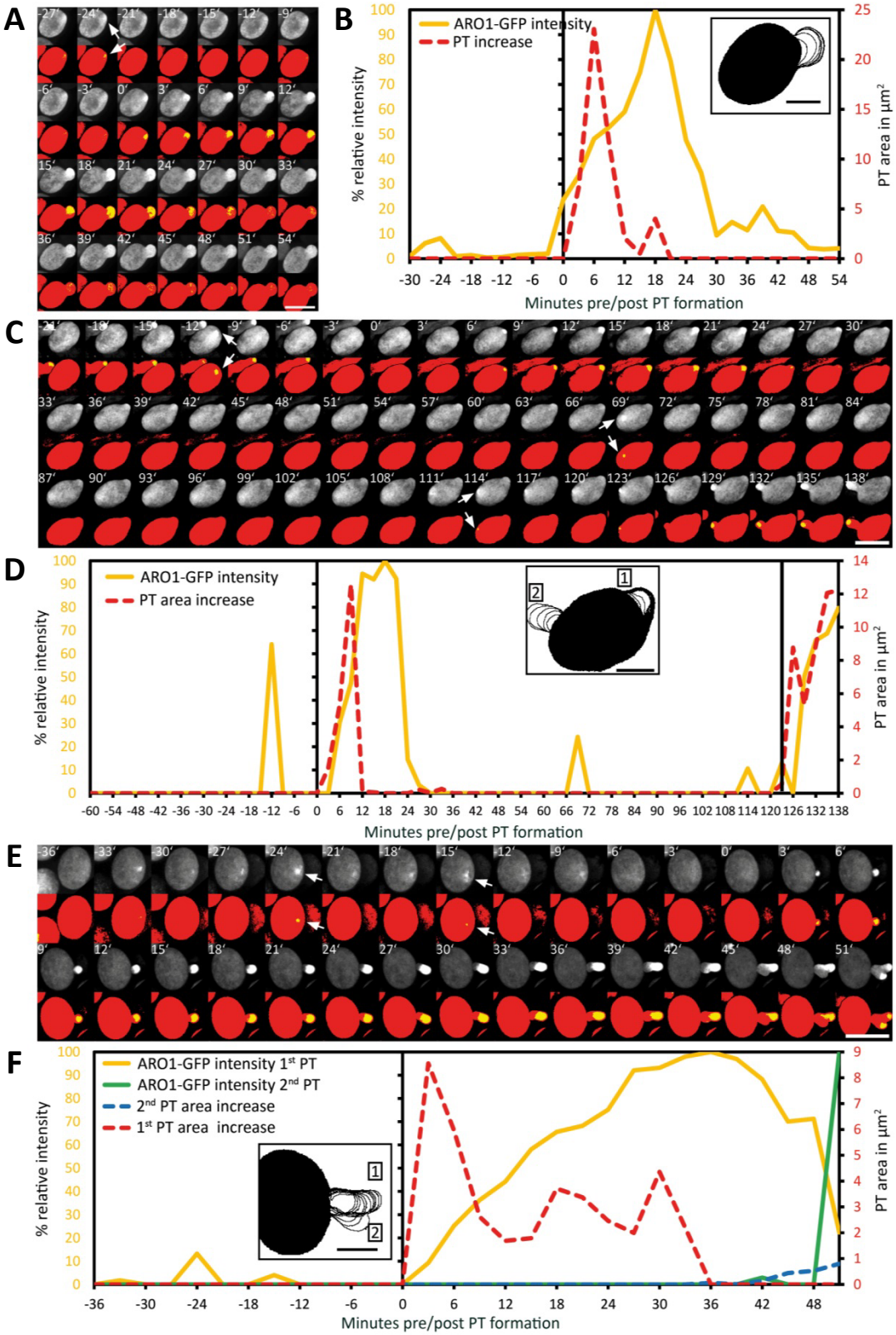

Figure 2.5 | Exceptional pollen germination events confirm the correlation between local vesicle accumulation and pollen tube emergence.

The breakdown of vesicle accumulation in the pollen tube bulge is accompanied with the failure to switch to rapid PT tip growth **(A)**, **(B)**. After unsuccessful transition to rapid PT tip growth, the pollen cell may also change the direction of polar vesicle trafficking, resulting in the establishment of a second germination site, as shown in **(C)** and **(D)**. A branching pollen tube is shown in **(E)** and **(F)**. After successful bulging the transition to rapid PT tip growth fails and a second growth site is selected, indicated by the accumulation of ARO1-GFP decorated vesi-

Figure 2.5 | ***continued.***

cles in the tip of the PT branch. Maximum intensity projected fluorescence raw images and composite thresholded images are shown in (A), (C) and (E). GFP fluorescence is shown in yellow (0.5 % of highest intensities) and in red (70 % of highest intensities), representing the ARO1-GFP maxima and the pollen cytoplasm. Frame-wise PT area increase and relative ARO1-GFP intensity are shown in (B), (D) and (F), where insets show frame-wise overlaid PT shape outlines. Time point 0' indicates the last frame before germination. Arrows point to ARO1-GFP intensity maxima before germination. Scale bars = 25 µm in (A), (C), (E) and 10 µm in insets in (B), (D), (F).

18 minutes after germination. However, during the following 12 minutes ARO1-GFP fluorescence rapidly decreased to only 10 %, detected 30 minutes after germination. The decrease in ARO1-GFP signal intensity was accompanied with arrested PT growth (**Figure 2.5 A, B**).

In one pollen grain a second tube was established during germination (**Figure 2.5 C, D**). A sharp ARO1-GFP intensity maximum appeared subjacent to the future site of PT outgrowth, 12 minutes before pollen germination, the area of the bulge increased after pollen germination and ARO1-GFP accumulated in the bulge. However, 21 minutes after germination, ARO1-GFP fluorescence rapidly decreased and during the following 45 minutes neither the PT area increased, nor was any ARO1-GFP intensity maximum observed. 69 minutes after first bulging, a new ARO1-GFP intensity maximum arose within the pollen grain, followed by another peak at the same site 45 minutes later. Nine minutes after the second ARO1-GFP fluorescence maximum the pollen grain started to germinate at this site. After bulging, ARO1-GFP steadily accumulated at the distal end of the second bulge and rapid PT elongation was successfully initiated (**Figure 2.5 C, D**).

In the case of a branching PT (**Figure 2.5 E, F**), two maxima of ARO1-GFP intensity occurred 24 and 15 minutes before pollen germination. During the following phase of bulging, ARO1-GFP signal intensity at the distal end of the bulge steadily increased and reached a maximum in the remarkable long transition phase, 36 minutes after germination. However, the switch to rapid PT growth did not occur at this site but a second growth site was selected, marked by ARO1-GFP signals appearing at the tip of the branching PT (**Figure 2.5 E**; 42 min). During the following 6 minutes ARO1-GFP signal intensity at the first tube tip rapidly decreased while the PT branch expanded. Nine minutes after the pollen tube initiated branching, another ARO1-GFP intensity maximum was detected in the new tip of the PT, while the signal in the old tip diminished (**Figure 2.5 E**, **F**; 51 min).

2.3.7 *The actin cytoskeleton polarizes prior to germination and undergoes characteristic changes during PT growth*

We used the *ARO1* promoter to drive moderate expression of the tagRFP-T-Lifeact fusion protein in pollen. DAPI staining was performed to visualize the nuclei of the vegetative cell and the sperm cells in pollen grains. Immediately after pollen mounting, the pollen actin cytoskeleton was not distributed with any polarity and showed homogenous accumulation in the cell periphery and pronounced fluorescent signals around the vegetative nucleus (**Figure 2.6 A, B**), which has also been reported for mature *Brassica napus* pollen (Hause et al., 1992; Gervais et al., 1994).

We germinated tagRFP-T-Lifeact expressing pollen in our micro-germination setup and observed that within half an hour before germination F-actin accumulated at the periphery of the pollen vegetative cell, opposite to the future site of PT outgrowth (**Figure 2.6 C-E**). Almost all (35 of 38) pollen grains showed this pattern of F-actin polarization before germination.

Within 15 minutes after pollen germination, we observed an increase in longitudinal actin cable formation pointing towards the PT axis and partially reaching into the tube (**Figure 2.6 C**). Very articulate actin reorganization appeared in all investigated PTs around 30 minutes after germination, when the PTs reached a mean size of 300 ± 17 μm^2. The actin cytoskeleton assembled at the site of PT outgrowth forming prominent longitudinal F-actin bundles that reached from the pollen grain into the PT. The formation of a large vacuole opposite to the germination site was observed simultaneously with the prominent F-actin assembly near the site of PT outgrowth (**Figure 2.6 C**). In later stages of PT growth, this dense assembly of F-actin cables was shifted into the PT (**Supplemental Movie S2.4**).

Again, we looked for exceptional germination scenarios and identified a PT that stopped growth after bulging (**Figure 2.6 D**) and a PT that initiated a second tube from one pollen grain (**Figure 2.6 E**). In the case of PT growth arrest after bulging, the F-actin polarized prior to germination at the pole opposite to the germination site and longitudinal actin cables reaching from the pollen grain into the PT bulge were present 15 minutes after germination. However after 30 minutes, the actin cytoskeleton started to depolarize and transition to rapid tip growth was not initiated (**Figure 2.6 D**).

In the case of additional tube formation from one pollen grain, 15 minutes before germination the actin cytoskeleton accumulated at the periphery, opposite to the future site of PT outgrowth but after bulge formation, the F-actin almost completely depolarized until 60 minutes after the first germination (**Figure 2.6 E**). F-actin repolarization was observed 75 minutes after the first germination event, opposing to the site where the second tube bulged later on. 15 to 30 minutes after the second F-actin polarization was observed at the periphery of the pollen vegetative cell, a second bulge was formed and underwent transition to rapid tip growth, showing all F-actin features of a normal growing pollen tube.

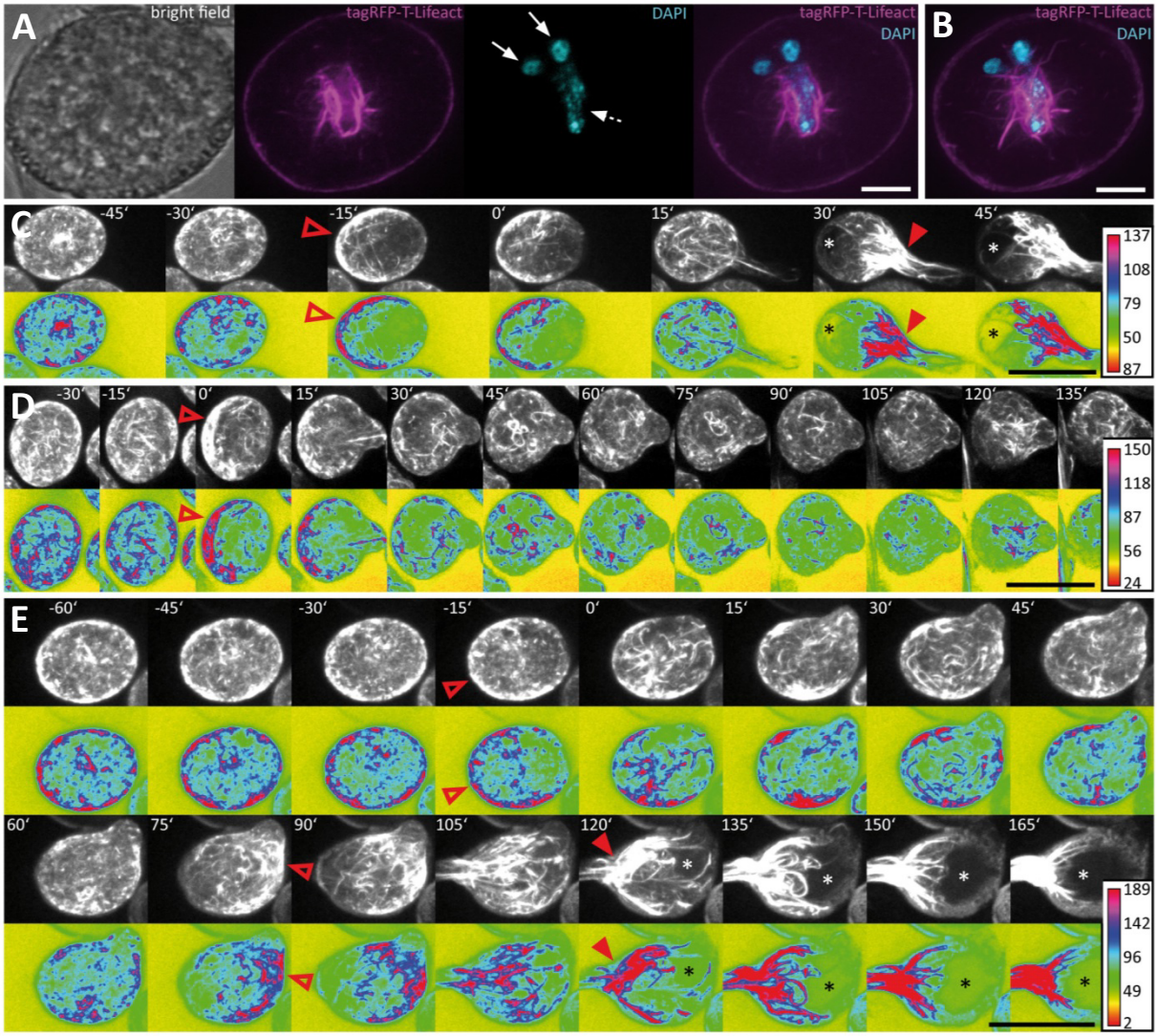

Figure 2.6 | The actin cytoskeleton undergoes characteristic changes during pollen germination.

Pollen expressing tagRFP-T-Lifeact was used for live-cell imaging of F-actin architecture and dynamics during pollen germination and growth. A single optical slice through a representative DAPI stained pollen grain is shown in **(A)**. Solid arrows mark the sperm cells and dashed arrows the vegetative nucleus. A composite maximum intensity projection of 19 optical slices is shown in **(B)**, the typical pattern of actin dynamics during pollen germinating is presented in **(C)**. A pronounced F-actin network accumulates at the periphery of the pollen vegetative cell, opposite to the future site of PT outgrowth (open arrowhead). Rapid PT tip growth is associated with vacuole formation (asterisk) and the massive appearance of parallel F-actin bundles extending from within the pollen grain, into the pollen tube (solid arrowheads). In **(D)** a PT that failed to switch to rapid PT tip growth after bulging is shown. The germination of a second PT after first unsuccessful bulging is shown in **(E)**. Maximum intensity projections of raw images and intensity based false-colored images are shown in (C), (D) and (E) with respective calibration bars. Open red arrowheads indicate polar F-actin accumulation at the periphery of the pollen vegetative cell. Solid red arrowheads point at massively accumulating F-actin bundles that extend into the PT. Asterisks mark vacuoles. Time point 0’ indicates the last frame before germination. Scale bar = 10 µm in (A), 5 µm in (B) and 25 µm in (C) to (E).

2.3.8 *Sperm cell transport starts when the switch to rapid tip growth has taken place*

We used a marker line showing RFP fluorescence in the sperm cell nuclei and GFP fluorescence in the sperm cell plasma membranes to investigate whether the two sperm cells are relocated into the PT at a distinct growth phase (**Supplemental Movie 2.5**). The GFP-labeled sperm cell membranes show that the two sperm cells are closely interlinked and that one long membrane extension connects one of the sperm cells to the nucleus of the vegetative cell (**Figure 2.7**), thereby forming a transport unit known as the male germ unit (MGU). In *Arabidopsis*, the entrance of the three MGU components into the pollen tube follows a regular order, both in planta (Lalanne and Twell, 2002) and in in vitro germinated pollen (Zhou and Meier, 2014): the vegetative nucleus always precedes the sperm cells during entrance into the pollen tube (Lalanne and Twell, 2002; own observations).

The tip of the GFP labeled long membrane extension of the leading sperm was used as a tracer for the position of the vegetative nucleus as it is hooked up to the vegetative nucleus. We defined the time point of MGU relocation into the PT when the tip of the sperm membrane extension became permanently visible outside the pollen grain (**Figure 2.7 A**, green arrowhead). From 34 PTs we calculated a mean PT size of 350 ± 13 µm² at the time point of MGU translocation into the PT (**Figure 2.7 B**), indicating that the sperm cell transport into the PT does not occur at random but when the PT has reached a certain length and growth phase. Two processes associated with rapid PT tip growth, the formation of a large vacuole within the pollen grain and the accumulation of prominent F-actin cables at the base of the growing PT (**Figure 2.7 B**), have already taken place when we detected the sperm membrane extension in the PT.

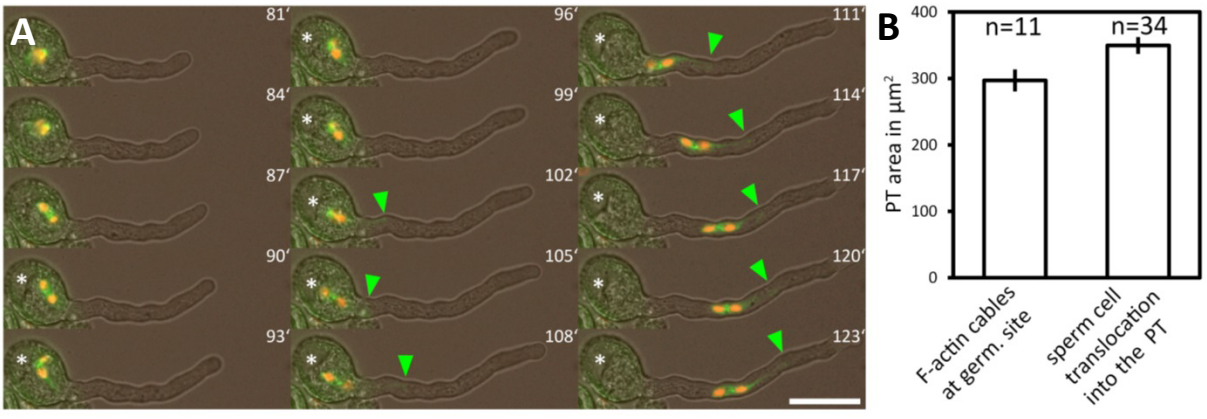

Figure 2.7 | The male germ unit is transported into the PT after the transition to rapid tip growth.

A marker line labeling both sperm nuclei (red fluorescence) and the sperm plasma membrane (green fluorescence) was used for time lapse imaging of pollen germination. **(A)** Green arrowhead points to the tip of the long sperm cell membrane extension physically associated to the vegetative cell nucleus, which has been transported into the pollen tube. Bar plots in **(B)** show average PT areas when F-actin bundles massively accumulate at the germination site (indication for rapid tip growth), compared to the mean PT area when the male germ unit is relocated into the PT. Scale bar = 25 µm.

2.4 Discussion

The pollen tube is an attractive model for the analysis of tip growth mechanisms on the molecular and cellular level, especially in plant species amenable to forward genetic screens and with excellent genomic and bioinformatic resources such as *Arabidopsis thaliana*. Nevertheless, quantitative imaging of growing *Arabidopsis* PTs remained challenging, due to highly variable pollen germination rates in different experiments.

Here, we describe an inexpensive and easy mounting technique to simultaneously track germinating pollen from up to 12 genetically different plants. Our multi-well germination-slide with modified pollen germination medium yields high germination percentages and allows live cell imaging and subsequent quantitative image analysis of the whole process of *Arabidopsis* pollen activation, germination, and the establishment of polar tip growth.

By using our setup and pollen from different fluorescent marker lines we were able to precisely describe the kinetics of *Arabidopsis* pollen germination in vitro. We expressed tagRFP-T-Lifeact in pollen to investigate F-actin dynamics during pollen activation, germination and tube growth, as Lifeact has become the actin marker of choice in the PT (Qu et al., 2015). Vesicles within the pollen grain and the germinating PT were visualized by ARO1-GFP (Gebert et al., 2008). The accumulation of ARO1-GFP in the apical region of growing pollen tubes and the rapid dissipation of this tip localization by Brefeldin A treatment is reminiscent of YFP-RabA4d, an exocytotic vesicle marker of pollen tubes (Lee et al., 2008; Szumlanski and Nielsen, 2009), and of GFP-Rab11b-tagged vesicles in tobacco pollen tubes (de Graaf et al., 2005; Cheung and Wu, 2008). Transport vesicles in the tip of angiosperm PTs are known to follow a reverse fountain-streaming pattern (for review see Bove et al., 2008; Cheung and Wu, 2008; Chebli et al., 2013), as is the case for ARO1-GFP (**Supplemental Movie 2.2**). By TIRF microscopy, a method that has been successfully used to image secretory vesicles in *Picea meyeri* PTs (Wang et al., 2006), we were able to show that ARO1-GFP is associated to vesicles in the pollen tube tip. The size of the punctate ARO1-GFP signals was approximately 200 nm in diameter, which is very close to the calculated size of 182 nm described for vesicles in *Arabidopsis* PTs (Ketelaar et al., 2008). Based on the vesicle-like appearance of ARO1-GFP in TIRF microscopy, its reverse fountain-streaming pattern and the BFA sensitive tip localization we conclude that ARO1-GFP shows a bona-fide vesicle association in the tip of growing pollen tubes.

2.4.1 *Germinating* Arabidopsis *pollen reveal characteristic tube morphologies and growth kinetics, accompanied with F-actin and vesicle polarization*

Tip growing cells confine cellular expansion to a small area. The occurrence of a single growth site includes at least two distinct phases: the initiation of growth and the elongation phase (Geitmann, 2010). Our quantitative imaging of tube morphologies and growth kinetics enabled us to dissect the early events of germination and to define characteristic features associated with

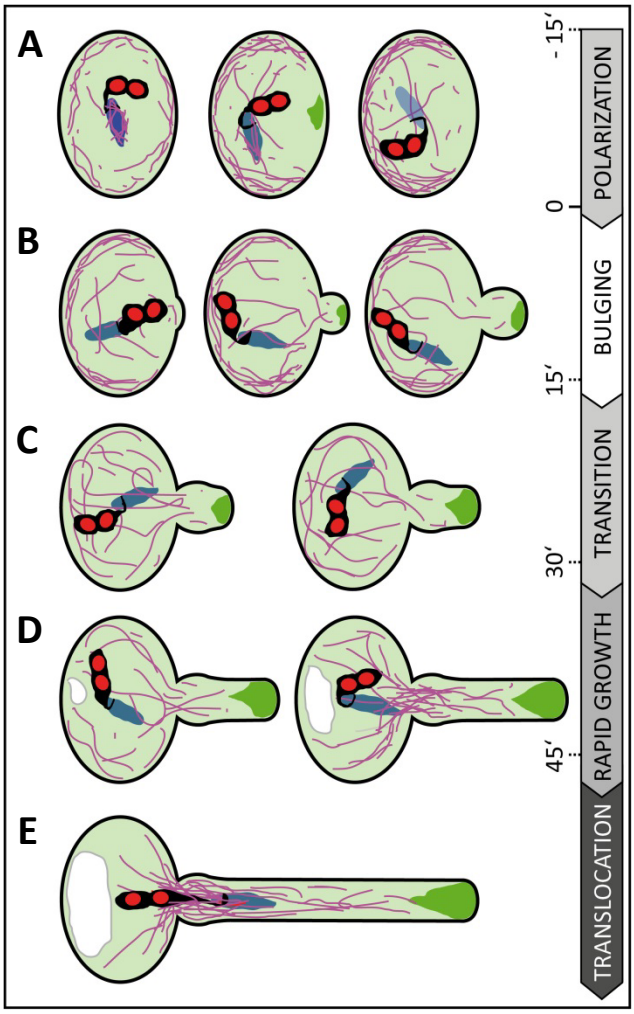

Figure 2.8 | Scheme summarizing subcellular changes observed during different phases of pollen germination and tube growth.

At least five distinct phases are recognized in our live cell imaging studies on in vitro germinating Arabidopsis pollen. **(A)** In early rehydrating pollen F-actin is uniformly distributed at the pollen cell cortex and forms prominent bundles around the vegetative nucleus. Polarization of the pollen grain is indicated by ARO1-GFP decorated vesicles, transiently accumulating subjacent to the future germination site approximately 3 to 20 minutes prior germination, and by F-actin accumulating at the cell periphery, in the half of the pollen vegetative cell opposite to the later germination site. **(B)** During the following bulging phase a local protuberance becomes visible, showing isodiametric expansion. ARO1-GFP decorated vesicles start to accumulate in the bulge and first longitudinal F-actin bundles extend from the grain into the bulge. **(C)** The transition phase is indicated when the bulge becomes slightly tubular-shaped. Transition to tip growth is accompanied by a strong accumulation of ARO1-GFP decorated vesicles in the shape of an inverted cone and by the reorganization of the actin cytoskeleton. The polar dense F-actin at the cell periphery of the pollen grain dissipates and long actin bundles, often oriented towards the emerging PT, arise. **(D)** During the subsequent phase of rapid tip growth the PT area increases significantly. A vacuole is formed in the pollen grain, across from the germination site and F-actin bundles start to extend from within the pollen grain into the pollen tube. The accumulation of ARO-GFP-decorated vesicles in the very tip of the growing pollen tube is most pronounced. **(E)** The translocation phase is initiated when the MGU becomes transported into the growing pollen tube. Sperm cell translocation is preceded by the formation of massive parallel F-actin bundles at the germination site. The vacuole in the pollen grain rapidly enlarges. Objects are not to scale. Color code: purple lines, F-actin; green areas, ARO1-GFP; red areas, sperm cell nuclei; black areas surrounding sperm cell nuclei, sperm cell membranes and cytoplasm; blue area, vegetative cell nucleus. Numbers indicate approximate time points for each phase before or after germination in minutes.

distinct phases (**Figure 2.8**). We observed successive phases of cell polarization before germination, bulge formation at the beginning of PT germination, the transition to polar growth and subsequent initiation of rapid tip growth.

The germination phase is characterized by an emerging pollen tube that shows isodiametric expansion at the germination site. Some longer F-actin bundles become visible during that phase, extending from within the pollen grain into the bulge (**Figure 2.8 B**). The growth rate of the expanding bulge, measured as increase in area over time, is rather slow during the first 15 minutes (16.7 ± 1.1 μm^2), compared with later tube growth of 57.0 ± 4.0 μm^2 at 45 to 60 minutes after germination. In our experimental setup this slower growth phase persists on average 30 minutes and includes the transition phase (**Figure 2.8 C**) in which the bulge slightly elongates and adopts a dome-shaped form before switching to the phase of rapid tip growth. Notably, we observed that the bulge expands while the accumulation of ARO1-GFP associated vesicles at the distal end of the bulge is slightly delayed. The fact that the *Arabidopsis* PT starts forming a uniformly expanding bulge before vesicles massively accumulate at the future site of polar growth suggest that the bulging phase represents a rather turgor-driven deformation process, like assumed by Geitmann (2010). It furthermore indicates that the transition phase was preceded by the selection of a defined plasma membrane region for local exocytosis within the bulge. Thus, the burst of PTs soon after germination, especially observed in a number of pollen mutants such as *aro1-3* and *seth4* (Gebert et al., 2008; Lalanne et al., 2004), may be a turgor-driven event when the establishment of a local growth site was unsuccessful.

ARO1-GFP labeled vesicles heavily accumulate at the distal end of the bulge and finally adopt an inverted cone-like shape (**Supplemental Movie 2.3**). In elongating PTs the inverted cone-shaped zone at their apex is referred to as the 'clear zone', because this region is almost exclusively occupied by vesicles but lacks refracting starch containing amyloplasts (Hepler and Winship, 2015). The establishment of the vesicle-rich 'clear zone' depends on acto-myosin-dependent long distance transport of vesicles towards the tip of the pollen tube. This transport is mediated by F-actin cables, which are oriented parallel to the longitudinal axis of the pollen tube and a cortical network of fine filaments located in the subapical region of the cell (Chebli et al., 2013; Cai and Cresti, 2009). Cortical actin filaments in the shank of angiosperm PTs are believed to be oriented with their barbed ends towards the apex, while the central actin bundles are thought to comprise filaments with the barbed ends pointing backwards (Chebli et al., 2013). The resulting reverse fountain-like cytoplasmic streaming observed in angiosperm pollen tubes is likely to be involved in maintaining the 'clear zone' by producing a constant shear between the anterograde and retrograde transport lanes, by which many of the vesicles, especially those near the surface of the inverted cone, will re-enter the tipward lanes and flow back to the apex (Hepler and Winship, 2015). Thus, the local accumulation and inverted cone-shaped appearance of ARO1-GFP labeled vesicles at the end of the bulging phase indicate that a distinct growth site has been selected,

which also becomes apparent by the change in pollen tube morphology and the increase in the median growth rate in the following transition phase (**Figure 2.8 C**).

When rapid tip growth is initiated (**Figure 2.8 D**), longitudinal actin cables extend from the pollen grain towards the apex of the pollen tube and the volume of the vacuole opposite the germination site continuously increases. We observed the appearance of massive F-actin bundles near the germination site, extending from the pollen grain into the pollen tube, when the pollen tube area reached the average size of 300 μm^2. Likewise, Rhodamine-phalloidin staining of *Pyrus communis* PTs showed articulate staining of actin at the PT base and of cables ranging into the tube (Tiwari and Polito, 1988). Notably, the male germ unit, comprising the two sperm cells associated to the vegetative cell nucleus, is transported from the pollen grain into the pollen tube only when the pollen tube completed its transition to rapid tip growth. In our experimental setup we detected the long membrane extension connecting the leading sperm cell to the vegetative nucleus in the pollen tube when its area is 350 ± 13 μm^2 (**Figure 2.8 E**), which equals to a PT length of 63 ± 2.3 µm. Zhou and Meier (2014) determined a pollen tube length of approximately 35 ± 10 µm when the vegetative cell nucleus permanently enters the PT. This difference may be attributed to a different experimental setup but also to the fact that Zhou and Meier (2014) used a marker line with a mCherry-labeled vegetative nucleus rather than labeled sperm nuclei and membranes as we did. While sperm cell nuclei are spheres, the vegetative nucleus is elongated and irregularly shaped and can reach a remarkable length (>20 µm) in the growing PT.

2.4.2 New insights into Arabidopsis *pollen activation, provided by live imaging of vesicle dynamics and F-actin*

Most pollen grains are metabolically quiescent and highly desiccated (Edlund et al., 2004). They need to attain a certain degree of hydration before they germinate, which will increase the turgor and transform the unpolar pollen grain to a highly polarized cell, a process termed pollen activation. In the past many studies were performed on morphological and ultrastructural changes in activated pollen revealing that, inter alia, the grain starts to organize its cytoskeleton and endoplasmic reticulum, and forms secretory vesicles (Raghavan, 1997 and references cited therein). Depending on the species examined, PTs either grow out of preformed germinal pores (apertures) or break directly through the exine wall, as is the case with *Arabidopsis* pollen grains. The presence of cytoplasmic vesicles subjacent to the aperture was detected by ultrastructural studies on pollen from *Lycopersicum peruvianum*, *Nicotiana alata* and *Narcissus pseudonarcissus* L. (Cresti et al. 1977, 1985; Heslop-Harrison and Heslop-Harrison 1992). However, it is not yet clear, how the pollen perceives external polarization signals and how they are transduced to select the site for tube emergence.

It was reported that the cytoplasmic Ca^{2+} concentration in *Arabidopsis* pollen increases at the potential germination site soon after hydration (Iwano et al., 2004) and that in vitro germination involves the formation of a 'germination plaque' at the future site of tube emergence, containing

cellulose, callose, pectin and at least partly de-esterified pectin (Hoedemaekers et al., 2015). When we performed our live cell imaging on the dynamics of ARO-GFP1 labeled vesicles in hydrating pollen grains we observed the initial appearance of weak transient ARO1-GFP signals, arising at various areas of the pollen cell periphery. However, approximately 3 to 20 minutes before germination either one or two very strong fluorescent peaks of ARO1-GFP labeled vesicles appeared in the region where the PT protoplast will break through the exine, suggesting targeted vesicle secretion and probably local softening of the cell wall at this site. This would be in line with previous assumptions that vesicles filled with cell wall material and cell wall-modifying enzymes are directed towards the future emergence site to produce a local weak point at which the turgor-driven bulge formation is initiated afterwards (Krichevsky et al., 2007; Geitmann and Ortega, 2009; Cai et al., 2011).

The polarization of the actin cytoskeleton towards the site of tube emergence has been reported in activated *Pyrus communis* pollen (Tiwari and Polito, 1988) by using rhodamine-phalloidin labeling. Similar observations were made by TRITC-phalloidin staining for actin in hydrated *Narcissus pseudonarcissus* pollen (Heslop-Harrison and Heslop-Harrison, 1992). Notably, we did not observe a similar pattern of polarization in our live imaging setup with hydrating *Arabidopsis* pollen grains expressing tagRFP-T-Lifeact: F-actin mainly accumulated at the cell periphery opposite to the future germination site and no conspicuous polarization towards the site of tube emergence was observed before PT bulging. We assume that the spatial configuration of actin arrays at the periphery of the other half of the activated *Arabidopsis* pollen grain may form a mechanical counter-bearing for the turgor-driven PT bulging.

Species-dependent variations in F-actin polarization during pollen grain activation would be conceivable, on the other hand previous reports using actin-binding proteins or their actin-binding domains have shown that each F-actin marker produces a different labeling pattern (Thomas et al., 2006; Wilsen et al., 2006; Cheung et al., 2008). However, the distribution of the actin cytoskeleton in hydrating *Arabidopsis* pollen grains by fluorescent phalloidin has, to our knowledge, not been investigated in detail and will be difficult to interpret without having any information about the cellular dynamics before and after the moment of fixation.

2.5 Conclusions

Our live imaging studies on germinating *Arabidopsis* pollen tubes using the described mounting technique revealed characteristic growth phases and kinetics, together with specific spatiotemporal changes in vesicle transport and actin cytoskeletal organization. The method presented here allows the phenotypic assessment of larger numbers of in vitro germinating *Arabidopsis* pollen from wild-type and mutant plants by live imaging. It facilitates the analyses of morphological alterations and growth kinetics, and the identification and subcellular localization of players contributing to cell polarity formation and growth site selection in germinating pollen.

2.6 Summary

Pollen tubes are an excellent system for studying the cellular dynamics and complex signaling pathways that coordinate polarized tip growth. Although several signaling mechanisms acting in the tip-growing pollen tube have been described, our knowledge on the subcellular and molecular events during pollen germination and growth site selection at the pollen plasma membrane is rather scarce. To simultaneously track germinating pollen from up to 12 genetically different plants we developed an inexpensive and easy mounting technique, suitable for every standard microscope setup. We performed high magnification live-cell imaging during *Arabidopsis* pollen activation, germination, and the establishment of pollen tube tip growth by using fluorescent marker lines labeling either the pollen cytoplasm, vesicles, the actin cytoskeleton or the sperm cell nuclei and membranes. Our studies revealed distinctive vesicle and F-actin polarization during pollen activation and characteristic growth kinetics during pollen germination and pollen tube formation. Initially, the germinating *Arabidopsis* pollen tube grows slowly and forms a uniform roundish bulge, followed by a transition phase with vesicles heavily accumulating at the growth site before switching to rapid tip growth. Furthermore, we found the two sperm cells to be transported into the pollen tube after the phase of rapid tip growth has been initiated. The method presented here is suitable to quantitatively study subcellular events during *Arabidopsis* pollen germination and growth, and for the detailed analysis of pollen mutants with respect to pollen polarization, bulging, or growth site selection at the pollen plasma membrane.

CHAPTER 3 *Functional Conserved Armadillo Repeat Only Proteins Act in the Network of Polarity Signaling and Polarized Secretion of* Arabidopsis *Root Hairs*

This chapter was submitted for publication (Vogler et al., submitted). Frank Vogler, Stefanie Sprunck and Pascal Braun designed the experiments. Molecular cloning, the generation of transgenic plant lines and genetic crossings were performed by F.V., as well as bioinformatics analyzes, RT-PCR experiments, phenotyping, physiological experiments, drug treatments, complementation assays and all microscopic techniques. In vivo pull-down experiments, sample preparation for LC-MS/MS analyzes and immunoblot experiments were carried out by F.V.. Jens Steinbrenner and F.V. performed independent yeast two-hybrid screenings at the liquid handling platform of P.B. at the TU Munich. J.S. screened full length DB-ARO constructs and F.V. screened full length and deletion AD- and DB-constructs. Binary yeast two-hybrid verification was performed in quadruplicates by F.V. and P.B.. Direct yeast two-hybrid protein interaction studies between ARO and Exo70 proteins were carried out by Ivan Kulich and Zdeňka Vojtíková (Laboratory of Viktor Žárský, Institute of Experimental Botany of the Academy of Sciences of the Czech Republic, Prague). Transient expression in tobacco leaves, microscopy and quantitative image analyzes were performed by F.V. who also prepared all figures and tables and wrote the manuscript with input from the coauthors.

3.1 Introduction

Cell polarity, generally understood as the asymmetry within a cell, is a key feature of almost all cells (Thompson, 2013). For plants, cell polarity is required over the whole life cycle in all facets of development, morphogenesis and growth (Yang, 2008). Polar growth within a cell can be restricted to a few locations, or can occur at only one single site from which a tubular protrusion emerges (Geitmann and Ortega, 2009). Fungal hyphae, like those of the mucosal disease-causing human pathogen *Candida albicans* (Sudbery, 2011), neurons, algal rhizoids, moss protonemata and higher plant root hairs and pollen tubes grow by an exclusive expansion at a region close to the very tip of a single cell (Geitmann and Ortega, 2009).

Extreme cases of polarized cell growth are often attended by highly specialized functions, as is the case for root hairs and pollen tubes. Root hairs (trichoblasts) are single-epidermis cell protrusions that enormously increase surface and diameter of the root and hence improve plant anchorage and perception of extracellular conditions and nutritional states. Furthermore, they facilitate the uptake of water and ions from the environment and the interactions with other soil organisms (Hofer, 1991; Grierson et al., 2014). By root hair mutant analyzes, the process of root hair development was subdivided morphologically and genetically in the distinct processes of trichoblast

cell fate determination, local swelling formation (also called bulging), transition to tip growth and finally polar elongation (Schiefelbein and Sommerville, 1990; Parker et al., 2000). Pollen tubes of flowering plants start to emerge from the pollen grains upon landing on the stigma of a receptive pistil, with the goal to deliver their non-motile sperm cell cargo to the embryo sacs that are deeply embedded in the protective female floral tissues (Raghavan, 2003). On its journey the pollen tube has to integrate dozens of signals to penetrate the stigma and to direct its growth towards the ovule to render possible double fertilization (Higashiyama and Takeuchi, 2015). As recently shown for *Arabidopsis thaliana*, in vitro pollen tube growth kinetics also comprises distinct phases including bulging, transition to tip growth and rapid tip elongation (Vogler et al., 2015).

Root hairs and pollen tubes possess a highly polarized intracellular organization with a growth-controlling zone that resides at the very tip. The apical dome is a hot-spot for polarized exo- and endocytosis (Camapanoni and Blatt, 2007; Ketelaar et al., 2008) to provide new plasma membrane, cell wall materials and regulatory proteins for sustained growth. Critical cellular activities during tip growth are a tip-derived calcium gradient, the spatial organization and dynamics of F-actin, polarized membrane trafficking, the local activity of ion channels and plasma membrane receptor-like kinases, the production of reactive oxygen species (ROS), and controlled cell wall modifications (Cheung and Wu, 2008; Qu et al., 2015; Qin and Dong, 2015). Key regulators of polar tip growth are signaling pathways controlled by small Rho of plant (ROP) GTPases, Ca^{2+}, and phosphoinositides (Ischebeck et al., 2008; Craddock et al., 2012; Guan et al., 2013). Rab GTPases serve as master regulators for intracellular membrane trafficking and the exocyst complex plays essential roles in secretory vesicle targeting and docking at the plasma membrane during exocytosis (Nielsen et al., 2008; Žárský et al., 2013).

Small GTPase ROPs are fundamental signaling switches for cell polarity. They cycle between the GTP-bound active and GDP-bound inactive forms and bind to their downstream effector proteins in a GTP/GDP-dependent manner, in response to external cues. The spatial restriction of active ROPs to the growing tip is crucial for tubular expansion of both, root hairs and pollen tubes (Kost, 2008; Craddock et al., 2012). The regulation of ROP activity is mainly controlled by two classes of proteins, the guanine nucleotide-exchange factors (RhoGEFs) and GTPase activating proteins (RhoGAPs) which function in dynamic ROP activation and inactivation and thus influence the polar tip growth machinery including actin dynamics and vesicle trafficking.

We have shown earlier that one member of the conserved family of plant-specific ARMADILLO REPEAT ONLY (ARO) proteins, ARO1, is important for polar tip growth in *Arabidopsis* pollen tubes (Gebert et al., 2008). *ARO1* loss-of-function mutants are male sterile and show about 50 % mutant pollen tubes that are very short and thick or directly burst after germination. Pharmacological treatments as well as live-cell imaging and TIRF microscopy revealed that ARO1 is associated to vesicles of the secretory machinery in the growing tip of pollen tubes (Gebert et al., 2008; Vogler et al., 2015). While *ARO1* is expressed exclusively in gametophytes, transcripts of the other three members of the small *Arabidopsis* gene family (*ARO2, ARO3, ARO4*) were not detectable

in pollen but in tissues of the sporophyte (Gebert et al., 2008). However, so far no role for the sporophyte-expressed *ARO* genes has been assigned.

Here we show that the double knock-out of two members of the *ARO* gene family, *ARO2* and *ARO3*, interferes with proper root hair tip growth. Root hairs of *aro2 aro3* double mutants are short and bloated and arrest development prior to polar elongation. Functional redundancy of ARO1, ARO2, and ARO3 proteins is demonstrated, as mutant pollen and root hair phenotypes can be restored by ectopic expression of another ARO family member. However, the more distant ARO4 can only partially rescue mutant phenotypes.

Promoter and gene reporter studies revealed that *ARO3* expression is enriched in trichoblasts, while *ARO2* is additionally expressed in other root tissues. *ARO2* and *ARO3* as C-terminal GFP fusion localize to the vesicle-rich clear zone of actively growing root hairs. Tip-localization of ARO3-GFP is Brefeldin A (BFA) sensitive, suggesting its association to vesicles of the secretory machinery, similar to ARO1-GFP in pollen tubes (Gebert et al., 2008).

By expressing fluorescent marker proteins in root hairs of the wild-type and *aro2 aro3-1* mutant we observed that mutant root hairs display a disturbed F-actin organization and an enlarged YFP-ROP2 area at the distal plasma membrane of the root hair bulge. Most notable has been the completely nonpolar localization of the YFP-RabA4b-labeled Trans-Golgi Network (TGN) and secretory vesicles (SV) in the *aro2 aro3-1* mutant root hairs. A role for ARO3 in polarized membrane trafficking was furthermore supported by yeast two-hybrid and pull-down experiments using ARO3 as bait. These experiments revealed ARO3 protein interactions with a ROP-ENHANCER 1 (REN1)-like RhoGAP and Pleckstrin homology domain protein (RhoGAP/PH), with the vesicle-tethering complex subunit Exo70E2 and the dynamin-like GTPase Root Hair Defective 3 (RHD3), suggesting ARO3 to be a molecular linker between the secretory machinery and ROP signaling.

3.2 Material and Methods

All oligonucleotide primers used in this work are specified in the **Supplemental Data** file.

3.2.1 Plant material and plant growth

The T-DNA insertion lines *aro1-3* (SALK_033785), *aro2-1* (SALK_003387), *aro3-1* (SALK_136769), *aro3-2* (SAIL_1157_F02), *rhogap/ph-1* (SALK_11590), *exo70e2-1* (GA-BI_072F12) and *rhd3-7* (SALK_106309) were generated by the Salk Institute Genomic Analysis Laboratory (SALK [Alonso et al., 2003]), Syngenta (SAIL [Sessions et al., 2002]) and GABI-Kat (Rosso et al., 2003). The double mutants *aro2 aro3-1* and *aro2 aro3-2* were generated by crossing respective T-DNA lines. The $ARO1_{pro}$*:ARO1-GFP* line was from Gebert et al. (2008) and the $Lat52_{pro}$*:GFP* line from Twell et al. (1990). *Arabidopsis thaliana* (ecotype Columbia-0 [Col-0]) plants were grown on soil under a long photoperiod (16 h of light, 22 °C, 70% humidity).

3.2.2 Bioinformatic analyzes

ARO protein sequences were aligned using the ClustalW algorithm implemented in the EMBL-EBI platform (www.ebi.ac.uk). A phylogenetic tree was computed with SeaView 3.2 using the Neighbor-Joining method. Identity and similarity matrices were created with the SIAS tool (http://imed.med.ucm.es/). *ARO* expression values were extracted from microarray data using the GENEVESTIGATOR software (Zimmermann et al., 2004). Disordered protein regions were predicted by ELM on http://elm.eu.org (Dinkel et al., 2013).

3.2.3 Analysis of T-DNA insertion lines and Reverse Transcriptase PCR

Genomic DNA was isolated using the innuPREP Plant DNA kit (Analytik Jena). T-DNA integrations were identified by PCR using gene-specific primer pairs for *aro1-3* (a1LP/a1RP), *aro2-1* (a2LP/a2RP), *aro3-1* (a3LPsalk/a3RPsalk), *aro3-2* (a3LPsail/a3RPsail), *aro4-1* (a4LP/a4RP), *rhogap-1* (rhogapLP/rhogapRP) and *exo70e2-1* (exo70e2LP/exo70e2RP) as well as a combination of the T-DNA specific primers LBb1.3 (SALK-lines), LB3 (SAIL-line) or GK_08409 (GABI-line) with gene-specific primers. The Dynabeads® mRNA DIRECT™ Kit was used to isolate mRNA from leaves of T-DNA insertion lines. The SuperScript® III Reverse Transcriptase and Oligo(dT) primers were used for cDNA synthesis according to the manufacturer's recommendations (Life Technologies). Genomic DNA contamination of cDNA was excluded by PCR using intron flanking housekeeping gene primers (ACT3LP/ACT3RP). Expression levels of *ARO* genes were tested with gene specific primers (a2LP/a2RP, a3salkLP/a3salkRP and a4LP/a4RP).

3.2.4 Generation of constructs

Promoter sequences of *ARO* genes were amplified from Col-0 genomic DNA using the primer pairs A2pLP/A2pRP (*ARO2*), A3pLP/A3pRP (*ARO3*) and A4pLP/A4pRP (*ARO4*) and cloned into the pENTR™D/TOPO® vector according to the manufacturer's recommendations (Life Technologies). To drive NLS3xeGFP reporter expression, entry clones were recombined with the pGII-NLS3xeGFP destination vector (Zheng et al. 2011) by LR Clonase® reaction according to the manufacturer's protocol (Life Technologies).

The *ARO2*$_{pro}$*:ARO2* and *ARO3*$_{pro}$*:ARO3* sequences were amplified from Col-0 genomic DNA with the A2pLP/A2RPmdc and A3pLP/A3RPmdc primer pairs and cloned into pENTR™D/TOPO®. Entry clones were recombined with pMDC206-sGFP (derived from pMDC206 [Curtis and Grossniklaus, 2003], Ulrich Hammes, unpublished) by LR Clonase® reaction to obtain constructs for ARO2-GFP and ARO3-GFP expression under its' endogenous promoters.

Ectopic ARO expression was driven by the *ARO1* promoter in pollen and by the *ARO3* promoter in root hairs. Both promoters were amplified from genomic DNA with the primers A1pSac/A1pSpe and A3pSac/A3pSpe that generated 5' *Sac*I and 3' *Spe*I restriction sites in the amplicons. The *35S* promoter of pB7FWG2.0 or pH7FWG2.0 (Karimi et al., 2002) was excised by *Sac*I/*Spe*I digestion and replaced by ligation of the *ARO1* or the *ARO3* promoter to obtain the pB7-ARO1$_{pro}$:GW-GFP and pH7-ARO3$_{pro}$:GW-GFP destination vectors. The coding sequences (CDS) of *ARO1*, *ARO2*, *ARO3* and *ARO4* were amplified from genomic DNA using the primers A1LP/A1RP, A2LP/A2RP, A3LP/A3RP and A4LP/A4RP and cloned into pENTR™D/TOPO®. The resulting entry vectors pENTR-ARO3 and pENTR-ARO4 were recombined with pB7-ARO1$_{pro}$:GW-GFP and the entry vectors pENTR-ARO1 and pENTR-ARO4 with pH7-ARO3$_{pro}$:GW-GFP by LR Clonase® reaction. To generate a construct for ectopic expression of ARO2-GFP under control of the *ARO1* promoter, the *ARO2* CDS was amplified from genomic DNA and used to replace the ARO1 CDS in pLNG-ARO1$_{pro}$:ARO1-GFP (Gebert et al., 2008). The expression cassette from the resulting pLNG-ARO1$_{pro}$:ARO2-GFP vector was transferred into p95-NOS (DNA Cloning Service) by *Sfi*I digestion and ligation to obtain the binary vector p95N-ARO1$_{pro}$:ARO2-GFP.

The *35S*$_{pro}$*:eGFP* construct was generated by *eGFP* amplification from pB7FWG2.0 (Karimi et al., 2002) with the primers eGFPLP/eGFPRP, insertion of the PCR product into pENTR™D/TOPO® and LR Clonase® reaction with the destination vector pB2GW7 (Karimi et al., 2002).

The *UBI10*$_{pro}$*:tagRFP-T-Lifeact* construct was created by recombination of pENTR-tagRFP-T-Lifeact (Vogler et al., 2015) with the pMDC123 (Curtis and Grossniklaus, 2003)-based destination vector pKB31 (Ulrich Hammes, unpublished) by LR Clonase® reaction. *Arabidopsis* plants were transformed by floral dipping (Clough and Bent, 1998).

For yeast two-hybrid interaction screening, full-length or fragment *ARO1-4* sequences were amplified from genomic DNA (for details see **Supplemental Data**), cloned into pENTR™D/TOPO® and recombined with AD and DB yeast expression destination vectors (Dreze et al., 2010) by LR Clonase® reaction.

To test interactions between ARO and Exo70 proteins, we performed an independent directed yeast two-hybrid assay. As all *ARO* and *Exo70* genes represent single exon genes, genomic DNA has been used for amplification of the CDS. Amplified fragments were purified, digested and ligated into pGBKT7 and pGADT7 (Clontech). Restriction sites are indicated in the primer list (**Supplemental Data**). All constructs have been sequenced.

Constructs for transient expression in tobacco leaves were created by amplification of candidate genes from root cDNA, cloning into pENTR™D/TOPO® and recombination with destination vectors harboring *GFP* or *mCherry* fluorophores under control of the estradiol inducible *lexA-46 35S* promoter (Bleckmann et al., 2010) by LR Clonase® reaction.

3.2.5 Root hair mutant characterization

To analyze root hairs, seeds were surface-sterilized by washing twice with 70 % EtOH, 0.1 % Triton X-100 for 10 minutes, followed by washing twice with 96 % EtOH for 5 minutes and subsequent washing twice with water. Seeds were placed on plates containing MES buffered half-strength MS medium (M0255, Duchefa), 2 % sucrose, pH 5.7 and solidified with 1 % PhytoAgar (Duchefa). Root hair-inducing growth media lacking phosphate were prepared according to Müller and Schmidt (2004) or were generated by adding 1-Naphthaleneacetic acid (NAA [Duchefa]) in a final concentration of 100 nM from a 100 µM stock solution to the above described half-strength MS medium. Plates were stratified for 2 days at 4 °C in the dark and root hairs were analyzed 10-14 days after sowing. The number of root hair bulges was counted and root hair length was measured manually for 10 seedlings per genotype and treatment in ImageJ. Oneway-ANOVAs with subsequent Bonferroni-corrected pairwise t-tests were calculated with SPSS 22 (IBM).

3.2.6 Drug treatments

14 days old seedlings of ARO3-GFP expressing lines in the *aro2 aro3-1* mutant background were treated with the drug BrefeldinA (BFA [Sigma]) dissolved in DMSO at a final concentration of 25 µM and 0.2 % DMSO in 2 % sucrose. Equal amounts of the solvent in 2 % sucrose were used as controls. Images were acquired 30 to 45 minutes after roots treatments.

3.2.7 Complementation assays

Root hairs of mutant or wild-type plants, or plants expressing complementation constructs in the mutant background were measured manually as segmented lines using ImageJ. For each genotype, the 50 basal most root hairs of 5 plants were measured. Homozygous lines ectopically expressing *ARO2-4* constructs in pollen were crossed with the *aro1-3*/+ mutant (Gebert et al., 2008). In at least three independent experiments for each genotype, pollen was germinated in vitro on solidified germination medium (Li et al., 1999) and analyzed according to Gebert et al. (2008). All plant genotypes were confirmed by PCR using gene specific primers (see **Supplemental Data**) and by sequencing of PCR products. Mean values were compared in oneway-ANOVAs and subsequent pairwise Bonferroni-corrected t-tests using SPSS 22 (IBM).

3.2.8 Microscopy

Seedlings and roots were analyzed on a ZEISS Discovery V8 Zoom Stereo microscope or a ZEISS Axioskop FL epifluorescence microscope. At the Stereo microscope, a 495 nm excitation and a 500-550 nm band pass emission filter were used for GFP imaging. Microscopy of petri dishes with in vitro germinated pollen tubes, imaging of plants expressing the NLS3xeGFP reporter constructs and monitoring of BFA treated root hairs was performed on an inverted Eclipse TE2000-S microscope (Nikon). To image GFP fluorescence, a 495 nm excitation and a 503-538 nm band pass emission filter were used. Expression of fusion proteins in roots and root hairs was analyzed at an inverted TCS SP8 confocal laser scanning microscope (Leica). The pinhole was always set to maximum 1 airy unit. GFP was excited with a 488 nm laser line, YFP with a 514 nm laser line and tagRFP-T and mCherry with a 561 nm laser line. HyD™ detectors were used for fluorophore emission detection. GFP emission was detected from 500-545 nm, YFP emission from 520-560 nm and tagRFP-T and mCherry emission from 580-640 nm. Live cell imaging of growing pollen tubes was performed according to Vogler et al. (2015) on solidified pollen germination medium (Li et al., 1999). Surface sterilized seeds were placed on growth medium containing cover slip-bottom chamber slides (x-well®, Sarstedt) allowing non-invasive monitoring of root hair growth. Live cell imaging of root hairs and pollen tubes was performed on a ZEISS Cell Observer Spinning Disc (Yokogawa CSU-X1) confocal microscope system. GFP was excited with a 488 nm laser line and emission was detected from 505-545 nm. All images were processed and analyzed in ImageJ (http://rsbweb.nih.gov/ij, version 1.45).

3.2.9 In vivo pull-down and Western Blotting

Roots of sterile cultured 2-3 week-old plants grown on MES buffered half-strength MS medium (M0255, Duchefa), 2 % sucrose, pH 5.7, solidified with 1 % PhytoAgar (Duchefa) and supplemented with 50 nM NAA (Duchefa) were cut, frozen in liquid nitrogen, homogenized and resuspended in protein extraction buffer (50 mM Tris/HCl pH 7.5, 150 mM NaCl, 10 mM

EDTA, 0.5 % Triton X-100, 5 mM DTT, 1 mM PSF, 50 µM MG132, Protease Inhibitor Complete [Roche]). Cell debris was centrifuged twice for 5 minutes at 13,000 g and 4 °C. The supernatant was diluted 1:5 with dilution buffer (50 mM Tris/HCl pH 7.5, 150 mM NaCl, 10 mM EDTA, 5 mM DTT, 1 mM PMSF, 50 µM MG132, Protease Inhibitor Complete [Roche]). After adding 20 µL of washed GFP-Trap_M beads (Chromotek) the suspension was inverted at 20 rpm for 1 hour at 4 °C. A magnetic rack was used to remove the supernatant. Beads were washed three times with cold wash buffer (50 mM Tris/HCl pH 7.5, 150 mM NaCl, 10 mM EDTA, 0.1 % Triton X-100). Samples were boiled in 2x sample buffer at 95 °C for 5 minutes prior to SDS-PAGE. Bands were cut of the gel, proteins isolated and trypsin digested prior to LC-MS/MS analysis on an Ultimate 3000 RSLC nano (Dionex) and a UHR-Q-TOF system (Maxis Plus, Bruker). Duplicate SDS gels were used for Western Blot analyzes. Blots were probed with a monoclonal anti-GFP primary antibody (Roche) and a HRP conjugated anti-mouse secondary antibody (Sigma).

3.2.10 Yeast two-hybrid screening

Screening of ARO protein interaction partners was performed on a robotic high-throughput platform according to Dreze et al., (2010). For this, a collection of about 8,000 *Arabidopsis* open reading frames (*Arabidopsis* Interactome Mapping Consortium, 2011) was extended with about 4,000 additional open reading frames. This collection was screened in AD and DB direction against all four full-length ARO proteins, as well as against 28 ARO protein fragments which lacked N- or C-terminal domains, Armadillo Repeat Domains, or the Spacer Domains (for details see **Supplemental Data**). Interactions were tested on –LTH + 1 mM 3-Amino 1,2,4-triazole (3AT) media and autoactivation was tested on –LH + 1mM 3AT + 1 mg/L cycloheximide (CHX) plates. Yeast interactions were verified in quadruplicates and scored as positive only if interactions were visible in at least 3 of 4 cases according to Dreze et al. (2010).

The directed yeast-two hybrid assay between ARO and Exo70 proteins, was performed using the Matchmaker GAL4 Two-Hybrid System 3 (Clontech), following the manufacturer's instructions. The yeast strain AH109 (MATa, trp1-109, leu2-3, 112, ura3-52, his3-200, gal4Δ, gal80Δ, LYS2 GAL1UAS-GAL1TATA-HIS3, MEL1, GAL2UAS-GAL2TATA-ADE2, URA3 MEL1UAS-MEL1TATA-lacZ) was simultaneously transformed with both constructs for all combinations presented. Yeasts were plated on –LT media and then transferred to –LTH + 1mM or 10 mM 3AT media and pictured after 4 days.

3.2.11 Transient gene expression in tobacco leaves

An estradiol-inducible transient expression system was used for transformation of 4-week-old *Nicotiana benthamiana* plants according to Bleckmann et al. (2010) with the exception that

we did not use the silencing suppressor p19. Transgene expression was induced 48 h after infiltration with 20 µM β-estradiol in 0.1 % Tween20 and 20 h before microscopy.

3.2.12 Accession numbers

Sequence data from this article can be found in GenBank/EMBL or *Arabidopsis* Genome Initiative identifiers: At4g34940 (*ARO1*), At5g66200 (*ARO2*), At4g36030 (*ARO3*), At3g26600 (*ARO4*), At5g19390 (*RhoGAP/PH*), At5g61010 (*Exo70E2*), At3g13870 (*RHD3*).

3.3 Results

3.3.1 The promoters of the closely related ARO2 and ARO3 genes are active in root hair cells

We generated transgenic plants that express the GUS reporter under control of each of the promoter of sporophyte-expressed *ARO* genes (At5g66200 (*ARO2*), At4g36030 (*ARO3*), At3g26600 (*ARO4*)) and investigated the reporter activity in 10 day old seedlings (**Figure 3.1 A-C** and **Figure S3.1**). Both, the *ARO2* and *ARO3* promoter were active in the tip and the base of the cotyledons, the first leaves, in the stipules, the hypocotyls and in the roots. The *ARO3* promoter showed a pronounced reporter activity throughout the root. The *ARO2* promoter is highly active in the primary root and in the root cap of primary and lateral roots. Overall, the activity of both promoters in the tissues of germinated seedlings was similar to a large extent except for root caps and the expression level in root hairs. By contrast, the GUS reporter driven by the *ARO4* promoter revealed a different pattern of activity (**Figure 3.1 C** and **Figure S3.1 D, G, J, M**). Here we observed strong reporter signals in the hypocotyl, the stem, stipules, the vasculature of leaves and in stomata. In the root, *ARO4* promoter activity was detected adjacent to the hypocotyl, in the vasculature and in the tip excluding the root cap. Only weak reporter signals were seen in other parts of the root.

The similarities between the *ARO2* and *ARO3* promoter activity are also reflected by their phylogenetic relationship. Within the small *Arabidopsis* ARO protein family, ARO2 and ARO3 are the most closely related ones (**Figure 3.1 D** and **Table S3.1**). Both proteins are also closely related to ARO1. The lowest identity and similarity is found in comparisons with ARO4.

To obtain a refined pattern of *ARO* expression in roots and other tissues and cell types of *Arabidopsis*, we analyzed publically available microarray data using the GENEVESTIGATOR database (Zimmermann et al., 2004) (**Figure 3.1 E** and **Figure S3.1**). As expected, *ARO1* was not expressed anywhere in the root. The *ARO2* and *ARO4* genes showed a uniform expression in all root tissues and cell types, but the expression level was markedly higher for *ARO2* than for *ARO4*. In contrast, *ARO3* showed a non-uniform expression pattern. While in the root tip, the root

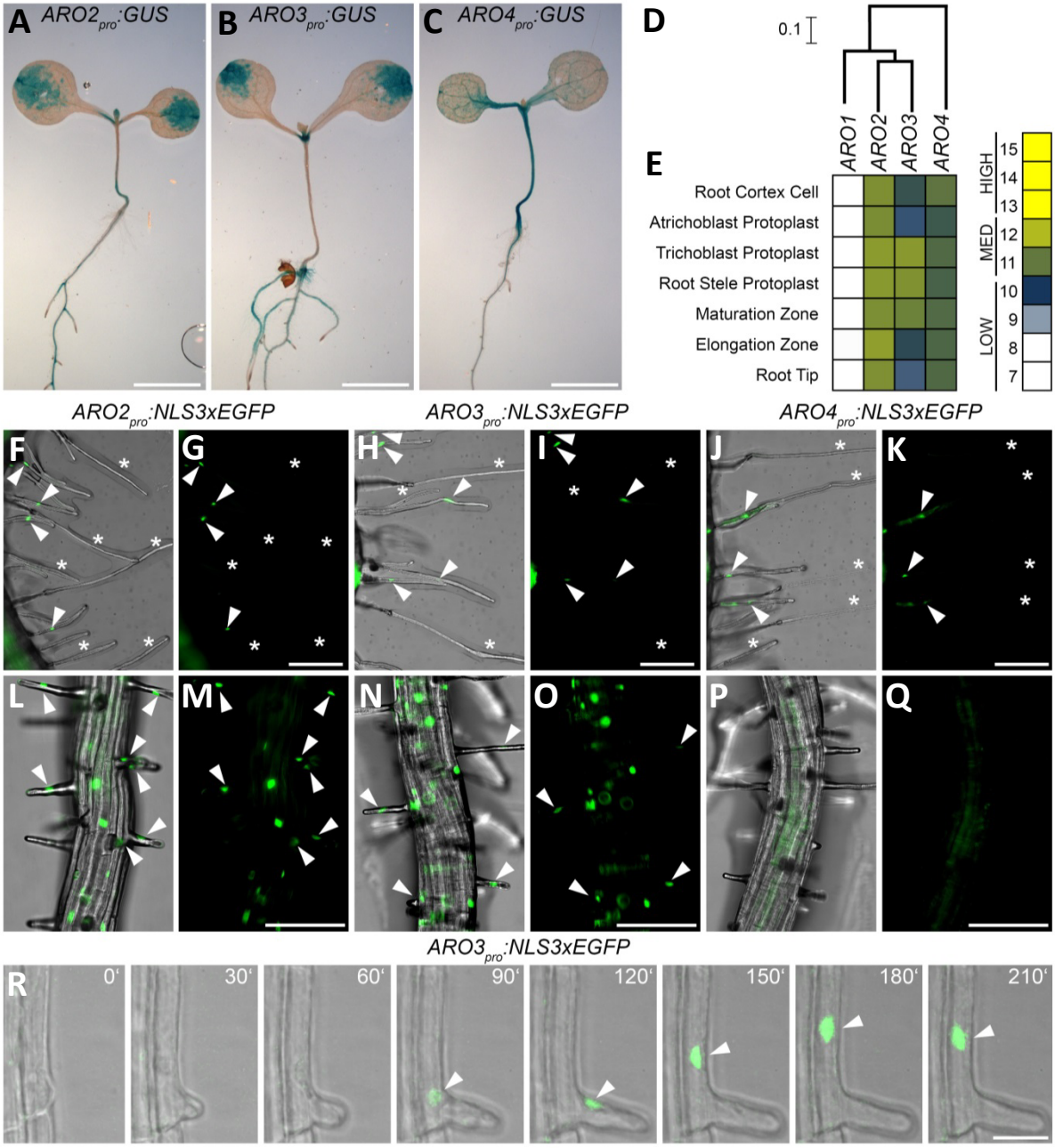

Figure 3.1 | Expression of *ARO* genes in *Arabidopsis* roots.

(A) to **(C)** *ARO2 -4* promoter activity in 10 day old seedlings as indicated by the GUS reporter system. Note the similarity in the activity of the *ARO2* and *ARO3* promoters in leaves and roots. **(D)** Phylogenetic relationship of *Arabidopsis* ARO proteins using the ClustalW alignment and the Neighbor-Joining algorithm. Bar = amino acid substitutions per site. **(E)** Expression of *ARO2-4* genes in different root parts and root cell types according to the GENEVESTIGATOR microarray database (Zimmermann et al., 2004). Numbers give log2-fold expression values. **(F)** to **(K)** Activity of the *ARO2-4* promoters in 4 day old parts of the root is indicated by the NLS3xeGFP reporter signal. Arrowheads indicate root hairs with nuclear localized reporter signals. Asterisks indicate root hairs that do not show reporter activity. **(L)** to **(Q)** Activity of the *ARO2-4* promoters in the root differentiation zone is indicated by the NLS3xeGFP reporter signal. Arrowheads indicate root hairs with nuclear localized reporter signals. **(R)** Time course of the NLS3xeGFP reporter signal under control of the *ARO3* promoter in a root hair cell. Arrowheads indicate reporter fluorescence in the nucleus. Numbers indicate minutes after acquisition start. Bars = 100 µm in (A) to (C) and (F) to (Q) and 15 µm in (R).

elongation zone, in atrichoblast protoplasts and root cortex cells the *ARO3* expression was low, a considerably higher expression level was observed in the root maturation zone, the root stele and in trichoblast protoplasts (**Figure 3.1 E**).

To further validate the microarray-based expression data with a cellular resolution, we created transgenic lines in which the *ARO2* to *4* promoters were used to drive the expression of a nuclear localized NLS3xeGFP reporter. We investigated roots of representative T3-lines on the presence of nuclear localized GFP using epi-fluorescence microscopy (**Figure 3.1 F-R**). In older parts of the root where most of the root hairs had already stopped polar elongation, root hair cells showed no or only weak reporter signals when the NLS3xeGFP expression was driven under control of the *ARO2-4* promoters (**Figure 3.1 F-K**). In contrast, newly emerging root hair cells from the root maturation zone showed strong nuclear localized reporter signals when under control of the *ARO2* or *ARO3* promoter (**Figure 3.1 L-O**). Notably, no reporter signal was observed in growing root hair cells from the root maturation zone when the *ARO4* promoter was used to drive reporter expression (**Figure 3.1 P-Q**).

In a time-lapse imaging experiment we investigated the appearance of the *ARO3* promoter driven NLS3xeGFP reporter signal in developing root hair cells. Shortly after trichoblast bulging and prior to the polar elongation of the root hair, the nuclear localized reporter signal became visible (**Figure 3.1 R**). Although there is likely a certain delay between the true start of promoter activity and the microscopic detectability of the NLS3xeGFP reporter, we concluded that the considerable late occurrence of the reporter signal is indicative of a function of the ARO3 protein in later stages of root hair formation but not root hair differentiation or bulging.

3.3.2 Double knock-out of ARO2 *and* ARO3 *causes short and swollen root hairs*

In a reverse genetics approach we analyzed T-DNA insertion lines for *ARO2* (*aro2-1*), *ARO3* (*aro3-1* and *aro3-2*), and *ARO4* (*aro4-1*). In all cases, the homozygous single T-DNA insertion lines did not show any obvious phenotype in aerial parts or in roots (**Figure S3.2**). We confirmed the absence of *ARO2, ARO3* and *ARO4* transcripts in the T-DNA insertion mutants by RT-PCR (**Figure 3.2 A-D** and **Figure S3.2**). In all cases, the T-DNA insertions generated null alleles.

We assumed that ARO2 and ARO3 proteins could act functionally redundant as the ARO2 and ARO3 proteins are closely related (**Figure 3.1 D** and **Table S3.1**) and the *ARO2* and *ARO3* promoters showed a comparable pattern of activity (**Figure 3.1 A**). We therefore generated the *aro2 aro3-1* and *aro2 aro3-2* double homozygous knock-out lines by crossing the respective single knock-outs and investigated the progeny. Whereas in aerial parts of the double knock-out lines no phenotype was observable and root lengths were comparable (**Figure S3.2**), both lines exhibited identical severe defects in root hair development (**Figure 3.2 E-I**). In the double mutants,

the root hairs were shorter and thicker than in wild-type plants. We also observed root hairs that were either burst or showed extreme swellings at the base or the tip (**Figure 3.2 H**).

To confirm that the root hair mutant phenotype is caused by the loss of functional ARO protein, we complemented the double homozygous mutant with an *ARO3$_{pro}$:ARO3-GFP* construct. By that we fully restored wild-type root hair morphology (**Figure 3.3 A**).

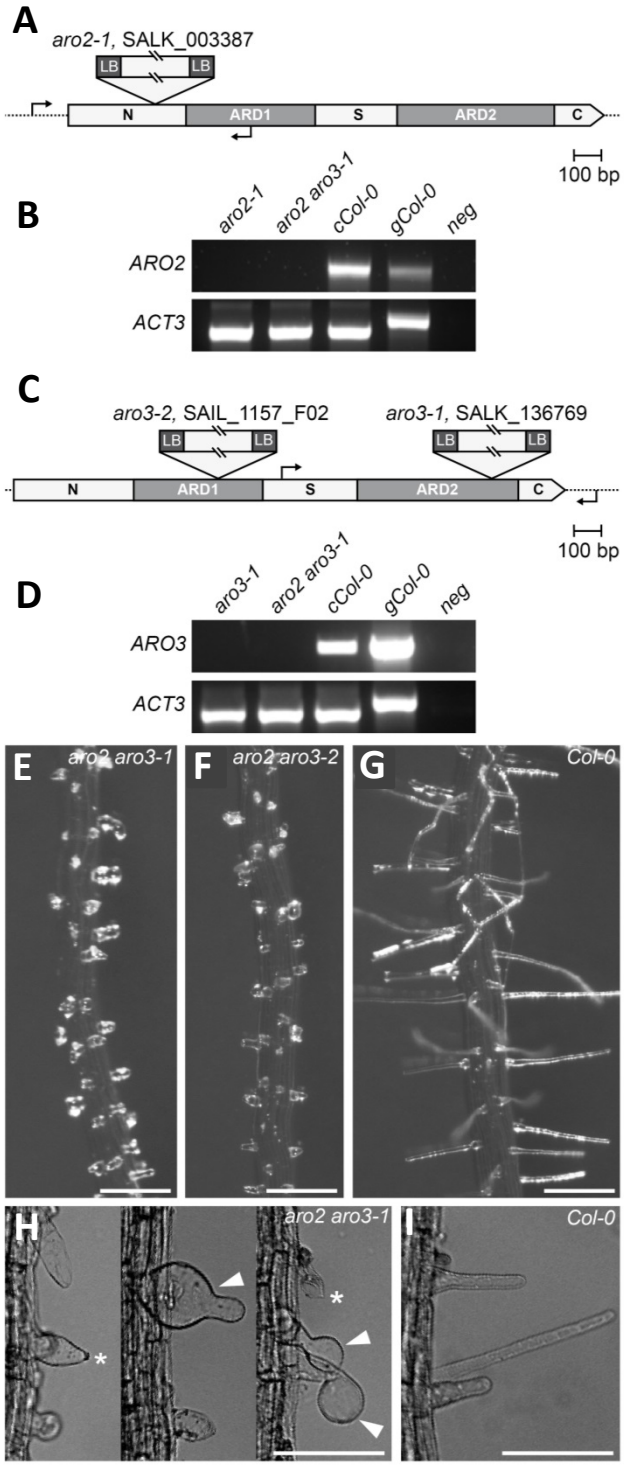

Figure 3.2 | Phenotyping of *aro2 aro3* double knock-out mutants.

A) and **(C)** Genomic structure of the *ARO2* and *ARO3* genes. Armadillo Repeat Domains according to Gebert et al. (2008) are indicated by light grey boxes. Positions of tandem-inverse integrated T-DNAs are indicated for the *aro2-1, aro3-1* and *aro3-2* insertions. Arrows indicate genotyping and expression analysis primer positions and dashed lines 5' and 3' UTR sequences. N, N-terminal domain; ARD, armadillo repeat domain; S, spacer region; C, C-terminal domain. Bars = 100 base pairs in (A) and (C). **(B)** and **(D)** RT-PCR using cDNA generated from leaf mRNA isolated from the *aro2-1* and *aro3-1* single and the *aro2 aro3-1* double T-DNA insertion lines as well as from wild-type. Wild-type gDNA and water were used as PCR controls. Gene specific primers for *ARO2* and *ARO3* were used as well as gene-specific, intron-spanning primers for *Actin 3 (ACT3)* which results in a larger *ACT3* amplicon on gDNA. **(E)** and **(F)** Morphology of roots of double homozygous *aro2 aro3-1* and *aro2 aro3-2* T-DNA insertion mutants. **(G)** Morphology of wild-type roots grown on the same plates as the mutants. **(H)** Different root hair morphologies observed for the *aro2 aro3-1* mutant. Asterisks indicate burst root hairs. Arrowheads point to root hairs that showed ballooning at the base or the tip. **(I)** Morphology of wild-type root hairs grown and imaged under identical conditions. Bars = 250 µm in (E) to (G) and 50 µm in (H) and (I).

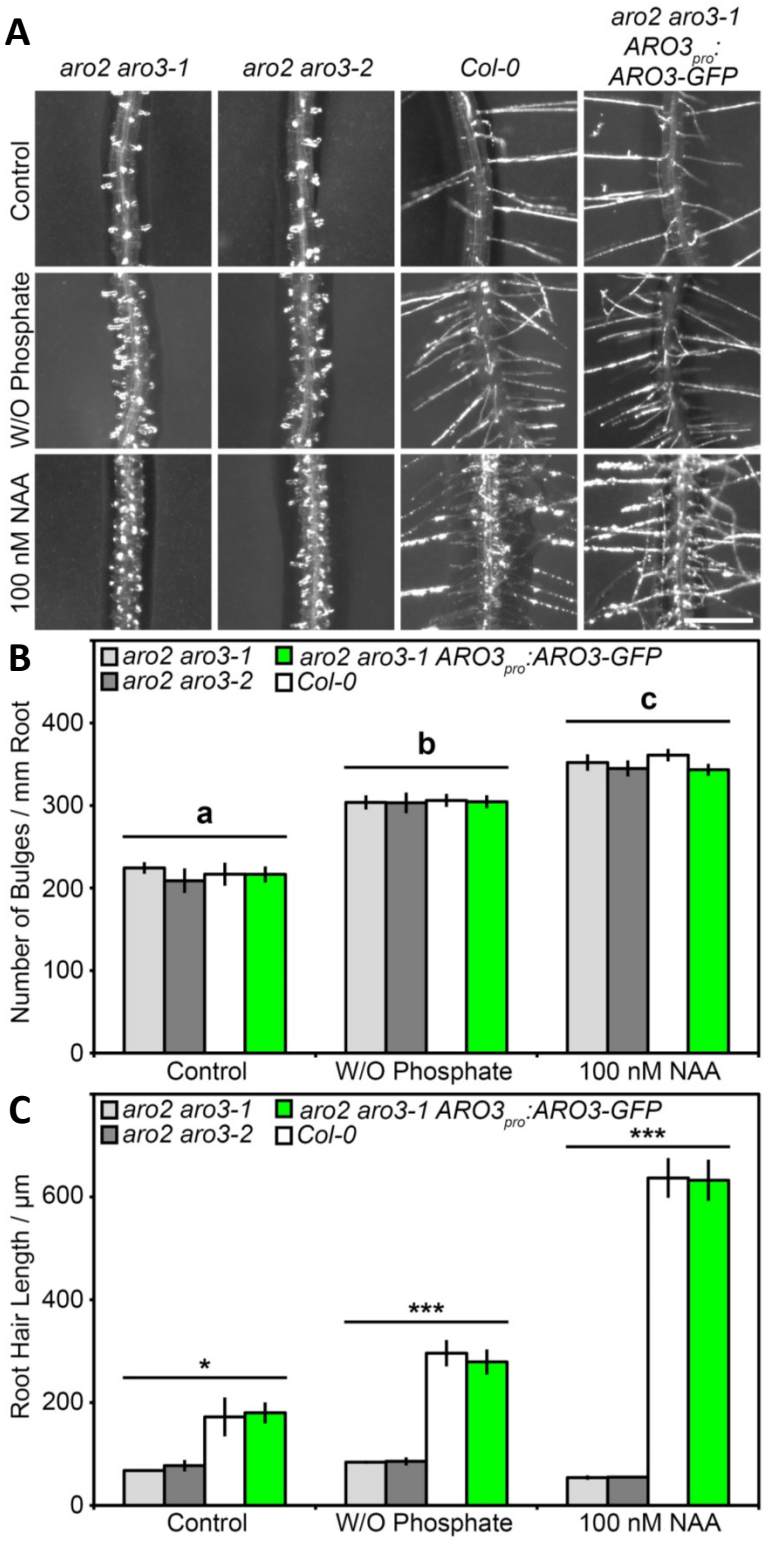

Figure 3.3 | Characterization of the *aro2 aro3-1/2* double mutant phenotypes.

(A) Seeds of the *aro2 aro3-1* and *aro2 aro3-2* double knock-out lines, as well as seeds of the wild-type and complementing mutant plants were grown on control medium and on root hair-inducing media that either lacked phosphate or contained the auxin analog NAA. **(B)** and **(C)** Mean (±1SE, n=10) number of bulges per mm root and root hair length of the mutant and control lines grown on control and on root hair-inducing media. Bars with different letters in (B) display significant differences ($p < 0.05$). Asterisks in (C) indicate significant differences ($p < 0.05$*, $p < 0.01$**, $p < 0.001$***). Bar = 500 µm in (A).

3.3.3 The ARO2 and ARO3 proteins act during polar root hair elongation

In *Arabidopsis* the development of a root hair from a trichoblast cell comprises the stages of cell fate determination, the formation of a local swelling, the so called bulge, the transition to tip growth and the root hair elongation by polar tip growth (Schiefelbein and Somerville, 1990; Parker et al., 2000). To identify which stage of root hair development is compromised by the loss of the ARO2 and ARO3 protein function, we further characterized the *aro2 aro3-1* and *aro2 aro3-2* double mutants by their behavior on different growth media. In wild-type roots, the lack of phosphate in growth media leads to an increased number of root hair initiation sites and an increased length of root hairs (Müller and Schmidt, 2004; Wada et al., 2015). Root hair mutants can behave differently under this growth regime. Besides lack of phosphate, auxin and auxin analogs are also known to increase the density and length of root hairs in wild-type plants (Ishida et al., 2008) but not in some root hair mutants (Masucci and Schiefelbein, 1994).

We grew the wild-type and complemented mutant control plants, as well as our double mutants on media lacking phosphate according to Müller and Schmidt (2004), or supplemented with 100 nM NAA according to Duan et al. (2010) (**Figure 3.3 A**). In accordance with the literature, we observed an increased density of root hair initiation sites and an increase in root hair length in the wild-type and in the complementing mutant (**Figure 3.3 B, C**). Notably, also the double knock-out lines formed a comparable higher number of root hair initiation sites (**Figure 3.3 B**). By contrast, the root hair length of the mutant lines was not altered, neither on medium lacking phosphate, nor on medium supplemented with auxin (**Figure 3.3 C**). Mutant root hairs stopped growing shortly after bulge formation in the transition phase to tip growth and showed a short and swollen morphology.

According to the growth behavior of the *aro2 aro3* double mutants, we conclude that the ARO2 and ARO3 proteins function in the two stages of root hair development, the transition to polar tip growth and the elongation stage of the growing root hair.

3.3.4 Trichoblast enriched ARO3-GFP localizes to the tip of growing root hairs

Given the importance of the ARO2 and ARO3 proteins for proper root hair development, we investigated the subcellular localization of complementing C-terminal GFP fusion proteins under control of the endogenous promoters. Whereas ARO2-GFP was weakly expressed in many root cell types including trichoblasts (**Figure 3.4 A-C**), the ARO3-GFP fusion protein was strongly enriched in trichoblasts (**Figure 3.4 D-I**). Both fusion proteins accumulated polar in the tip of growing root hairs (**Figure 3.4 C-H**). The pronounced tip localization of ARO3-GFP fusion protein was visible only in actively growing root hairs (**Figure 3.4 J, K**). In full-grown root hairs, no ARO3-GFP signal was visible anymore (**Figure 3.4 L, M**). ARO3-GFP showed an articulate polar accumulation in that part of the actively growing root hair, which is known as vesicle-rich clear zone (**Figure 3.4 N-P**).

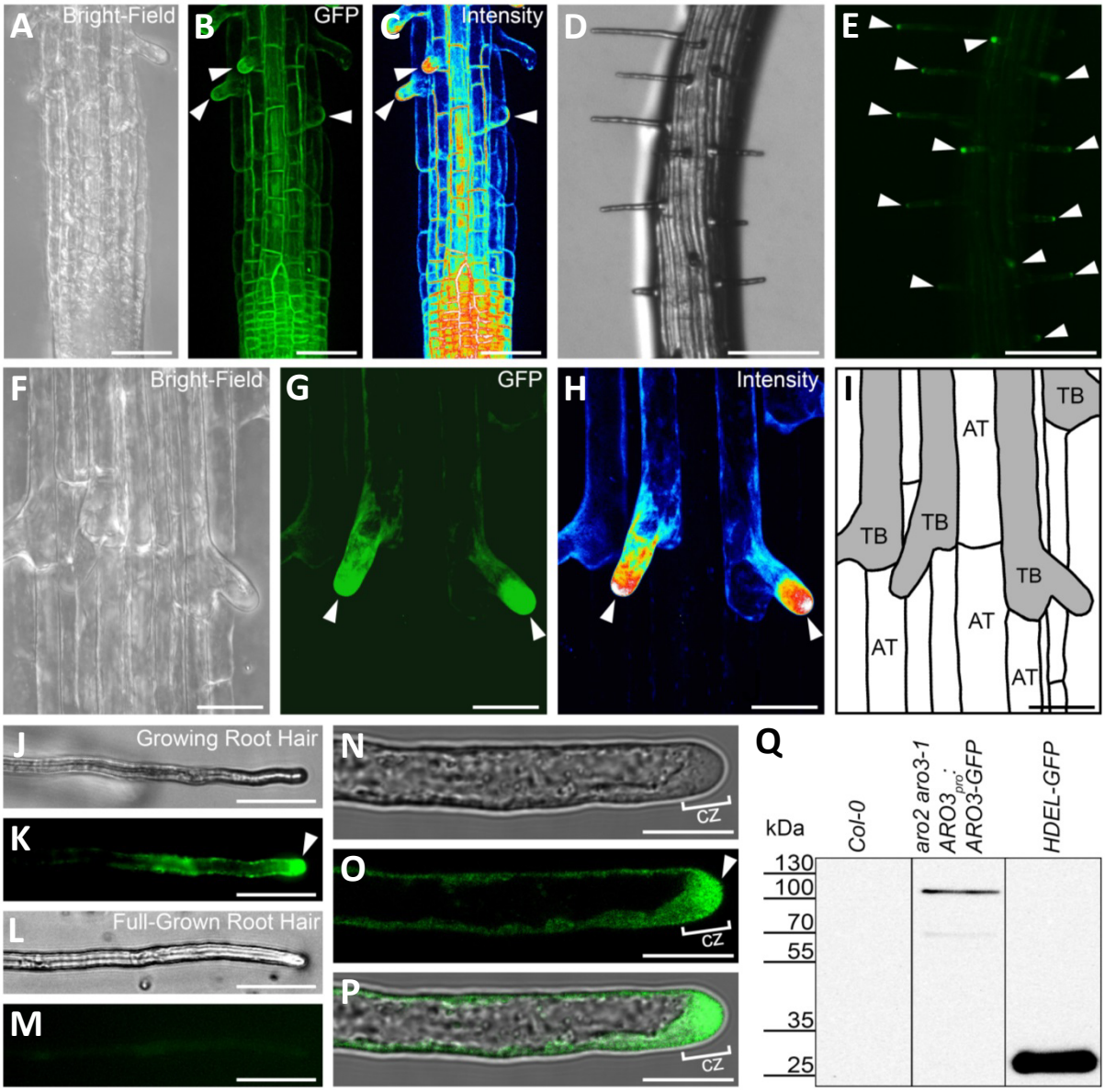

Figure 3.4 | Localization of the ARO2-GFP and ARO3-GFP fusion proteins in the root.

(A) to **(C)** The ARO2-GFP fusion protein is detected ubiquitously in the root. In root hairs it accumulates at the tip. Shown are maximum intensity projections of 100 optical slices of (A) bright-field channel, (B) GFP channel and (C) intensity false-colored GFP channel. **(D)** and **(E)** In *aro2 aro3-1* mutant lines complemented with *ARO3*$_{pro}$*:ARO3-GFP*, the fusion protein accumulates at the tip of growing root hairs. **(F)** to **(I)** The ARO3-GFP fusion protein shows polar localization in trichoblast cells (TB, gray) but not in atrichoblast cells (AT). Shown are maximum intensity projections of 151 confocal slices of (F) bright-field channel, (G) GFP channel and (H) intensity false-colored GFP channel. **(J)** and **(K)** ARO3-GFP is polar localized in an actively growing root hair. **(L)** and **(M)** In a full-grown root hair of the same root as in (J) and (K) and imaged and processed under identical conditions, no ARO3-GFP signal is detectable. **(N)** to **(P)** The ARO3-GFP fusion protein accumulates in the tip-localized clear zone of growing root hairs. (N) In the bright-field image, the clear zone (cz) of a growing root hair is visible at the tip. (O) Single optical slice (0.23 µm) of polar distributed ARO3-GFP in the root hair. (P) Merged image of (N) and (O). **(Q)** Western Blot analysis of root protein extracts probed against a monoclonal GFP antibody. Arrowheads indicate polar accumulations of fusion proteins in root hairs. Bars = 50 µm in (A) to (C), 200 µm in (D) and (E), 25 µm in (F) to (M) and 10 µm in (N) to (P).

We performed western blot analysis with a monoclonal GFP antibody to confirm that our fluorescence observations in the microscope were derived from the ARO3-GFP full-length fusion protein (**Figure 3.4 Q**). At the size of the predicted mass of 102 kDa, a clear band was visible in extracts from ARO3-GFP expressing plants, but not in extracts from wild-type plants. Another very faint band was observed at 70 kDa, which likely results from a degradation product as it was absent in the wild-type control.

The subcellular localization of ARO3-GFP in root hairs reminded us to the subcellular localization of ARO1-GFP in growing pollen tubes (Gebert et al., 2008; Vogler et al., 2015). To further compare their subcellular localizations, we performed live-cell imaging of growing pollen tubes expressing *ARO1$_{pro}$:ARO1-GFP* and root hairs expressing *ARO3$_{pro}$:ARO3-GFP*. As shown by Vogler et al. (2015), the polarization of ARO1-GFP in the pollen grain is already observed before a pollen tube is formed (**Figure 3.5 A**). When the pollen tube starts rapid tip growth (from time frame 120' on in **Figure 3.5 A**), the tip-localized ARO1-GFP signal strongly increased.

In the root hair, ARO3-GFP accumulated polar at the tip after bulging and shortly before the stage of rapid elongation (**Figure 3.5 B**). Comparable to ARO1-GFP in pollen tubes, the polar accumulation of ARO3-GFP at the tip was high when the root hair was actively elongating. When the root hair growth slowed down (last frame of **Figure 3.5 B**), the localization of ARO3-GFP began to depolarize from the tip. Besides the GFP signal observed at the tip, we also detected signals that were located in the nucleus of the growing root hair. Also for ARO1-GFP a nuclear localization in the pollen tube forming vegetative cell was observed (Gebert et al., 2008). However, different to ARO1-GFP in activated pollen grains we did not observe a polarization of ARO3-GFP in the trichoblast prior to root hair formation, which may be attributed to the different cell types with different growth kinetics (Ketelaar et al., 2008).

Taken together, our results from knock-out and subcellular localization studies indicate that the polar localization of ARO2 and ARO3 at the tip of actively elongating root hairs is, comparable to the tip-localization of ARO1 in pollen tubes (Gebert et al. 2008), crucial for proper polar cell growth.

3.3.5 Tip-localization of ARO3-GFP is BFA-sensitive

The subapical clear zone at the very tip is present only in actively growing root hairs (Ovečka et al., 2005) and known to be densely packed with secretory vesicles (Campanoni and Blatt, 2007). The RabA4b-labeled secretory vesicles and Trans-Golgi Network (Kang et al., 2011), as well as the endomembrane markers FM1-43 and FM4-64 strongly accumulate in this apical, vesicle-rich clear zone of growing root hairs (Preuss et al., 2004; Ovečka et al., 2005). It has been reported that the tip-localization of endomembrane markers, as well as the polar elongation of the root hair, are inhibited by Brefeldin A (BFA) (Ovečka et al., 2005), a drug that effectively blocks vesicular secretion in tip growing cells.

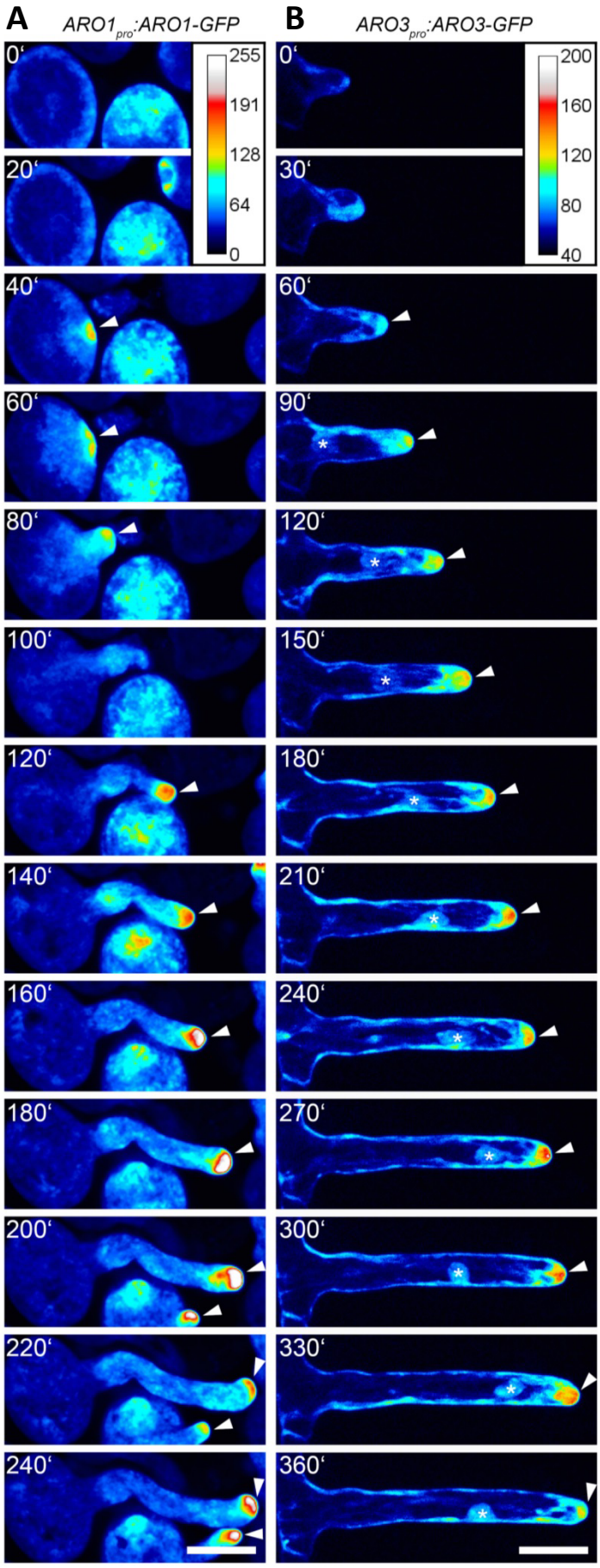

Figure 3.5 | Similar to ARO1-GFP in pollen tubes, ARO3-GFP is tip-localized in root hairs during polar tip growth.

(A) In growing pollen tubes, ARO1-GFP is localized polar at the tip (arrowheads). **(B)** After bulge formation, the ARO3-GFP fusion protein is localized polar at the tip of a growing root hair (arrowheads). After rapid elongation, the strong accumulation of ARO3-GFP at the tip of the root hair diminishes (360’ frame). Numbers indicate minutes after acquisition start. Images show maximum intensity projections of (A) 11, or (B) 21 optical slices. Bars = 15 µm in (A) and (B).

To test whether the polar tip-localization of ARO3-GFP in growing root hairs is associated with vesicular secretion, we treated *aro2 aro3-1* mutant plants complemented with *ARO3$_{pro}$:ARO3-GFP* with BFA, or, as solvent control, with DMSO. In the control treatment, ARO3-GFP was still localized polar in the root hair tip after 30 minutes (**Figure 3.6 A, B**). However, 30 minutes after treatment with 25 µM BFA, the polar localization of ARO3-GFP at the root hair tip was abolished (**Figure 3.6 C, D**). Instead, we observed an accumulation of the ARO3-GFP signal in the subapex (**Figure 3.6 D**, arrowheads). Furthermore, the ARO3-GFP signal accumulated in spherical structures of varying sizes in the basal part of the root hair (**Figure 3.6 E, F**). 45 minutes after BFA treatment, the ARO3-GFP signal was almost completely removed from the tip region of the root hair and the fluorescent fusion protein accumulated even more articulate in larger spherical structures that were also apparent in the bright-field image (**Figure 3.6 G, H**, arrowheads).

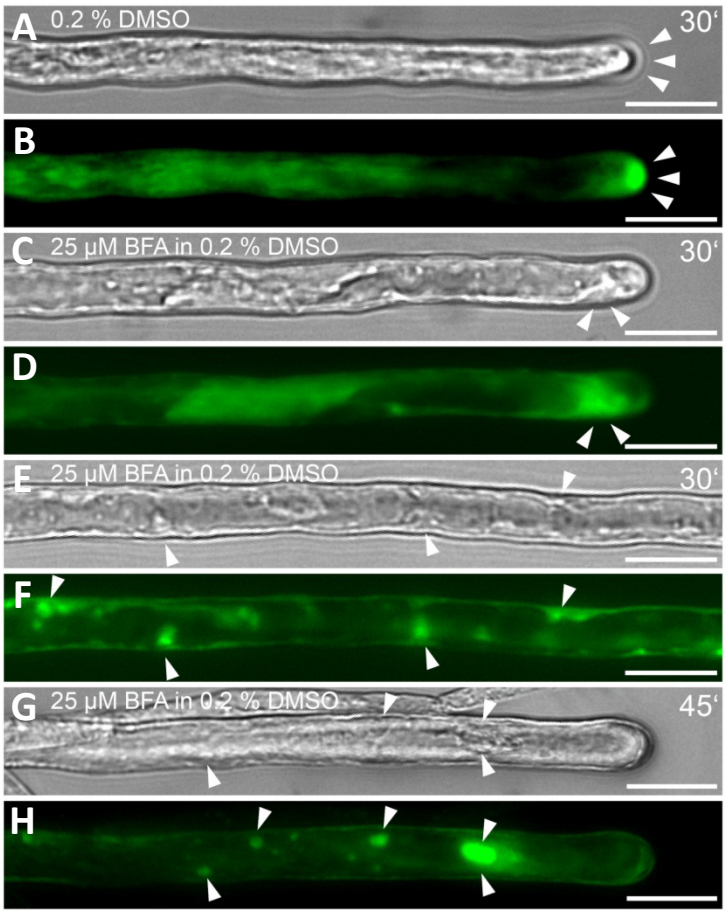

Figure 3.6 | The polar localization of ARO3-GFP in root hairs is BFA dependent.

(A) and **(B)** A root hair expressing ARO3-GFP in the *aro2 aro3-1* mutant background. 30 minutes after treatment with 0.2 % DMSO, the ARO3-GFP localization is still polar at the tip of the root hair (arrowheads). **(C)** to **(F)** Root hair cell expressing ARO3-GFP in the *aro2 aro3-1* mutant background 30 minutes after treatment with 25 µM BFA in 0.2 % DMSO. (C) and (D) Apical region of a BFA treated root hair. The tip-localization of ARO3-GFP is abolished and strong signals appear at the sub-apex (arrowheads). (E) and (F) Basal region of a BFA treated root hair. ARO3-GFP accumulates in large spherical structures (arrowheads). **(G)** and **(H)** 45 minutes after BFA treatment, the tip-localization of ARO3-GFP is completely lost and an accumulation of the fusion protein in large spherical bodies is observed (arrowheads). Bars = 10 µm.

It is known that treatment with BFA leads to a rapid blockage of ARF dependent vesiculation at the Golgi apparatus, and to the formation of large BFA-induced membrane aggregations, so called BIAs (Nebenführ et al., 2002; Šamaj et al., 2006). The BFA induced depolarization of ARO3-GFP from the clear zone and its subsequent accumulation in larger spherical structures indicates that ARO3 is at least partially associated to the membranous secretory system of root hairs.

3.3.6 The ARO protein family is functionally conserved

The close similarity between the *aro2 aro3-1* root hair mutant phenotype and the *aro1-3*/+ pollen tube mutant phenotype (Gebert et al., 2008), as well as the comparable subcellular localization of ARO3-GFP in growing root hairs and ARO1-GFP in growing pollen tubes (**Figure 3.5**), led us to the hypothesis that the ARO proteins could be functionally redundant.

To tests this, we used the double homozygous *aro2 aro3-1* mutant and transformed it with an $ARO2_{pro}$*:ARO2-GFP* or $ARO3_{pro}$*:ARO3-GFP* construct to restore the wild-type situation. Furthermore we used an $ARO3_{pro}$*:ARO1-GFP* or $ARO3_{pro}$*:ARO4-GFP* construct for ectopic expression of ARO1-GFP, or overexpression of ARO4-GFP in the double mutant. We performed genetic and phenotypic analyzes of the resulting T2-lines, which were double homozygous for the *aro2* and *aro3-1* insertions, and heterozygous and thus segregating for the respective complementation construct. The non-complemented mutant showed only short and swollen root hairs that were significantly different from wild-type root hairs in terms of morphology and length (**Figure 3.7 A, B, G**). The expression of ARO2-GFP and ARO3-GFP in the mutant background restored the root hair morphology and length to wild-type levels (**Figure 3.7 C, D, G**). Similarly, the ectopic expression of ARO1-GFP was able to fully rescue the *aro2 aro3-1* mutant phenotype back to wild-type levels (**Figure 3.7 E, G**). However, when we expressed ARO4-GFP under control of the *ARO3* promoter in the *aro2 aro3-1* mutant background, proper root hair morphology was restored (**Figure 3.7 F**), but root hairs were significantly shorter than those in the wild-type, or in one of the other complementing lines (**Figure 3.7 G**).

We verified the functional complementation by genetic segregation analyzes (**Table 3.1**). In wild-type plants, short and swollen root hairs were never observed. Likewise, root hairs of the wild-type morphology were not observed in the *aro2 aro3-1* or the *aro2 aro3-2* mutant, or in the *aro2 aro3-1* mutant expressing cytoplasmic GFP ($35S_{pro}$*:GFP*). However, the re-introduction of ARO2 or ARO3, the ectopic expression of ARO1 or the overexpression of ARO4 as C-terminal GFP fusions in the *aro2 aro3-1* mutant background resulted in wild-type to mutant segregation patterns of nearly 3:1 that satisfies a Mendelian inheritance pattern.

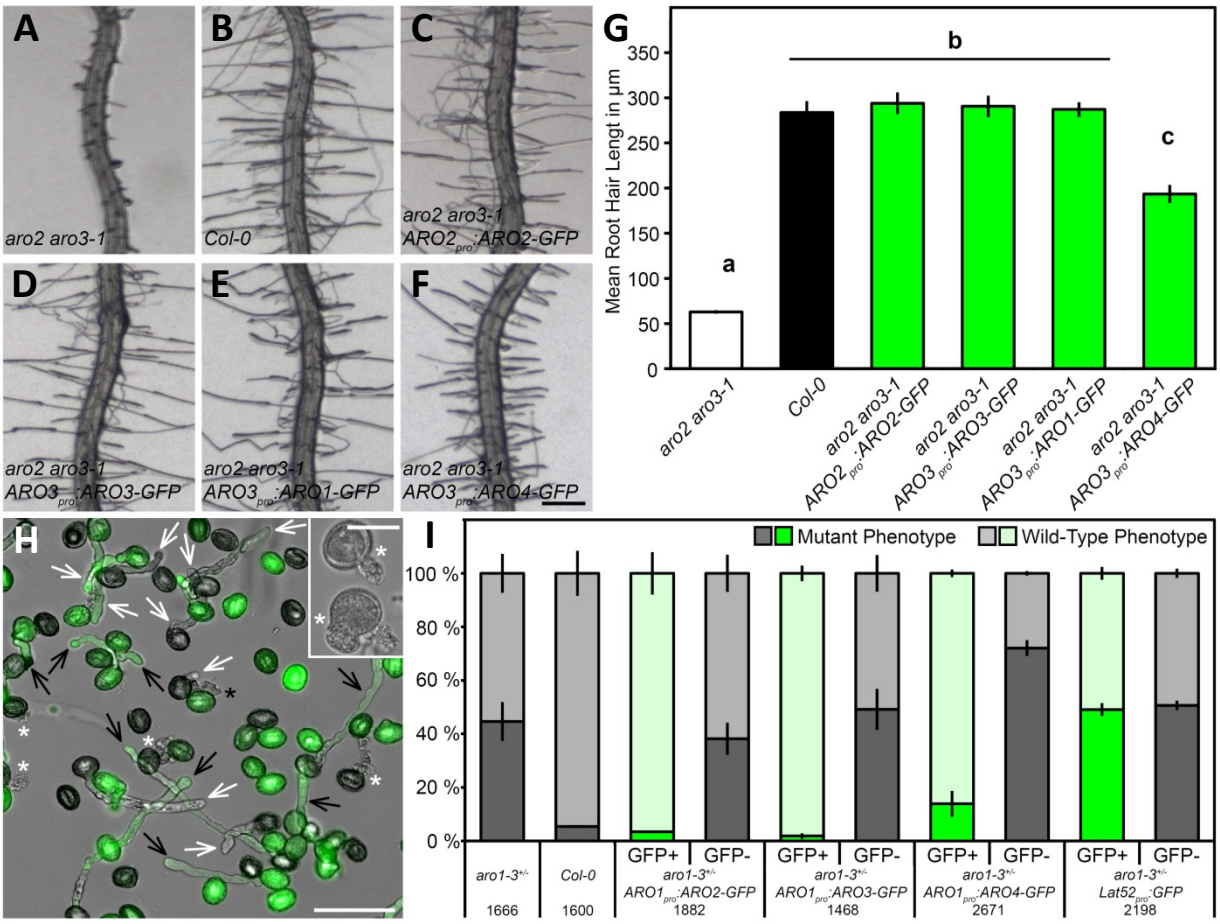

Figure 3.7 | Root hair and pollen tube mutant complementation by ectopic ARO expression.

(A) to **(G)** The *aro2 aro3-1* root hair mutant phenotype can be rescued by the reintroduction of ARO2-GFP or ARO3-GFP, or by ectopic expression of ARO1-GFP in the mutant background. Ectopic expression of ARO4-GFP only partially rescues the mutant phenotype. (A) to (F) Root hair morphology of *aro2 aro3-1* mutant or wild-type plants, and of lines harboring complementation or ectopic expression constructs in the mutant background. (G) Mean (±1SE, n=5) length of root hairs of plants from the different genotypes. Significant differences ($p < 0.001$) are indicated by different letters. **(H)** and **(I)** The *aro1-3* pollen tube mutant phenotype can be fully complemented by ectopic expression of ARO2-GFP or ARO3-GFP, but can only be partially complemented by ectopic expression of ARO4-GFP. (H) In vitro pollen tube growth mutant complementation assay according to Gebert et al. (2008). Pollen tubes were evaluated for mutant (asterisks) or wild-type (arrows) appearance and for the presence (black) or absence (white) of GFP fluorescence. Inset shows typical *aro1-3* mutant pollen tubes that are short and thick, or directly burst after germination. (I) Mean percentage (±1SE, n=3) of pollen exhibiting mutant or wild-type phenotypes and arranged by the presence or absence of GFP fluorescence. Numbers of counted pollen are indicated below the genotypes. Bars = 250 µm in (F), 50 µm in (H) and 25 µm in inset of (H).

We also wanted to test whether the *aro1-3* pollen tube mutant phenotype can be complemented by ectopic expression of the sporophytic *ARO* genes. For this purpose we crossed the male sterile heterozygous *aro1-3*/+ mutant with homozygous plants expressing ARO2-GFP, ARO3-GFP or ARO4-GFP under control of the *ARO1* promoter. Investigating the subcellular localization in growing pollen tubes revealed the polar tip localization of the fusion proteins, comparable to ARO1-GFP in the *aro1-3* background (**Figure S3.3**). Cytoplasmic GFP expressed in the

aro1-3/+ mutant under the control of the pollen specific *Lat52* promoter did not show this pronounced tip localization.

To perform an in vitro pollen tube growth complementation assay we used a T-DNA line heterozygous for the *aro1-3* insertion and the respective complementation constructs according to Gebert et al., (2008). Briefly, in vitro germinated pollen was scored for the wild-type or the mutant phenotype, and for the presence or absence of the complementation construct by means of GFP fluorescence (**Figure 3.7 H**). Without any complementation construct, approximately 50 % of the *aro1-3*/+ pollen showed the burst or short and thick pollen tube mutant phenotype (**Figure 3.7 I**) described by Gebert et al., (2008). Wild-type pollen also showed a background level of abnormal pollen tubes that ranged at about 5 %. When we ectopically expressed either ARO2-GFP or ARO3-GFP in the *aro1-3* mutant pollen, those pollen tubes that did not carry the complementation construct showed mutant phenotypes comparable to the non-complemented mutant. In contrast, those pollen tubes that carried the complementation construct, showed phenotypes comparable to wild-type pollen (**Figure 3.7 I**). However, when we complemented the *aro1-3*/+ mutant by *ARO1*$_{pro}$*:ARO4-GFP*, we observed that about 16 % of the GFP-positive pollen still showed a mutant phenotype, indicating that ARO4-GFP is only partially able to rescue the *aro1-3*/+ mutant. As a control, we also expressed cytoplasmic GFP in the *aro1-3*/+ mutant pollen tubes which did not result in any altered ratio of mutant to wild-type pollen phenotypes (**Figure 3.7 I**).

Table 3.1 | Segregation pattern of root hair phenotype in complementation assay.

Background [a]	Construct [b]	Wild-Type [c]	Mutant [d]	Ratio [e]
Col-0		183	0	
aro2 aro3-1		0	109	
aro2 aro3-2		0	74	
aro2 aro3-1	*ARO2*$_{pro}$*:ARO2-GFP*	116	39	3.0/1
aro2 aro3-1	*ARO3*$_{pro}$*:ARO3-GFP*	107	38	2.8/1
aro2 aro3-1	*ARO3*$_{pro}$*:ARO1-GFP*	197	62	3.2/1
aro2 aro3-1	*ARO3*$_{pro}$*:ARO4-GFP*	107	36	3.0/1
aro2 aro3-1	*35S*$_{pro}$*:GFP*	0	283	

[a] Wild-type or double homozygous T-DNA lines.

[b] Transgenic lines heterozygous for the complementation constructs.

[c] Number of plants with root hair length and width comparable to Col-0 plants.

[d] Number of plants with root hairs short and swollen.

[e] Wild-type to mutant phenotype.

To obtain a genetic verification of our pollen tube mutant complementation assays, we screened the progeny of plants double heterozygous for *aro1-3* and a respective complementation construct for the occurrence of plants that are double homozygous (**Figure S3.4**). While heterozygous *aro1-3* never produces homozygous offspring due to the lack of male transmission (Gebert et al., 2008), all the three complementation lines were able to produce homozygous *aro1-3* plants, indicating that ARO2-GFP, ARO3-GFP and ARO4-GFP are able to take over the ARO1 function in pollen tubes on a genetic basis.

The scheme shown in **Figure 3.8** summarizes the *aro2 aro3-1* root hair and the *aro1-3*/+ pollen tube mutant complementation by re-introduction, ectopic expression or overexpression of gametophytic or sporophytic AROs.

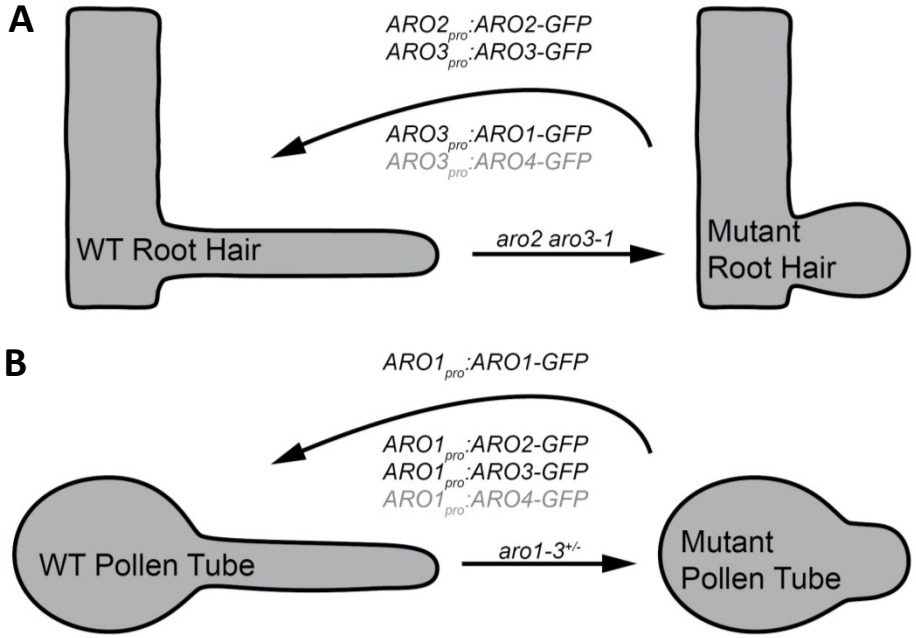

Figure 3.8 | Summary of ARO functional redundancy.

(A) The polar cell growth defects of mutant *aro2 aro3-1* root hairs can be complemented by the reintroduction of sporophyte expressed ARO2 or ARO3. Ectopic expression of gametophyte-specific ARO1 in the *aro2 aro3-1* mutant background also fully restores wild-type root hair formation. The mutant phenotype can only be partially complemented by ARO4 expression. **(B)** The polar cell growth defects of mutant *aro1-3* pollen tubes can be rescued by the reintroduction of the gametophyte-specific ARO1 (Gebert et al., 2008), or by the ectopic expression of ARO2 or ARO3. Ectopic expression of ARO4 in the *aro1-3* mutant background only partially restores wild-type pollen tube growth.

3.3.7 *The subcellular localization of polarity markers is altered in the* aro2 aro3-1 *mutant*

We investigated the F-actin organization, the distribution of the TGN/SV secretory machinery and the localization of ROP2, the RhoGTPase mainly involved in root hair polarity signaling (Jones et al., 2002), by introducing an *$UBI10_{pro}$:tagRFP-T-Lifeact*, a *$35S_{pro}$:YFP-RabA4b* or a *$ROP2_{pro}$:YFP-ROP2* construct in the wild-type and in the *aro2 aro3-1* mutant (**Figure 3.9**).

In accordance with earlier publications (Miller et al., 1999; Ketelaar, 2013), in wild-type root hairs, the actin cytoskeleton was organized mainly in thick, longitudinal and interconnected bundles further down the base of the root hair, while fine F-actin was visible in the apical part (**Figure 3.9 A**). The YFP-RabA4b labeled TGN/SV secretory system was localized polar at the tip of the growing root hairs and occasionally appeared in fluorescent spots down the base of wild-type root hairs (**Figure 3.9 B**, arrowheads), like described by Preuss et al. (2004, 2006). YFP-ROP2 accumulated in the plasma membrane at the root hair initiation site, the tip of the bulge and the tip of the growing root hair (**Figure 3.9 C**, arrowheads), concordant with earlier findings (Jones et al., 2002; Xu and Scheres, 2005).

In our *aro2 aro3-1* mutant, the prominent bundles of F-actin did not show a preferential longitudinal orientation as in the wild-type, but exhibited a more net-like organization with thick bundles also randomly oriented towards the flanks or the tip of the root hair bulge, forming some pronounced nodes near the plasma membrane (**Figure 3.9 D**, arrowheads). Notably, the tip-localized YFP-RabA4b labeled secretory system was completely absent in the *aro2 aro3-1* mutant root hairs. Instead, YFP-RabA4b appeared randomly in fluorescent spots at the flanks and tips of the mutant root hairs (**Figure 3.9 E**, arrowheads). The YFP-RabA4b labeled spots in *aro2 aro3-1* mutant root hairs showed a distribution comparable to the pronounced nodes of the tagRFP-T-Lifeact labeled actin cytoskeleton. Comparable to the wild-type, during root hair initiation in the *aro2 aro3-1* mutant trichoblast, YFP-ROP2 was localized polar at the site of the emerging root hair. However, it did not show the pronounced localization to the plasma membrane but accumulated in dot-like structures in the cytoplasm beneath the plasma membrane (**Figure 3.9 F**, arrowheads). In the widened *aro2 aro3-1* mutant bulge, YFP-ROP2 was polarized to the tip comparable to the wild-type. In these early stages of root hair development the YFP-ROP2 polarization in the *aro2 aro3-1* mutant resembled that of the wild-type root hairs except its more granular-like fluorescence below the plasma membrane. However, after bulging and in the defective transition stage to polar tip growth, a remarkably enlarged ROP2 area became visible at the root hair plasma membrane. YFP-ROP2 signals spread from the tip along the sub-apex towards the flanks of the bloated root hairs (**Figure 3.9 F**, arrowheads).

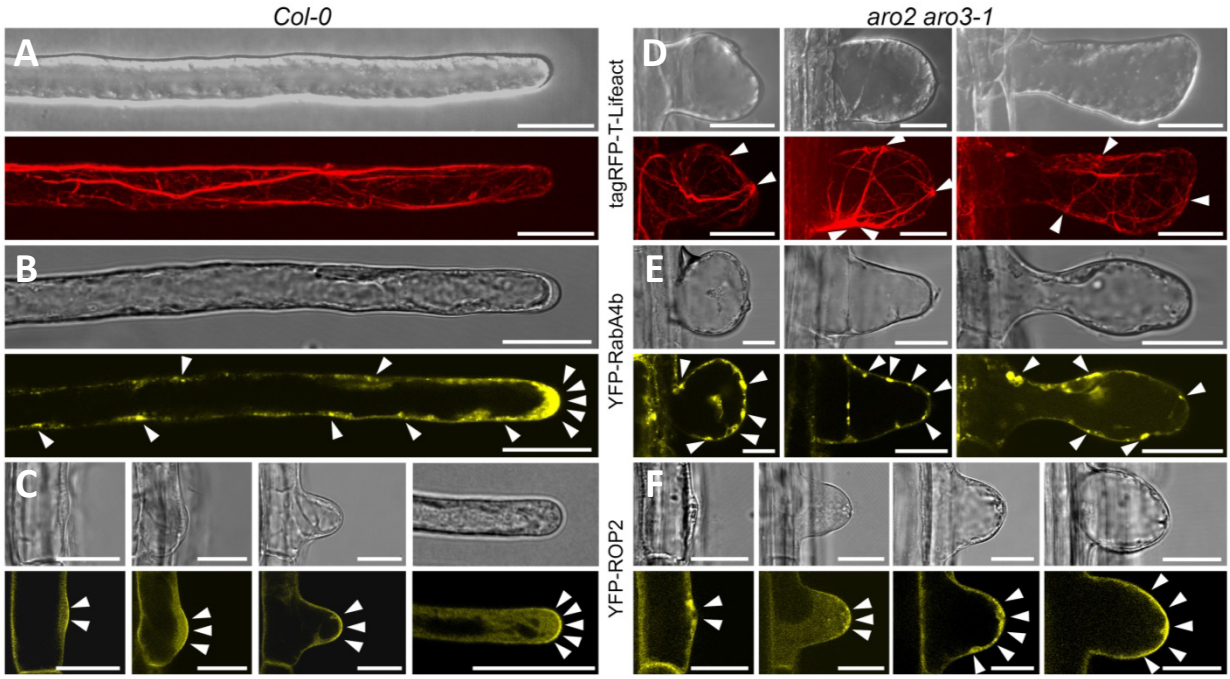

Figure 3.9 | Subcellular localization of polarity markers in the *aro2 aro3-1* mutant or in wild- type root hairs.

(A) to **(C)** Organization of the actin cytoskeleton, the secretory system and localization of the RhoGTPase ROP2 in wild-type root hairs. (A) Wild-type root hairs expressing the actin marker tagRFP-T-Lifeact. (B) Wild-type root hairs expressing the TGN and secretory vesicle marker YFP-RabA4b. (C) Localization of YFP-ROP2 in wild-type root hairs. **(D)** to **(F)** Organization of the actin cytoskeleton, the secretory system and localization of the RhoGTPase ROP2 in *aro2 aro3-1* mutant root hairs. (D) Exemplary *aro2 aro3-1* mutant root hairs arrested after bulge formation or in the transition to polar growth expressing the actin marker tagRFP-T-Lifeact. (E) Exemplary *aro2 aro3-1* mutant root hairs arrested after bulge formation or in the transition to polar growth expressing the TGN and secretory vesicle marker YFP-RabA4b. (F) Subcellular localization of YFP-ROP2 in *aro2 aro3-1* mutant root hairs during hair initiation, bulge formation, or arrested after bulge formation or in the transition to polar growth. Arrowheads point to local assemblies of subcellular markers. (A), (D) Show maximum intensity projections. (B), (C), (E) and (F) show single optical slices. Bars = 20 µm.

3.3.8 A RhoGAP and Pleckstrin homology-domain containing protein, Exo70E2 and RHD3 are ARO3 interactors

The 42 amino acid Armadillo (ARM) repeat motif has been identified in the name-giving segment polarity mutant *armadillo* (Pfeifer and Wieschaus, 1990). Each ARM motif comprises three alpha helices, and tandem arranged ARM repeats fold together to a right-handed superhelix that serves as platform for protein-protein interactions (Samuel et al., 2006; Tewari et al., 2010). The four *Arabidopsis* ARO proteins comprise two separate ARM domains (ARD1, ARD2) with four to five armadillo repeat motifs (ARM) and no other known protein domain (Gebert et al., 2008).

To identify putative ARO interaction partners in *Arabidopsis*, we used two different approaches. First, we screened an extended collection of approximately 12,000 *Arabidopsis* open reading frames (*Arabidopsis* Interactome Mapping Consortium, 2011) against all 4 full-length ARO proteins for yeast two-hybrid interaction using a robotic screening platform. We also included 28

ARO protein deletion constructs in this screen, which lacked combinations of the N-terminus, the armadillo repeat domains (ARD), the spacer region or the C-terminus (for an overview, see **Supplemental Dataset**), to enhance its sensitivity. Afterwards, we verified yeast two-hybrid candidate proteins by subsequent direct quadruplicate interaction testing according to Dreze et al. (2010).

In the yeast two-hybrid screen we were able to identify a RhoGAP and Pleckstrin homology-domain containing protein (AT5G19390, hereafter termed RhoGAP/PH) and the exocyst complex subunit Exo70E2 (AT5G61010) as robust yeast interactors of full-length ARO3 (**Figure 3.10 A**). Furthermore, a weak interaction was observed between Exo70E2 and the ARO3 deletion lacking either the C-terminus ($ARO3_{\Delta C}$), or the ARD2 domain and the C-terminus ($ARO3_{\Delta ARD2,C}$). No interactions were observed with all the other ARO3 deletions.

In a directed yeast two-hybrid screen we tested which of the ARO proteins are able to interact with Exo70E2 or the pollen-enriched paralogues Exo70C1, Exo70H3 or Exo70H5 (Li et al., 2010). This directed yeast two-hybrid screen was performed completely independent of the first screen by means of constructs, yeast strains and experimenters. Again, we found a robust interaction of Exo70E2 and ARO3 and additionally a weak interaction of Exo70H3 and ARO3. However, this weak interaction was not detectable on higher stringency selection media (**Figure 3.10 B**).

In a second approach, we performed GFP pull-down experiments with protein extracts from *aro2 aro3-1* mutant plants complemented with ARO3-GFP, followed by LC-MS/MS analysis. The ARO3-GFP pull-down MS data set was further refined by eliminating false positive proteins, i.e. proteins that were also identified in pull-down experiments with ER-GFP expressing plant lines, or from wild-type plants, using an identical procedure. Among the proteins exclusively found in the ARO3-GFP pull-down, we identified 5 peptides of ROOT HAIR DEFECTIVE 3 (RHD3). We further tested the interaction of RHD3 with the ARO proteins in a directed yeast two-hybrid assay and found that full-length ARO3 reliably interacted with RHD3 (**Figure 3.10 A**).

We investigated single T-DNA insertion lines of the ARO3 interactors RhoGAP/PH (*rhogap/ph-1*), Exo70E2 (*exo70e2-1*) and RHD3 (*rhd3-7*) on their root hair morphology (**Figure S3.5**). The single insertion lines *rhogap/ph-1* and *exo70e2-1* did not show any altered root hair morphology compared to the wild-type. As already described by Zhang et al. (2013), the *rhd3-7* mutant root hairs were shorter and wavier than wild-type root hairs. Although *rhd3-7* root hairs were still slightly longer compared to *aro2 aro3-1* root hairs and did not show comparable swellings, they also arrested in the phase of polar tip growth.

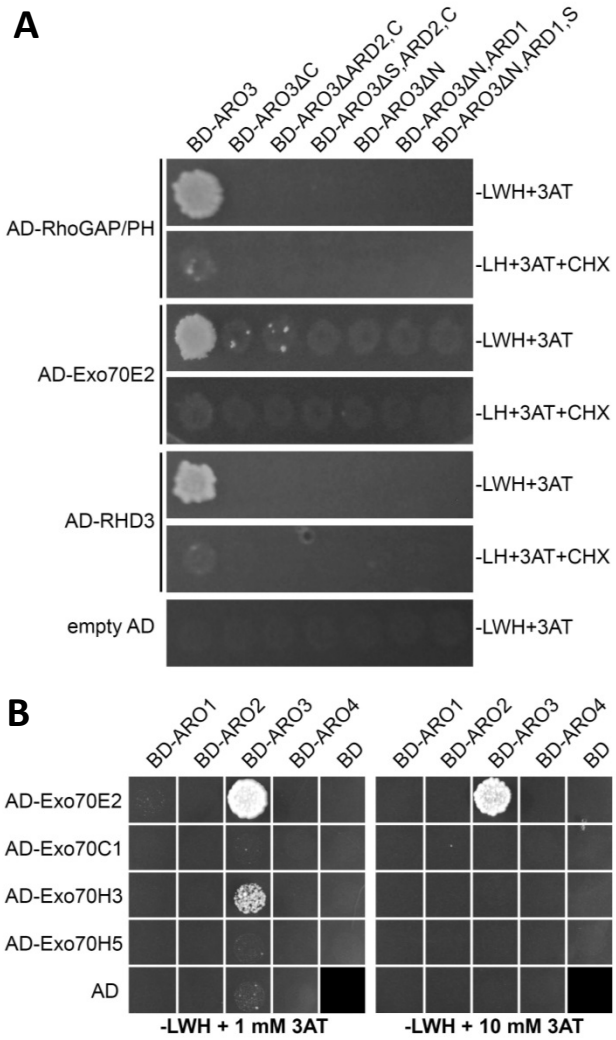

Figure 3.10 | ARO3 interaction partners in *Arabidopsis*.

(A) In a yeast two-hybrid screen, we identified a RhoGAP and Pleckstrin homology domain containing protein (RhoGAP/PH) and Exo70E2 as interaction partners of ARO3. In pull-down experiments with functional ARO3-GFP from root tissue, we identified RHD3 as interaction partner and validated the interaction in the yeast two-hybrid system. Besides full-length AROs we also tested AROs deletion constructs, lacking different domains or combinations of domains. Interactions were tested on –LWH+3AT and auto-activation on –LH+3AT+CHX plates. The yeast two-hybrid assay and subsequent quadruplicate interaction verification was performed according to Dreze et al. (2010). **(B)** ARO3 specifically interacts with Exo70E2, but also shows a weak interaction with Exo70H3. Note that this verification represents a second, completely independent directed yeast two-hybrid interaction test.

3.3.9 ARO3 colocalizes with its interactors in different subcellular locations

We used an estradiol inducible transient tobacco leaf expression system to perform colocalization experiments with ARO3-mCherry and its identified interaction partners as GFP fusions. As we observed a considerable putative cytoplasmic localization of ARO3-GFP in our stable *ARO3$_{pro}$:ARO3-GFP* lines (Figures 4, 5 and 6), we first tested colocalization of ARO3-mCherry and eGFP in the tobacco system (**Figure 3.11 A-D**). In medial optical sections through the epidermis cells, we observed that ARO3-mCherry and eGFP colocalized in the cytoplasm

(**Figure 3.11 A**) and in cytoplasmic strands (asterisks in **Figure 3.11 A**). This colocalization was confirmed by overlapping mCherry and eGFP peaks in a line intensity plot (**Figure 3.11 B**). However, in cortical optical sections, ARO3-mCherry and eGFP colocalized in the cytoplasm (**Figure 3.11 C**) but ARO3-mCherry showed an additional localization in small, dot-like structures (arrowheads in **Figure 3.11 C**). In the line intensity plot, these dot-like accumulations appear as articulate peaks that overlay with peaks of eGFP marked cytoplasmic strands (**Figure 3.11 D**). The dot-like accumulation of ARO3mCherry was also observed when expressed alone (**Figure S3.6 A**).

When we tested the colocalization of ARO3-mCherry and its interactor RhoGAP/PH as C-terminal GFP fusion, we found that both are localized in the cytoplasm and in cytoplasmic strands in medial optical sections (**Figure 3.11 E**). The colocalization of ARO3mCherry and RhoGAP/PH in the cytoplasm is also indicated by the line intensity plot (**Figure 3.11 F**).

When we co-expressed ARO3-mCherry and RHD3-GFP, we observed in cortical optical sections that RHD3-GFP nicely marks the ER (**Figure 3.11 K**), like reported by Zheng and Chen (2011). ARO3-mCherry localized mainly in the cytoplasm around the ER, but also showed a dot-like localization (arrowheads in **Figure 3.11 K**). As visible from the merged image and from the line intensity plot (**Figure 3.11 K-L**), these dots (arrowheads) localize in close proximity to the RHD3-GFP labeled ER strands (arrows).

Induced expression of Exo70E2-GFP tobacco leaf epidermal cells led to the formation of intense, spherical fluorescent accumulations, mainly visible in cortical optical sections (arrowheads in **Figure 3.11 G** and **Figure S3.6 B**). These cytoplasm-located, dot-like structures were mostly of homogenous size, but occasionally also were of larger size (arrow in **Figure 3.11 G**). Notably, ARO3-mCherry colocalized with Exo70E2-GFP in these spherical structures (arrowheads in **Figure 3.11 G**) as revealed in cortical optical sections, beside its cytoplasmic location. The line intensity plot shows that ARO3-mCherry and Exo70E2-GFP have high intensities in these dot-like structures (arrowheads in **Figure 3.11 H**). In a time-lapse imaging experiment, we observed that the Exo70E2-GFP and ARO3-mCherry positive dots were slowly moving. However, this movement rather resembled a waggling at a fixed place than a long-distance translocation (**Figure 3.11 I, J**).

Taken together, its protein interactions and subcellular co-localizations place ARO3 in the molecular machinery of cell polarity signaling and polarized membrane trafficking in the growing root hair.

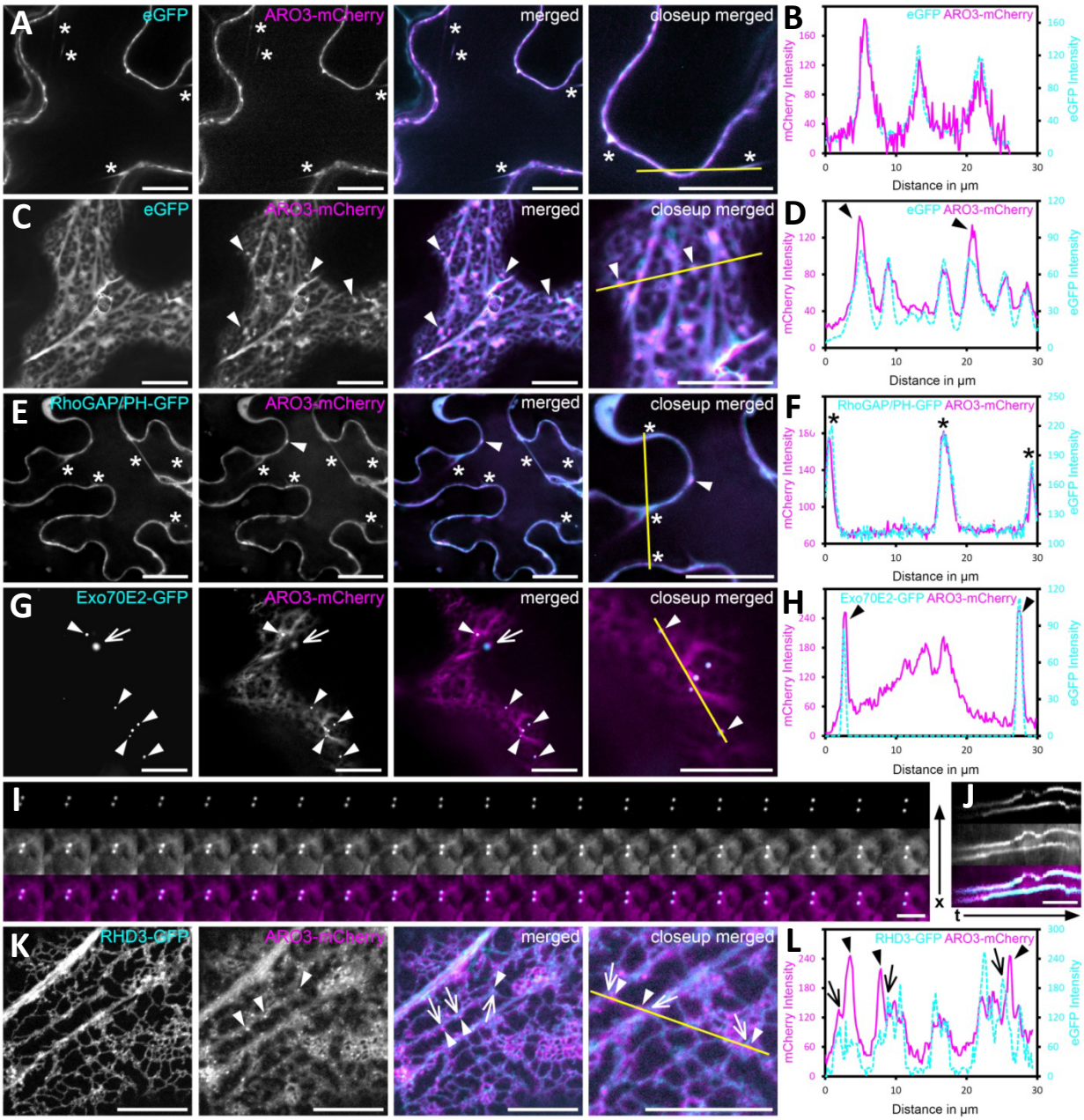

Figure 3.11 | Transient colocalization of protein interaction pairs in tobacco leaves.

(A) to **(D)** ARO3-mCherry localization is cytosolic with additional accumulation in spherical structures. (A) and (B) Median section of a cell co-expressing cytosolic GFP and ARO3-mCherry. Both channels overlap and show (B) similar line plots. Colocalization in cytoplasmic strands is indicated by asterisks. (C) and (D) Cortical section of a cell co-expressing cytosolic GFP and ARO3-mCherry. Both channels overlap but ARO3-mCherry exhibits additional localization in spherical structures that are located in the cytoplasm (arrowheads) and appear as articulate peaks in the **(D)** line plots. **(E)** and **(F)** RhoGAP/PH-GFP colocalizes with ARO3-mCherry in the cytoplasm (asterisks) as also indicated by the (F) line plots. ARO3-mCherry shows additional localization in spherical structures (arrowheads). **(G)** and **(H)** Exo70E2-GFP and ARO3-mCherry colocalizes in punctate structures in the cell cortex (arrowheads). Whereas ARO3-mCherry also localizes to the cytoplasm, Exo70E2-GFP only appears in spherical structures. **(I)** Time lapse imaging of co-migrating Exo70E2-GFP and ARO3-mCherry positive dots. Frame interval = 3 seconds. **(J)** Kymograph of 115 time frames showing colocalized Exo70E2-GFP and ARO3-mCherry spherical structures. **(K)** and **(L)** ARO3-mCherry positive spherical structures localize in close proximity of the ER that is labeled by RHD3-GFP. Arrowheads show punctate ARO3-mCherry accumulations that are in close proximity to RHD3-GFP labeled ER tubules. Yellow lines in (A), (C), (E), (G) and (K) indicate positions of plot profiles. All microscopic images show single optical sections. Bars = 20 µm, except (I) and (J) 5 µm.

3.4 Discussion

3.4.1 Differential expression but functional conservation among ARO proteins in polar tip growth

Members of a flowering plant gene family may show a preferential or specific expression in either the gametophytic or the sporophytic generation (Preuss et al., 2004; Szumlanski and Nielsen, 2009; Zhang et al., 2009; Nguema-Ona et al., 2012; Ichikawa et al., 2014). The *ARO* gene family in *Arabidopsis* exhibits a clear gametophyte-sporophyte separated expression pattern with *ARO1* as the one member that is expressed in the male gametophyte (Gebert et al., 2008). To investigate the developmental role of the three sporophyte-expressed *ARO* family members we performed detailed expression studies using promoter reporter transgenic lines and publicly available microarray data. Although especially *ARO3* exhibited a strong trichoblast-enriched expression pattern the single null mutants *aro3-1* and *aro3-2* did not show a root hair phenotype. The proposed functional redundancy with *ARO2*, also expressed in root hairs, was confirmed by the root hair phenotype of *aro2 aro3* double mutants which furthermore suggests that *ARO4* is acting in other cell types of *Arabidopis*, e.g. in guard cells where it showed high expression (**Figure S3.1**).

The observed defects in the polar elongation of *aro2 aro3* double mutant root hairs resembles the phenotype of *aro1-3*/+ mutant pollen tubes (Gebert et al., 2008) and indicate that ARO proteins play a general role in polar tip growth. According to their expression profiles, *Arabidopsis* root hairs and pollen tubes appear to cluster closely together (Becker et al., 2014) and may express a common set of genes involved in the regulation of polar tip growth. This is also reflected by a large body of publications showing that root hairs and pollen tubes are significantly similar by means of processes underlying their polar elongation by tip growth (Šamaj et al., 2006; Kost, 2008; Lee and Yang, 2008; Yang, 2008; Qin and Yang 2011).

However, besides genes known to act on polar elongation in both cell types (Schiefelbein et al., 1993; Song et al., 2006; Synek et al., 2006), there have been gene families identified of which some members show a pollen tube enriched, and others a root hair enriched expression profile (Li et al., 1999; Jones et al., 2002; Preuss et al., 2004; Szumlanski and Nielsen, 2009; Won et al., 2009; Zhang et al., 2009; Nguema-Ona et al., 2012; Ichikawa et al., 2014).

Functional substitutability between pollen tube and root hair-expressed proteins of the same family has rarely been experimentally addressed (Baumberger et al., 2003; Preuss et al., 2006; Coimbra et al., 2009; Zhang et al., 2009; Wada et al., 2015). It has been demonstrated, for example, that the pollen tube growth defect of the *raba4d* mutant could be partially rescued by the expression of root hair *RabA4b* (Szumlanski and Nielsen, 2009). However, as the single knockout of *RabA4b* does not result in a root hair defect (Preuss et al., 2004), a vice versa complementation with the gametophyte specific *RabA4d* could not be tested. We found the ectopically expressed ARO1 to be able to rescue the root hair mutant defect in *aro2 aro3-1* and, vice versa, the

ectopic expression of ARO2 or ARO3 in the *aro1-3*/+ pollen mutant background completely restored the wild-type state, suggesting a high degree of functional conservation between the gametophytic ARO1 and the sporophytic ARO2 and ARO3.

3.4.2 ARO protein function recapitulates phylogeny

Besides the full phenotypic and genetic complementation of the *aro2 aro3-1* root hair or *aro1-3*/+ pollen mutants by expression of ARO1, ARO2 or ARO3, we could show that ARO4 is not able to fully rescue the mutant phenotypes as the short and swollen phenotype of mutant root hairs disappeared but root hairs were still significantly shorter than those of the wild-type or of ARO1, ARO2 or ARO3 complemented mutant lines. From both approaches, however, we were able to generate genetically complemented homozygous T-DNA insertion lines (**Table 3.1** and **Figure S3.4**), indeed proofing at least a partial functional redundancy for ARO4.

Interestingly, ARO4 appears to be the most distantly related member of the whole protein family (**Figure 3.1 A** and **Table S3.1**). Especially the spacer region, which separates the two armadillo repeat domains ARD1 and ARD2, is much shorter in ARO4 compared to any of the remaining three AROs (Gebert et al., 2008). This highly flexible and intrinsically disordered region could fulfill an important role in ARO protein function. Intrinsically disordered protein regions can have regulatory roles by their structural formation or post-translational modifications (Iakoucheva et al., 2004; Dyson and Wright, 2005).

3.4.3 ARO3 functions in establishing polar tip-growth of root hair cells

The apical clear zone at the tip of actively growing root hairs and pollen tubes is almost exclusively occupied by densely packed vesicles that facilitate the polar elongation process by rapid exo- and endocytosis (Cheung and Wu, 2008; Ketelaar et al., 2008; Hepler and Winship, 2015). We could show earlier that in the growing pollen tube, ARO1-GFP is mainly localized to the apical clear zone, where it partially colocalizes with the endocytic styryl dye FM4-64, and moves in a reverse fountain-streaming pattern (Vogler et al., 2015). Furthermore, as shown by confocal and TIRF microscopy, ARO1-GFP in pollen tubes appears in small, dot-like structures (Gebert et al., 2008; Vogler et al., 2015). Treatment of pollen tubes with the secretion inhibiting drug BFA or the actin depolymerizing drug Latrunculin B resulted in a loss of ARO1-GFP depletion from the tip (Gebert et al., 2008). Therefore it was concluded that ARO1 is associated with vesicles and that the observed partial co-localization with F-actin cables in the shank of pollen tubes results from the transport of ARO1-GFP labeled secretory vesicles along the actin cytoskeleton (Gebert et al., 2008; Vogler et al., 2015).

The two close ARO1 relatives, ARO2 and ARO3, polarize to the tip of growing root hairs. As both *aro2 aro3* double mutants show short and swollen root hairs but no defects in root hair ini-

tiation, we conclude that ARO2 and ARO3 proteins function in a later stage of root hair formation such as transition to tip growth and/or rapid elongation. This is furthermore substantiated by the fact that in the developing root hair the reporter signal from *ARO3* promoter driven NLS3xeGFP became detectable first after bulge formation. Also, ARO3-GFP first accumulated at the tip of growing root hairs during the transition to elongation and disappeared when root hair growth stopped. Finally, the BFA-sensitive tip-localization of ARO3-GFP suggested that ARO3 is either involved in polar vesicle transport to the clear zone or exerts its function in the root hair tip.

We propose a role for ARO3 in the regulatory network of polar tip growth, because *aro2 aro3-1* root hairs exhibit a lack of polarized membrane trafficking, an enlarged ROP2 area at the apical plasma membrane after bulging and a change in the actin cytoskeleton organization. RabA4b is localized to the secretory vesicle (SV)–forming regions of the TGN and to SVs (Kang et al., 2011) and shows a polar, Latrunculin B sensitive accumulation at the tip of growing root hairs (Preuss et al., 2004, 2006). The massive mislocalization of the polarity marker YFP-RabA4b in the *aro2 aro3-1* mutant root hairs show that they are not able to establish a polar organized TGN or polar oriented SV flow, ultimately leading to growth arrest after bulging or in the transition to polar elongation.

3.4.4 ARO3 interactors suggest a mechanistic role in the negative regulation of ROP and in targeted vesicle secretion

Rho GTPase-activating proteins (RhoGAPs) are important mediators in polarity signaling as they inactivate GTP bound Rho GTPases by stimulating their low intrinsic hydrolase activity (Kost, 2008). Among the *RhoGAP* genes identified in *Arabidopsis* (Hwang et al., 2008), there is a cluster of three members that encodes RhoGAP proteins with an additional Pleckstrin homology (PH) domain, which is known to be able to bind to phospholipids (Wang and Shaw, 1995). The only characterized member of this small protein family is the ROP1 ENHANCER 1 (REN1), which plays a primary role in restricting the action of active, GTP-bound ROP1 to the pollen tube tip. REN1 loss-of-function results in short and ballooned pollen tubes reminiscent to the phenotype of pollen tubes expressing constitutive active ROP1 (Hwang et al., 2008).

Notably, we identified one of the so far unexplored REN1-like RhoGAP and Pleckstrin homology domain containing protein (RhoGAP/PH; AtREN3) as ARO3 interactor. It is thus tempting to speculate that the observed short and ballooned root hair phenotype of *aro2 aro3* mutants results from the lack of polar targeting of RhoGAP/PH via vesicle-associated ARO3 to the tip region of the root hair. The local delivery of RhoGAP/PH would, in turn, affect the restriction of Rho GTPase activity to the tip. Consistent with this assumption is our observation that ROP2, an essential regulator of root hair tip growth (Jones et al., 2002), shows a much wider localization on the plasma membranes of *aro2 aro3-1* mutant root hairs. However, we did not observe chang-

es in root hair morphology in the *rhogap/ph-1* T-DNA insertion line investigated in this study (**Figure S3.6**), which may be due to the action of other RhoGAPs in the root hairs of *Arabidopsis*, for example its close homolog AtREN2.

REN1 localizes to the apical cap and exocytic vesicles in the pollen tube tip, suggesting that its polar localization is dependent on exocytosis activities (Hwang et al., 2008; Guan et al., 2013). Notably, the second identified ARO3 interactor is Exo70E2, a key component in the recruitment of the octameric exocyst complex which is required for tethering and fusion of secretory vesicles at the plasma membrane at the sites of polarized exocytosis (Sztul and Lupashin, 2006; Žárský et al., 2013; Ding et al., 2014a,b). *Exo70E2* is strongly expressed in the root hair region of young seedlings while other *Exo70* family members are highly expressed in pollen tubes (Synek et al., 2006; Chong et al., 2010; Li et al., 2010), comparable to the differential expression pattern of *ARO3* and *ARO1* in root hairs and pollen tubes. The knock-out of *Exo70A1* leads to defects in polar cell growth of root hairs and stigmatic papillae, but also to reduced fertility due to abnormal pollen germination (Synek et al., 2006).

The interaction of ARO3 and Exo70E2 is supported by the observation that both proteins co-localized in small, co-migrating spherical structures in the cell periphery of transiently expressing tobacco leaf epidermis cells, while ARO3 additionally localizes in the cytoplasm and the ER of the cells. The appearance of Exo70E2 as small dots in stably and transiently transformed tobacco and *Arabidopsis* cells has been shown previously (Chong et al., 2010; Wang et al., 2010; Ding et al., 2014b). Polarized exocytosis is vital for cell polarity establishment and it is conceivable that the interaction of ARO3 and Exo70E2 recruits either the membrane tethering exocyst complex or its Exo70E2 component to secretory vesicles and thereby to the sites of active exocytosis and polarized cell growth. However, functional redundancy is very likely among the family of 23 Exo70 proteins (Synek et al., 2006; Cvrčková et al., 2012), which may explain both the lack of phenotype in root hairs of the *exo70e2* single mutant (**Figure S3.5**) and the fact that we did not observe an interaction of Exo70E2 with ARO2.

Also the third ARO3 interacting protein ROOT HAIR DEFECTIVE 3 (RHD3), identified in ARO3-GFP pull-down experiments and verified by yeast 2-hybrid interaction, is implicated in the control of vesicle trafficking. In transient colocalization assays, ARO3-decorated punctate structures were localized in direct proximity to RHD3-labeled ER tubules. RHD3 is a GTPase involved in the membrane traffic between the Golgi and the endoplasmic reticulum and was found to be crucial for shaping the ER architecture (Zheng and Chen, 2011; Zhang et al., 2013; Lai et al., 2014). However, RHD3 has also been described to be important for proper vesicle distribution in the tip of growing root hairs (Galway et al., 1997) and F-actin organization (Hu et al., 2003). Both, *ARO3* (this study) and *RHD3* (Schiefelbein and Sommerville, 1990; Parker et al., 2000) act genetically in the stage of root hair elongation. The knock out of *RHD3* leads to abnormal root hairs with a shorter and wavy morphology (Schiefelbein and Sommerville, 1990; Wang et al., 1997), also observed in the *rhd3-7* mutant used in this study. Still, there are differ-

ences between the *rhd3-7* and *aro2 aro3* mutant phenotypes (**Figure S3.5**), which may be attributed to the minimal spatial overlap of ARO3 and RHD3 in the cellular membrane trafficking machinery or to the redundant action of two close RHD3 homologs, *RL1* and *RL2* (Zhang et al., 2013).

Based on the cellular functions of the identified ARO3-interactors, the behavior of marker proteins for vesicle secretion, F-actin and polar plasma domain organization in *aro2 aro3* root hairs and the transient co-localization studies we suggest that ARO3 acts as a molecular linker in the spatiotemporal control of RhoGTPase signaling and secretory vesicle targeting.

3.5 Summary

Tip growth of pollen tubes and root hairs is dependent on secretory vesicle targeting and exocytosis at the dome-shaped apex of the growing cell. *Arabidopsis* pollen tubes lacking the gametophyte-expressed ARMADILLO REPEAT ONLY 1 (ARO1) protein are very short and swollen with defective actin organization. However, no function has been assigned for the sporophyte-expressed family members ARO2 to ARO4. Here we show that ARO2- and ARO3-GFP polarize towards the vesicle-rich clear zone in actively growing root hairs. Mutant *aro2 aro3* root hairs fail to undergo polar tip growth, lack polarized membrane trafficking, exhibit changes in actin cytoskeleton organization and reveal an enlarged ROP2 area at the plasma membrane. The expression of ARO1 in *aro2 aro3* mutant root hairs and the complementation of *aro1-3*/+ mutant pollen tubes with ARO2 and ARO3 fully restore polar tip growth. In screens for ARO3 interactors we identified a RhoGAP and Pleckstrin homology domain containing protein (RhoGAP/PH), the vesicle-tethering complex subunit Exo70E2 and ROOT HAIR DEFECTIVE 3 (RHD3), which in transient expression assays co-localize with ARO3 in distinct compartments of the secretory pathway. Taken together, our results highlight the functional conservation of gametophytic and sporophytic ARO proteins and their importance in the molecular network of polarity signaling and polarized membrane trafficking of root hairs.

CHAPTER 4 *Brassinosteroids Promote* Arabidopsis *Pollen Germination and Growth*

The work in this chapter was published as Vogler et al.,, (2014). The experiments were conceived and designed by Stefanie Sprunck and Frank Vogler. Christina Schmalzl and F.V. performed in vitro pollination experiments and F.V. designed and conducted pollen tube live cell imaging. The *CYP90A1:NLS-3xeGFP* reporter line was created by Martin Bircheneder and analyzed by M.B., Maria Englhart and F.V.. In vivo pollen tube growth experiments and analyzes were carried out by M.E. and F.V.. Schemes and figures were prepared by M.E.. The manuscript was written by F.V. with support of S.S..

4.1 Introduction

The pollen tube of flowering plants displays a unique cellular structure that is formed in order to transport two immobile sperm cells to the ovule, where the two female reproductive cells are located (Sprunck, 2010; Dresselhaus and Franklin-Tong, 2013). After the pollen grain lands, attaches and rehydrates on the receptive papillae on top of the stigma, it forms a tubular protrusion that navigates through the female tissues of the pistil to the female gametophyte, where it finally delivers its sperm cell cargo to undergo fertilization (Palanivelu and Tsukamoto, 2012). In an extreme form of polarized growth, the pollen tube cell rapidly elongates only at the very tip.

With growth rates up to 1 cm h^{-1} (Mascarenhas, 1993), pollen tubes, belong to the most rapidly elongating plant cells, and for example in maize, they can reach astonishing lengths of more than 30 cm. Besides their fundamental role in fertilization, pollen tubes serve as outstanding systems to study the cell biology and biochemistry of polarity and tip growth and have greatly facilitated the identification of essential players of the cell polarity machinery (Qin and Yang, 2011). At the molecular level, pollen tube tip growth depends on a RhoGTPase- and Ca^{2+}-based signaling network regulating actin cytoskeleton dynamics, and tip-targeted exocytosis (Cheung and Wu, 2008; Yang, 2008; Qin and Yang, 2011). This self-organizing system enables pollen grains to germinate and to form pollen tubes in vitro in the absence of external signals, making live cell imaging studies possible.

Assays on in vitro pollen germination and growth have been established for many decades (e. g. Fan et al., 2001; Taylor and Hepler, 1997; Li et al., 1999; Mouline et al., 2002; Rodriguez-Enriquez et al., 2013). From these studies, we also know that in vitro pollen germination rates, pollen tube growth rates, and final tube lengths are far lower than those observed in planta, which is attributed to female factors stimulating pollen germination, tube growth and growth directionality (Johnson and Preuss, 2002; Chae and Lord, 2011; Takeuchi and Higashiyama, 2011). Especially with *Arabidopsis*, the 'flagship' of molecular plant studies and best-studied flowering plant

so far, in vitro pollen germination and growth remain difficult despite many significant improvements (e. g. Johnson-Brousseau and McCormick, 2004; Boavida and McCormick, 2007; Bou Daher et al., 2009; Rodriguez-Enriquez et al., 2013). Therefore, many studies employ bicellular pollen from species such as lily or tobacco which perform much more reliable in vitro.

The pollen tube journey in the pistil follows the reproductive tract, which comprises the stigma, style, the septum epidermis or transmitting tract, and the funiculus. Some species such as lily exhibit a hollow style, in which pollen tubes grow along the extracellular matrix (ECM) of the septum epidermis, whereas others, such as *Arabidopsis*, form an intercellular-rich transmitting tissue within the style and the septum to facilitate pollen tube growth (Lennon et al., 1998). It is evident that the morphology of the transmitting tract and its nutrient-rich ECM is important for facilitating pollen tube growth over a long distance but relatively little is currently known about the nature of growth-promoting ECM components (Crawford and Yanofsky, 2008; Chae and Lord, 2011; Palanivelu and Tsukamoto, 2012). Mutants defective in proper transmitting tract formation show reduced fertility and impaired in vivo pollen tube growth (Crawford et al., 2007; Crawford and Yanofsky, 2011; Smith et al., 2013). Thus, quantitative germination and efficient pollen tube growth along the reproductive tract represent the 'conditio sine qua non' for fertilization, seed set and yield.

Factors known to affect pollen tube growth or directionality are, for example, inorganic ions (e. g. Brewbaker and Kwach, 1963; Boavida and McCormick, 2007; Bou Daher et al., 2009), small organic molecules (e. g. Mo et al., 1992; Palanivelu et al., 2003; Qin et al., 2011; Yu et al., 2014, Wu et al., 2014) and proteins (reviewed in Higashiyama 2010; Chae and Lord, 2011; Palanivelu and Tsukamoto, 2012; Beale and Johnson, 2013). But also the effects of plant hormones on pollen germination and growth have been in the focus of some studies. It could be shown that auxin and gibberellins promote in vitro pollen germination and growth, whereas abscisic acid shows an inhibiting effect (Hewitt et al., 1985; Singh et al., 2002; Chen and Zhao, 2008; Wu et al., 2008a, b).

Brassinosteroids (BRs) are known for their ability to promote cell elongation, and many BR synthesis or perception mutants show extreme dwarf phenotypes (reviewed in Clouse, 2011). Besides many other physiological responses, BR signaling affects reproductive organ initiation and formation: On the female side, BRs contribute to the number of ovule primordia and, thus, the number of seeds (Huang et al., 2012). Male sterility, described in genetic studies of dwarf BR mutants, is the result of abnormal tapetal development, reduced pollen number per locule, and of a defect in pollen release after anther dehiscence (Ye et al., 2010). Furthermore, the reduced filament length in BR-deficient and BR insensitive mutants prevents dehiscent anthers to shed their pollen on the stigma (Choe et al., 1998; Kim et al., 2005). BRs were also reported to enhance pollen germination and growth in *Prunus avium, Camellia japonica* (Hewitt et al., 985), *Prunus dulcis* (Sotomayor et al., 2012), tomato (Singh and Shono, 2005) and rice (Thussagunpanit et al., 2012). However, in tobacco, the growth-promoting effects of BRs on pollen remain contradicto-

ry. Whereas Hewitt et al. (1985) found a pronounced effect of BRs on pollen growth, Ylstra et al. (1995) could not detect any influence on elongation. Surprisingly, in the latter study, the mammalian steroid sex hormones testosterone, estradiol and progesterone, which are chemically related to BRs, were able to enhance tobacco pollen germination and growth. The effect of BRs on *Arabidopsis* pollen germination and growth has, to our knowledge, not been investigated despite its significance as model plant organism.

Here, we examined whether exogenously applied 24-epibrassinolide (epiBL) is able to stimulate *Arabidopsis* in vitro pollen germination and pollen tube growth rates, and to promote final pollen tube lengths. The promoter activity of one of the key enzymes in BR biosynthesis, *CYP90A1/CPD* (Szekeres et al., 1996), was studied in the reproductive tract by a *CYP90A1/CPD* promoter:reporter construct. Furthermore, we pollinated pistils of the wild-type and of *cyp90a1*-1 BR biosynthesis and *bri1-10* BR perception mutants with a marker line expressing cytoplasmic green fluorescent protein (GFP) in the vegetative cell of the pollen tube to investigate the influence of sporophytically derived BRs on in vivo pollen tube growth.

Our results indicate that BRs significantly promote both pollen germination and pollen tube growth. The addition of 10 µM epibrassinolide (epi-BL) to *Arabidopsis* pollen germination media can significantly improve in vitro pollen germination and growth, while epiBL concentrations above 20 µM revealed inhibitory effects. In a live cell imaging approach, we noticed an increase of cell elongation rates up to almost fivefold when germination media were supplemented with 10 µM epiBL. Notably, the promoter of the BR biosynthesis gene *CYP90A1/CPD* is highly active in the cells of the transmitting tract and CYP90A1/CPD-deficient plants show significantly reduced in vivo pollen tube growth. In summary, our results suggest that pollen tube tip growth through the reproductive tract of the *Arabidopsis* pistil is enhanced by BRs.

4.2 Material and Methods

4.2.1 Plant material and growth conditions

All plants were grown in growth chambers under long-day conditions (16 h light, 20 °C, 70 % humidity) after 2 days stratification at 4 °C in the dark. Seeds of the heterozygous T-DNA lines *cyp90a1-1* (SALK_023532) and *bri1-10* (SALK_041648), generated by the Salk Institute Genomic Analysis Laboratory (Alonso et al., 2003), were surface sterilized by washing with 70 % Ethanol and with 1 % NaOCl / 0.1 % Mucasol® (Schülke and Mayr GmbH) and grown on 0.5 Murashige Skoog (Duchefa Biochemie B.V.) medium containing 1 % Phytagar (Carl Roth GmbH and Co. KG). After 3 weeks, homozygous dwarf mutant plants were transferred to soil and grown under equal conditions. Pots were watered once a week with 1 g/L fertilizer solution (Hakaphos Blau, COMPO GmbH and Co. KG).

4.2.2 In vitro pollen tube growth experiments

Pollen germination experiments were carried out on pollen germination medium (PGM) as described by Li et al., (1999), solidified with 0.5 % Agarose (Low Melt Preparative Grade Agarose; BIO-RAD Laboratories 162-0017) in 35-mm disposable petri dishes. Final concentrations of PGM containing 5, 10, 20, 30, 40 and 50 µM 24-epibrassinolide (epiBL; Sigma-Aldrich E-1641) were prepared by adding the respective volume of a 2 mM epiBL stock solution dissolved in 90 % ethanol to 3.0 mL hand warm PGM. We used epiBL to test the bioactivity of BRs on *Arabidopsis* in vitro pollen, as it is a highly active stereoisomer of brassinolide, the most active natural BR (Mandava, 1988). Furthermore, epiBL has been isolated from *Arabidopsis* seeds (Schmidt et al., 1997), it is known to rescue BR phenotypes (e.g., Ephritikhine et al., 1999; Steber and McCourt, 2001; Szekeres et al., 1996) and it was successfully used to study the effect of exogenously applied BRs (e.g., Hewitt et al., 1985; Müssig et al., 2003; Singh and Shono, 2005). After plates dried under the sterile bench with open lid for 1 h, they were directly used for pollination experiments. In a pilot experiment, no inhibiting effects of the solvent concentrations on pollen germination were recorded. Plates were hand-pollinated with pollen from Col-0 wild-type plants by gently dabbing anthers with a forceps so that a tiny spot of pollen grains with a diameter of approximately 300 µm was released to the plates (**Figure S4.1 A**). Pollen from one flower was used to add one spot to every plate, containing no or different epiBL concentrations. To compensate for varying pollen quality between different flowers and to reduce temporal bias resulting from preparation, the order of pollination was varied as shown in **Figure S4.1 B**. Pollinated plates were kept inside a damp box at 20 °C in light for 3 h. A total of five experiments were conducted for statistical analyses. Final pollen tube lengths were determined after incubation for 20 h. Pollen germination and pollen tube lengths were recorded in the order of pollination on an inverse NIKON Eclipse 2000-S microscope equipped with a ZEISS Axio-Cam MRm CCD camera using a 20x/0.4 NA air objective and Normarski contrast. According to Stanley and Liskens (1974), pollen was assigned as germinated when a tube of at least the length of one pollen grain was clearly visible. After image stitching, pollen tube lengths were measured manually in FIJI (Schindelin et al., 2012) as segmented lines from the pollen coat to the pollen tube tip. Pollen tube length data from all epiBL concentrations were sub divided in percentiles (pollen tube length up to: 1, 21.22 µm; 2, 26.69 µm; 3, 33.99 µm; 4, 45.53 µm; 5, 58.84 µm; 6, 78.14 µm; 7, 109.84 µm; 8, 163.41 µm; 9, 244.69 µm; 10, and longer) and frequencies of observed pollen tube lengths were assigned to the respective epiBL regimes. Data on pollen germination fitted normal distribution and were subjected to a one way ANOVA followed by pairwise Tukey HSD post hoc testing. Pollen tube length data did not fit normal distribution and therefore were analyzed by Kruskal–Wallis tests. Statistical analyses were performed in IBM SPSS Statistics 19.

4.2.3 Live cell imaging of pollen tube growth

To investigate the time course of pollen germination and pollen tube elongation, we developed a micro germination chamber slide. PGM supplemented with 1 % Low Melt Preparative Grade Agarose (BIO-RAD Laboratories) was pipetted in the micro chamber, and *ARO1p:ARO1-GFP* pollen (Gebert et al., 2008) was added manually by removing single anthers with a forceps and gently dabbing on the center of the solidified medium. The chamber was sealed with a cover slip. For imaging, a 40x/1.3 NA oil immersion objective at an inverted ZEISS Cell Observer Microscope connected to a CSU-X1 Yokogawa Spinning Disc Confocal unit and a ZEISS Axio Cam MRm CCD camera was used. GFP was excited with a 488 nm laser line and emission was detected with a 525/40 nm band pass filter. In order to follow pollen tube growth z trajectories, at each position a 20 µm stack was acquired. Pollen tube elongation was measured frame wise by manually tracking the pollen tube tip in maximum intensity projections using FIJI (Schindelin et al., 2012). Statistical significance was determined by t-tests in IBM SPSS Statistics 19.

4.2.4 Gene expression profiles according to the GENEVESTIGATOR microarray database

Expression profiles of *CYP90A1/CPD, BRI1, BRL1* and *BRL3* were analyzed using the GENEVESTIGATOR microarray database (Zimmermann et al., 2004). Available log2-fold expression values for these genes were displayed relative to the signal intensity on the 22 k ATH1 array. Number of samples used for calculating mean values ± 1SE were as follows: embryo, 38; endosperm, 11; pollen, 52; pistil, 29; carpel, 2; stigma, 3; ovary, 4; ovule, 2; silique, 372; seed, 323; seedling, 2,330; shoot, 4,504; leaf, 2,849; and root, 1,063.

4.2.5 Molecular cloning and microscopy of reporter lines

A 2,018-bp promoter fragment upstream of the *CYP90A1/CPD* (At5g05690) coding sequence was amplified from Col-0 genomic DNA with the oligonucleotide primers CYP90A1pFW (5'-CACCTTTCTATATCATGTCCTTAAAAAGTATACCG-3') and CYP90A1pREV (5'-TGAAGAAGAAGATGATGATGAGAGAAGAAGAG-3') and was inserted into pENTR™/D-TOPO® vector according to the manufacturer's recommendation (Life Technologies). he resulting pENTR-CYP90A1p vector was used for LR Clonase™ (Life Technologies) recombination reaction with the pGreenII-based binary Gateway® destination vector pGII-NLS3XGFP (Zheng et al., 2011), derived fromNLS:3xEGFP::nost (Takada and Jürgens, 2007). The resulting expression vector CYP90A1p:NLS:3xEGFP was transformed into the *Agrobacterium tumefaciens* strain GV3101 (pMP90, pSOUP) and used for *Arabidopsis* Col-0 transformation by the floral dip method (Clough and Bent1998). Offspring was selected after germination by spraying a BASTA® (Bayer Crop Science) solution (200 mg/L, 0.1 % Tween®20) three times within the first two weeks of growth. Seven independent transgenic lines were investigated on reporter activity in T1 and later generations at an inverted ZEISS LSM510 Confocal Laser

Scanning Microscope (CLSM) with a 10x/0.3 NA dry or a 40x/1.3 NA oil immersion objective. The 488 nm argon laser line was used for GFP excitation, and emission was detected from 505 to 550 nm with a PMT. To image the reproductive tract, the valves of the pistil were removed, style and stigma cut longitudinally along the replum axis and the septum was placed horizontally to scrape off the ovules from the ovary by hand with hypodermic needles (0.4 x 20 mm, B. Braun Melsungen AG; for schematic overview of pistils see **Figure 4.4 B, D, E**). Ovules were dissected and mounted as described by Sprunck et al., (2012). Transmitting tract cross sections were obtained by manually cutting pistils clamped between polystyrene blocks with a razor blade. Reporter activity was studied in pistils of different flower stages according to Smyth et al., (1990).

4.2.6 Pollination experiments and in vivo pollen tube growth

For pollination experiments, we used pistils of *Arabidopsis* wild-type Columbia-0 (Col-0) plants and the dwarf mutant progeny of *cyp90a1-1*/+ and *bri1-10*/+. Prior to pollination, wild-type plants and mutants were emasculated and randomly hand-pollinated after 2–3 days with pollen harboring the *Lat52p:GFP* transgene (Twell et al., 1990), which drives expression of cytoplasmic GFP in the vegetative cell of the pollen tube. To take account of varying pollen qualities, pollen from one donor plant served to pollinate an average of 13 pistils of each of the three genotypes. Five independent experiments were conducted at different days. 5 to 6 hours after pollination, carpels were manually removed and pistils were mounted in a droplet of 100 mM Na_2HPO_4/NaH_2PO_4 (pH 7.4) buffer. Pollen tubes growing through the transmitting tract were exposed to the objective by positioning the pistil with the septum horizontally. Imaging was performed on an inverted Leica SP8 CLSM with a 20x/0.75 NA multi immersion objective. The 488 nm laser line of an argon laser was used for excitation of GFP. Emission was detected from 500 to 535 nm by a hybrid detector as well as chlorophyll autofluorescence from 580 to 690 nm by a PMT. The whole pistil was recorded in z-stacks of 3 AU single optical slices at overlapping positions with subsequent image stitching. Within the pistil, pollen tube tips were marked in maximum intensity projections and the pollen tube length was measured as parallel straight lines perpendicular to a vertical line drawn at the topmost point of the papillae in FIJI (Schindelin et al., 2012). Mean pollen tube lengths were compared in pairwise t-tests in IBM SPSS Statistics 19.

4.3 Results

4.3.1 Epibrassinolide promotes in vitro germination of Arabidopsis *pollen*

The effect of BRs on in vitro pollen germination was investigated by applying *Arabidopsis* pollen on small petri dishes containing solidified PGM supplemented with the final concentrations of 5, 10, 20, 30, 40 and 50 µM epibrassinolide (epiBL). Plates with epiBL-free PGM were used as reference. For our experiments, we dissected dehiscent anthers from open flowers of plants grown under standard long-day conditions, without any further efforts to improve the de-

scribed variability of *Arabidopsis* pollen germination (Johnson-Brousseau and McCormick, 2004; Boavida and McCormick, 2007). In vitro pollination experiments were performed in a standardized procedure (**Figure S4.1**) to balance out varying pollen qualities and time lags associated with image acquisition. Pollen germination was recorded after 3 h of incubation in five independent experiments. In total 8,143 pollen were counted. Low germination rates were obtained on plates with epiBL-free PGM (4.54 ± 1.65 %, mean ± 1 standard error of mean) (**Figure 4.1 A, B**), while germination rates increased by almost 23 % when 5 µM epiBL was added (27.15 ± 7.43 %; $p = 0.458$). Significantly higher germination rates were observed when media were supplemented with 10 µM and 20 µM epiBL, with mean values of 41.68 ± 8.56 % ($p = 0.044$) and 42.71 ± 8.03 % ($p = 0.036$), respectively. By contrast, higher concentrations of 30 µM (33.35 ±10.93 %) and 40 µM (15.93 ± 12.07 %) epiBL caused intermediate germination rates that were not statistically significant to media without epiBL ($p = 0.197$; $p = 0.952$). With a mean of 2.44 ± 1.62 %, the concentration of 50 µM epiBL led to germination rates that were even lower than those obtained without epiBL ($p = 1.000$), indicating that high BR concentrations may have an inhibitory effect on pollen germination. In conclusion, pollen germination rates 3 h after pollen application showed a clear dose dependency leading to highest germination rates for media supplemented with 10 to 20 µM epiBL.

4.3.2 Pollen tube growth rates are stimulated by epiBL

In addition, we tested the effect of epiBL on the pollen tube growth rates. After 3 h of incubation on plates with epiBL-free PGM and PGM supplemented with the final concentrations of 5, 10, 20, 30, 40 and 50 µM epiBL, pollen tubes were measured manually as segmented lines from the pollen coat to the tube tip. Similar to the germination rate, we also observed a dose dependency pattern for pollen tube lengths (**Figure 4.1 C**; light gray boxes). On media without epiBL, pollen tubes reached a median length of 56.94 µm and a maximum length of 339.09 µm. The addition of 5 and 10 µM epiBL to the growth media resulted in significantly longer ($p = 0.002$; $p < 0.001$) pollen tubes with medians of 103.41 and 130.09 µm and maximum length of 575.43 and 542.63 µm, respectively. In contrast, a median of only 64.50 µm and a maximum length of 392.15 µm was observed on media with 20 µM epiBL, and this was comparable to the results obtained without epiBL ($p = 1.000$). Notably, higher epiBL concentrations revealed an inhibitory effect on pollen tube elongation. Median and maximum pollen tube length decreased on media with 30 µM (27.84 and 332.67 µm), 40 µM (32.18 and 118.52 µm) and 50 µM (21.89 and 47.46 µm) epiBL (**Figure 4.1 C**). This resulted in statistically significant shorter pollen tubes compared to media that were not supplemented with epiBL ($p < 0.001$, $p = 0.001$, $p < 0.001$). Final pollen tube lengths were measured 20 h after pollination (**Figure 4.1 C**, dark gray boxes). By that time the median pollen tube length reached 175.14 µm ($n = 159$) and the maximal pollen tube length 375.90 µm on plates without epiBL. On plates supplemented with 5 µM epiBL, a median pollen tube length of 231.31 µm ($n = 139$) and a maximal pollen tube

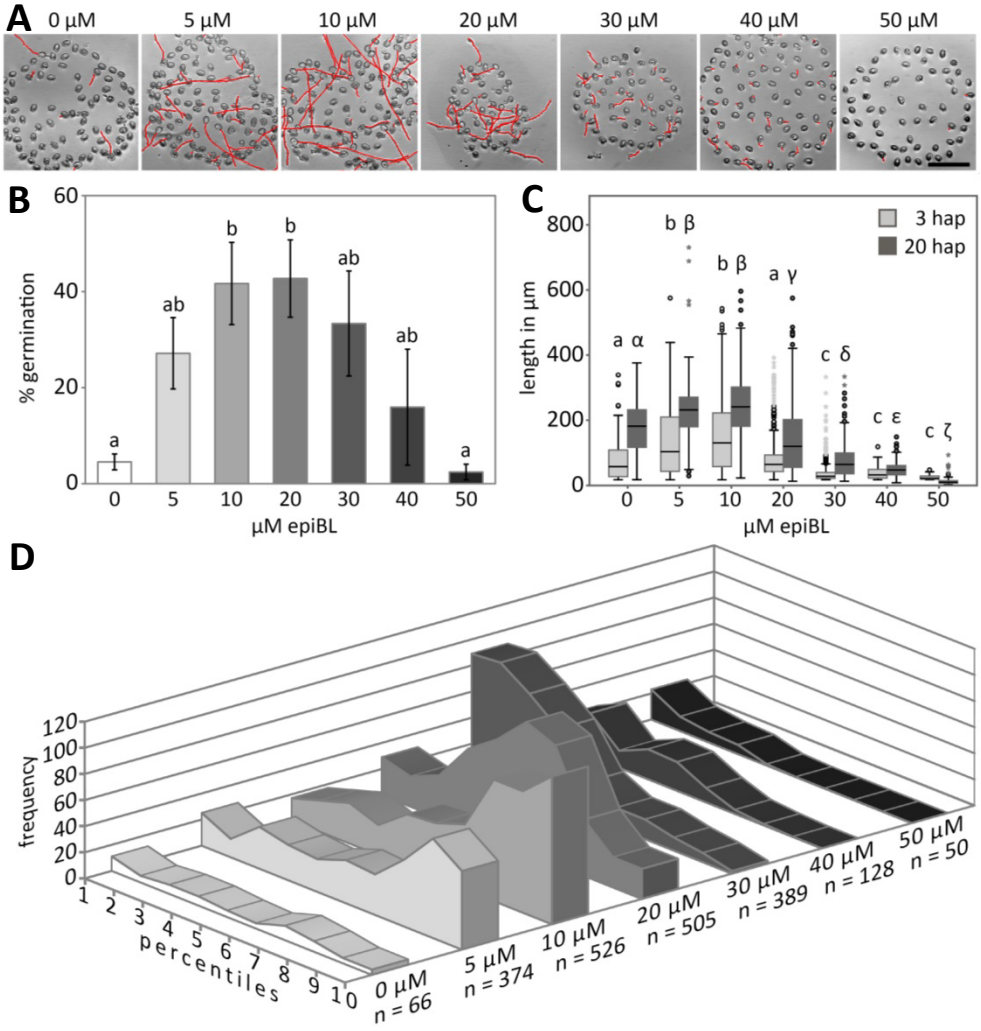

Figure 4.1 | Epibrassinolide promotes in vitro pollen germination and tube growth in a dose-dependent manner.

Arabidopsis *thaliana* (Col-0) pollen was germinated on media supplemented without and with increasing concentrations of epiBL. **(A)** Pollen grains after 3 h of incubation. Germinated pollen was counted and pollen tube lengths (red segmented lines) were measured. Note that the original images are shown in **Figure S4.1**. **(B)** Percentage of pollen germination (mean ± 1SE) and **(C)** box plot depicting the distributions of measured pollen tube length on epiBL-free plates and plates containing increasing concentrations of epiBL 3 (light gray) or 20 (dark gray) h after pollination (hap). Whiskers extend maximum 1.5-fold the interquartile range (IQR) from the box. Outliers between 1.5 and 3 IQR are indicated by circles and extremes with higher 3 IQR by *asterisks*. **(D)** Pollen tube lengths were assigned to percentiles and plotted for each epiBL concentration. Percentiles were assigned as follows: up to *1,* 21.22 µm; *2,* 26.69 µm; *3,* 33.99 µm; *4,* 45.53 µm; *5,* 58.84 µm; *6,* 78.14 µm; *7,* 109.84 µm; *8,* 163.41 µm; *9,* 244.69 µm; *10,* and longer. Different letters on top of the bars of *b* and *c* indicate statistically significant differences ($p < 0.05$). Arabic or Greek letters in (C) indicate statistically significant differences between pollen tube lengths at concentrations of 3 or 20 hap. Scale bar = 100 µm.

length of 730.62 µm were obtained after 20 h. Plates containing 10 µM epiBL resulted in a median pollen tube length of 252.33 µm (n = 136) and a maximum pollen tube length of 596.11 µm. As this resembles the pattern observed already after 3 h the sustained effect of epiBL on PT growth, and not just a temporary acceleration of PT elongation, is indicated. In order to investigate the distribution of pollen tube lengths within individual pollen populations more precisely, pollen tube lengths measured after 3 h of incubation were assigned to percentile classes that we

calculated from the entire dataset (**Figure 4.1 D**). When pollen was germinated on plates without epiBL, all pollen tube percentiles were represented almost equally. A pronounced accumulation of the highest percentiles could be observed when pollen was grown on media supplemented with 5 µM (percentiles 8–10; 163.41 µm and above) or 10 µM (percentiles 7–10; 109.84 µm and above) epiBL. This frequency peak was shifted to intermediate length percentiles in the 20 µM epiBL treatment (percentiles 4–7; 45.53 to 163.41 µm) and to even lower percentiles in the 30 µM (percentiles 1-5; up to 78.14 µm) and 40 µM (percentiles 1-4; up to 58.84 µm) epiBL treatments. In the latter case, no pollen tube lengths were obtained that belonged to the percentiles 9 or 10. When pollen was germinated on plates supplemented with 50 µM epiBL, only one pollen tube out of 50 was observed that belonged to the 5th percentile and none above. Most frequently pollen tube lengths were assigned to the first percentile in this treatment indicating an inhibitory effect of high epiBL concentrations on pollen tube elongation (**Figure 4.1 D**). The higher median pollen tube length and the affiliation of pollen grown on plates containing 5–10 µM epiBL to higher pollen tube length percentiles could be attributed to either an acceleration of pollen germination or to a promotion of cell elongation. To address this experimentally, we set up a live imaging approach to quantify pollen tube elongation rates shortly after pollen germination (**Figure 4.2 A, B**). We found that the addition of 10 µM epiBL to the PGM led to a highly significant ($p < 0.001$) increase of pollen tube growth rates from a mean of 34.8 µm h^{-1} ($n = 61$) to a mean of 153.6 µm h^{-1} ($n = 70$) compared to media lacking epiBL within the first hour of growth (**Figure 4.2 C**). Thus, we can clearly show that the longer pollen tubes observed on media containing 5-10 µM epiBL are attributed to higher cell elongation rates. Taken together, we conclude that epiBL promotes both in vitro pollen germination and pollen tube elongation in a dose-dependent manner. The addition of 10 and 20 µM epiBL to PGM showed the most beneficial effect on *Arabidopsis* pollen germination, while pollen tubes grew best on media supplemented with 10 µM epiBL, which is therefore the dose recommended to optimize in vitro growth conditions, and to improve the problems of poor pollen germination rates and slow PT growth in the model plant *Arabidopsis thaliana*.

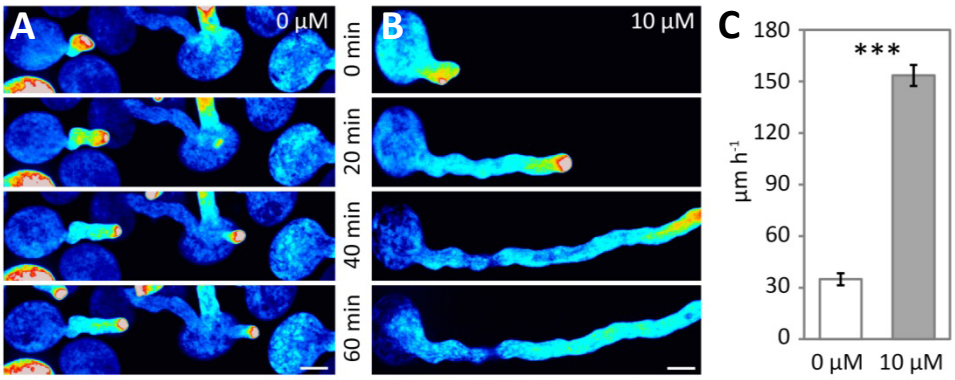

Figure 4.2 | Pollen tube growth rates are significantly stimulated by epibrassinolide.

Live imaging of pollen of an *ARO1p:ARO1-GFP* marker line (Gebert et al. 2008), germinating on media **(A)** without and **(B)** with 10 µM epiBL. **(C)** The mean elongation rate of pollen tubes growing on epiBL-free medium (0 µM, n = 70) is much slower, compared to that of pollen tubes growing on medium supplemented with a final concentration of 10 µM epiBL (n = 71; $p < 0.001$). False color code represents increasing fluorescence intensity from blue to white. Bars indicate mean ± 1SE. Scale bars = 10 µm.

4.3.3 The promoter of CYP90A1/CPD *is highly active in the transmitting tissue of the* Arabidopsis *pistil but not in pollen*

The observed in vitro effects of epiBL on pollen encouraged us to investigate the role of BRs on in vivo pollen tube growth. We therefore investigated the expression pattern and promoter activity of one of the key enzymes in BR biosynthesis, *CYP90A1/CPD*. According to the GENEVESTIGATOR microarray database (Zimmermann et al., 2004), the *CYP90A1/CPD* gene is expressed in many *Arabidopsis* tissues (**Figure 4.3 A**; light gray columns), showing high expression values in the female parts of the flower such as stigmas, carpels and ovules, and medium expression values in the pistil and the ovary. Notably, *CYP90A1/CPD* expression in pollen is very low, according to published microarray data, which is also the case for *BRI1* (*BRASSINOSTEROID INSENSITIVE 1*) encoding the main BR receptor in *Arabidopsis* (**Figure 4.3 A**; dark gray columns). To analyze the pattern of *CYP90A1/CPD* promoter activity on a single-cell resolution using optical sectioning in developing anthers, microspores and ovaries of *Arabidopsis*, we expressed the sensitive NLS:3xeGFP reporter under control of a 2,018 bp fragment upstream of the *CYP90A1/CPD* start codon. We investigated the *CYP90A1/CPD* promoter activity by imaging the nuclear GFP fluorescence in developing anthers, in microspores and pollen, and in growing pollen tubes (**Figure 4.3 B-M**). While strong GFP signals were observed in nuclei of cells in the stomium region, and in the differentiated stomium of the anther (**Figure 4.3 B-I**), *CYP90A1/CPD* promoter activity was barely detectable in developing pollen (**Figure 4.3 J-L**). Besides some autofluorescence of the pollen coat, no specific GFP signal was visible in polarized uninucleated microspores (**Figure 4.3 J**). Weak GFP fluorescence was detected in the vegetative cell and the generative cell nucleus of bicellular pollen (**Figure 4.3 K**), which decreased in mature pollen (**Figure 4.3 L**). No *CYP90A1/CPD* promoter activity was detectable in germinated pollen (**Figure 4.3 M**). Thus, the very weak promoter activity of *CYP90A1/CPD* in pollen is consistent with the low expression

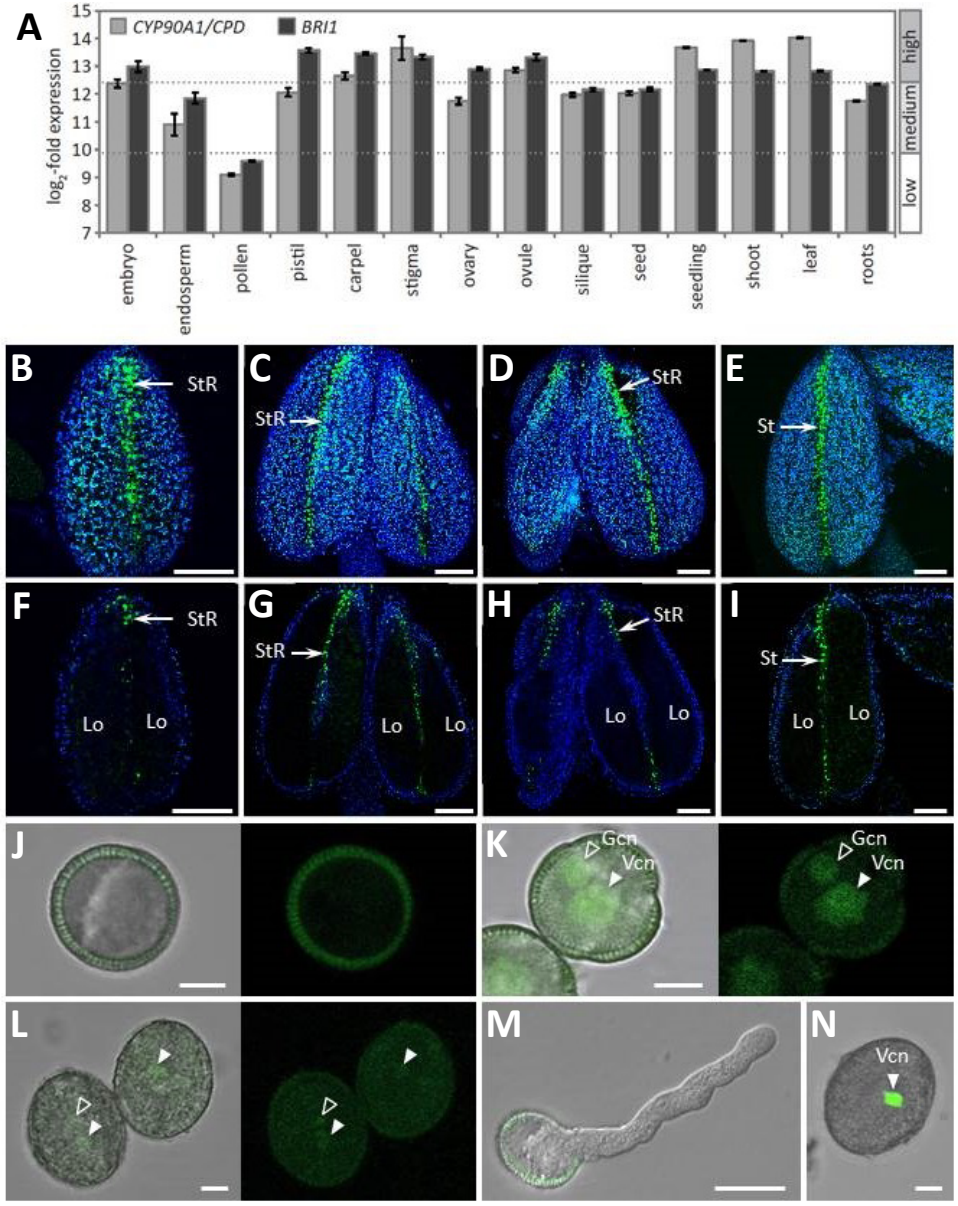

Figure 4.3 | *CYP90A1/CPD* and *BRI1* are highly expressed in female reproductive tissues but show very low expression in pollen.

(A) Log2-fold expression values of *CYP90A1/CPD* (light gray) and *BRI1* (dark gray), relative to the signal intensity on the 22 k ATH1 array according to the GENEVESTIGATOR microarray database. **(B)** to **(M)** Promoter activity of *CYP90A1/CPD* during anther and pollen development and in growing pollen tubes. **(N)** Positive control (marker line expressing NLS-3xeGFP in the vegetative cell nucleus (Vcn) of tricellular pollen). (B) to (I) Developing anthers and pollen of plants expressing the NLS-3xEGFP reporter under control of a 2,018 bp *CYP90A1/CPD* promoter fragment (*CYP90A1p:NLS-3xEGFP*), analyzed by CLSM. Flower stages were defined according to Smyth et al. (1990). Strong fluorescence of NLS- 3xeGFP is visible in nuclei of cells in the stomium region (StR) and in the differentiated stomium (St). No fluorescence is visible in the locules (Lo), where the microspores/pollens are located. Anthers of flower stages 7–8 are shown in (B) and (F); stage 9 in (C) and (G); stage 11 in (D) and (H), stage 13 in (E) and (I); In vitro germinated pollen is shown as merged image in (M). Weak GFP signals could be detected in the vegetative cell (Vcn) and generative cell nucleus (Gcn) of bicellular pollen (K), which become even weaker in tricellular pollen (L). No *CYP90A1/CPD* promoter activity was detected in polarized uninucleated microspores (J) and in germinated pollen (M). Maximum intensity projections of single optical slices are shown in (B) to (E), median optical sections through the anthers of (B) to (E) are shown in (F) to (I). Chlorophyll autofluorescence is shown in blue. Single optical sections through microspores and pollen are shown in (J) to (L), and (N). Scale bars = 50 µm in (B) to (I), 5 µm in (J) to (L) and (N) and 20 µm in (M).

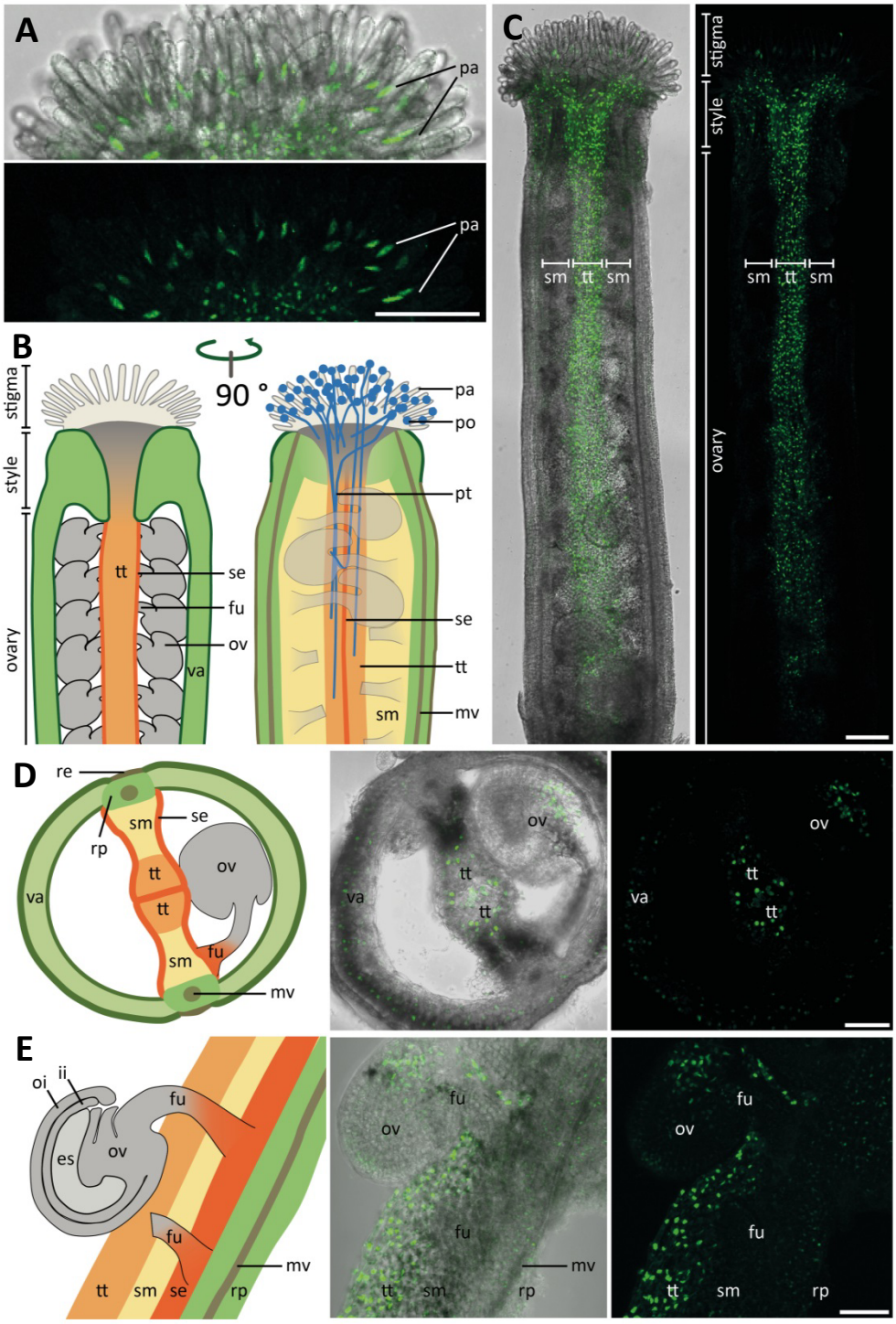

Figure 4.4 | The promoter of *CYP90A1/CPD* is highly active in the reproductive tract of *Arabidopsis*.

The activity of the *CYP90A1/CPD* promoter is shown in pistils by nuclear fluorescence of a *NLS:3xeGFP* reporter construct. **(A)** Reporter fluorescence in the papillar cells of the stigma. **(B)** Schematic overview of the Arabidopsis pistil and the pollen tube pathway along the reproductive tract. **(C)** Reporter fluorescence in a pistil expressing *CYP90A1p:NLS:3xeGFP* at the time point of flowering. Strongest fluorescence is detected in the papillae and in the cells of the transmitting tract while it is much weaker in the other tissues of the pistil. **(D)** In pistil cross and **(E)** longitudinal sections, strongest fluorescence is seen in the nuclei of the transmitting tract cells, and of the integument cells that form the micropylar opening of the ovule. Abbreviations: es, embryo sac; fu, funiculus; ii, inner integument; mv, medial vascular bundle; oi, outer integument; ov, ovule; pa, papillae; po, pollen; pt, pollen tube; rp, replum; se, septum epidermis; sm, septum; tt, transmitting tract; va, valves. Scale bars = 100 µm in (A) and (C) and 50 µm in (D) and (E).

values of *CYP90A1/CPD* in published microarray experiments. We also investigated the *CYP90A1/CPD* promoter activity of the cells of developing and mature pistils by CLSM (**Figure 4.4, Figure S4.3).** Weak nuclear GFP signals could be detected throughout the pistil. However, the highest reporter signals were observed in the papillae (**Figure 4.4 A**) and along the transmitting tissue (**Figure 4.4 C-E**), which in *Arabidopsis* begins at the stigma–style boundary of the pistil and extends through the style and septum along the apical–basal axis of the ovary (Lennon et al., 1998). Strong *CYP90A1/CPD* promoter activity was also observed in the micropylar region of the ovule integuments (**Figure 4.4 D, E**). The articulate reporter fluorescence in the reproductive tract was visible from flower stage 11, most pronounced in stages 12 and 13 and started to diminish from stage 14 (**Figure 4.3**). In other parts of the carpels and the ovules as well as in the septum tissue, which is located adjacent to the transmitting tract, only a weak promoter activity was observed (**Figure 4.4 C-E**). The strong promoter activity of *CYP90A1/CPD* in the papillae and along the reproductive tract suggests these tissues to be very active in C-3 oxidation of early brassinosteroid intermediates, which is catalyzed by CYP90A1/CPD (Ohnishi et al., 2012).

4.3.4 Pollen tube growth is retarded in BR-deficient pistils

We chose two T-DNA insertion mutants, one for CYP90A1/CPD (SALK_023532; *cyp90a1-1*), and one for the main BR-perceiving receptor BRI1 (SALK_041648; *bri1-10*) to examine pollen tube growth through their female reproductive tracts. Homozygous offspring of both T-DNA insertion lines (**Figure S4.4**) showed the characteristic dwarf phenotype of BR-deficient and BR-insensitive mutants (Clouse, 1996; Szekeres et al., 1996; Noguchi et al., 999; Kwon and Choe, 2005). The flowers of both mutants were smaller, compared to the wild-type, with shorter sepals, petals and filaments and protruding pistils (**Figure 4.5 A**). Mutant pistils were about one-third shorter compared to the wild-type (**Figure 4.5 B**), with no obvious phenotypic differences between the two mutants. In accordance to Ye et al., (2010), we observed less pollen production in *cyp90a1-1* and *bri1-10*, compared to the wild-type, with defects in releasing the pollen from dehiscent anthers, especially in *bri1-10*. The reduced length of the filaments furthermore prevented the dehiscent anthers of *cyp90a1-1* and *bri1-10* to shed pollen on the stigma, like described previously (Choe et al., 1998; Kim et al., 2005). After performing self- and reciprocal crosses between pistils and pollen of the wild-type (*Arabidopsis* Col-0), *cyp90a1-1* and *bri1-10* mutants, we initially used the aniline blue-based fluorescent staining (Mori et al., 2006) to detect pollen tubes growing through the pistil. However, the micropylar regions of unfertilized mutant ovules generally revealed very strong callose-derived signals, impeding the detection of pollen tubes within the mutant pistils. We therefore investigated the growth of wild-type pollen expressing *Lat52p:GFP* after hand-pollinating emasculated pistils of *cyp90a1-1*, *bri1-10*, and of the wild-type. Six hours after pollination, the carpels were removed and the pollen tubes within the reproductive tract, identified by their cytoplasmic GFP fluorescence, were imaged by CLSM. Measuring individual pollen tube lengths as parallel straight lines from the top of the stigma to the re-

spective pollen tube tip in the transmitting tract revealed that pollen tubes grown through the reproductive tract of Col-0 wild-type pistils (n = 189) reached a mean of 1,261 ± 57.07 µm and thus were significantly longer than pollen tubes grown in *cyp90a1-1* pistils with a mean of 905 ± 54.16 µm (n = 76; p = 0.08). Pollen tubes grown through the reproductive tract of *bri1-10* reached a mean of 1,050 ± 56.48 µm (n = 47; p = 0.010) (**Figure 4.5 C, D**). In each of the 5 independent experiments, we could observe that pollen tubes grown through the reproductive tract of *cyp90a1-1* were significantly shorter than those grown in *bri1-10* (p = 0.029). Taking the pollen tube length and the time interval from hand pollination to microscopic analysis into account, we calculated average in vivo pollen tube growth rates of 210 µm h^{-1} when pollen tubes grew through the wild-type reproductive tract. By contrast, the average pollen tube growth rate was 150.6 µm h^{-1} when wild-type pollen grew through the reproductive tract of *cyp90a1-1*. In *bri1-1* pistils, the average growth rate of wild-type pollen through the reproductive tract was 174.6 µm h^{-1} and thus higher than in *cyp90a1-1* pistils. In summary, our results show that pollen tube growth through the transmitting tract of a BR-deficient mutant is significantly reduced compared to the wild-type and the BR receptor mutant *bri1-10*. The observed promoting effect of epiBL on in vitro pollen tube growth, the strong promoter activity of *CYP90A1/CPD* in the cells of the reproductive tract, and the reduced in vivo growth rate of pollen tubes in the transmitting tract of the BR-deficient *cyp90a1-1* mutant suggest that the cells of the female reproductive tract provide BR compounds to accelerate pollen tube growth through these tissues.

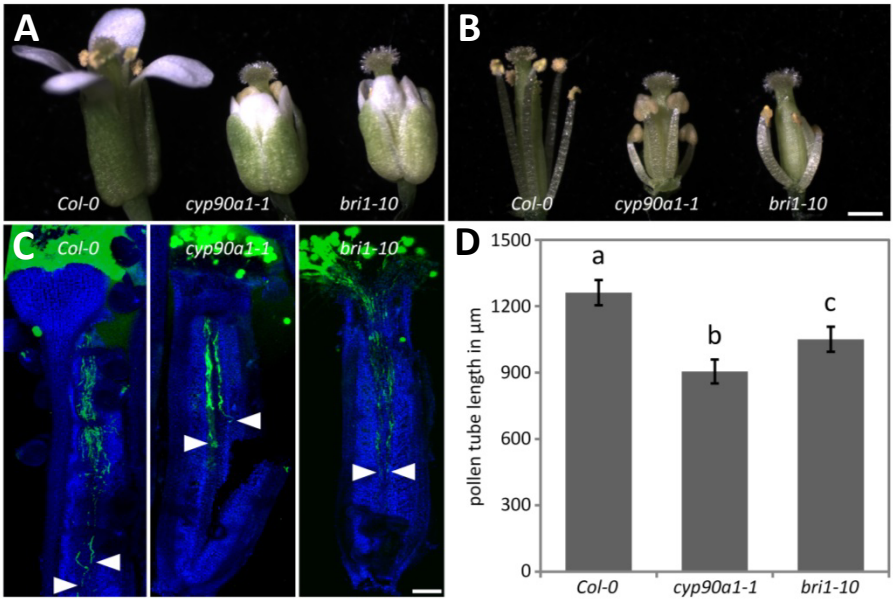

Figure 4.5 | Pollen tubes grow shorter in BR-deficient pistils of *cyp90a1-1*.

(A) and **(B)** Flowers of *cyp90a1-1* and *bri1-10* mutants are shorter compared to the wild-type (Col-0) and have reduced sepal, petal and filament length. **(C)** After hand pollination with pollen expressing cytoplasmic GFP (green), and removing the carpels from the pistils, single pollen tube tips (arrowheads) can be imaged within the transmitting tract of Col-0, *cyp90a1-1* and *bri1-10* pistils by CLSM. Chlorophyll autofluorescence is shown in blue in the false color image. **(D)** 6 h after pollination, mean ± 1SE pollen tube length was shortest in the *cyp90a1-1* mutant. Different letters on top of the bars indicate significant differences ($p < 0.05$). Scale bars = 500 µm in (B) and 100 µm in (C).

4.4 Discussion

4.4.1 Arabidopsis *pollen reacts on epiBL in a dose-dependent manner*

High pollen germination rates, morphologically normal pollen tube growth and elongation rates comparable to those obtained in pistils are substantial when in vitro grown pollen tubes are used to study cellular processes involved in polarity and tip growth. Despite much effort that has been put in optimizing in vitro germination and growth of *Arabidopsis* pollen (e. g. Li et al., 1999; Fan et al., 2001; Palanivelu et al., 2003; Johnson-Brousseau and McCormick, 2004; Boavida and McCormick, 2007) experiments with this plant species are still demanding and suffer from high variations (Bou Daher et al., 2009; Rodriguez-Enriquez et al., 2013). The general observation that in vitro cultured pollen is outperformed by in vivo grown pollen in terms of germination efficiency and pollen tube elongation rates is commonly attributed to the lack of stimulating chemical substances produced by the female floral tissues (Lord and Russell, 2002; Johnson and Preuss, 2002). Indeed, it has been clearly shown that pollen germination on media next to excised female tissues such as stigmas, stigmas and styles, or ovules was strongly enhanced. Exudates from these tissues also promote *Arabidopsis* pollen tube growth in a dose-dependent manner (Qin et al., 2011).

Among chemical substances that have been identified so far to be produced by the flower tissues and to promote in vitro pollen germination are gamma-amino butyric acid (Palanivelu et al., 2003; Yu et al., 2014), spermidine (Wu et al., 2010), and sulfinylated azadecalins (Qin et al., 2011). Flavonols stimulate pollen germination in *Brassica oleracea*, petunia, tobacco and tomato (Sedgley 1975; Mo et al., 992; Ylstra et al., 1992). The plant hormones auxin and gibberellic acid enhanced pollen germination and growth in *Prunus avium* (Hewitt et al., 1985), *Torenia fournieri* (Wu et al., 2008a), tobacco (Chen and Zhao, 2008) as well as *Arabidopsis* (Singh et al., 2002). While for some plant species a stimulating effect of BRs on pollen germination and growth was reported (Hewitt et al., 1985; Singh and Shono, 2005; Sotomayor et al., 2012; Thussagunpanit et al., 2012), there are also contradictory results on the role of BRs in pollen tube growth (Hewitt et al., 1985; Ylstra et al., 995).

In our study, we found that epiBL is able to stimulate *Arabidopsis* pollen germination and growth in a dose dependent manner. After 3 h, germination rates increased up to tenfold when media were supplemented with 10 or 20 µM epiBL. The median length as well as the maximum final length of pollen tubes almost doubled when media were supplemented with 10 µM epiBL, while epiBL concentrations higher than 20 µM inhibited both pollen germination and elongation growth, resulting in bell-shaped dose-response curves. Compared to bioassays using other *Arabidopsis* tissues, the physiological responses of pollen require a rather high concentration of exogenously supplied epiBL: Root elongation was shown to be promoted by 0.1 nM epiBL (Müssig et al., 2003), lateral root development by 10 nM brassinolide (Bao et al., 2004) and hypocotyl length in the presence of light by 1 µM epiBL (Yang et al., 2005). However, active BRs occur at very low concentration in shoots, and even lower concentrations were detected in roots (Bancos et

al., 2002), while pollen is known to be one of the richest sources of BRs (Grove et al., 1979; Fujiokaand Sakurai, 1997; Shimada et al., 2003; Bajguz and Tretyn, 2003; and references cited therein).

The observed lack of *CYP90A1/CPD* promoter activity in mature *Arabidopsis* pollen indicates high endogenous levels of bioactive BRs, as they are known to repress transcription of the *CYP90A1/CPD* gene (Mathur et al., 1998). It seems plausible that much higher exogenous BR levels are necessary to induce physiological responses in *Arabidopsis* pollen, as its sensitivity for BR might be much lower compared to other tissues. This assumption is furthermore supported by the observation that *BRI1*, the main BR perceiving receptor in *Arabidopsis*, is expressed at very low levels in pollen (**Figure 4.3A**). Moreover, *Arabidopsis* pollen shows also very low expression levels for *BRL1* and *BRL3* in published microarray data (**Figure S4.2**). These two genes were described to encode functional BRI1-like (BRL) receptor kinases (Caño-Delgado et al., 2004). The fact that Singh and Shono, (2005) found the most stimulating effect of BRs on tomato pollen at 1 µM furthermore suggests that the concentration optimum of BR action on pollen and, thus, the pollen sensitivity for active BRs may vary depending on the plant species.

By time-lapse live cell imaging, we could show that the BR-induced increase of pollen tube lengths that we observed at 10 µM epiBL was caused by significantly enhanced cell elongation rates rather than just by accelerating pollen germination. With a mean of 34.9 µm h^{-1}, the growth rates obtained on media without epiBL were comparable to those reported earlier with a range of 20-50 µm h^{-1} (Qin et al., 2011; Rodriguez-Enriquez et al., 2013; Yetisen et al., 2011). However, on media containing 10 µM epiBL, the mean growth rate of pollen tubes increased to 153.6 µm h^{-1}, which comes much closer to the in vivo pollen tube growth rate that in our experiments reached about 210 µm h^{-1} in wild-type pistils. Although we show that the pollen tube growth rates can be significantly increased by epiBL, still there is a discrepancy to the final tube lengths of pollen growing through a pistil. Our maximum pollen tube lengths reached up to 731 µm, and this is in the range of maximum in vitro pollen tube lengths that have been reported earlier (Cheung and Wu, 2008; Rodriguez-Enriquez et al., 2013). In vivo, pollen tubes are able to grow even longer, and this may be due to the supply of energy and other known or as yet unknown factors, provided by the ECM of the transmitting tissue. Likewise, the interplay of distinct chemical substances in the ECM could have an additive effect in promoting tube growth. It is conceivable, for instance, that different plant hormones can act additively on pollen germination and growth, as suggested by Wu et al., (2008b).

In a recent comprehensive study on in vitro pollen germination, Rodriguez-Enriquez et al., (2013) found that pollen germination was significantly stimulated on a cellulose-rich matrix that more closely mimicked the conditions present on the dry stigma species *Arabidopsis*. However, with a mean growth rate of 22.5 µm h^{-1}, pollen tube elongation was not increased and was in the range of growth rates reported earlier (Yetisen et al., 2011). It will be interesting to find out whether the optimized pollen germination technique by Rodriguez-Enriquez et al., (2013) in

combination with the supply of 10 µM epiBL in the germination medium will yield *Arabidopsis* pollen germination and growth rates comparable to those observed in pistils.

4.4.2 BRs are beneficial but not essential for pollen tube germination and growth

In vitro pollen tube growth is significantly increased on media containing 10 µM epiBL, and wild-type pollen tubes grow significantly slower through *cyp90a1-1* pistils compared to wild-type or *bri1-10* pistils. Exogenously provided BRs thus appear to stimulate pollen tube elongation both in vitro and in vivo. Notably, pollen of *bri1-116* and *cpd* were reported to be able to germinate and to grow through pistils after hand pollination, although *bri1-116* pollen was slower in self-pollination experiments compared to the wild-type (Ye et al., 2010). Likewise, pollen from a *cyp90a1* mutant is able to germinate and to grow in vitro (own observations), suggesting that the CYP90A1/CPD catalyzed C-3 oxidation of early brassinosteroid intermediates (Ohnishi et al., 2012) is not particularly relevant for pollen function. This is contrary to an earlier report by Szekeres et al. (1996) who described the *cpd* mutant to be male sterile because the pollen fails to elongate. Ye et al. (2010) investigated the male sterility phenotype of *bri1-116* and *cpd* in more detail and found that it is attributed to a couple of reasons: While the short filaments of mutant anthers physically impair the transfer of pollen to the stigma, developing anthers of *cpd* and *bri1-116* also exhibit a reduced number of microspore mother cells, lower pollen number per locule, altered exine and tapetum formation, and reduced pollen release from the locules. Notably, we observed a strong *CYP90A1/CPD* promoter activity in the stomium region, which is the final breakage site for anther dehiscence, supporting the importance of BR signaling for pollen release.

Little is known about the function of the high endogenous BR levels in pollen. The general ability of *cpd* pollen to germinate and to grow through the pistil (Ye et al., 2010) implies that high levels of endogenous BRs are per se not essential but might be beneficial for *Arabidopsis* pollen germination on the stigma, for example under suboptimal conditions. On the other hand, BR synthesis in *cpd* pollen might also be bypassed, for example, by exploiting BR intermediates or reversibly inactivated BR storage compounds provided by the reproductive tract, or by using an alternative route in the grid-like BR biosynthesis pathway (reviewed in Vriet et al., 2013). The fact that *bri1-116* pollen grows slower compared to the wild-type (Ye et al., 2010) furthermore suggests that BR perception is either not essential but beneficial for elongating pollen tubes or that BRI1 and other BR-perceiving receptors act redundantly in pollen. The investigation of in vitro pollen germination and tube growth of *cpd*, *bri1* and *bri1/brl* double or triple mutants, and the biochemical analysis of BR levels in the transmitting tract of *Arabidopsis* will be necessary to address these questions.

4.4.3 *BRs: provided by the transmitting tract of* Arabidopsis *to stimulate pollen tube growth?*

It has been shown in many species that the tissues of the reproductive tract play an important role in guiding pollen tubes by means of their morphology and by releasing pollen tube growth-promoting substances in the ECM (Crawford and Yanofsky, 2008). The fact that epiBL stimulates in vitro pollen germination and tube growth and that apical–basal pollen tube growth through *cyp90a1-1* pistils is significantly reduced compared to the wild-type suggests that BR is one of these substances. However, the strong promoter activity of *CYP90A1/CPD* in the reproductive tract indicates that in these cells, BR homeostasis is regulated by the formation of storage intermediates or conjugated BR metabolites (Fujioka and Yokota, 2003; Bajguz, 2007), as bioactive BRs would lead to the repression of *CYP90A1/CPD* transcription (Mathur et al., 1998). Likewise, data from microarray experiments show high expression values of *CYP90A1/CPD* in style and ovary tissues. This is in contrast to earlier studies by Mathur et al. (1998) where β-Glucuronidase reporter activity under control of a 964 bp *CYP90A1/CPD* promoter fragment could only be detected in the cauline leaves and sepals of *Arabidopsis* inflorescences but not in the pistil. However, the observed differences in promoter activities can be due to the much longer promoter region used in our studies (2,018 bp), and the presence of additional cis-elements necessary to drive *CYP90A1/CPD* expression in the pistil, which may lack in the shorter promoter fragment used by Mathur et al. (1998).

The importance of BRs for the formation and the function of the transmitting tract has already been proposed because the bHLH transcription factor CESTA/HALFFILLED (CES/HAF) turned out to be a positive regulator of BR-biosynthetic gene expression, including *CYP90A1/CPD* (Poppenberger et al., 2011). CES/HAF acts redundantly with two other bHLH transcription factors, BEE1 and BEE3 (Crawford and Yanofsky, 2011), which are BR regulated (Friedrichsen et al., 2002). Notably, the *haf/bee1/bee3 (hbb)* triple mutant shows reduced seed set especially in the lower part of the silique and strongly reduced in vivo pollen tube growth rates compared to the wild-type, which has been attributed to the dramatically reduced ECM production in the transmitting tract of the mutant (Crawford and Yanofsky, 2011). Notably, the expression of *CES/HAF* and *CYP90A1/CPD* overlaps in the tissues of the reproductive tract, which is regarded as a pollen tube superhighway (Johnson and Preuss, 2002) since pollen tubes grow faster, longer and more straightforward within this tissue than in vitro.

In summary, our results suggest that the growth-promoting properties of the reproductive tract of *Arabidopsis* depend, at least partly, on BR compounds, which are provided by the cells of the reproductive tract to promote pollen germination on the stigmatic papillae, and to boost pollen tube growth for rapid double fertilization.

4.5 Summary

Pollen tubes are among the fastest tip-growing plant cells and represent an excellent experimental system for studying the dynamics and spatiotemporal control of polarized cell growth. However, investigating pollen tube tip growth in the model plant *Arabidopsis* remains difficult because in vitro pollen germination and pollen tube growth rates are highly variable and largely different from those observed in pistils, most likely due to growth-promoting properties of the female reproductive tract. We found that in vitro grown *Arabidopsis* pollen respond to brassinosteroid (BR) in a dose-dependent manner. Pollen germination and pollen tube growth increased nine- and fivefold, respectively, when media were supplemented with 10 µM epibrassinolide (epiBL), resulting in growth kinetics more similar to growth in vivo. Expression analyses show that the promoter of one of the key enzymes in BR biosynthesis, *CYP90A1/CPD*, is highly active in the cells of the reproductive tract that form the pathway for pollen tubes from the stigma to the ovules. Pollen tubes grew significantly shorter through the reproductive tract of a *cyp90a1* mutant compared to the wild-type, or to a BR perception mutant. Our results show that epiBL promotes pollen germination and tube growth in vitro and suggest that the cells of the reproductive tract provide BR compounds to stimulate pollen tube growth.

CHAPTER 5 *Male–female Communication Triggers Calcium Signatures During Fertilization in* Arabidopsis

The work of this chapter was published in *Nature Communications* (Denninger et al., 2014). Frank Vogler contributed to this work by molecular cloning of the membrane marker P_{Lat52}*:tagRFP-T-REM*, the generation of transgenic *Arabidopsis* lines and by crossing these lines with a sperm cell marker line. He screened the progeny of these lines to obtain the double marker LHR that is shown in **Figure 5.1**, **Figure 5.2**, **Figure 5.3**, **Figure 5.4**, **Figure S5.4** and in all **Supplemental Movies**. Furthermore F.V. provided knowledge input on the development of the semi in-vivo fertilization assay. F.V. contributed to the manuscript by writing the respective parts of this work.

5.1 Introduction

Fertilization in eukaryotes involves species-specific recognition, local interaction, attachment and eventually fusion of two gametic cells of opposite sex. The fertilization process in flowering plants (angiosperms) is especially complex and requires communication between the cells of two haploid gametophytes (Dresselhaus and Franklin-Tong, 2013). The pollen tube comprises the male gametophyte and consists of a vegetative tube cell that carries two immotile sperm cells. The female gametophyte is composed of the two female gametes (egg and central cell) and accessory cells at opposite poles. Two synergid cells adjoining the egg cell are located at the micropylar entry of the ovule, while antipodal cells neighboring the central cell are found at the chalazal pole. After sperm cell delivery and fusion of two gamete pairs, a process termed as double fertilization, the fertilized central cell develops into the endosperm and the fertilized egg cell gives rise to the embryo. Numerous cell–cell communication events take place during the attraction of the male towards the female gametophyte and their mutual interaction. It was reported that synergid cells are responsible for pollen tube attraction by secreting species specific chemotactic peptides (Márton et al., 2005; Okuda et al., 2009; Márton et al., 2012; Takeuchi and Higashiyama, 2012). Moreover, they recognize arriving pollen tubes involving cell surface receptors (Escobar-Restrepo et al., 2007; Capron et al., 2008; Kessler et al., 2010) and control sperm release (Amien et al., 2010; Woriedh et al., 2013). After pollen tube burst, the two sperm cells rapidly reach the cleft between egg and central cell representing the site of gamete interaction and fusion (Hamamura et al., 2011). Sperm cells interact with female gametes and become activated by egg cell-secreted small proteins (Sprunck et al., 2012). The molecular mechanisms by which the male and female gametes recognize each other and the intracellular signaling events that result in synergid cell death, female gamete activation, control of successful plasmogamy and the prevention of multiple sperm fusion (polyspermy) remain to be identified.

In animals, calcium plays a key role during fertilization as a secondary messenger of cell–cell interaction events and triggers, for example, the establishment of a fertilization membrane to prevent polyspermy (Gilkey et al., 1978; Miao et al., 2012; Iwao, 2012). While the role of calcium signaling during double fertilization in flowering plants still remains to be unveiled, it is known that calcium signaling plays a key role in cell–cell recognition, for example, during the innate immune response to pathogens or the establishment of symbiosis (Ma and Berkowitz, 2007; Oldroyd et al., 2009). Calcium has also known functions during the early stages of fertilization, which include promoting pollen tube growth, guidance and eventually the regulation of its burst (Holdaway-Clarke et al., 1997; Schiøtt et al., 2004; Iwano et al., 2012; Boisson-Dernier et al., 2013). Recently, it was also reported that the arrival of the pollen tube causes $[Ca^{2+}]_{cyto}$ oscillations in synergid cells (Iwano et al., 2012). This observation opened up the question how the pollen tube and the synergid cells interact with each other to trigger these oscillations, whether this occurred through direct contact or through signals that act at a distance.

The first evidence that calcium indeed is also involved during gamete fusion was obtained from in vitro fertilization experiments. Gamete fertilization in maize mediated by calcium chloride was shown to occur in a cell-specific manner and leads to a block of polyspermy (Faure et al., 1994). More detailed studies have reported that Ca^{2+} influx occurred in this in vitro system after egg–sperm fusion and spreads as a wave front from the fusion site towards the whole cell lasting for up to 30 min (Digonnet et al., 1997; Antoine et al., 2000; Antoine et al., 2001). The authors further observed that fusion, but not gamete adhesion triggered a transient $[Ca^{2+}]_{cyto}$ rise in fertilized egg cells and found that cell wall material is formed after fusion likely representing a block to polyspermy functionally similar to the fertilization membrane in animals. These data strongly support the notion that calcium signaling may be of similar importance during double fertilization in plants compared with fertilization in animals. However, in vitro investigations are limited as double fertilization mechanisms involve many timely and accurately regulated cellular interactions to guarantee reproductive success.

To visualize when and how calcium transients are triggered during the whole double fertilization process in vivo, and to enable studies on the functional role(s) of $[Ca^{2+}]_{cyto}$ changes during fertilization, we used an enhanced genetically encoded fluorescent calcium sensor. This sensor consists of a calcium binding domain fused to two fluorophores that are spectrally overlapping. Their proximity and orientation depends on the conformation of the binding domain. Calcium binding therefore results in differential Förster Resonance Energy Transfer (FRET) between the donor and acceptor fluorophores. Most widely used in plants are Yellow Cameleon sensors (Miyawaki et al., 1997; Nagai et al., 2004; Monshausen, 2008; Krebs et al., 2012) that contain a calmodulin-based calcium-binding domain. It has been argued, however, that due to the high degree of conservation of calmodulin, cellular pathways might interfere with the sensor, and vice versa (Heim and Griesbeck, 2004). This led to the development of the calcium sensor CerTN-L15, a sensor with enhanced folding, increased brightness and a calcium-binding domain based on troponin C,

a protein exclusively found in myocytes (Heim et al., 2007). Thus, it is unlikely that CerTN-L15 exhibits strong interactions with plant proteins.

By using a modified semi-in vivo system (Palanivelu and Preuss, 2006) and expressing the improved calcium sensor CerTN-L15 from various female gametophyte cell-type-specific promoters, we were able to monitor $[Ca^{2+}]_{cyto}$ signatures by live-cell imaging throughout the whole double fertilization process in the model plant *Arabidopsis*. We report that direct contact with the pollen tube apex and not its shank region triggers polarized $[Ca^{2+}]_{cyto}$ oscillations in synergids cells. Furthermore, we link sperm cell dynamics at the gamete fusion site to specific Ca^{2+} signatures in both egg and central cells. We show that first Ca^{2+} transients precede fertilization, indicating that they might be required for early events such as female gamete activation. A second Ca^{2+} transient solely in the egg cell appears associated to sperm–egg fusion and might trigger later events such as a block to polyspermy.

5.2 Material and Methods

5.2.1 Generation of CerTN-L15 expressing plants

The coding sequence of CerTN-L15 (Heim et al., 2007) was amplified using the primers P12 (5'-GGGGACAAGTTTGTACAAAAAAGCAGGCTGCCACCATG-3') and P16 (5'-GGGGACCACTTTGTACAAGAAAGCTGGGTTCA-3'). The resulting PCR product was used in a BP-reaction (Gateway Technology manual; Life Technologies) with the donor vector pDONR207 (Invitrogen) resulting in pDONR207-CerTN-L15. *Sac*I/*Spe*I restriction digest was performed to remove the 35S promoter of the destination vectors pB2GW7 and pH2GW7 (Karimi et al., 2007), respectively, which was subsequently replaced by the promoters of either AtEC1.1 (Sprunck et al., 2012) (454 bp upstream of the start codon of At1g76750), AtMYB98 (Kasahara et al., 2005) (1.494 bp upstream of the start codon of At4g18770) or AtDD65 (Steffen et al., 2007) (1.246 bp upstream of the start codon of At3g10890). The *EC1.1* promoter was amplified using the primers P9 (5'-CAAAAGCTGGAGCTCTCTAGAG-3') and P10 (5'-GGCCGACTAGTATCCTTCTCAAC-3') from the plasmid pEC1.1-GUS12. The promoter *pMYB98* was amplified with the primers P7 (5'-ATGGAGCTCGCGTCGACAGTTG-3') and P8 (5'-AGGGACTGACTAGTGGATC-3') from the plasmid pN7-Myb-EC1 (S. Sprunck, unpublished). *pDD65* was amplified using the primers pDD65_FW (5'-AGTGAGCTCAATCAAAATTTAACATTTAAATAAAGTC-3') and pDD65_REV (5'-TGATTACTAGTATCCTTTTCTACTTTGTTTTTGTTTTTGTGCT-3') from *Arabidopsis* Col-0 genomic DNA (*Sac*I and *Spe*I restriction sites underlined in primer sequences). CerTN-L15 (pDONR207-CerTN-L15) was recombined into the four destination vectors pB2GW7, pB2GW7-pEC1, pB2GW7-pMYB98 and pH2GW7-pDD65 by LR reaction (Gateway technology, Life Technologies) according to the manufacturer's protocol. Resulting expression constructs (p35S::CerTN-L15, pEC1::CerTN-L15, pMYB98::CerTN-L15 and pDD65::CerTN-L15) were transformed into

Arabidopsis Col-0 plants by floral dipping (Clough and Bent, 1998). Transformants were selected according to their selection marker and fluorescent properties.

5.2.2 *Generation of the double marker line LHR*

The promoter *pLat52* was amplified from *Lat52::GFP* expressing plants (Twell et al., 1990) using the primers FV01 (5'-GGGGGAGCTCATACTCGACTCAGAAGGTATTG-AGG-3') and FV02 (5'-GGGGACTAGTTTTAAATTGGAATTTTTTTTTTTGG-3') and cloned into the destination vector pB2GW7 (Karimi et al., 2007) by replacing the *35S* promoter using the introduced *Sac*I and a *Spe*I sites, resulting in the destination vector pVOLat52GW. *TagRFP* was amplified from pTagRFP-C (Evrogen) with the primers ptagRFPfwd (5'-CACCATGGTGTCTAAGGGCGAAGAGCTG-3') and ptagRFPrev (5'-TGGCTGATT-ATGATCAGTTATCTAGATCC-3') followed by insertion into the pENTR/D-TOPO vector according to the manufacturer's protocol (Gateway Technology manual; Life Technologies) to obtain pENTR-tagRFP. To yield pENTR-tagRFP-T, site-directed mutagenesis was performed (Quik Change II Site-Directed Mutagenesis Kit, Agilent) using the primers tagRFP-TPOINT (5'-CTGGAAGGCAGAACCGACATGGCCCTG-3') and TagRFP-TPOINTrev (5'-CAG-GGCCATGTCGGTTCTGCCTTCCAG-3'). A C-terminal 109 nucleotide sequence of MtSYMREM1 (Konrad et al., 2014), covering the C-terminal remorin anchor, was amplified from pDONR207-MtSYMREM1 with the primers FV03 (5'-GGGGAATTCTGGGGAAGA-AATCCTCAAGGTAGAG-3') and FV04 (5'-CCCCGGATCCCTAACTGAAAAACCTTA-AACCGCTG-3'). The resulting PCR product was cloned into pENTR-tagRFP-T using the introduced *Eco*RI and *Bam*HI restriction sites (underlined) to obtain pENTR-tagRFP-T-REM. The expression construct pP_{Lat52}:tagRFP-T-REM was created by LR reaction (Gateway Technology, Life Technologies) with pENTR-tagRFP-T-REM and pVOLat52GW. To create the double marker line Lat52:tagRFP-T-REM; HTR10:HTR10-mRFP (LHR), pP_{Lat52}:tagRFP-T-REM was used to transform plants homozygous for HTR10:HTR10-mRFP (Ingouff et al., 2007) by floral dipping (Clough and Bent, 1998). Transformants were selected according to their selection marker and fluorescent properties.

5.2.3 *Growth conditions of* Arabidopsis thaliana

Arabidopsis plants were either grown under short day conditions (8 h light, 20 °C, 50 – 70 % relative humidity) for 4–6 weeks followed by long day conditions (16 h light, 20 °C, 50 – 70 % relative humidity) or continuously grown under long day conditions.

5.2.4 Root imaging

Roots were prepared for imaging using the RootChip, a microfluidic perfusion device as described previously (Grossmann et al., 2011; Grossmann et al., 2012). In brief, seeds were sterilized, placed on cut pipet tips (5 mm) that were filled with MS medium (Murashige and Skoog, 1962) and incubated for 4 days under long day conditions in a growth chamber (16 h, 20 °C, 50–70 % relative humidity). Seedlings were transferred to the RootChip and incubated for one additional day in liquid MS medium. Images were acquired every 3 s. Growing roots were continuously perfused with ½ strength MS medium and treated with square pulses of 200 mM mannitol over 5 min.

5.2.5 Semi-in vivo pollen tube growth assay

Semi-in vivo experiments were performed with modifications from the originally described assay (Palanivelu and Preuss, 2006) using modified pollen germination medium (PGM)(Li et al., 1999) containing 18 % sucrose, 0.01 % boric acid, 1 mM $MgSO_4$, 1 mM $CaCl_2$, 1 mM $Ca(NO_3)_2$, 5 mM MES and 0.75 % ultrapure agar (Version 1) or 0.175 % agarose (peqGold Universal) (Version 2). The pH was adjusted to 7.0 with 200 mM KOH. The pistils and ovules that were used in all experiments were dissected from flowers with not yet opened anthers to ensure that only pollen used for pollination will fertilize the observed ovules. Preparation of pistils was performed by removing the leaves and anthers from the flower with forceps (Dumont No. 5) followed by cutting the pistil at junction of style and ovary with a razorblade and placing it upright on solidified PGM. Pollen was used from freshly opened anthers and put directly on the stigma of the cut pistils. For dissection of ovules, a pistil was cut open at the replum with the tip of a 27-gauge needle and the ovules were removed from the placenta using the needle. All dissections were performed on a microscope slide with double-sided tape to fix the tissue, but the contact of all tissue parts used for the assay with the adhesive tape was avoided.

5.2.6 Modified semi-in vivo assay

Version 1: A round plastic chamber (Ø 1 x 1 cm), which was covered and sealed on one side with a microscope slide, was completely filled with 1 mL fresh PGM containing 0.75 % agar. Medium was solidified for 30 min. The pollinated pistils and the individual ovules were placed on the medium surface. Afterwards, the chamber was covered by a cover slip with spacers of modelling clay, in a way that an air cushion was created between specimen and cover glass. The chamber was incubated at room temperature with light for 3 to 5 h. When the pollen tubes left the cut pistil and grew towards the dissected ovules, the chamber was turned cover glass-side down, the microscope slide was removed and the air cushion was released slowly, by puncturing the modelling clay with a needle. Thus, the agar helped to immobilize the tissue at the cover slip

without disturbing the arrangement of the pistil and the ovules. After an additional incubation for 30 min, the chamber was used for imaging.

Version 2: All preparations were done under humidified conditions with a relative humidity of > 80 % by dissecting under a hood containing a humidifier. Pistils were cut and placed vertically on solid PGM containing 0.75 % (w/v) agar. Stigmas of the pistils were pollinated and incubated for 3 h in the humidified chamber with light. Just before pollen tubes emerged from the pistil (usually ~ 3.5 h after pollination), pistils were transferred into a two-well microscope µSlide (IBIDI) that was filled with half solid PGM containing 0.175 % (w/v) agarose. Before filling the µSlide with PGM, a 0.5-mm thick silicon mat with small slots, cut in the center of the silicon layer, was placed on the bottom of the µSlide wells. Pistils were carefully pushed through the PGM to the bottom of the slide and fixed horizontally in the edges of the slots in the silicon layer. Afterwards, the ovules were dissected and transferred to the µSlide. They were pushed through the PGM with thin glass needles, pulled with a micropipette puller (P-97, Sutter Instruments), and placed in front of the cut pistils. The slides were covered with a lid and incubated in the humidified chamber with light. When pollen tubes had reached the ovules the µSlide was transferred to the microscope for imaging.

5.2.7 Microscopy

Imaging of the RootChip experiments was performed on an inverted epifluorescence microscope (LeicaDMIRE2) using a 10x objective (Leica, 0.40 N.A., Air). For excitation of the sensor, a Polychrome V monochromator light source (TILL Photonics, Germany) was used. Fluorescence signals were detected using a Dual View beam splitter (Photometrics, USA) containing an ET470/24m and ET535/30m filter setup and an EMCCD camera (QuantEM:512SC; Photometrics).

Semi-in vivo experiments were either done on an inverted Leica DMI6000B microscope using a 40x objective (Leica, 1.25 N.A., Oil) equipped with a Yokogawa (Japan) CSU-X Spinning Disk confocal head and a motorized stage (ASI, USA) for automated multi position imaging or on a Leica SP8 inverted confocal laser scanning microscope using a 40x objective (Leica, 1.3 N.A, oil). Using the Leica DMI6000B microscope, fluorophores were excited at a wavelength of 441 nm (Cerulean), 514 nm (Citrine) and 561 (RFP/tagRFP) using a multiband dichroic mirror (445/515/561 nm dichroic beam splitter, Semrock, USA) and the fluorescence signal was detected with an Evolve EMCCD camera (Photometrics, USA) using band-pass emission filters (475/42, 540/15 narrow, 605/64 RFP, Semrock). Exposure times were 100 ms (Citrine), 300 ms (Cerulean) and 600 ms (RFP). Acquisition was controlled using SlideBook 5.0 software (Intelligent Imaging Innovations, USA). Using the Leica SP8, fluorophores were excited with the same wavelengths described for the spinning disk system. Emission was detected using band-pass filter settings (Cerulean: 462–510 nm; Citrine: 520–550 nm and RFP/tagRFP: 570–666 nm).

5.2.8 Image processing and data analysis

Image processing and analysis were performed using FIJI (http://fiji.sc/). To correct for movements or growth, images were registered using the StackReg plug-in (http://bigwww.epfl.ch/thevenaz/stackreg/). To create false color ratiometric images for FRET experiments, the Ratio Plus plug-in (http://rsbweb.nih.gov/ij/plugins/ratio-plus.html) and a 16-colour lookup table were used. For false color ratiometric images as shown in **Figure 5.1 B**, raw data were processed as follows: multiplication of both 'FRET' channels (acceptor emission under donor excitation) with the reference channel (acceptor emission under acceptor excitation), 32-bit conversion, application of a mean filter with a radius of five pixels to both images, thresholding (Otsu-method) over the stack histogram. Dividing the acceptor channel by donor channel resulted in the ratiometric image (16-colour lookup table).

Analysis of FRET ratio changes was performed by calculating the ratio of fluorescence intensities of acceptor and donor under donor excitation using the Multi Measure plug-in (http://www.optinav.com/imagej.html) in specific regions of interest (**Figure S5.6**). The regions were 50 x 50 mm in root experiments and 4 x 4 mm squares for subcellular analysis or polygons in shape of the synergid cells for single cell analysis. The values of those measurements were further analyzed in Excel. The ratios of acceptor and donor were normalized ((Ratio[t]Ratio[t_0])/Ratio[t_0]) to display the relative ratio change over time. For the analysis of the $[Ca^{2+}]_{cyto}$ oscillation in synergids, the individual 4 x 4 mm regions were aligned as described (**Figure 5.2 D**) and the regions were moved over time, following the position of the growing pollen tube tip. The amplitudes of the ratio changes in individual regions were calculated and the amplitude values of one oscillation event were normalized to the amplitude in region D1/L1. To define significant $[Ca^{2+}]_{cyto}$ oscillations in synergid cells, a base line was determined as the mean ratio change over 10 min of FRET measurement before a pollen tube was in contact with the synergid cell. To determine the significance of amplitudes, the traces were smoothened applying a sliding average of three time points, the first derivative was calculated and the s.d. of the baseline (30 min without cell–cell interaction) of the resulting curve was determined. Amplitudes exceeding the s.d. of the baseline by fivefold (5 x σ) were considered significant.

Tracking of sperm cells was performed with the FIJI Track Mate plug-in (http://fiji.sc/TrackMate) and resulting coordinates were plotted using excel. Kymographs for the analysis of sperm cell movement at the gamete fusion site were generated using the Multiple Kymograph plug-in (http://www.embl.de/eamnet/html/body_kymograph.html) along a segmented line that covered the track of each sperm cell separately. To compare the movement speed of the two sperm cells, the individual Kymographs were aligned with the starting point of the sperm cell movement overlaying with each other.

5.3 Results

5.3.1 Sensor based recording of cell-specific calcium changes

To monitor $[Ca^{2+}]_{cyto}$ during the whole double fertilization process, we expressed the Ca^{2+} sensor *CerTN-L15* (Heim et al., 2007) under control of cell-type-specific promoters in synergid cells (*MYB98*-promoter; AT4G18770 (Kasahara et al., 2005)), egg cell (*EC1.1* promoter; AT1G76750 (Sprunck et al., 2012) and the central cell (*DD65*-promoter; AT3G10890 (Steffen et al., 2007) as indicated (**Figure 5.1 A**). This sensor is based on the Ca^{2+} binding domain of troponin C and two spectrally overlapping fluorescent molecules cerulean and citrine that act as donor and acceptor for FRET, respectively. As the CerTN-L15 sensor has not been used in plants before, we first validated its functionality in roots expressing the sensor constitutively under control of a *35S* promoter, using a microfluidic device that allows imaging under controlled perfusion of roots (Grossmann et al., 2011). Repeated pulsed treatments with a hyperosmotic solution resulted in $[Ca^{2+}]_{cyto}$ signatures with a minor increase in FRET ratio during the treatment-induced root shrinkage and a steep incline of the FRET ratio after wash-out and return to original root length, followed by a gradual return of the FRET ratio to the baseline (**Figure S5.1**). This characteristic signature has been observed before using Yellow Cameleon sensors (Krebs et al., 2012; Kiegle et al., 2000) indicating that CerTN-L15 is functional in plants.

5.3.2 Pollen tube apex triggers calcium signatures in synergids

To record $[Ca^{2+}]_{cyto}$ signatures in cells of the female gametophyte, we performed our measurements on excised *Arabidopsis* ovules arranged around a pollinated pistil (Palanivelu and Preuss, 2006). This semi-in vivo setup was modified to achieve automated time-lapse imaging at high spatiotemporal resolution. When CerTN-L15 was expressed in synergid cells, we observed repeated FRET ratio changes consistent with $[Ca^{2+}]_{cyto}$ increases in (Antoine et al., 2000) out of (Digonnet et al., 1997) experiments when the pollen tube successfully interacted with the synergid cells (**Figure 5.1 B,C**). The $[Ca^{2+}]_{cyto}$ transients occurred with variable periodicity within and among cells with a time interval of 100–200 s and durations of 50–170 s per individual transient. (**Figure 5.1 D, Figure S5.2 A, Supplemental Movies 5.1** and **5.2**). Burst of pollen tubes and receptive synergid cell occurred between 30 and 50 min after interaction with synergid cells. $[Ca^{2+}]_{cyto}$ oscillations with low amplitude (lower graphs in **Figure 5.1 D**) did not result in burst. When pollen tubes failed to target the micropyle of the ovule or did not reach the synergid cells, we detected spontaneous weak $[Ca^{2+}]_{cyto}$ fluctuations in two out of 16 trials (**Figure 5.1 D**, lower panel). In both cases, fluctuations were less regular and showed significantly reduced amplitude by comparison with the signatures observed when pollen tubes successfully approached the synergid cells. We conclude from these observations that limited $[Ca^{2+}]_{cyto}$ oscillations can occur spontaneously in synergid cells at a low likelihood. Only pollen tubes that successfully enter the ovule and interact with the synergid cells induce high persistent and effective $[Ca^{2+}]_{cyto}$ oscillations.

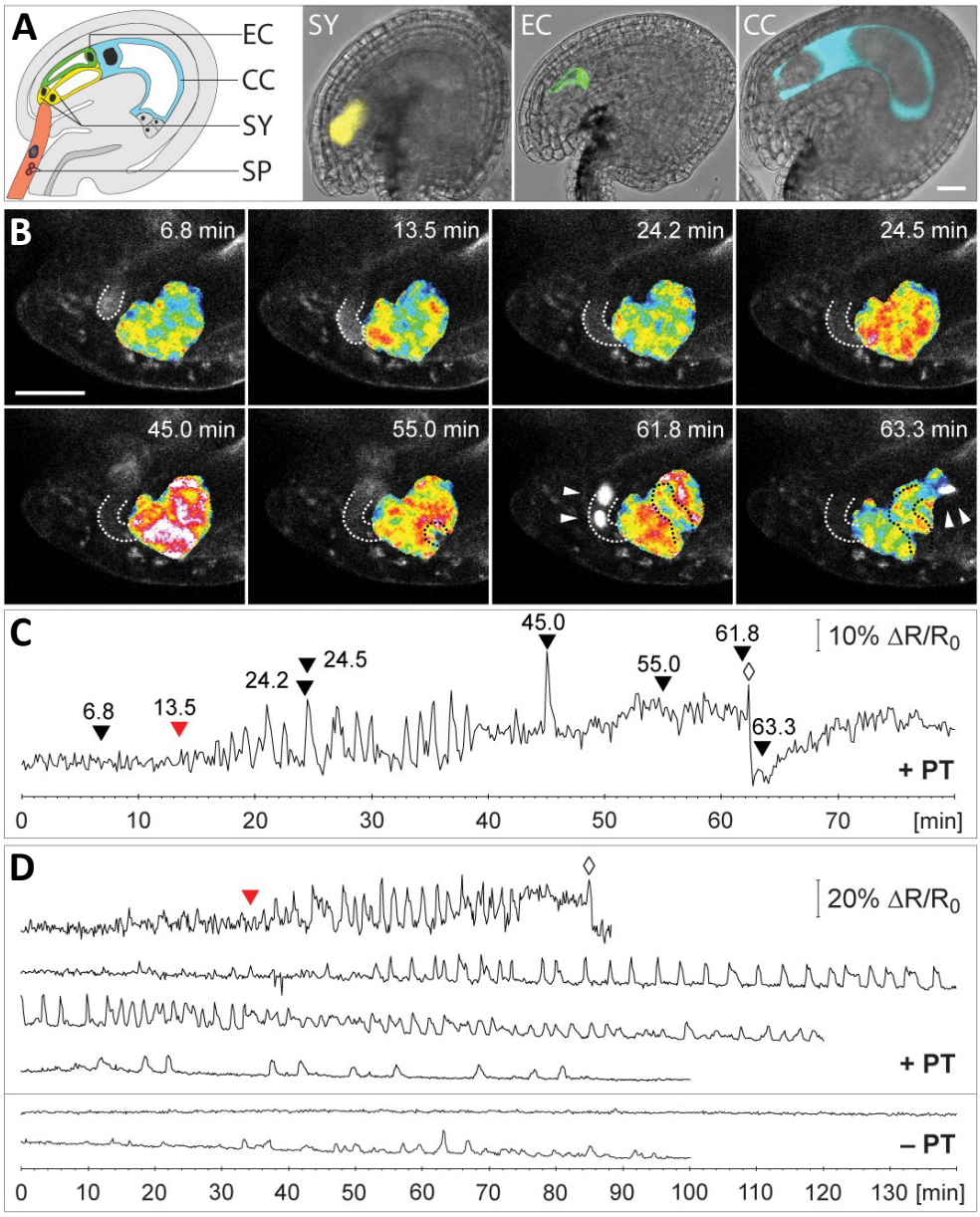

Figure 5.1 | $[Ca^{2+}]_{cyto}$ signatures in synergid cells during pollen tube arrival and discharge.

(A) Expression of the calcium sensor CerTN-L15 in specific cells of the female gametophyte. Left panel: Schematic of an ovule and approaching pollen tube (PT, orange) containing two sperm cells (SP, red). The female gametophyte consists of two synergid cells (SY, yellow), one egg cell (EC, green) and one central cell (CC, cyan). Right panels: merged bright field and confocal images of ovules expressing CerTN-L15 in specific cell types (promoters are in parentheses): SY (*pMYB98*), EC (*pEC1*) and CC (*pDD65*). **(B)** Arrival and discharge of a PT at the SYs. Time series of a PT of the LHR marker line displaying the tube apex (outline of the PT is indicated by dotted lines) approaching SYs (false colour ratiometric images of pMYB98:CerTN-L15). SPs (arrowheads) of this marker line are discharged about 62 min after recording was initiated. The following stages are visible: arrival of a PT (6.8 min), first PT contact with SY (13.5 min), before (24.2 min) and during (24.5 min) an oscillation of $[Ca^{2+}]_{cyto}$, growth of PT around SY (45.0 min, 55.0 min), PT shortly before (61.8 min) and after (63.3 min) release of SPs. See corresponding **Supplemental Movie 5.1**. **(C)** $[Ca^{2+}]_{cyto}$ signature of SYs. Normalized ratio changes of CerTN-L15 in cells shown in (B). Arrowheads indicate time points of images in (B). Red arrowhead: first physical contact of PT and SY, diamond: pollen tube burst **(D)** Variations of $[Ca^{2+}]_{cyto}$ signatures in SYs. Selection of representative $[Ca^{2+}]_{cyto}$ measurements in SYs in the presence (+ PT, upper panel) or absence of a PT (- PT, lower panel). Red arrowhead marks the time point where the first physical contact of a PT and the synergid could be observed, diamond indicates pollen tube burst. The first graph of the lower panel (- PT) shows typical $[Ca^{2+}]_{cyto}$ recording of SY without PT. The second graph displays an exceptional case of spontaneous $[Ca^{2+}]_{cyto}$ oscillations in SY without a PT being present. This behaviour was observed in two out of 13 cases. Scale bars = 20 µm.

Consistent with recently published work (Lesham et al., 2013), we observed that the pollen tube did not burst in the filiform apparatus as suggested previously (reviewed in Lesham et al., 2013). Instead the pollen tube grew for up to 60 min in close proximity and around the synergid cells towards the gamete fusion site before rupture and synergid cell death occurred (**Supplemental Movie 5.1**).

To investigate whether communication between the pollen tube and the synergid cells occurs already at a distance, or if physical cell–cell contact is required, we monitored the onset of Ca^{2+} oscillations as a function of the distance between the two cells. To this end, we visualized the pollen tube apex by developing a novel marker (*P_{LAT52}:RemCA-tagRFP*) targeting tagRFP with the carboxyl-terminal (C-terminal) anchor sequence of remorin to the plasma membrane of pollen tubes and introduced it into a homozygous sperm nuclei marker line (*$P_{H3.3}$:H3.3-mRFP*, Ingouff et al., 2007) resulting in the double marker line LHR (Lat52:tagRFP-T-REM; HTR10:HTR10-mRFP; see Methods for details). In all eight measurements where the onset of $[Ca^{2+}]_{cyto}$ oscillations in synergid cells and the advance of the pollen tube tip could be monitored simultaneously, the first substantial $[Ca^{2+}]_{cyto}$ transients (ratio change 45 s of baseline of first derivative, see Methods) were detected when the distance between the two cells could no longer be resolved (**Figure 5.1 B, C**). In three of the 25 experiments, the position of the two synergid cells allowed separate measurements of cytoplasmic CerTN-L15 fluorescence within each cell. We observed that the amplitude and frequency of $[Ca^{2+}]_{cyto}$ oscillations depended on the relative distance and position of the pollen tube tip and either of the two synergid cells. Only the synergid cell in direct contact with the pollen tube tip showed continuous $[Ca^{2+}]_{cyto}$ oscillations (**Figure 5.2 A, B**).

To support this finding and to investigate whether the synergid $[Ca^{2+}]_{cyto}$ signatures represent global or localized responses, we analyzed 78 $[Ca^{2+}]_{cyto}$ peaks and detected the highest amplitude in immediate proximity to the contact site of synergid cell and pollen tube tip (**Figure 5.2 C**). Progressing pollen tube growth resulted in relocation of the local $[Ca^{2+}]_{cyto}$ maximum that matched the shifted site of contact with the pollen tube tip. To measure whether indeed only the apex or the entire surface of the pollen tube has the capability to elicit a Ca^{2+} signature in the synergid cells, we mapped the local amplitudes $[Ca^{2+}]_{cyto}$ peaks (n = 78) in synergid cells in 4 x 4 mm bins across the whole cell. We found that the sensor amplitude gradually decreased with increasing distance from the pollen tube tip (**Figure 5.2 D**, **Figure S5.2 B**), consistent with the observation that $[Ca^{2+}]_{cyto}$ is highest at the site where the cells are in direct contact. Moreover, we found that the local sensor amplitude in the synergid cell was the highest in closest proximity to the pollen tube apex and not the shank of the tube (**Figure 5.2 D, Figure S5.2 B**).

Taken together, the separate measurements of neighboring synergids and the correlation of pollen tube position and localized synergid response demonstrate that physical contact specifically with the pollen tube apex is necessary to induce and maintain $[Ca^{2+}]_{cyto}$ oscillations in the synergid cell. Our measurements in synergid cells further show that there exists not just one excitable zone, but rather large areas of the synergid cell surface are capable of sensing contact with the pollen tube.

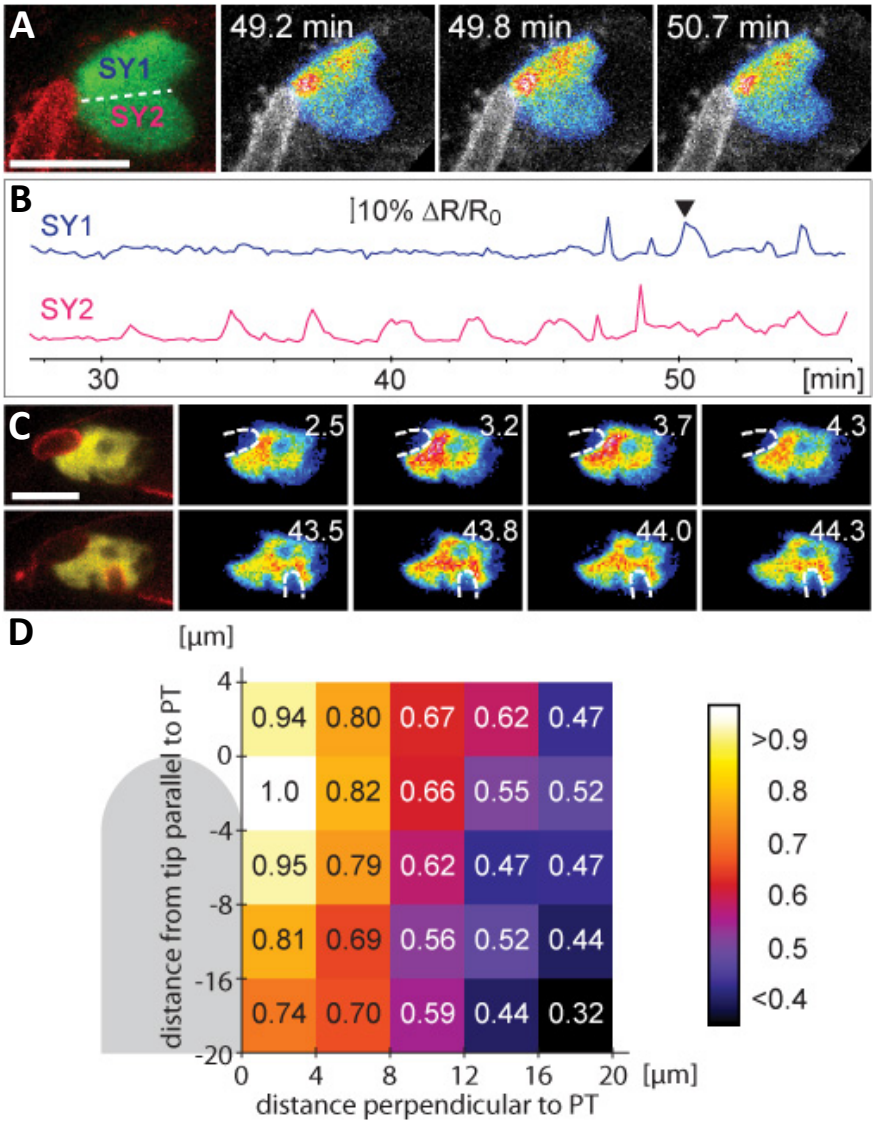

Figure 5.2 | $[Ca^{2+}]_{cyto}$ signature in the synergid cell depends on physical interaction with the pollen tube apex.

(A) CerTN-L15 signals observed in each of the two SYs separately. Left panel: Merged confocal image of a LHR PT tip (red) in contact with both pMYB98:CerTN-L15 expressing SYs (YFP signal of CerTN-L15 in green). Both SYs can be seen separately (SY1 and SY2). Right panels: one representative $[Ca^{2+}]_{cyto}$ transient (beginning, maximum, end) occurring only in SY1, which is in contact with the PT. LHR pollen is shown in grey scale, ratio changes of CerTN-L15 in SYs are displayed as heat map. **(B)** Ratio changes recorded for both SYs. The ratio changes of CerTN-L15 were measured in the two SYs separately Arrowhead marks the $[Ca^{2+}]_{cyto}$ transient shown in (A). **(C)** Local $[Ca^{2+}]_{cyto}$ transients in relation to PT tip position. Two $[Ca^{2+}]_{cyto}$ transient of one time series are shown. $[Ca^{2+}]_{cyto}$ transients with LHR PT tip in contact with the filiform apparatus (upper row) and after being grown around the SYs (lower row). Left panel in both rows: merged confocal image of a LHR PT tip (red) in contact with pMYB98:CerTN-L15 SYs (YFP signal of CerTN-L15 in yellow). Right panels of both rows: Time points of corresponding time series before, during and after a transient of $[Ca^{2+}]_{cyto}$ in the SYs (ratio of CerTN-L15 displayed in pseudo colour). The maximum of the $[Ca^{2+}]_{cyto}$ is different in both rows and correlates with the position of the PT tip (dotted line indicates the position of the PT according to the signal shown in the left panel). **(D)** Mapping of amplitudes of $[Ca^{2+}]_{cyto}$ transients in relation to the distance to PT tip. Left: schematic of a PT tip in contact with a SY. Right: amplitudes of $[Ca^{2+}]_{cyto}$ elevations were measured in 4 x 4 µm regions (indicated as squares) over the SY in time series registered to the PT tip. Measured amplitudes of the maximum number of detected $[Ca^{2+}]_{cyto}$ transients in five independent experiments. Numbers in each square display the normalized average amplitude height. For statistical data see **Figure S5.2 B**. Scale bars = 20 µm.

5.3.3 Sperm cell delivery causes calcium signals in female gametes

Once the pollen tube has ruptured and released its content including the two sperm cells, the process of fertilization enters the next stage, the specific interaction and fusion of the two sperm cells with the egg and the central cell, respectively. To investigate whether the interactions between male and female gametes also invoke Ca^{2+} transients and whether there is a correlation between calcium signatures and sperm cell movement, we measured $[Ca^{2+}]_{cyto}$ in egg and central cells separately.

When measuring CerTN-L15 signals in the central cell during successful pollen tube rupture (n = 14), we observed a sharp increase in $[Ca^{2+}]_{cyto}$ lasting for approximately 1 min immediately following pollen tube burst and deformation of the central cell in the area of sperm arrival due to explosive release of pollen tube contents (**Figure 5.3 A, B**, t = 0 min; **Supplemental Movie 5.3**). Beyond this short transient, significant $[Ca^{2+}]_{cyto}$ transients were not detectable, independent of fertilization success (see further examples in **Figure S5.3**).

In the egg cell, we also observed an immediate deformation of its shape that coincided with the pollen tube burst and the rapid delivery of sperm cells (**Figure 5.3 C**). Analysis of $[Ca^{2+}]_{cyto}$ levels during these events (n = 26) revealed again a sharp increase that coincided with cell deformation and sperm cell arrival (**Figure 5.3 D**, t = 0 min). In some experiments, deformation of the egg cell was caused by the growing pollen tube (**Figure 5.3 C**, arrows at time points 17 min and 8 min). However, in these cases, calcium transients were never detected (**Figure 5.3 D**; **Figures S5.4 A, B** and **S5.6 B, Supplemental Movies 5.4, 5.5**). This indicates that mechanical stimulation of the egg cell is not sufficient to cause the detected elevation of $[Ca^{2+}]_{cyto}$.

While the sharp $[Ca^{2+}]_{cyto}$ peak at t = 0 occurred in both female gametes simultaneously during pollen tube burst, an additional extended $[Ca^{2+}]_{cyto}$ transient with more gradual rise and fall times was detected only in the egg cells (**Figures 5.3 D** and **5.4 C**, **Figures S5.3** and **S5.6 C**). This second $[Ca^{2+}]_{cyto}$ transient appeared on average 3.8 min (±1.9, n = 12) after the pollen tube burst and lasted on average for 3.1 min (±0.66, n = 12). The second $[Ca^{2+}]_{cyto}$ transient was detected in all successful fertilization events (n = 10) as shown in **Figure 5.4 C**. When fertilization was not successful, the second $[Ca^{2+}]_{cyto}$ transient could not be detected in 13 out of 15 measurements (**Figure 5.4 D, Figure S5.4 A, B, Supplemental Movie 5.5**). This indicates a functional link between the second extended $[Ca^{2+}]_{cyto}$ transient and successful fertilization.

5.3.4 Egg cell-specific calcium signature during plasmogamy

To reveal the role of the second $[Ca^{2+}]_{cyto}$ transient for plasmogamy, we analyzed the timing of associated events in more detail. In animal oocytes, a $[Ca^{2+}]_{cyto}$ elevation occurs after the sperm–egg fusion. In plants, two female gametes are fertilized by two sperm cells. This double fertilization event is supposed to require molecular events such as cell–cell recognition, gamete attachment, sperm cell separation, gamete membrane fusion, egg activation and cell wall modi-

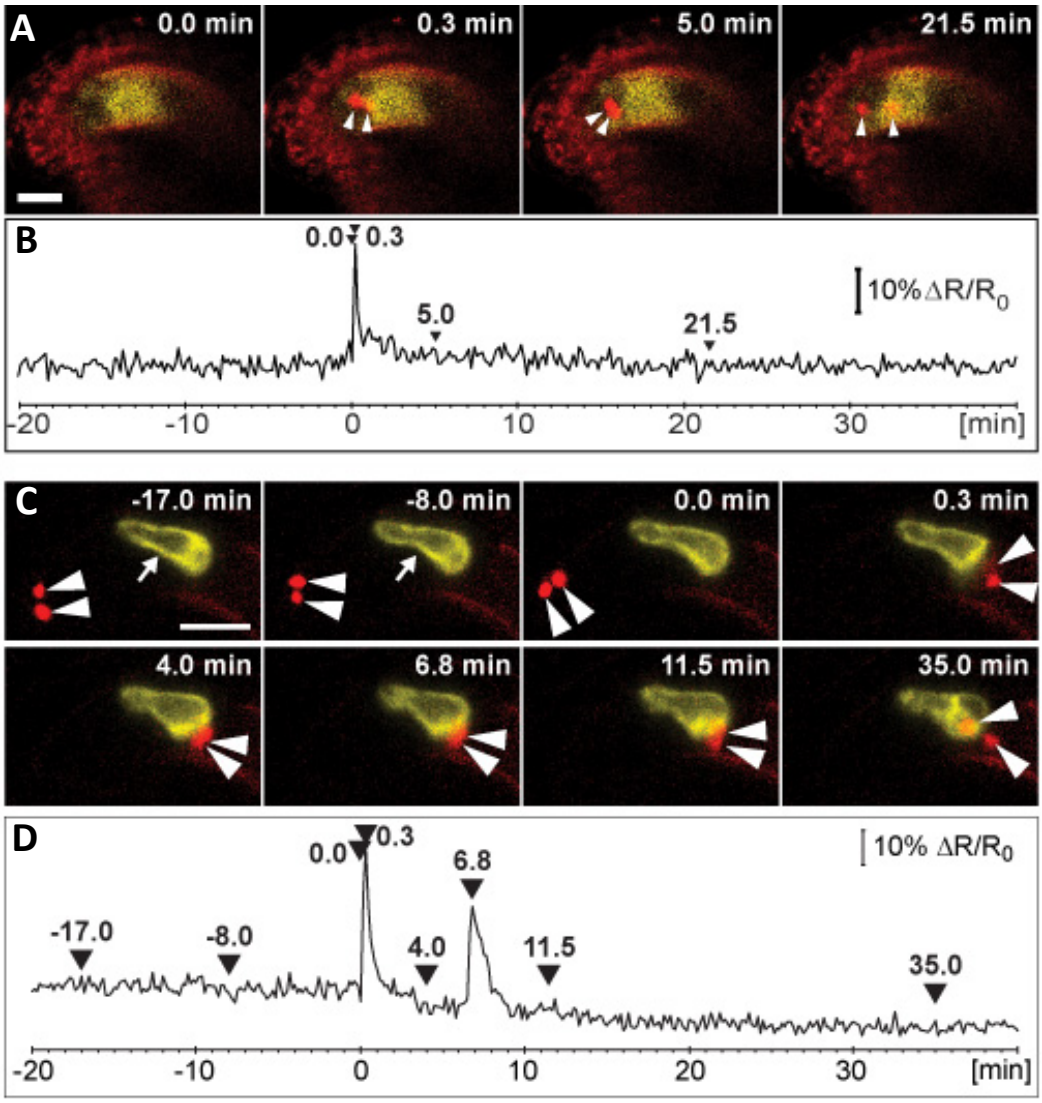

Figure 5.3 | $[Ca^{2+}]_{cyto}$ signatures in female gametes during double fertilization.,

(A) Time series showing arrival of labelled SPs (indicated by arrow heads; LHR marker line) at the gamete fusion site and subsequent plasmogamy with the central cell (CC) expressing pDD65:CerTN-L15 (yellow). Images show major steps of the gamete fusion process: directly before PT rupture (0.0 min), after PT rupture and SP arrival (0.3 min), during arrest phase of SPs at the fusion site (5.0 min) and after plasmogamy showing movement of SP nucleus towards CC nucleus (21.5 min). Scale bar: 20 µm. See also Supplementary Movie 3. **(B)** $[Ca^{2+}]_{cyto}$ transients in the CC during fertilization. Normalized ratio of CerTN-L15 in CC of time series shown in (A). Arrowheads indicate time points corresponding to images shown in (A). A single ratio change of 27% occurs during SP release (time point 0.3 min). **(C)** Time series of a LHR pollen fertilizing an ovule expressing pEC1:CerTN-L15 in the egg cell (EC, yellow). From -17.0 to 0.0 min) the PT is in contact with SYs (not visible). SPs (red, marked by arrowheads) release occurred at 0.0 min. Arrest of SPs is visible at the fusion site (4.0 min), movement of one SP nuclei inside egg cytoplasm (6.8 - 11.5 min) is followed by separation of SP nuclei (11.5 - 35 min) indicating fertilization success. See corresponding **Supplemental Movie 5.4**. **(D)** $[Ca^{2+}]_{cyto}$ signals in the EC during fertilization. Normalized ratio changes of CerTN-L15 in the EC of time series shown in (C) Arrowheads with time correspond to the images shown in (C). Ratio changes can be seen directly after SP release (0.0 min) and during the arrest phase of the SPs at the fusion site (6.8 min) but not after SP separation (11.5 – 35.0 min). Scale bar = 20 µm.

fications that take place between both male–female gamete pairs. Any of these processes may involve calcium signaling. While it is challenging to directly address each process separately, the timing of events before fertilization can be dissected by using a marker line that labels sperm nu-

clei and tracking their movement at the fusion site (Hamaumra et al., 2011). Since both sperm cells do not possess any propelling mechanism, their movement presumably results from elastic deformations and pressure exerted by neighboring cells or differential surface interactions. Hamamura et al. (2011) reported that sperm delivery is composed of three steps. They are delivered as a pair (i) and after a period of immobility lasting about 7.4 min (ii) they both fuse almost simultaneously about 8.5 min after release with either female gamete without any preference (iii).

To correlate the second $[Ca^{2+}]_{cyto}$ transient with stages of sperm delivery and fusion, we tracked the sperm nuclei after pollen tube rupture and analyzed their trajectories for consistent movement patterns. The sperm cell, which eventually fused with the egg cell, was termed SPEC, while the sperm cell that would fuse with the central cell was termed SPCC (**Figure 5.4 A**). After pollen tube rupture, we observed four distinct phases of sperm movement, which typically occurred over a travelled distance of 10 mm (**Figure 5.4 B**): after delivery, both cells moved initially quickly together along parallel trajectories (phase I, **Figure 5.4 B**, orange trajectories); a second phase is initiated by a sudden sideward movement of SPEC apart from SPCC (**Figure 5.4 A, B**, single asterisks) followed by slow movement, rotation and temporary arrest (phase II, **Figure 5.4 B**, green), while SPCC movement was also slowed down (phase III, **Figure 5.4 B**, blue); after a second sudden positional shift, now of SPCC (**Figure 5.4 A, B**, double asterisks), both separated sperm nuclei then made final movements inside the female gametes (phase IV, **Figure 5.4 B**, violet) indicating fertilization success. Plotting the intensities of each SP in an overlaying kymograph visualizes their velocity over time (**Figure S5.4 C**). After the arrival of both cells (t = 0), an initial rapid parallel movement (orange phase), followed by a slowdown and the eventual separation due to backwards movement of SPCC is visualized. The occurrence of both shifts of SPEC and SPCC in opposite directions is clearly visible in all successful fertilization attempts (n = 10) but absent when fertilization failed (n = 13).

The shifts were also observed in both failed fertilization attempts where the second broader $[Ca^{2+}]_{cyto}$ transient was detected but the sperm nucleus did not continue to move towards the nucleus of the female gamete (data not shown). In a single measurement, where delayed or incomplete plasmogamy was observed, we could detect two broader $[Ca^{2+}]_{cyto}$ transients in the egg cell and also two sudden shifts of SPEC (**Figure 5.4 E, Figure S5.4 D**). These exceptions indicate that the shift can occur repeatedly and therefore could precede successful gamete fusion, eventually representing the event of initial sperm cell adhesion to the female gamete before fusion occurs.

To correlate the $[Ca^{2+}]_{cyto}$ signatures in egg cells and the sperm cell movement patterns, we further analyzed the occurrence and timing in all measurements where both events could be unequivocally detected (n = 10). We found that the sudden movement of SPEC at the end of sperm movement phase (i) generally coincided with the onset of the second broader $[Ca^{2+}]_{cyto}$ transient (R^2 = 0.9894; time difference between shift and onset of $[Ca^{2+}]_{cyto}$ transient was 5 ± 13 s; **Figure 5.4 F**, **Supplemental Movie 5.4**). We interpret this finding as strong evidence for a functional link between gamete interaction, Ca^{2+} signaling in the egg cell and successful plasmogamy.

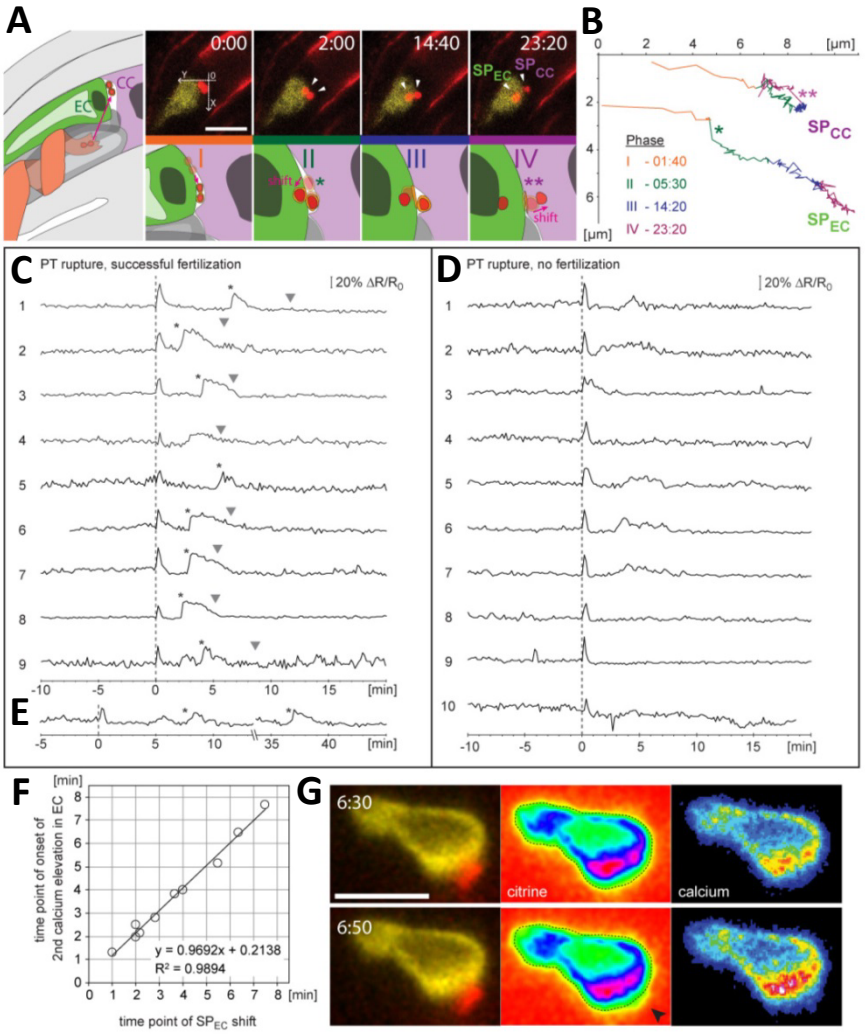

Figure 5.4 | A second $[Ca^{2+}]_{cyto}$ transient in egg cells is associated with successful fertilization.

(A) Left: scheme depicting SP release from a PT growing around receptive SY (drawn in grey). After burst SP are located at fusion site between EC and CC. Upper panel: time series of LHR SP (red, arrowheads) fertilizing an egg cell expressing the CerTN-L15 sensor (yellow). SP_{EC}: sperm cell fusing with egg cell, SP_{CC}: sperm fusing with central cell. Lower panel: scheme of different phases of sperm cell movement before and during fusion. *Phase I:* parallel movement of sperm cells after arrival along fusion site. *Phase II:* sideward shift of SP_{EC} (single asterisk) towards EC. *Phase III:* arrest of SP_{CC} and movement of SP_{EC} nucleus towards EC nucleus. *Phase IV:* sideward shift of SP_{CC} (double asterisk) and subsequent fast sperm nuclei separation. **(B)** Tracking movement of both sperm cells at fusion site of experiment shown in (A). Different colours of the tracks indicate the four different phases and numbers indicate end points of each phase after sperm delivery in minutes. Shift of SP_{EC} occurs at 1:40 min (single asterisk) and shift of SP_{CC} at 14:20 min (double asterisk). **(C)** $[Ca^{2+}]_{cyto}$ signals in the EC during successful fertilization. Graphs are normalized and aligned to time of PT rupture (0.0 min). Asterisks mark shift of SP_{EC}, arrowheads mark fast separation of both sperm nuclei indicating successful fertilization of both female gametes. In all cases two Ca^{2+} transients occur: a short single transient during PT rupture and a longer extended transient after SP_{EC} shift (*Phase II*). **(D)** Variety of $[Ca^{2+}]_{cyto}$ signals in the EC during unsuccessful fertilization. Only a single Ca^{2+} transient occurs upon pollen tube rupture (0.0 min). **(E)** Exceptional case of EC fertilization. Ratio change of pEC1:CerTN-L15 is shown. SP_{EC} displays two shifts (asterisk) before fusing with the EC. Each shift is followed by a Ca^{2+} transient in the EC (Corresponding kymograph see **Figure S5.4 D**). **(F)** Correlation of SP_{EC} shift towards EC and beginning of second Ca^{2+} transient in EC (n = 10). Formula of linear regression and calculated coefficient of determination (R^2) are given. **(G)** Diffusion of sensor molecules into sperm cells upon gamete fusion. Time points before (top row) and after SP_{EC} shift (bottom row). Left column, fluorescent micrographs of egg cell (yellow, citrine signal of CerTN-L15) and LHR sperm cell nuclei (red). Middle column, false colour representation of egg cell citrine signal. The dotted line displays the egg cell outline before the SP_{EC} shift. The arrowhead indicates spreading of citrine signal towards the position of sperm cells. Scale Bars = 20 µm.

To determine the time point of plasmogamy as precise as possible, we therefore followed the rational that upon fusion of the plasma membranes of both gametes, cytosolic calcium sensor molecules would immediately diffuse into the sperm cell cytoplasm resulting in detectable citrine fluorescence around the sperm cell nucleus. In four measurements of successful fertilization, measurements were possible as egg cell and SPEC were positioned in the focus plane such that both the fluorescent signals overlapped only minimally. In all four experiments, we were able to detect the spreading of citrine fluorescence signal from the egg cell towards the direction of the sperm cell position immediately after the SPEC shift, coinciding with the broader $[Ca^{2+}]_{cyto}$ transient (**Figure 5.4 G, Figure S5.5**). In summary, this observation indicates that all three processes, sperm cell shift, onset of the broad $[Ca^{2+}]_{cyto}$ transient and gamete fusion occur all in concert and within less than 20 s.

5.4 Discussion

Innovations in specimen handling and application of a sensitive calcium reporter have allowed live-cell observations and detection of cell-type-specific Ca^{2+} signatures during the entire double fertilization process in the model plant *Arabidopsis*. Measuring $[Ca^{2+}]_{cyto}$ in vivo in the female gametophyte at high resolution was previously hampered due to the low accessibility of the deeply embedded cells for imaging. We have optimized a previously reported semi-in vivo fertilization assay that allows live-cell observations by using excised ovules and semi-in vitro grown pollen tubes (Palanivelu and Preuss, 2006). Adaptation of this system for confocal fluorescence imaging and expression of sensors driven by cell specific promoters resulted in reduced background and improved sensitivity. We decided to use the troponin C-based sensor CerTN-L15 as it is expected to be less affected by or interfering with cellular processes as it is the case for calmodulin-based sensors (Heim et al., 2007). The improved brightness and high sensitivity of this sensor also present significant advantages for imaging through several cell layers (Heim et al., 2007; Garaschuk et al., 2007; Kaestner, 2012) and thus enabled us to record changes in $[Ca^{2+}]_{cyto}$ inside the ovule at subcellular resolution.

The described experimental setup allowed studies yielding strong evidence for a functional role of Ca^{2+} signaling during virtually all steps of the double fertilization process in angiosperms. We were able to confirm recently reported $[Ca^{2+}]_{cyto}$ oscillations in synergid cells during pollen tube interaction (Iwano et al., 2012) and provide further insights into cell–cell communication between these cells and the provoked $[Ca^{2+}]_{cyto}$ transients. One open question was, for example, whether the communication between the pollen tube tip and synergid cells occurs already at a distance as concluded earlier (Iwano et al., 2012) or whether direct cell–cell contact is required. Our measurements show that irregular $[Ca^{2+}]_{cyto}$ elevations can occur spontaneously in synergid cells at a low likelihood, but do not cause cell death. In addition, we observed that only pollen tubes that successfully enter the ovule and interact with the synergid cells induce high persistent $[Ca^{2+}]_{cyto}$ oscillations that may ultimately trigger synergid cell death and pollen tube burst. Usage

of a novel marker for the pollen plasma membrane further indicated that physical contact of the pollen tube apex was necessary to induce and maintain $[Ca^{2+}]_{cyto}$ oscillations only in the synergid cell, which was in direct contact with the tube apex. Recently components of the FERONIA (FER) signaling pathway were shown to be involved in the initiation of calcium oscillations and for coupling these with programmed cell death (Ngo et al., 2014).

Stimulus-induced $[Ca^{2+}]_{cyto}$ oscillations have been frequently observed in plants. It was reported that their period, amplitude and waveform encode information about stimulus and trigger required to activate specific signaling responses, to regulate protein activity and eventually to alter gene expression (Dodd et al., 2010). The spiking nature of the synergid transients is typical for rapidly released Ca^{2+} from intra- or extracellular stores followed by slower removal (Meyer and Stryer, 1988). Observations of comparable $[Ca^{2+}]_{cyto}$ spiking signatures in legume root hairs, for example, induced by symbiotic infection with rhizobial bacteria or mycorrhizal fungi, identified the origin of the $[Ca^{2+}]_{cyto}$ wave at the cell nucleus (Erhardt et al., 1996; Kosuta et al., 2008; Chabaud et al., 2011) and therefore depend on specific metabotropic receptors at the plasma membrane that perceive and convey the extracellular signal (Oldroyd and Downie, 2008). In contrast, during physical stimulation of root epidermal cells, observed $[Ca^{2+}]_{cyto}$ transients originated from the site of stimulation at the cell periphery (Monshausen et al., 2009), suggesting extracellular stores or peripheral ER as sources of Ca^{2+} and possibly the involvement of stretch-activated calcium channels (Nakagawa et al., 2007). The localized transients of $[Ca^{2+}]_{cyto}$ in synergid cells also occur in immediate proximity to the cell contact site, which is reminiscent of mechano-sensing. The oscillation signature, however, is similar to that observed during symbiotic infections and thus suggests an involvement of metabotropic receptors and the existence of feedback mechanisms of Ca^{2+}-induced Ca^{2+} release (Uhlén and Fritz, 2010). The regulation of such oscillatory increases of $[Ca^{2+}]_{cyto}$ commonly occurs through the receptor-mediated activation of phospholipase C, which increases the levels of Inositol-1,4,5-trisphosphate (InsP3) that further triggers InsP3-receptor-mediated Ca^{2+} release from internal storages.

The signaling cascades that might be provoked by $[Ca^{2+}]_{cyto}$ increase in the synergid cells are currently unknown. During self-incompatibility in poppy, it was shown that $[Ca^{2+}]_{cyto}$ increase is correlated with the generation of reactive oxygen species and NO signaling resulting in cell death. Downstream targets include, for example, components of the cytoskeleton and mitogen-activated protein kinases (Wilkins et al., 2014). Both synergid cells undergo cell death either during pollen perception or after successful fertilization (Beale et al., 2012; Völz et al., 2013). We observed that only synergid cells showing high and continuous amplitudes burst during pollen tube interaction. This finding supports previous reports also in animal cells showing that high sustained $[Ca^{2+}]_{cyto}$ levels are toxic to cells and may result in cell death both during necrosis and apoptosis (Orrenius, 2003). The identification and analysis of calcium-dependent signaling components in synergid cells will now be an exciting area of future research activities. Reactive oxygen species were recently reported to mediate pollen tube burst in $[Ca^{2+}]_{cyto}$-dependent processes (Duan et al., 2014) sug-

gesting the existence of similar mechanisms during synergid cell death. It will be of similar importance to identify the pollen tube apex-derived stimulus and synergid cell surface receptors involved in triggering the described $[Ca^{2+}]_{cyto}$ oscillations. Our results on $[Ca^{2+}]_{cyto}$ oscillations support the notion of a short-range signal secreted from the pollen tube apex that is perceived by receptor(s) of synergid cells triggering a feedback mechanism that cause localized, oscillating release of Ca^{2+}. The FERONIA receptor-like kinase and the glycosylphosphatidylinositolanchored LORELEI protein are candidate synergid cell surface proteins that have previously been shown to be required for pollen tube burst (Escobar-Restrepo et al., 2007; Capron et al., 2008). Moreover, a secreted peptide, RALF (RAPID ALKALINIZATION FACTOR) was recently shown to activate FERONIA in the root (Haruta et al., 2014). Whether RALF peptides secreted from the pollen tube apex activate FERONIA at the surface of synergid cells inducing $[Ca^{2+}]_{cyto}$ oscillations remains to be determined. Further studies should also involve mutants with defects in phospholipaseC / InsP3 signaling and metabotropic receptors (see above). Altogether, these mutants will be instrumental in elucidating the functional importance of the localized $[Ca^{2+}]_{cyto}$ oscillations in the synergid–pollen tube interaction.

During the next act of plant double fertilization, the fusion of sperm cells with both female gametes, an involvement of Ca^{2+} transients was long suggested by pioneering work applying in vitro fertilization studies with maize egg and sperm cells (Digonnet et al., 1997; Antoine et al., 2000; Antoine et al., 2001). It was reported that Ca^{2+} influx occurred after egg–sperm fusion and spreads as a wave front from the fusion site towards the whole cell. However, these studies did not allow to image $[Ca^{2+}]_{cyto}$ dynamics during the whole fertilization process and thus overlooked, for example, the first $[Ca^{2+}]_{cyto}$ transient in both female gametes that is correlated with sperm cell release. The function of this first elevation remains unclear. It might also be correlated with mechanic deformation of female gametes, albeit we did not observe $[Ca^{2+}]_{cyto}$ transients in egg cells, which were occasionally deformed by pollen tubes (see above). It was, however, recently shown that egg cells secrete EC1 protein after pollen tube burst to activate sperm cells and thus enable them to fertilize female gametes (Sprunck et al., 2012). Thus, the egg cell itself requires activation shortly after the sperm cell release. Further studies will elucidate whether egg activation at this phase requires Ca^{2+} signaling. Mammalian egg cells are activated by a series of $[Ca^{2+}]_{cyto}$ oscillations that occur shortly after egg–sperm membrane fusion (for review see Swann and Ku, 2008), thus differing significantly from the single elevation that we have observed during pollen tube burst. A major difference between previously reported in vitro and our semi-in vivo studies is the length of $[Ca^{2+}]_{cyto}$ elevations. It was reported that the $[Ca^{2+}]_{cyto}$ transient after in vitro gamete fusion lasted for up to 30 min, while we observed that the comparable second extended $[Ca^{2+}]_{cyto}$ transient lasted on average only for 3 min. Moreover, the signature of this $[Ca^{2+}]_{cyto}$ transient is different and seems to consists of a few very short spikes, which could not be resolved individually. In agreement with the above-mentioned in vitro studies, we conclude that this $[Ca^{2+}]_{cyto}$ transient was provoked by fusion rather than adhesion. A functional role of the reported Ca^{2+} influx could not be addressed during in vitro studies. We were able to ultimately correlate the second

$[Ca^{2+}]_{cyto}$ transient with plasmogamy and fertilization success. In a parallel study, Hamamura et al. (2014) found highly similar $[Ca^{2+}]_{cyto}$ signatures during egg cell fertilization using the calcium sensor YC3.60. In line with our findings, the authors also identified a correlation between the occurrence of the second $[Ca^{2+}]_{cyto}$ transient and successful fertilization. In a mutant of the *HAP2/GCS1* gene, which has known roles in pollen tube guidance and fertilization, sperm cells were delivered properly but gamete fusion never occurred. Consistently, the authors found that in this mutant the second $[Ca^{2+}]_{cyto}$ transient in the egg cell was not detectable. It will, however, remain challenging to elucidate the exact role of Ca^{2+}–dependent signaling during this short fertilization phase.

In mammals, two separate fusion phases are distinguished after gamete adhesion takes place: a marginal and a separating phase (Okabe, 2013). During the marginal phase, fusion is initiated and the second phase, which has a different topological character, fusion is completed during a process similar to endocytosis. We suggest that this process is similar in plants. In accordance with the topology of the marginal phase, we observed egg cell cytoplasm extending towards the sperm cell followed by a quick shift of the sperm cell towards the inside of the egg, which might be consistent with the separating phase characterized by endocytosis at the plasma membrane. Moreover, we have observed few cases that showed additional $[Ca^{2+}]_{cyto}$ elevations displaying the signature of the extended second transient. We assume that fusion was initiated in these cases, but not completed allowing additional fusion events associated with $[Ca^{2+}]_{cyto}$ transients. Markers labelling the plasma membrane and cytoskeleton of gametes in combination with Ca^{2+} sensors whose signals can be optically separated from the gamete surface will help to explain these observations. While diffraction-limited confocal imaging of fertilization presents a significant advance, unequivocal visualization of membrane fusion may also require substantially improved spatial resolution. It also remains to be determined which downstream responses are triggered by these relatively short $[Ca^{2+}]_{cyto}$ transients. It is very likely that the structure of the cytoskeleton undergoes local changes and reorganization to initiate the first fusion phase and to enable the transport of the sperm nucleus towards the egg nucleus. It was also discussed that $[Ca^{2+}]_{cyto}$ transients initiate the formation of cell wall material after fusion likely representing a block to polyspermy functionally similar to the fertilization membrane in animals (Antoine et al., 2001). In animal oocytes, $[Ca^{2+}]_{cyto}$ waves triggered by fusion with the first sperm elicit immediate exocytosis of extracellular matrix-modifying enzymes to quickly block polyspermy (Miao et al., 2012). In vitro fertilization studies in maize showed the formation of cell wall components already 30 s after gamete fusion (Kranz et al., 1995) indicating a quick release of cell wall components likely from Trans-Golgi vesicles stored in the egg cell. Whether this leads to a block of polyspermy, whether it also occurs in vivo and depends on Ca^{2+} signaling remains to be determined. However, the timing and the observation that central cell fusion lacks the second $[Ca^{2+}]_{cyto}$ transient and allows polyspermy (Scott et al., 2008) suggest that the egg cell-specific $[Ca^{2+}]_{cyto}$ transient might also be involved to generate a quick block to polyspermy. In vitro fertilization studies using egg and central cells of tobacco confirm our finding that the second transient Ca^{2+} elevation is lacking in central cells (Peng et al., 2009).

In conclusion, we have reported $[Ca^{2+}]_{cyto}$ dynamics during the entire double fertilization process and were able to correlate the timing of Ca^{2+} signatures with cellular events including localized cross-talk between the pollen tube apex and synergid cells, pollen tube burst and sperm delivery, as well as gamete activation and fusion culminating in fertilization success and likely a polyspermy block to the egg cell. These studies thus significantly extend our knowledge about the timing of double fertilization events and deepen our understanding about the role of Ca^{2+} signaling during the individual processes. Future studies are necessary to unveil the molecular players involved in $[Ca^{2+}]_{cyto}$ induction, signal maintenance and/or oscillation as well as the downstream targets regulating Ca^{2+} dependent processes to finally understand its role during double fertilization.

5.5 Summary

Cell–cell communication and interaction is critical during fertilization and triggers free cytosolic calcium ($[Ca^{2+}]_{cyto}$) as a key signal for egg activation and a polyspermy block in animal oocytes. Fertilization in flowering plants is more complex, involving interaction of a pollen tube with egg adjoining synergid cells, culminating in release of two sperm cells and their fusion with the egg and central cell, respectively. Here, we report the occurrence and role of $[Ca^{2+}]_{cyto}$ signals during the entire double fertilization process in *Arabidopsis*. $[Ca^{2+}]_{cyto}$ oscillations are initiated in synergid cells after physical contact with the pollen tube apex. In egg and central cells, a short $[Ca^{2+}]_{cyto}$ transient is associated with pollen tube burst and sperm cell arrival. A second extended $[Ca^{2+}]_{cyto}$ transient solely in the egg cell is correlated with successful fertilization. Thus, each female cell type involved in double fertilization displays a characteristic $[Ca^{2+}]_{cyto}$ signature differing by timing and behavior from $[Ca^{2+}]_{cyto}$ waves reported in mammals.

CHAPTER 6 Egg Cell–Secreted EC1 Triggers Sperm Cell Activation During Double Fertilization

This chapter was published in *Science* (Sprunck et al., 2012). Frank Vogler generated the *HTR10p:HTR10-mRFP1; HTR10p:TET9-GFP* sperm cell nuclei and membrane double marker by crossing (**Figure 6.4**; **Figure S6.10**) and performed all quantitative plot profile analyzes (**Figure 6.2**, **Figure S6.3** and **Figure S6.4**). F.V. developed the method for releasing sperm cells from semi-in vivo grown pollen tubes and subsequent in vitro peptide application. F.V. performed experiments, data and statistical analysis on HAP2-YFP subcellular localization (**Figure 6.4**). F.V. contributed to the manuscript by writing the respective parts of the work.

6.1 Introduction

Sexual reproduction depends on the successful union of two gametes of opposite sex at fertilization. In flowering plants such as *Arabidopsis thaliana*, sexual reproduction is distinct in that two gamete fusion events take place in a coordinated manner, a phenomenon termed "double fertilization" (Berger et al., 2008). Two nonmotile sperm cells are delivered by a pollen tube into the female gametophyte (embryo sac) that harbors two dimorphic female gametes (**Figure 6.1 A).** One sperm fuses with the egg cell, giving rise to the embryo, whereas the second sperm cell fuses with the central cell to develop the triploid endosperm. Although this distinct mode of reproduction was discovered more than a century ago (Nawashin, 1898; Guignard, 1899) and recent live-cell imaging has shed some light on the behavior of *Arabidopsis* sperm nuclei during double fertilization (Hamamura et al., 2011), almost nothing is known about the molecules mediating gamete interactions.

To date, the evolutionary conserved HAP2 (HAPLESS 2)/GCS1 (GENERATIVE CELL SPECIFIC 1) is the only sperm protein known to be essential at a late step in gamete interactions (Mori et al., 2006; von Besser et al., 2006), and its role as a fusogen is strongly supported by the observation that HAP2-deficient gametes of *Chlamydomonas* and *Plasmodium berghei* are able to adhere but fail to fuse (Liu et al., 2008).

6.2 Results and Discussion

Based on a transcriptomics approach that uses isolated egg cells of wheat (Sprunck et al., 2005), we discovered a family of *Arabidopsis* genes with sequence similarity to the largest wheat egg cell–specific transcript cluster, termed *EC-1 (EGG CELL 1)*. We found transcripts of the five *Arabidopsis EC1-like* genes (*EC1.1, EC1.2, EC1.3, EC1.4,* and *EC1.5*) only in female reproduc-

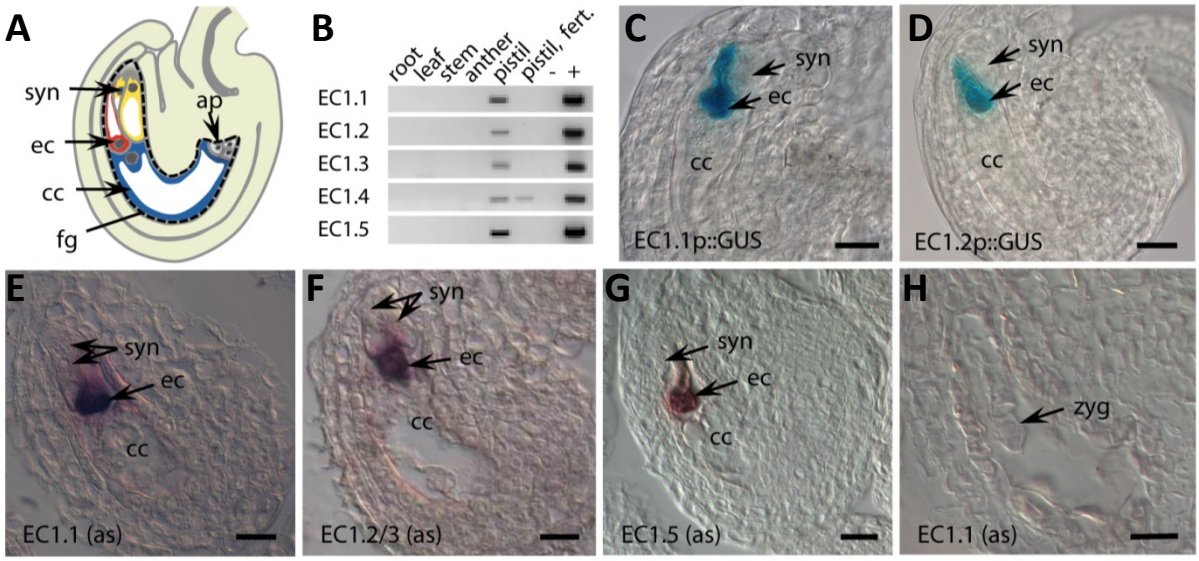

Figure 6.1 | The *EC1* gene family is specifically expressed in the egg cell.

(A) Schematic of an *Arabidopsis* ovule harboring the haploid generation, termed "female gametophyte" (dashed line), which comprises two female gametes (egg cell and central cell) and two accessory cell types (synergids and antipodal cells). **(B)** Reverse transcription polymerase chain reaction (RT-PCR) detects *EC1* transcripts only in female reproductive tissues. **(C), (D)** Egg cell–specific β-glucuronidase (GUS) reporter activity, driven by the *EC1.1* (C) and *EC1.2* (D) promoters. **(E)** to **(H)** Expression pattern of *EC1* as detected by in situ hybridization on ovules. *EC1* transcripts are present only in egg cells (E) to (G) but not in zygotes (H). ap, antipodal cells; as, antisense RNA; cc, central cell; ec, egg cell; fert., fertilized; fg, female gametophyte; syn, synergid cell; zyg, zygote; -, water control; +, genomic DNA. Scale bars = 20 µm.

tive tissues (**Figure 6.1 B**). Egg cell–specificity of *EC1* was shown by expressing the β-glucuronidase (GUS) reporter under control of individual *EC1* promoters (**Figure 6.1 C, D**) and by in situ hybridization to tissue sections. Transcripts of *EC1* genes are specifically present in the egg cell (**Figure 6.1 E-G**) but are not detectable early after fertilization (**Figure 6.1 H** and **Figure S6.1 B**), whereas GUS remains active in zygotes and early embryos (**Figure S6.1 D-F**).

EC1 proteins belong to the large and unexplored group of ECA1 (EARLY CULTURE ABUNDANT 1) gametogenesis-related cysteine-rich proteins characterized by their conserved cysteine-spacing signature (Silverstein et al., 2007). Within 118 ECA1 proteins of *Arabidopsis*, the EC1 family forms a distinct subclade (**Figure S6.2 A**). Notably, we identified EC1-like genes or transcripts only in flowering plant species, including the basal angiosperm *Amborella trichopoda*, and not in gymnosperms, ferns (*Adiantum sp.*), Bryophytes (*Physcomitrella patens*), or green algae (*Volvox sp.; Chlamydomonas sp.*). Protein-sequence analyses revealed common features of EC1 proteins, such as a predicted N-terminal signal peptide for secretion and a similar predicted intramolecular disulfide bond arrangement (**Figure 6.2 A**). Two conserved signature sequences, termed S1 and S2, were identified by multiple sequence alignments with representatives from monocots, dicots, and basal angiosperms (**Figure S6.2 B**).

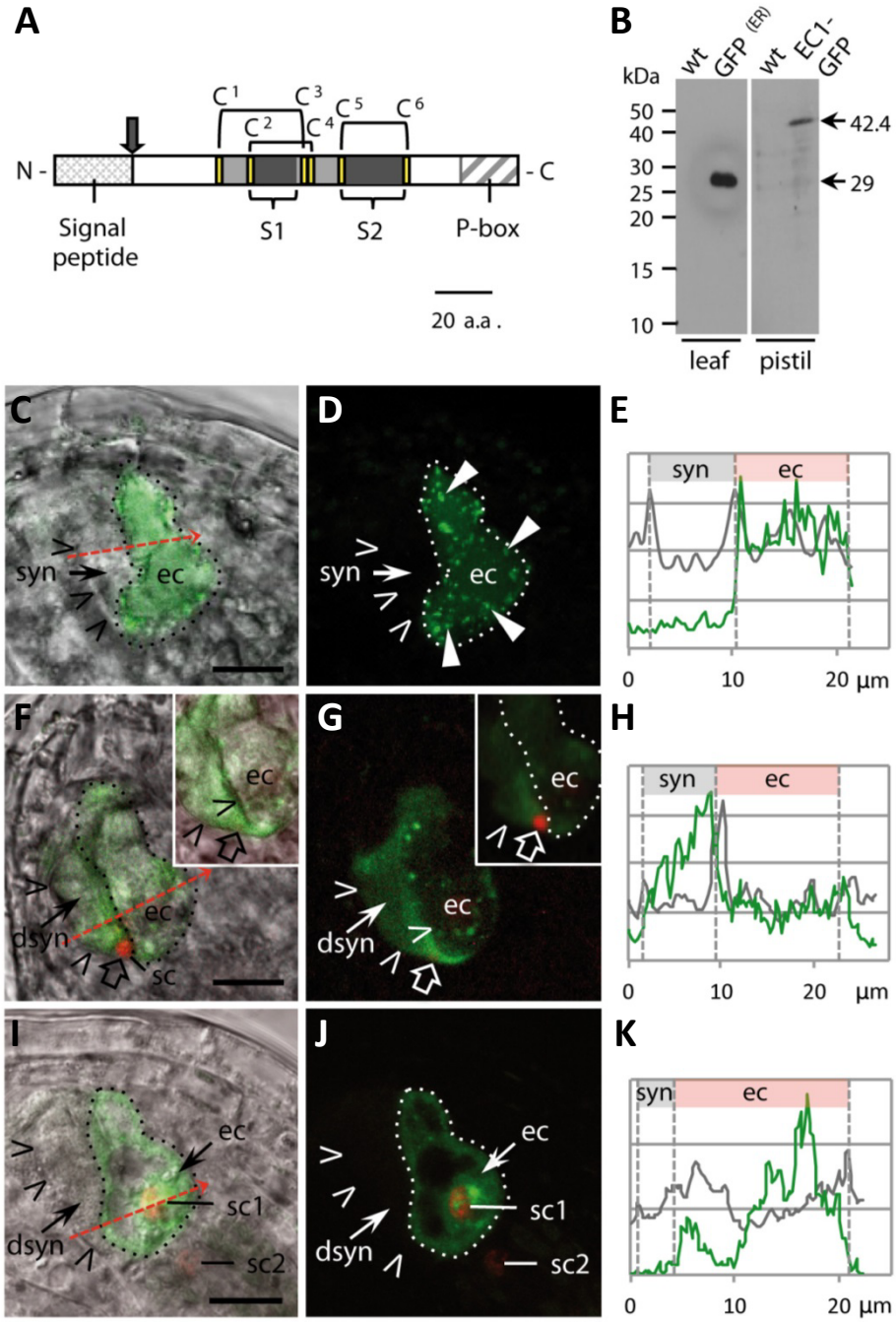

Figure 6.2 | Triggered secretion of small cysteine-rich EC1 proteins.

(A) Schematic of EC1 precursor protein. Predicted N-terminal signal peptide cleavage site (arrow). Prolines at the C terminus (P-box), two signature motifs (S1 and S2), and a conserved cysteine-spacing signature (C^1 to C^6) forming three predicted disulfide bonds (black lines) are shown. **(B)** Western blot showing the 42.4-kD EC1-GFP fusion in a pistil protein extract, compared with endoplasmic reticulum–localized GFP (29 kD) from leaves. **(C)** to **(H)** EC1-GFP is secreted upon sperm cell arrival. Merged bright-field and fluorescence images at a single z plane (C), (F) and **(I)** and corresponding fluorescence images (D), (G) and **(J)** are shown together with plot profiles of relative signal intensities (E), (H) and **(K)** detected along a line drawn across one synergid cell and the egg cell (red arrows in C, F, and I). x axis, distances (in micrometers) along the drawn line; y axis, relative signal intensities of GFP (green) and reciprocal grayscale values [1/bright field; gray]. Dashed lines denote the position of cell borders. (C) to (E) EC1-GFP signals are visible as vesicle-like structures (solid arrowheads) in the cytoplasm of unfertilized egg cells but not outside the egg cell. (F to H) EC1-GFP is detected extracellularly when the sperm cells (red nuclei) reach the gamete fusion sites (open arrows). Insets

Figure 6.2 | *continued.*

and (G) represent different focal planes. One sperm nucleus is out of focus. (I to K) Control. Egg cell–expressed cytoplasmic ARO1- GFP is not detected extracellularly during gamete interactions. dsyn, degenerating synergid; sc, sperm cell. Dotted lines delimit egg cell borders; open arrowheads point at synergid cell borders. Scale bars = 10 µm. See **Figures S6.3** and **S6.4** and **Supplemental Movies 6.1** and **6.2** for additional data.

To investigate the subcellular localization of EC1, we stably expressed a translational fusion of EC1.1 and the green fluorescent protein (GFP) under control of the *EC1.1* promoter. The calculated molecular mass of the EC1.1-GFP fusion, excluding the leader peptide, corresponds to its size in anti-GFP Western blots (**Figure 6.2 B**), arguing against posttranslational proteolytic processing of EC1. We found EC1-GFP to accumulate in spherical vesicle-like structures within the unfertilized egg cell, but never as extracellular signal (**Figure 6.2 C-E**, and **Figure S6.3**).

To study EC1-GFP localization during the short-lived event of double fertilization, we used a red fluorescent marker for sperm nuclei (Ingouff et al., 2007). Upon sperm cell arrival in the female gametophyte and during double fertilization, EC1-GFP signals are detected extracellularly, especially in the apical region of the degenerating synergid cell (**Figure 6.2 G**), which is where gamete fusions will take place (Sprunck, 2010; Hamamura et al., 2011). Quantification of GFP fluorescence in the egg cell and the flanking synergid cell during gamete interaction and fusion revealed that signal intensities are gradually increasing towards the egg cell membrane (**Figure 6.2 H** and **Figure S6.4**), indicating regulated exocytosis of EC1-GFP by the egg cell during gamete interactions. By contrast, extracellular GFP signals were never observed in control egg cells expressing a GFP fusion of ARO1 (ARMADILLO REPEAT-ONLY 1) (**Figure 6.2 K** and **Figure S6.4**), a cytoplasmic and endomembrane-associated gametophyte specific Armadillo repeat protein found to be essential for polar pollen tube growth (Gebert et al., 2008).

Recent live-cell imaging revealed that the sperm cells remain in the boundary region between the egg and the central cell for only 7.4 ± 3.3 min before they fuse (Hamamura et al., 2011). We therefore proposed the narrow time slot of EC1 secretion to be associated with sperm-egg recognition or adhesion, with egg cell signaling, or with a polyspermy block on the egg cell.

However, the five *EC1* genes appear to be functionally redundant, as we did not find negative effects on fertility in single, double, or triple knock-out mutants (**Figure S6.5**). *EC1.2* and *EC1.3* are tandem arranged on chromosome 2 and, thus, are not suitable to generate double mutants. We used the strong *EC1.1* promoter for simultaneous knock-down of *EC1.2* and *EC1.3* expression in the egg cell via RNA interference (RNAi), but we did not find any effect on fertility (**Figure S6.5**). We only observed reduced seed set when we down-regulated *EC1.2/3* in egg cells of the triple knock-out *ec1.1/4/5* (**Figure 6.3 B** and **Figure S6.5**; referred to as *ec1-RNAi*). Reciprocal backcrosses and segregation ratios of self-fertilized *ec1-RNAi* lines revealed the expected female gametophytic effect on transfer DNA transmission, resulting in only heterozygous or wild-type (WT) offspring (**Tables S6.1** and **S6.2**). Despite the lower transcript abundance of *EC1.2* and

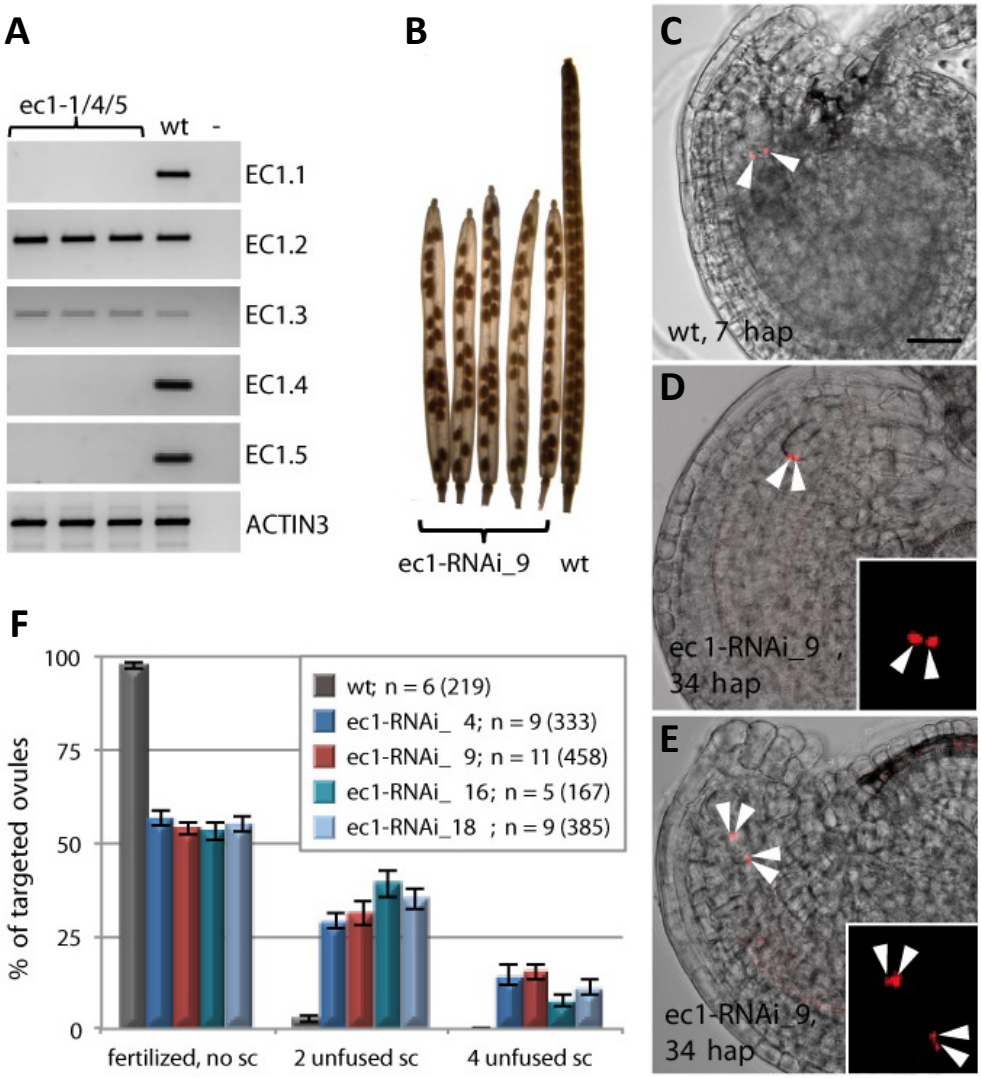

Figure 6.3 | The *EC1* gene family is essential for gamete fusion and for blocking supernumerary sperm cell delivery.

(A) *ec1.1/4/5* is a triple knock-out, shown by RT-PCR. **(B)** The reduced seed set was observed only in siliques of the quintuple knock-down *ec1-RNAi.* **(C)** to **(E)** Confocal images of sperm nuclei (red) in the wild-type and in *ec1-RNAi* ovules. (C) Sperm cells (arrowheads) fusing with WT female gametes at 7 hap. (D and (E) *ec1-RNAi* ovules with two (D) or four (E) unfused sperm cells (arrowheads). **(F)** Quantitative assessment of *ec1*-RNAi phenotypes at 30 to 40 hap. Phenotypes of ovules targeted by a pollen tube were classified as indicated. Mean values ±SEM (error bars) are shown [n = numbers of siliques counted (number of ovules)]. Scale bar in (C) = 20 µm.

EC1.3 in heterozygous *ec1-RNAi* pistils (**Figure S6.6**), both embryo sac development (**Figure S6.7**) and pollen tube reception (**Figure S6.8**) were comparable to the same processes in WT ovules.

To study the *EC1* knock-down phenotype in more detail, we pollinated pistils of the wild-type and four independent *ec1-RNAi* lines with the sperm marker HTR10-mRFP1 (Ingouff et al., 2007). The evaluation of ovules at 30 to 40 hours after pollination (hap) revealed that *ec1-RNAi* ovules allow sperm release but block gamete fusion (**Table S6.3**).We found that 43.5 to 46.7% of *ec1-RNAi* embryo sacs had two, or even four, unfused sperm cells (**Figure 6.3 D-F**), whereas

in the wild-type, both sperm cell delivery and fusion are completed within 6 to 10 hap (**Figure 6.3 C**) (Faure et al., 2002). Notably, multiple-sperm cell delivery in *ec1-RNAi* ovules involves both synergids (**Figure S6.9**). We conclude that, due to failed gamete fusion, the second synergid of an *ec1-RNAi* ovule continues to secrete pollen tube attractants, even after the first pollen tube has successfully discharged its sperm pair into the receptive synergid cell. This suggests a gamete fusion-based molecular mechanism preventing multiple-pollen tube attraction and is in accordance with recent observations of mutants with defective sperm cells that fail to fuse (Beale et al., 2012; Kasahara et al., 2012). It is vital to ensure that both gamete fusion events take place in a timely and efficient manner, because typically only one pair of sperm cells is delivered into the embryo sac, and both female gametes need to be fertilized for reproductive success. The two sperm cells of flowering plants are known to be physically associated (arrowhead in **Figure 6.4 A**) (McCue et al., 2011), and this connection may ensure the simultaneous delivery of both sperm cells to the gamete fusion sites.

To address the question of whether EC1 secretion serves as a precisely timed signal for sperm cell separation, we generated transgenes expressing a GFP-labeled membrane protein (TET9-GFP) in sperm cells to visualize the sperm membranes during double fertilization. Both the intercellular sperm connection and the cytoplasmic projection that is known to connect the front sperm (sc1) with the vegetative nucleus (McCue et al., 2011) are visible (**Figure 6.4 A, B**). Notably, the physical link between the two sperm cells appears to be membrane-enriched (arrowhead in **Figure 6.4 B**). This membranous link remains between the unfused sperm cells in *ec1-RNAi* ovules (**Figure 6.4 C, D**). However, we also detect the physical association at the time point of sperm-egg fusion in WT embryo sacs (**Figure 6.4 E, F**), arguing against a role for EC1 in sperm separation. After plasmogamy, remnants of the membranous link are visible at the apical edge of the degenerating synergid (**Figure 6.4 G, H**), where they stay attached, even when the synergid collapses. At that stage, we also find traces of GFP-labeled sperm membranes at the surface of the fertilized egg cell, most likely representing the sperm-egg fusion site (**Figure S6.10**).

Gamete-interaction studies in other organisms revealed that gamete adhesion and/or binding initiates a signaling cascade that leads to the activation of the male gamete and to the exposure of fusogenic membrane regions (Hirohashi et al., 2008; Inoue et al., 2011; Neill and Vacquier, 2004; Grote, 2010; Pan and Snell 2000). So far, the only known flowering plant candidate gamete fusogen is HAP2/GCS1, a sperm-expressed single-pass transmembrane domain protein (Mori et al., 2006; von Besser et al., 2006). Notably, fluorescent signals of HAP2–yellow fluorescent protein (YFP) in sperm cells of semi–in vivo grown *Arabidopsis* pollen tubes are endomembrane-associated and not located at the sperm surface (**Figure 6.4 I, J**) (Wong and Johnson, 2010), implying the need for membrane remodeling to acquire full fertilization competence when the sperm cells reach their fusion sites. However, the weak fluorescence of HAP2-YFP prevented us from detecting any redistribution of HAP2/GCS1 within the ovule.

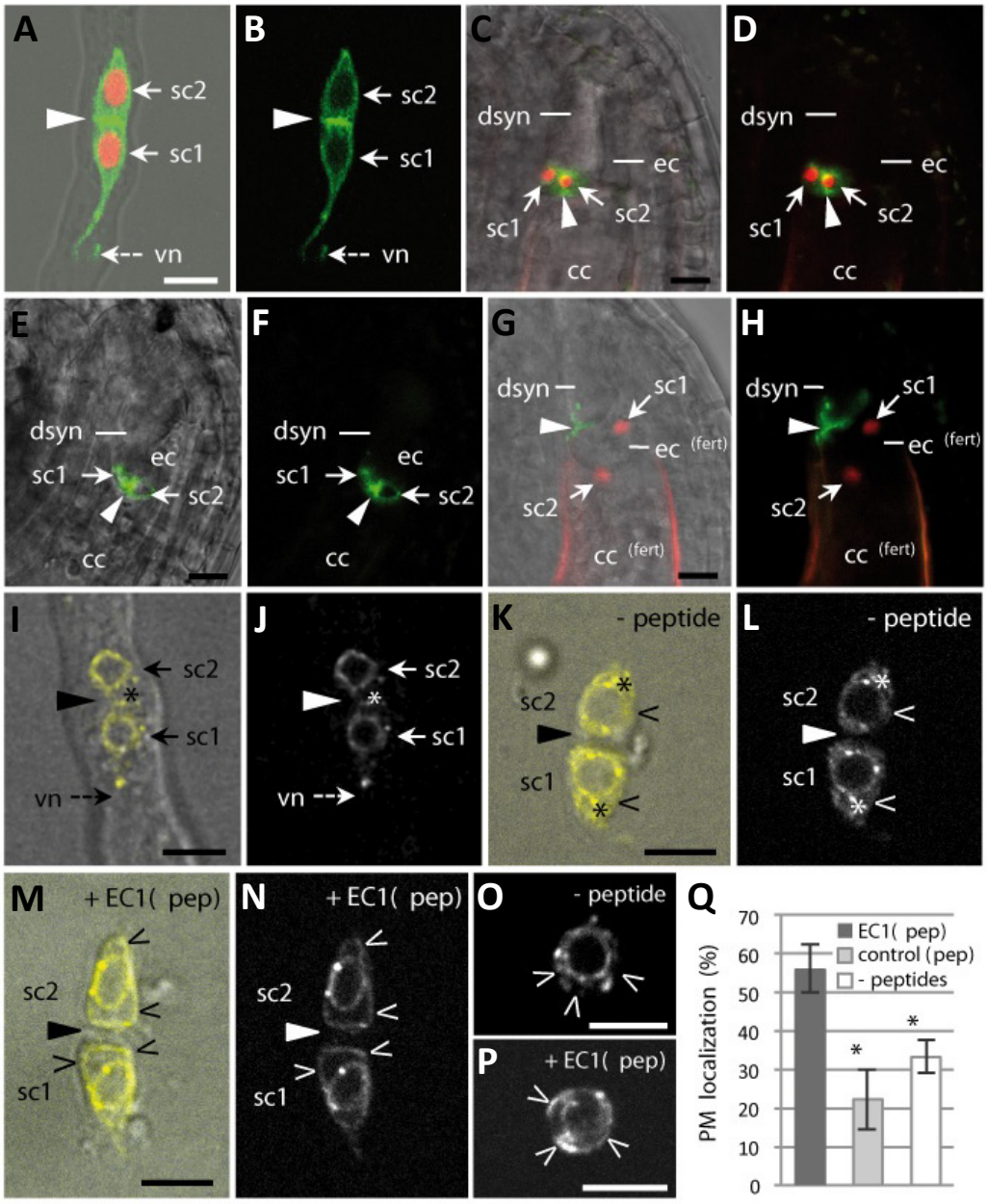

Figure 6.4 | EC1 peptides activate the sperm endomembrane system.

(A) and **(B)** Confocal images of sperm cell marker line simultaneously labeling sperm nuclei (red) and sperm membranes (green). Note the membranous connection between the sperm cells (solid arrowheads) and the cytoplasmic projection associated with the vegetative nucleus (dashed arrows). **(C)** to **(F)** Sperm membranes stay physically connected (solid arrowheads) during gamete interaction, in both *ec1-RNAi* (C) and (D) and WT ovules (E) and (F). **(G)** and **(H)** After plasmogamy, the membranous connection (solid arrowheads) is visible at the apical edge of the degenerating synergid. **(I)** to **(P)** Spinning disc images of sperm cells expressing HAP2-YFP. (I) and (J) HAP2-YFP localization in the endomembrane system of sperm cells within a semi–in vivo growing pollen tube. Solid arrowheads point at the position of the membranous intercellular connection. (K) and (L) Sperm cell pair released in peptide-free control solution, showing endomembrane-associated HAP2-YFP (asterisks). (M) and (N) HAP2-YFP localization at the plasma membrane (arrowheads) of sperm cells treated with EC1.1 peptidemix [EC1(pep)]. (O) Single sperm cell in a peptide-free control solution. (P) HAP2-YFP at the plasma membrane (arrowheads) of EC1(pep)-treated single sperm cell. **(Q)** Quantitative assessment of HAP2-YFP localization at plasma membranes of EC1(pep)-treated sperm cells, compared with randomized control peptides and a peptide-free solution. Mean values (±SEM) of at least three independent experiments with ≥20 sperm cells each are shown. Asterisks indicate statistically significant difference from the controls (*$P < 0.05$), according to Student's t test. vn, vegetative nucleus. Scale bars = 5 µm.

To investigate the effect of exogenously applied EC1 on HAP2-YFP localization, we developed a bioassay with sperm cells freshly released from semi-in vivo grown pollen tubes. Because all attempts to express recombinant EC1 or to generate synthetic EC1 proteins failed, we tested the effect of two synthetic EC1.1 peptides, comprising the signature motifs S1 and S2 (**Figure 6.2 A**). Neither peptide alone showed an obvious effect on sperm cells, but when we treated the sperm cells with an equimolar peptide mixture [EC1(pep)], the HAP2-YFP signal significantly shifted towards the sperm plasma membrane, compared with controls treated with a mixture of two randomized peptides based on the same amino acids or a peptide-free solution (**Figure 6.4 K-Q**).

Taken together, our results strongly suggest that EC1 is a protein factor controlling *Arabidopsis* gamete fusion by mediating sperm activation. We propose that the regulated secretion of EC1 by the egg cell upon sperm-egg interaction ensures the appropriate localization of the cell-fusion machinery in distinct sperm membrane domains to accomplish gamete fusion. Although both sperm cells stay close together after being delivered at the site where the two fusion events take place, we show that they remain spatially separated from one another, which may be a strategy to avoid polyspermy and to guarantee reliable and efficient double fertilization after achieving full fertilization competence. The observed mutual gamete activation furthermore suggests a complex mode of intercellular communication between the flowering plant egg and sperm cell before fusion. This may include the on-time delivery of other, yet undiscovered fertilization molecules to the gamete surfaces.

Although the reproductive strategy of flowering plants is considerably different from those of other sexual reproducing organisms, we report here on some essential common processes and principles. Our results indicate that, like the male gametes of other species, *Arabidopsis* sperm cells must be activated to acquire fertilization competence. However, animal sperm become activated after interacting with the outer vestment of the egg, whereas the egg responds by undergoing the cortical reaction only after fusion (Neill and Vacquier, 2004; Parrington et al., 2007; Hirohashi et al., 2008; Inoue et al., 2011). Thus, the mutual activation of *Arabidopsis* gametes before fusion points to an evolutionary link between flowering plant fertilization and fertilization in unicellular sexual reproducing organisms such as yeast and *Chlamydomonas* (Pan and Snell, 2000; Grote, 2010), where both mating-type gametes become activated before fusion.

6.3 Material and Methods

6.3.1 Plant materials and growth conditions

Arabidopsis thaliana (accession Col-0) SALK T-DNA insertion lines (Alonso et al., 2003) were obtained from the Nottingham *Arabidopsis* Stock Centre (NASC). FLAG mutant lines (accession WS-4) were obtained from the Versailles INRA collection (Samson et al., 2004). T-DNA insertion lines used in this work are *ec1.1* (SALK_016232), *ec1.3* (SALK_117981), *ec1.4*

(SALK_048709), and *ec1.5* (FLAG_456H12). Mutant and wild-type (Col-0) seeds were sown on soil (65 % substrate, 25 % sand, 10 % expanded clay), stratified for 2 days at 4 °C in the dark, and grown at 20 °C under a short photoperiod (9 h / 5 h light / dark cycles) for 4 weeks, followed by a long photoperiod (16 h / 8 h light / dark cycles) to induce flowering. For sterile growth seeds were surface sterilized for 3 min in 70 % ethanol, followed by a 2 min treatment in 1 % NaOCl / 0.1 % Mucasol® (Merz Consumer Care GmbH). Seeds were then washed three times in sterile H_2O, dispersed in sterile 0.1 % agarose and placed on half-strength MS medium (Murashige & Skoog, Duchefa) containing vitamins and MES buffer, solidified with 0.8 % Phytagar. For hygromycin selection the medium was supplemented with 30 µg/mL Hygromycin, when PAT (Phosphinotricin-Acetyltransferase) was used as a selection marker, seedlings were germinated on soil and sprayed at least three times with 200 mg/L glufosinate ammonium (BASTA®; Bayer Crop Science) supplemented with 0.1 % Tween-20.

6.3.2 Expression studies by RT-PCR

RT-PCR based expression analysis was performed using isolated mRNA, as described previously (Gebert et al., 2008). For semi-quantitative PCR and quantitative RT-PCR, wild-type and *ec1-RNAi* flowers of stage 11-12 (Smyth et al., 1990) were emasculated and five to eight pistils of each plant were collected two days later for mRNA isolation. PCR reactions were performed with each 1 µL of cDNA as template. Specificity of RT-PCR primers for *EC1.1* (At1g76750), *EC1.2* (At2g21740), *EC1.3* (At2g21750), *EC1.4* (At4g39340), and *EC1.5* (At5g64720) was confirmed by PCRs with genomic DNA and cDNA of individual T-DNA knock-out lines. *Actin3* (At3g53750) was used as reference gene for standard RT-PCR, the gene for *EUKARYOTIC TRANSLATION INITIATION FACTOR 4G* (*eIF4G*, At3g60240) served as a reference for relative quantification using the ΔΔCt method (Livak and Schmittgen, 2001). The following primer pairs were used for analyzing gene expression: *Act3* ACT3fw (5'-GATTTGGCATCACACTTTCTACAATG-3') ACT3rev (5'-GTTCCACCACTGAGCACAATG-3') *eIF4G* eIF4Gfw (5'-CGGCGATGTTCTTGGGAGTG-3') eIF4Grev (5'-CCGGTTAGGTGCATGAGGTTTG-3') *EC1.1* RT_EC1.1fw (5'-ACAGTGACAGCTCGCCCTCTC-3') RT_EC1.1rev (5'-AGTCATTGCCATCACAGTAACCTT-3') *EC1.2* qRT_EC1-2fw (5'-ACAAAACAAAAACCCCAAAAAGAA-3') qRT_EC1-2rev (5'-GAAGGCGCCGGAGAAGAA-3') *EC1.3* qRT_EC1-3fw (5'-ACGCCGTTGATGTCATTACCACT-3') qRT_EC1-3rev (5'-ACGTCAGCGAGGAACATTTATCAA-3') *EC1.4* EC1-4fw (5'-CCAGCGGAGTCATCAACCAACATA-3') EC1-4rev (5'-GGAGACGGAGCCGGAGAAGAGT-3') *EC1.5* EC1-5fw (5'-GCGCCGGAAACTTGATGGACT-3') EC1-5rev (5'-GGCGCCGGTGAAGGAGATAAT-3').

6.3.3 *In situ hybridization*

Nonradioactive *in situ* hybridization was performed as originally described by (Vielle-Calzada et al., 1999) with minor modifications for hybridizations to ovule and embryo sections as detailed in (Sieber et al., 2004) and (Köhler et al., 2003), respectively. Flowers of different developmental stages (immature flower buds, emasculated flowers, flowers with pollinated pistils) were used for making 8 µm thin sections for hybridizations. For generating RNA probes by in vitro transcription the 3'-UTR and part of the open reading frame of *EC1.1* and *EC1.2*, and *EC1.5* including 5´ and 3´-UTRs were amplified by PCR and cloned into pCR®II-TOPO® (Invitrogen). Primers used for amplification were as follows: *EC1.1* 1-1fw*Xba*I (5'-ATCTGTCTAGAAATGG-CTTC-3') 1-1rev*Xba*I (5'-TTTATTCTAGAAAGTAATAACAG-3') *EC1.2* 2a-*Bgl*IIfw (5'-AAA-GAAAGATCTATGGCTTCTAAC-3') 2a-*Sal*rev (5'-TCATTAGTCGACTTTGCATACATC--3') *EC1.5* 1-5(-34)fw (5'-CTCTTACAAAAAATCCATAACAC-3') 1-5(+494)rev (5'-TAA-CTTAAAATATAAAGGGAAAGC-3') Plasmids were linearized using *BamH*I (sense) or *Xho*l (antisense) and purified by two times of phenol/chloroform extractions followed by precipitation. Run off transcripts of linearized plasmids (0.5 µg/µL in DEPC-treated water) were generated by using T7 and SP6 polymerases for in vitro transcription. After hybridization, the slides were viewed with a Leica DMR or a Zeiss Axioplan microscope under differential interference contrast (DIC) and pictures were taken with a digital camera for microscopes (Magnafire model S99802, Optronics, USA).

6.3.4 *Preparing ovules and siliques for microscopy*

For differential interference contrast (DIC) microscopy the ovules and developing seeds were dissected on glass slides in chloral hydrate/glycerol/water (8:1:2, w/v/v), for fluorescence microscopy or CLSM they were dissected in 50 mM sodium phosphate buffer (pH 7.5). Using a stereomicroscope, the pistils/siliques were dissected from other floral organs and slit open along both sides of the septum using a hypodermic needle (0.4 x 20 mm, Braun). After removing the carpels, the septum with attached ovules was transferred into a droplet of mounting solution, the placenta was separated lengthwise into two halves using two hypodermic needles and a cover slip was carefully lowered onto the drop of mounting medium. For fluorescence microscopy and CLSM ovules were analyzed immediately. For DIC microscopy, slides were kept for 30 min to 2 hours at room temperature before analyzing the samples at the Axioskop FL (Zeiss) with DIC optics. Seed set of siliques was investigated and photographed after clearing almost mature siliques overnight in 9:1 (v/v) ethanol:acetic acid, followed by the incubation in 90 % (v/v) ethanol. Before stereomicroscopy (Zeiss Discovery.V8), siliques were transferred into 70 % Ethanol (v/v). Pictures were captured using a Zeiss Axiocam MRc5.

6.3.5 Pollen tube reception and double fertilization

Mature pistils from emasculated wild-type, *EC1.1p:EC1.1-GFP* and *ec1-RNAi* flowers were crossed with pollen of the marker lines *ARO1p:GUS* (Gebert et al., 2008), *HTR10p:HTR10-mRFP1* (Ingouff et al., 2007), or with the double marker *HTR10p:TET9-GFP*; *HTR10p:HTR10-mRFP1*. To monitor double fertilization by CLSM wild-type and *EC1.1p:EC1.1-GFP* pistils were dissected from 6 to 10 hours after hand pollination in phosphate buffer as described above. Pollinated *ec1-RNAi* pistils were dissected 30 to 40 hours after hand pollination. A Nikon ECLIPSE TE2000-S inverted microscope was used to quantify the unfused sperm cell phenotype, using the filter set F36-506 (EX 575/15; DM 593; BA 624/40). Pollen tube reception was investigated 24 hours after pollinating pistils of emasculated wild-type and *ec1-RNAi* flowers with *ARO1p:GUS* pollen by GUS histochemical staining. Pistils were slit open along both sides of the septum and transferred into GUS-staining solution (10 mM EDTA, 2 mM $K_4Fe(CN)_6$, 2 mM $K_3Fe(CN)_6$, 0.1% Triton X-100, 1 mg/mL X-Gluc (Applichem) in 50 mM sodium phosphate buffer, pH 7.0) and incubated at 37 °C overnight. Pistils were washed three times in sodium phosphate buffer before they were dissected in chloral hydrate/glycerol/water (8:1:2, w/v/v) and analyzed by DIC microscopy, as described above. Images were captured using the Zeiss AxioVision camera and software (release 4.6).

6.3.6 Confocal Laser Scanning Microscopy (CLSM)

A Zeiss Axiovert 200M inverted microscope equipped with a confocal laser scanning module (LSM 510 META) was used for CLSM. GFP was excited by 488 nm and detected with a BP 505-550 filter, mRFP1 was excited by 543 nm and detected using a BP 560-615 filter. Optical sections were generally between 0.39 and 0.48 µm each, using a 40x or 63x magnification. Capture and processing of images were done using the AxioCam HRc camera, the Zeiss LSM 510 META software, and the Zeiss LSM image browser version 3.5.0.359. Plot profiles on fluorescence and grayscale data in individual optical slices were generated using ImageJ. Fluorescence intensity profiles along the length of a line, drawn across one synergid cell and the flanking egg cell, were plotted together with reciprocal grayscale values for the transmitted light channel (1/BF) to obtain both fluorescence and grayscale signals as local maxima. The cell borders of the egg cell and the synergid (or degenerating synergid) cell were identified in pixel-sized grayscale images and included as dashed lines in the plot profiles by measuring cell widths on the plot axis.

6.3.7 Generation of constructs and plant transformation

EC1p:GUS constructs. Genomic regions of *EC1.1* and *EC1.2* were amplified from *Arabidopsis thaliana* (Col-0) using *Pfu* DNA Polymerase (MBI Fermentas) and the primer pair pEC1.1 (5'-TGCCTTATGATTTCTTCGGTTTC-3') / EC1.1rev1 (5'-TCAGAGTCATTGCCATCACAGTAACCTT-3'), and pEC1.2 (5'-AAGCATTTGCGTTTGGTTTATC-3') /

tEC1.2rev (5'-AATGCGGTTTTAGTCACACG-3'), respectively. The PCR products were cloned into pCR®2.1-TOPO® (Invitrogen) and subsequently used to amplify a 457 bp region 5´ upstream of the *EC1.1* start codon by using the primer pair M13rev (vector primer) / EC1.1-*Pst*I (5'-CCATTTCTCTGCAGATTGATAA-3'), and a 893 bp region 5´ upstream of the *EC1.2* start codon using the primer pair M13rev / EC1.2-*Bgl*II (5'-CCATAGATCTTTCTTTTTGG-GG-3'). PCR fragments were restricted with *Pst*I (*EC1.1* promoter) and *Bam*HI/*Bgl*II (*EC1.2* promoter), respectively. The binary expression vector *EC1.1p:GUS* was created by cloning the *Pst*I digested *EC1.1* promoter fragment upstream of β-glucuronidase (GUS-INT) (Vancanneyt et al., 1990) using dephosphorylated vector *pMG2002* (M. Gahrtz, unpublished), after the maize *Ubiquitin* (*UBI*) promoter was removed by *Pst*I digest. The binary expression vector *EC1.2p:GUS* was created by ligating the *Bam*HI/*Bgl*II-digested *EC1.2* promoter fragment into *Bam*HI/*Bgl*II digested *pMG2002*. *EC1p:EC1-GFP*. A C-terminal fusion of eGFP (enhanced green fluorescence protein; (Pang et al., 1996)) to EC1.1, expressed under control of the *EC1.1* promoter, was generated by amplifying genomic *EC1.1* using *Pfu* DNA polymerase (MBI Fermentas) and the primers E1F (5'-GCCTTATGATTTCTTCGGTT-3') and E1R (5'-GCAGGAGTGTAAAGAT-GAAT-3'). A second amplification was performed using the modified primers EC1-PF2 (5'-CCCCGAATTCCTTATGATTTCTTCGGT-3') and EC1-R (5'-CTCGGATCCGGGT-TAGAAGGAGAA-3'). After restriction with *Eco*RI and *Bam*HI, the fragment was cloned into the *Eco*RI-*Bam*Hl sites of the binary vector *p7U-GFP* (DNA Cloning Service, Hamburg) to generate *EC1p:EC1-GFP*. *EC1p:RNAi(EC1.2/3).* The ORF of *EC1.2* was amplified from genomic DNA using the primer set 1.2Eco (5'-CCGCCGAATTCTATGGCTTCTAACAC-3') / 1.2Bam (5'-CCTCGGATCCATCAAAGTTTCACAGAG-3') and 1.2Eco/1.2 Mlu (5'-CTCTACGCG-TCATCAAAGTTTCACAGAG-3'), respectively. After the restriction digest with *Eco*RI / *Bam*-HI the first PCR fragment was cloned in antisense orientation into the *Eco*RI / *Bam*HI digested vector *pEC1-iF2*, between the *EC1.1* promoter and the *FAD2* intron (At3g12120), to generate the intermediate *EC1.2-antisense* construct. The sense fragment was digested with *Eco*RI / *Mlu*I and ligated behind the *FAD2* intron into *EC1.2-antisense* using *Mlu*I and *Mfe*I. Subsequently, the resulting expression cassette *EC1.2-RNAi* was transferred via *Sfi*I digest into the vector *p7N* (DNA Cloning Service, Hamburg) to generate the binary vector *EC1p:RNAi(EC1.2/3).* For hygromycin selection in plants, the expression cassette *EC1.2-RNAi* was subcloned into the binary vector *p6U* (DNA Cloning Service, Hamburg). The high sequence similarity of *EC1.2* and *EC1.3* results in simultaneous down-regulation of *EC1.2* and *EC1.3* in the egg cell.

HTR10p:TET9-GFP. A PCR fragment covering the *HTR10* promoter was amplified by PCR from genomic DNA using the primer pair HTR10fw_SacI (5'-TGATTGAGCTCCGACCAAA-AACTTTCAAAATTT-3') / HTR10rev_SpeI (5'-TTCTACTAGTGAACGATGATGATGA-TGATAACC-3'). The GATEWAY destination vector pB7FWG2 (Karimi et al., 2002) was digested with *Sac*I/*Spe*I to remove the 35S promoter which was subsequently replaced by the *Sac*I/*Spe*I digested *HTR10* promoter fragment, resulting in the Gateway® destination vector *HTR10p:GW:GFP*. The coding sequence of the four transmembrane domain protein TET9

(At4g30430) was amplified from pistil cDNA using the primer pair Tet9-FW (5'-CACCAT-GGTACGTTTTAGTAACAGTCTTGTAGGAATACT-3') and Tet9-REV(-Stopp) (5'-AGA-ATTGTTGAAACCATTGGAACGGC-3') and cloned into the Gateway® Entry vector pENTR/D-TOPO (Invitrogen, Carlsbad, CA, USA). By *in vitro* recombination using the Gateway® LR Clonase® enzyme mix (Invitrogen) the *TET9* coding sequence was then transferred into the binary vector *HTR10p:GW:GFP*, generating the binary expression vector *HTR10p:TET9-GFP*. Individual binary expression vectors were delivered into *Agrobacterium tumefaciens* GV3101 (pMP90RK) which were then used to transform either *Arabidopsis* (Col-0), *ec1* T-DNA insertion mutants, or homozygous *HTR10p:HTR10-mRFP1* plants by the floral dip method (Clough and Bent, 1998).

6.3.8 Western Blot analysis of EC1-GFP

For one protein extraction, fifty mature pistils of each wild-type and *EC1p:EC1- GFP* (two days after emasculating stage 12 flowers, (Smyth et al., 1990)) were frozen in liquid nitrogen. Leaves of wild-type and *CaMV35Sp:mGFP–ER* expressing plants (Haseloff et al., 1997) were used for control protein extractions. After grinding, 300 µL of homogenization buffer (50 mM Tris / 0.05 % MES, pH 7.5; 330 mM sucrose; 100 mM KCl; 1 mM EDTA; 5 mM DTT; 1 "Complete" protease inhibitor tablet (Roche)) was added to each sample. The samples were centrifuged for 15 min at 1,000 x g and the supernatants subjected to two consecutive centrifugation steps (15 min, 10,000 x g; 75 min, 48,000 x g). The resulting supernatants were precipitated with 0.01 vol. of 2% DOC (sodium deoxycholate) / 0.1 vol. of 100 % TCA (trichloroacetic acid). The precipitated proteins were pelleted by centrifugation at 15,000 x g at 4 °C for 15 min. For SDS-PAGE the dried pellets were resuspended in 20 µL of 1 x SDS sample buffer, boiled, and entirely loaded on the gel. After electrophoresis, proteins were blotted onto a PVDF membrane (Bio-Rad) and EC1- GFP was detected using a monoclonal anti-GFP (Roche) and a HRP (horseradish peroxidase)-conjugated goat anti-mouse antibody (Sigma-Aldrich). The Immobilon Western Detection Reagent (Millipore) was used as a substrate for the HRP enzyme. The molecular masses of the detected EC1-GFP and ER-targeted GFP signals were extrapolated after determining the Rf value (distance migrated / gel length) for the immunosignals and the protein standards and plotting the log (MW) against Rf.

6.3.9 Sperm cell activation assay

In a modified semi-in vivo pollen germination assay (Palanivelu and Preuss, 2006), mature but virgin pistils were pollinated with the respective transgenic pollen (*HAP2p:HAP2-YFP; HTR10p-TET9-GFP*; or *HTR10p:HTR10-mRFP1 x HTR10p-TET9-GFP*) and cut at the junction between the style and ovary. The upper part of the pistil was placed upright on 35 mm petri dish with solidified pollen germination medium (PGM) (Li et al., 1999). After incubating the

pistils for 2 hours under humid conditions, they were transferred into a droplet of liquid PGM and incubated another 6-7 hours. Two HPLC-purified peptides (peptides covering the signature motifs S1 and S2, respectively, were synthesized since all trials to generate recombinant or synthetic EC1-1 proteins, or slightly shorter versions covering both signature motifs, failed) covering the EC1.1 signature motifs S1 (EC1(pep)S1: CSGELILFFLNGETYIGPG) and S2 (EC1(pep)S2: CWPTMIGVLGFTAQEGDMLQGY), and two randomized peptide versions based on the same amino acids (rS1: GEPLFGELCSLNIGFTYGI; rS2: GDFTMCTMIGWPLQEYGVLGAQ) were synthesized by Centic Biotec (Weimar, Germany) and INTAVIS Bioanalytical Instruments AG (Reutlingen, Germany), respectively. The lyophilized peptides were solubilized in DMSO, briefly sonicated and diluted with 100 mM Tris / HCl (pH 7.7) to 20 % (v/v) DMSO. Subsequently, peptides were diluted 1:20 in liquid PGM to obtain a final peptide concentration of 120 µmolar (solubilization was only partially possible, due to the high hydrophobicity of the peptides; therefore the effective concentration of the particular soluble peptide fraction cannot be estimated precisely) each in 2 % DMSO. Incubated pistils were either transferred in a droplet of EC1 peptide mix, in a droplet of randomized peptide-mix, or in a droplet of control solution prepared identical except the addition of peptides. The sperm cell pairs were released by cutting the pollen tubes emerging from the style with a sterile surgical blade. The preparation was carefully covered with a cover slip and incubated for 10 minutes in a moist chamber prior to microscopic analysis. Preliminary experiments with pollen tube-released sperm cells revealed that approximately 69 % (n = 168) of the sperm cells remained as a pair during this procedure, irrespective of whether they had been released in peptide-mix or in control solution. We assessed the sperm cells for the presence of a continuous HAP2-YFP signal along the sperm plasma membrane in at least three independent experiments with 20 analyzable sperm cells, each. Treatments with individual peptides (i.e. EC1(pep)S1 only, or EC1(pep)S2 only) did not show any obvious effect on subcellular HAP2-YFP localization, therefore we performed subsequent experiments with an equimolar mixture of both EC1 peptides (n = 4; 141 sperm cells), compared to mock-treated controls (n = 3; 143 sperm cells) and to sperm cells treated with an equimolar mixture of the two randomized peptides (n = 3; 97 sperm cells). The mean ± SEM and the statistical significant difference between EC1(pep)S1/S2 treated sperm cells and the controls were estimated according to Student's t test.

6.3.10 Spinning Disc Microscopy (SDM) and data evaluation

SDM was performed on a ZEISS Cell Observer spinning disc confocal microscope (Yokogawa CSU-X1) using a 100x/1.40 Oil DIC objective. HAP2-YFP fluorescence was excited with a 488 nm 100 mW OPSL laser and emission filtered through a 505-545 nm BrightLine HC 525/40 filter. Spinning disc confocal images were processed using ImageJ software (http://-rsbweb.nih.gov/ij, version 1.45). Changes in fluorescent signal localization were evaluated by analyzing fluorescent images and the respective DIC images. Graphs were drawn with data obtained

from at least three independent experiments, considering the standard error calculated by IBM SPSS Statistics 19.

6.3.11 Bioinformatics and sequence analysis

Wheat *EC-1* (*TaEC1*) cDNA sequences (Sprunck et al., 2005) were used to identify putative orthologs in *Arabidopsis thaliana* and rice with the Basic Local Alignment Search Tool (BLAST; http://blast.ncbi.nlm.nih.gov/). Subsequently, the *Arabidopsis EC1.1* coding sequence and the EC1.1 protein sequence were used as queries for BLASTP and TBLASTN searches, respectively, at different genome databases: The plant genome database (http://www.plantgdb.org/); the TIGR gene indices (http://compbio.dfci.harvard.edu/tgi/plant.html); the *Brachypodium distachyon* database; (http://www.brachypodium.org/), the *Medicago truncatula* database, version MT3.0 (http://www.medicago.org/); the EST assemblies from ancestral angiosperms (http://ancangio.uga.edu/content/aagp-home); and the *Amborella* Genome Database (http://amborella.huck.psu.edu/project). TargetP (http://www.cbs.dtu.dk/services/TargetP/) was used to predict the subcellular localization of EC1 and EC1-like proteins. The analyses for signal peptides targeting the proteins to the secretory pathway, and the prediction of putative signal peptide cleavage sites were performed using SignalP 4.0 (http://www.cbs.dtu.dk/services/SignalP/). Disulfide bond formation in EC1 and EC1-like proteins was predicted by PredictProtein (http://www.predictprotein.org/), and by DISULFIND (http://disulfind.dsi.unifi.it/). Multiple sequence alignment and molecular phylogeny was performed using SeaView Version 4.2.8. (Gouy et al., 2010). The MUSCLE algorithm (Edgar, 2004) was applied for multiple sequence alignments of mature EC1 protein sequences (after removing the predicted signal peptides). Alignments were imported into GeneDoc (http://www.nrbsc.org/gfx/genedoc/) for sequence editing and shading of conserved amino acids. For the construction of phylogenetic trees of ECA1 gametogenesis related CRPs (Silverstein et al., 2007) the protein sequences were aligned using the multiple sequence alignment program ClustalW2 (http://www.ebi.ac.uk/Tools/msa/clustalw2/) and the deduced phylogenetic tree was illustrated with PhyloDraw 0.8 software (Graphics Application Lab, Pusan National University).

6.4 Summary

Double fertilization is the defining characteristic of flowering plants. However, the molecular mechanisms regulating the fusion of one sperm with the egg and the second sperm with the central cell are largely unknown. We show that gamete interactions in *Arabidopsis* depend on small cysteine-rich EC1 (EGG CELL 1) proteins accumulating in storage vesicles of the egg cell. Upon sperm arrival, EC1-containing vesicles are exocytosed. The sperm endomembrane system responds to exogenously applied EC1 peptides by redistributing the potential gamete fusogen HAP2/GCS1 (HAPLESS 2/GENERATIVE CELL SPECIFIC 1) to the cell surface. Furthermore, fertilization studies with *ec1* quintuple mutants show that successful male-female gamete interactions are necessary to prevent multiple-sperm cell delivery. Our findings provide evidence that mutual gamete activation, regulated exocytosis, and sperm plasma membrane modifications govern flowering plant gamete interactions.

CHAPTER 7 Comprehensive Summary, Discussion and Outlook

The research focus of this thesis lies on the description of cell biological and molecular properties of polarity establishment and maintenance in *Arabidopsis* pollen tubes and root hairs, as well as on signaling events between both the pollen tubes and the sperm cells with the cells of the female gametophyte during double fertilization.

In ***Chapter 2*** of this thesis it is shown that in vitro pollen activation and germination is subdivided into several distinct developmental phases revealing characteristic growth kinetics, vesicle polarization and actin cytoskeleton dynamics. The ARO1 armadillo repeat protein is essential for proper polar pollen tube growth and its knock-out leads to male sterile mutants (Gebert et al., 2008). In the growing pollen tube, ARO1 highly accumulates at clear zone of the pollen tube tip. Here we show that already before pollen germination, ARO1 polarizes in the pollen grain at the future site of tube emergence. However, ARO1 does not exhibit a steady-state accumulation at this site, but its localization rather resembles one to two distinct maxima 12 to 3 minutes before pollen tube formation. Pharmacological treatments (Gebert et al., 2008), TIRF microscopy and live cell imaging (Vogler et al., 2015) revealed that ARO1 is associated to vesicles in the tip of growing pollen tubes. The distinct ARO1 maxima prior to pollen tube formation likely are associated with polarized secretion events, leading to the polar localization of cell wall material and cell wall modifying enzymes at a distinct site to initiate the local pollen coat weakening in order to allow subsequent tube emergence. Also very likely the formation of the only recently discovered germination plaque (Hoedemaekers et al., 2015) at the pollen tube emergence site could be related to the ARO1-labeled polar vesicle secretion events. The formation of the germination plaque is dependent on the *BURSTING POLLEN* (*BUP*) gene encoding a novel Golgi-located glycosyltransferase related to the plant-specific glycosyltransferase 4 (GT4) subfamily. The *bup* knock-out leads to short and thick pollen tubes that after germination often burst (Hoedemaekers et al., 2015). Interestingly, the *aro1-3* mutant also exhibits short and thick pollen tubes that often burst after germination (Gebert et al., 2008). Germination plaque formation in the *aro1-3* background therefore is an interesting open question.

Unlike the mechanistically similar root hair system, so far pollen tube mutants could not be clearly assigned to discrete developmental stages of protuberance formation, because a basic description of pollen tube growth kinetics was lacking. Based on quantitative live cell imaging, ***Chapter 2*** of this thesis also provides techniques for monitoring *Arabidopsis* pollen germination and a detailed description of the process of pollen tube formation. It is shown that after an initial slow bulging phase, ARO1-marked vesicles rapidly accumulate at the tip before the pollen tube enters a phase of rapid growth. Our data support the hypothesis that the initial pollen tube bulging represents a discrete and passive process (Geitmann, 2010). Based on the knowledge gained and the new experimental setup for quantitative live imaging of pollen during the different phases of activation, bulging and transition to rapid tip growth, it will be possible to characterize existing pol-

len mutants and to perform forward mutant screens to identify more genes involved in the different phases of pollen tube growth.

Notably, the function of the ARO protein family is not restricted to polar pollen tube growth but very likely to polarized vesicle targeting in general. In ***Chapter 3*** of this thesis the novel *aro2 aro3* root hair mutants are described. Comparable with *aro1-3* pollen tubes, *aro2 aro3* mutants exhibit short, thick and often burst root hairs. By genetic complementation we show that the ARO1, ARO2 and ARO3 proteins are able to functionally replace each other, while the more distant related ARO4 protein is only partially able to rescue the mutant phenotypes in pollen and root hairs. The single knock-out of *aro4* shows no obvious phenotype. However, as *ARO4* is strongly expressed in guard cells and other cell types of the leaf, it could act functionally redundant with ARO2 or ARO3 there. In collaboration with the group of Prof. Dr. Victor Žárský we were able to observe that trichome development is altered in *aro2 aro4* double knock-out mutants (I. Kulich and F. Vogler et al., unpublished), which will be investigated in more detail in the future.

The action of ARO proteins in different aspects of cell polarity is obviously regulated by their cell-type specific or preferential expression. We show that the highly root hair enriched ARO3 protein specifically accumulates in the vesicle-rich tip of the growing root hair and its localization is dependent on active secretion. Physiological experiments proofed that the ARO2 and ARO3 proteins function in the polar elongation step of root hair formation. The polar subcellular distribution of the TGN and secretory vesicles is defective in the *aro2 aro3* knock-out mutant as indicated by marker protein expression. This leads to the conclusion that functional redundant vesicle-associated ARO proteins are important for proper polarized secretion in tip growing cells. This is furthermore substantiated by the molecular interactions of ARO3 identified in this thesis. We could show in yeast two-hybrid or pull-down experiments that ARO3 interacts with *(i)* the exocyst vesicle tethering complex subunit Exo70E2, *(ii)* a yet uncharacterized Rho GTPase activating protein (RhoGAP) with a Pleckstrin homology domain and *(iii)* with the dynamin-like GTPase ROOT HAIR DEFECTIVE 3 (RHD3). As it is known that armadillo repeat proteins serve as versatile protein-protein interaction platforms (Samuel et al., 2006), the further characterization of these three ARO3 interacting proteins and the identification of potential additional interactors represent key steps in deeper understanding the ARO protein function in cell polarity control. In large scale *Arabidopsis* seedling phospho-proteomics approaches, for ARO2 and ARO3 phosphorylated peptides were identified (Durek et al., 2010). In collaboration with the group of Prof. Dr. Claus Schwechheimer (TU Munich) we were able to proof ARO2 and ARO3 phosphorylation by in vitro kinase assays (H. Shikata and F. Vogler et al., unpublished). To map the phosphorylation sites and to elucidate the regulation of ARO proteins by phosphorylation in respect of their molecular interactions will be another future task of paramount significance.

Besides regulating polar tip growth, there is also evidence that ARO proteins could play a more general role in cell polarization, for example in the polar response to invading pathogens. It was shown that ARO2 interacts with the oomycete effector protein HaRXL14 from *Hyaloperonospora*

arabidopsidis (Mukhtar et al., 2011). The role of ARO proteins during plant-pathogen interactions is currently investigated in a further collaboration (J. Steinbrenner and F. Vogler et al., unpublished).

Using ARO1-GFP expressing plants as a marker line, in ***Chapter 4*** of this thesis we show that *Arabidopsis* pollen germination and pollen tube growth responds in a dose-dependent manner to the plant hormone epiBL. We show that by adding epiBL to pollen germination media the often highly variable in vitro germination rates of *Arabidopsis* pollen can be significantly improved, as technically implemented in ***Chapter 1***. The promoter of one of the key enzymes in brassinosteroid biosynthesis, CYP90A1/CPD, is highly active along the reproductive tract of *Arabidopsis* pistils. In vivo pollen tube growth in wild-type, the *cyp90a1-1* brassinosteroid synthesis and the *bri1-10* brassinosteroid perception mutant revealed that brassinosteroids or their intermediates also promote pollen tube growth in the transmitting tract of the pistil. Therefore the often observed fact that in vitro pollen germination is not as efficient as in vivo pollen tube growth can be partially explained by the lack of brassinosteroid plant hormones. Highly sensitive chemical approaches, together with the development of brassinosteroid sensors for live cell imaging could further improve our understanding of the role of brassinosteroids in pollen tube growth promotion and guidance.

After pollen tubes have navigated through the female pistil tissues by polar expansion at the tip, they enter the ovule via the micropyle and reach the synergid cells of the female gametophyte. ***Chapter 5*** of this work employs ratiometric FRET live cell imaging to describe intracellular Ca^{2+} signatures of the synergid, egg and central cells during double fertilization. We were able to show that upon physical contact of the receptive synergid cell with the pollen tube membrane, it initiates high Ca^{2+} oscillations at the contact site with the tube tip. These high Ca^{2+} oscillations are necessary for synergid cell degeneration, likely by inducing cell death. Rapid synergid cell degeneration is important to avoid multiple pollen tube guidance into the ovule, termed polytubey (Beale et al., 2012). The egg and central cell show a high intracellular Ca^{2+} transient when the pollen tube bursts and the sperm cells are released. Additionally only in the egg cell a second Ca^{2+} peak occurs about 7 minutes after sperm cell release, when one of the sperm cells successfully fuses with the egg cell. This second Ca^{2+} peak in the egg cell could serve as a signal for polyspermy block and could initiate the subsequent karyogamy and zygote formation. Furthermore, the second Ca^{2+} in the egg cell also could function in cell signaling to the adjacent synergid or central cell. Although technically demanding, it would be of paramount interest to further experimentally address the timing of Ca^{2+} signaling, gamete membrane attachment and fusion, and the transport of the sperm nuclei after plasmogamy. Of great interest is also the timing of Ca^{2+} oscillations, the activation of the egg cell and the polarization and secretion of molecules from the egg cell.

Especially the timing of Ca^{2+} spikes in the egg cell and the release of the small cysteine-rich EC1 proteins is an interesting question that remains to be addressed.

In ***Chapter 6*** it is demonstrated that in *Arabidopsis* EC1 proteins are secreted after the sperm cells are released from the pollen tube. EC1 localizes to storage vesicles of the egg cell and before gamete fusion triggered EC1 exocytosis occurs. Knock-out/down of all five members of the *EC1* gene family leads to a significantly reduced seed set. In *ec1* quintuple mutant ovules a significantly higher number of two to four unfused sperm cells was observed. This indicates that in *Arabidopsis,* EC1 is an important female factor for rapid gamete fusion and for the subsequent block of pollen tube attraction and multiple sperm cell delivery. In ***Chapter 6*** a method for live cell imaging of sperm cells, released from semi-in vivo grown pollen tubes is presented. We used synthetic EC1 peptides to investigate their effect on sperm cells that express the putative fusogen GCS1/HAP2 as YFP fusion protein. The knock-out of GCS1/HAP2 results in sperm cells that are able to attach to the female gametes but are unable to fuse (Johnson et al., 2004; Mori et al., 2006). Notably, in sperm cells within the pollen tube or in released sperm cells of in vitro growing pollen tubes, GCS/HAP2 is localized in the endomembrane system. However upon treating the released sperm cells with EC1 peptides, GCS1/HAP2 is partially redistributed from the endomembrane system to the cell surface, likely activating the sperm cells for fusion. The established sperm cell isolation method can now serve to characterize the effects of different chemical substances, peptides and proteins on released sperm cells and allows investigating the involvement of other proteins or factors necessary for gamete activation and its downstream signaling.

Supplemental Data

The following digital Supplemental Data files can be found on the CD attached to the back cover of this thesis.

Chapter 2:	Figures S2.1 – S2.6
	Supplemental Movie 2.1 – 2.5
	Supplemental Movie Legends Chapter 2
Chapter 3:	Figures S3.1 – S3.6
	Table S3.1
	Supplemental Dataset Chapter 3
Chapter 4:	Figures S4.1 – S4.4
Chapter 5:	Figures S5.1 – S5.6
	Supplemental Movie 5.1 – 5.5
	Supplemental Movie Legends Chapter 5
Chapter 6:	Figures S6.1 – S6.10
	Table S6.1 – S6.3
	Supplemental Movie 6.1 – 6.2
	Supplemental Movie Legends Chapter 6
	Supplemental References Chapter 6

Publications

Chapter 2:

Vogler, F., Konrad, S.S.A., and Sprunck, S. (2015). Knockin' on pollen's door: live cell imaging of early polarization events in germinating *Arabidopsis* pollen. Front. Plant Sci. **6,** 246.

Chapter 3:

Vogler, F., Steinbrenner, J., Kulich, I., Vojtíková, Z., Braun, P., and Sprunck, S. (2015). Functional conserved ARMADILLO REPEAT ONLY proteins act in the network of polarity signaling and polarized secretion of *Arabidopsis* root hairs. ***submitted***.

Chapter 4:

Vogler, F., Schmalzl, C., Englhart, M., Bircheneder, M., and Sprunck, S. (2014). Brassinosteroids promote *Arabidopsis* pollen germination and growth. Plant Reprod. **27,** 153-167.

Chapter 5:

Denninger, P., Bleckmann, A., Lausser, A., Vogler, F., Ott, T., Ehrhardt, D.W., Frommer, W.B., Sprunck, S., Dresselhaus, T., and Grossmann, G. (2014). Male–female communication triggers calcium signatures during fertilization in *Arabidopsis*. Nat. Commun. **5,** 4645.

Chapter 6:

Sprunck, S., Rademacher, S., Vogler, F., Gheyselinck, J., Grossniklaus, U., and Dresselhaus, T. (2012). Egg cell–secreted EC1 triggers sperm cell activation during double fertilization. Science **338,** 1093-1097.

No own Chapter:

Sprunck, S., Hackenberg, T., Englhart, M., and Vogler, F. (2014). Same same but different: sperm-activating EC1 and ECA1 gametogenesis-related family proteins. Biochem. Soc. T. **42,** 401-407.

References

Alandete-Saez, M., Ron, M., and McCormick, S. (2008). *GEX3*, expressed in the male gametophyte and in the egg cell of *Arabidopsis thaliana*, is essential for micropylar pollen tube guidance and plays a role during early embryogenesis. Mol. Plant **1,** 586-598.

Alonso, J.M., Stepanova, A.N., Leisse, T.J., Kim, C.J., Chen, H., Shinn, P., Stevenson, D.K., Zimmerman, J., Barajas, P., Cheuk, R., Gadrinab, C., Heller, C., Jeske, A., Koesema, E., Meyers, C.C., Parker, H., Prednis, L., Ansari, Y., Choy, N., Deen, H., Geralt, M., Hazari, N., Hom, E., Karnes, M., Mulholland, C., Ndubaku, R., Schmidt, I., Guzman, P., Aguilar-Henonin, L., Schmid, M., Weigel, D., Carter, D.E., Marchand, T., Risseeuw, E., Brogden, D., Zeko, A., Crosby, W.L., Berry, C.C., and Ecker, J.R. (2003). Genome-wide insertional mutagenesis of *Arabidopsis thaliana*. Science **301,** 653-657.

Altschuler, S.J., Angenent, S.B., Wang, Y., and Wu, L.F. (2008). On the spontaneous emergence of cell polarity. Nature **454,** 886-889.

Alvarez, J.V., Pan, T.C., Ruth, J., Feng, Y., Zhou, A., Pant, D., Grimley, J.S., Wandless, T.J., Demichele, A., Investigators, I.S.T., and Chodosh, L.A. (2013). *Par-4* downregulation promotes breast cancer recurrence by preventing multinucleation following targeted therapy. Cancer Cell **24,** 30-44.

Amien, S., Kliwer, I., Marton, M.L., Debener, T., Geiger, D., Becker, D., and Dresselhaus, T. (2010). Defensin-like ZmES4 mediates pollen tube burst in maize via opening of the potassium channel KZM1. PLoS Biol. **8,** e1000388.

Antoine, A.-F., Faure, J.-E., Dumas, C., and Feijó, J.A. (2001). Differential contribution of cytoplasmic Ca^{2+} and Ca^{2+} influx to gamete fusion and egg activation in maize. Nature Cell Biol. **3,** 1120-1123.

Antoine, A., Faure, J.-E., Cordeiro, S., Dumas, C., Rougier, M., and Feijo, J. (2000). A calcium influx is triggered and propagates in the zygote as a wavefront during in vitro fertilization of flowering plants. Proc. Natl. Acad. Sci. **97,** 10643-10648.

***Arabidopsis* Interactome Mapping Consortium** (2011). Evidence for network evolution in an *Arabidopsis* interactome map. Science **333,** 601-607.

Arkowitz, R.A., and Bassilana, M. (2014). Rho GTPase-Phosphatidylinositol Phosphate interplay in fungal cell polarity. Biochem. Soc. Trans. **42,** 206-211.

Axelrod, J.D., and Bergmann, D.C. (2014). Coordinating cell polarity: heading in the right direction? Development **141,** 3298-3302.

Bajguz, A. (2007). Metabolism of brassinosteroids in plants. Plant Physiol. Bioch. **45,** 95-107.

Bajguz, A., and Tretyn, A. (2003). The chemical characteristic and distribution of brassinosteroids in plants. Phytochemistry **62,** 1027-1046.

Bancos, S., Nomura, T., Sato, T., Molnár, G., Bishop, G.J., Koncz, C., Yokota, T., Nagy, F., and Szekeres, M. (2002). Regulation of transcript levels of the *Arabidopsis Cytochrome P450* genes involved in brassinosteroid biosynthesis. Plant Physiol. **130,** 504-513.

Bao, F., Shen, J., Brady, S.R., Muday, G.K., Asami, T., and Yang, Z. (2004). Brassinosteroids interact with auxin to promote lateral root development in *Arabidopsis*. Plant Physiol. **134,** 1624-1631.

Baumberger, N., Steiner, M., Ryser, U., Keller, B., and Ringli, C. (2003). Synergistic interaction of the two paralogous *Arabidopsis* genes *LRX1* and *LRX2* in cell wall formation during root hair development. Plant J. **35,** 71-81.

Bayer, M., Nawy, T., Giglione, C., Galli, M., Meinnel, T., and Lukowitz, W. (2009). Paternal control of embryonic patterning in *Arabidopsis thaliana*. Science **323,** 1485-1488.

Beale, K.M., and Johnson, M.A. (2013). Speed dating, rejection, and finding the perfect mate: advice from flowering plants. Curr. Opin. Plant Biol. **16,** 590-597.

Beale, K.M., Leydon, A.R., and Johnson, M.A. (2012). Gamete fusion is required to block multiple pollen tubes from entering an *Arabidopsis* ovule. Curr. Biol. **22,** 1090-1094.

Becker, J.D., Takeda, S., Borges, F., Dolan, L., and Feijó, J.A. (2014). Transcriptional profiling of *Arabidopsis* root hairs and pollen defines an apical cell growth signature. BMC Plant Biol. **14,** 197.

Berger, F., Hamamura, Y., Ingouff, M., and Higashiyama, T. (2008). Double fertilization - caught in the act. Trends Plant Sci. **13,** 437-443.

Bi, E., and Park, H.-O. (2012). Cell polarization and cytokinesis in budding yeast. Genetics **191,** 347-387.

Bibikova, T., and Gilroy, S. (2002). Root hair development. J. Plant Growth Regul. **21,** 383-415.

Bleckmann, A., Alter, S., and Dresselhaus, T. (2014). The beginning of a seed: regulatory mechanisms of double fertilization. Front. Plant Sci. **5,** 452.

Bleckmann, A., Weidtkamp-Peters, S., Seidel, C.A., and Simon, R. (2010). Stem cell signaling in *Arabidopsis* requires CRN to localize CLV2 to the plasma membrane. Plant Physiol. **152,** 166-176.

Boavida, L.C., and McCormick, S. (2007). Temperature as a determinant factor for increased and reproducible in vitro pollen germination in *Arabidopsis thaliana*. Plant J. **52,** 570-582.

Boavida, L.C., Qin, P., Broz, M., Becker, J.D., and McCormick, S. (2013). *Arabidopsis* Tetraspanins are confined to discrete expression domains and cell types in reproductive tissues and form homo- and heterodimers when expressed in yeast. Plant Physiol. **163,** 696-712.

Boisson-Dernier, A., Lituiev, D.S., Nestorova, A., Franck, C.M., Thirugnanarajah, S., and Grossniklaus, U. (2013). ANXUR receptor-like kinases coordinate cell wall integrity with growth at the pollen tube tip via NADPH oxidases. PLoS Biol. **11,** e1001719.

Boisson-Dernier, A., Roy, S., Kritsas, K., Grobei, M.A., Jaciubek, M., Schroeder, J.I., and Grossniklaus, U. (2009). Disruption of the pollen-expressed *FERONIA* homologs *ANXUR1* and *ANXUR2* triggers pollen tube discharge. Development **136,** 3279-3288.

Bou Daher, F., Chebli, Y., and Geitmann, A. (2009). Optimization of conditions for germination of cold-stored *Arabidopsis thaliana* pollen. Plant Cell Rep. **28,** 347-357.

Bove, J., Vaillancourt, B., Kroeger, J., Hepler, P.K., Wiseman, P.W., and Geitmann, A. (2008). Magnitude and direction of vesicle dynamics in growing pollen tubes using spatiotemporal image correlation spectroscopy and fluorescence recovery after photobleaching. Plant Physiol. **147,** 1646-1658.

Brewbaker, J.L., and Kwach, B.H. (1963). The essential role of calcium ion in pollen germination and pollen tube growth. Am. J. Bot. **50,** 747-858.

Bulyha, I., Lindow, S., Lin, L., Bolte, K., Wuichet, K., Kahnt, J., van der Does, C., Thanbichler, M., and Søgaard-Andersen, L. (2013). Two small GTPases act in concert with the bactofilin cy-

toskeleton to regulate dynamic bacterial cell polarity. Dev. Cell **25,** 119-131.

Bunting, C., and Eades, C.C. (1926). The effect of mechanical tension upon the polarity of growing fibroblasts. J. Exp. Med. **44,** 147-149.

Cai, G., and Cresti, M. (2009). Organelle motility in the pollen tube: a tale of 20 years. J. Exp. Bot. **60,** 495-508.

Cai, G., Parrotta, L., and Cresti, M. (2015). Organelle trafficking, the cytoskeleton, and pollen tube growth. J. Integr. Plant Biol. **57,** 63-78.

Cai, G., Faleri, C., Del Casino, C., Emons, A.M.C., and Cresti, M. (2011). Distribution of callose synthase, cellulose synthase, and sucrose synthase in tobacco pollen tube is controlled in dissimilar ways by actin filaments and microtubules. Plant Physiol. **155,** 1169-1190.

Campanoni, P., and Blatt, M.R. (2007). Membrane trafficking and polar growth in root hairs and pollen tubes. J. Exp. Bot.**58,** 65-74.

Caño-Delgado, A., Yin, Y., Yu, C., Vafeados, D., Mora-García, S., Cheng, J.-C., Nam, K.H., Li, J., and Chory, J. (2004). BRL1 and BRL3 are novel brassinosteroid receptors that function in vascular differentiation in *Arabidopsis*. Development **131,** 5341-5351.

Capron, A., Gourgues, M., Neiva, L.S., Faure, J.-E., Berger, F., Pagnussat, G., Krishnan, A., Alvarez-Mejia, C., Vielle-Calzada, J.-P., and Lee, Y.-R. (2008). Maternal control of male-gamete delivery in *Arabidopsis* involves a putative GPI-anchored protein encoded by the *LORELEI* gene. Plant Cell **20,** 3038-3049.

Cárdenas, L. (2009). New findings in the mechanisms regulating polar growth in root hair cells. Plant Signal. Behav. **4,** 4-8.

Cárdenas, L., Lovy-Wheeler, A., Kunkel, J.G., and Hepler, P.K. (2008). Pollen tube growth oscillations and intracellular calcium levels are reversibly modulated by actin polymerization. Plant Physiol. **146,** 1611-1621.

Chabaud, M., Genre, A., Sieberer, B.J., Faccio, A., Fournier, J., Novero, M., Barker, D.G., and Bonfante, P. (2011). Arbuscular mycorrhizal hyphopodia and germinated spore exudates trigger Ca^{2+} spiking in the legume and nonlegume root epidermis. New Phytol. **189,** 347-355.

Chae, K., and Lord, E.M. (2011). Pollen tube growth and guidance: roles of small, secreted proteins. Ann. Bot. **108,** 627-636.

Chebli, Y., Kroeger, J., and Geitmann, A. (2013). Transport logistics in pollen tubes. Mol. Plant **6,** 1037-1052.

Chen, D., and Zhao, J. (2008). Free IAA in stigmas and styles during pollen germination and pollen tube growth of *Nicotiana tabacum*. Physiol. Plantarum **134,** 202-215.

Chen, X., and Friml, J. (2014). Rho-GTPase-regulated vesicle trafficking in plant cell polarity. Biochem. Soc. Trans. **42,** 212-218.

Chen, Y.-H., Li, H.-J., Shi, D.-Q., Yuan, L., Liu, J., Sreenivasan, R., Baskar, R., Grossniklaus, U., and Yang, W.-C. (2007). The central cell plays a critical role in pollen tube guidance in *Arabidopsis*. Plant Cell **19,** 3563-3577.

Cheung, A.Y., and Wu, H.-M. (2008). Structural and signaling networks for the polar cell growth machinery in pollen tubes. Annu. Rev. Plant Biol. **59,** 547-572.

Cheung, A.Y., Wang, H., and Wu, H.-M. (1995). A floral transmitting tissue-specific glycoprotein attracts pollen tubes and stimulates their growth. Cell **82,** 383-393.

Cheung, A.Y., Boavida, L.C., Aggarwal, M., Wu, H.-M., and Feijó, J.A. (2010). The pollen tube journey in the pistil and imaging the in vivo process by two-photon microscopy. J. Exp. Bot. **61,** 1907-1915.

Cheung, A.Y., Duan, Q.-H., Costa, S.S., de Graaf, B.H., Di Stilio, V.S., Feijo, J., and Wu, H.-M. (2008). The dynamic pollen tube cytoskeleton: live cell studies using actin-binding and microtubule-binding reporter proteins. Mol. Plant **1,** 686-702.

Choe, S., Dilkes, B.P., Fujioka, S., Takatsuto, S., Sakurai, A., and Feldmann, K.A. (1998). The *DWF4* gene of *Arabidopsis* encodes a Cytochrome P450 that mediates multiple 22α-hydroxylation steps in brassinosteroid biosynthesis. Plant Cell **10,** 231-243.

Chong, Y.T., Gidda, S.K., Sanford, C., Parkinson, J., Mullen, R.T., and Goring, D.R. (2010). Characterization of the *Arabidopsis thaliana* exocyst complex gene families by phylogenetic, expression profiling, and subcellular localization studies. New Phytol. **185,** 401-419.

Clough, S.J., and Bent, A.F. (1998). Floral dip: a simplified method for Agrobacterium-mediated transformation of *Arabidopsis thaliana*. Plant J. **16,** 735-743.

Clouse, S.D. (2011). Brassinosteroids. The *Arabidopsis* book. American Society of Plant Biologists **9,** e0151.

Clouse, S.D., Langford, M., and McMorris, T.C. (1996). A brassinosteroid-insensitive mutant in *Arabidopsis thaliana* exhibits multiple defects in growth and development. Plant Physiol. **111,** 671-678.

Coimbra, S., Costa, M., Jones, B., Mendes, M.A., and Pereira, L.G. (2009). Pollen grain development is compromised in *Arabidopsis agp6 agp11* null mutants. J. Exp. Bot. **60,** 3133-3142.

Cove, D.J. (2000). The generation and modification of cell polarity. J. Exp. Bot. **51,** 831-838.

Craddock, C., Lavagi, I., and Yang, Z. (2012). New insights into Rho signaling from plant ROP/Rac GTPases. Trends Cell Biol. **22,** 492-501.

Crawford, B.C., and Yanofsky, M.F. (2008). The formation and function of the female reproductive tract in flowering plants. Curr. Biol. **18,** 972-978.

Crawford, B.C., and Yanofsky, M.F. (2011). *HALF FILLED* promotes reproductive tract development and fertilization efficiency in *Arabidopsis thaliana*. Development **138,** 2999-3009.

Crawford, B.C., Ditta, G., and Yanofsky, M.F. (2007). The *NTT* gene is required for transmitting-tract development in carpels of *Arabidopsis thaliana*. Curr. Biol. **17,** 1101-1108.

Cresti, M., Pacini, E., Ciampolini, F., and Sarfatti, G. (1977). Germination and early tube development in vitro of *Lycopersicum peruvianum* pollen: ultrastructural features. Planta **136,** 239-247.

Cresti, M., Ciamolini, F., Mulcahy, D.L.M., and Mulcahy, G. (1985). Ultrastructure of *Nicotiana alata* pollen, its germination and early tube formation. Am. J. Bot. **72,** 719-727.

Csikász-Nagy, A., Sato, M., and Carazo Salas, R.E. (2013). Projecting cell polarity into the next decade. Philos. Tr. Soc. Lon. B. **368,** 20130001.

Curtis, M.D., and Grossniklaus, U. (2003). A gateway cloning vector set for high-throughput functional analysis of genes in planta. Plant Physiol. **133,** 462-469.

Cvrčková, F., Grunt, M., Bezvoda, R., Halá, M., Kulich, I., Rawat, A., and Žárský, V. (2012). Evolution of the land plant Exocyst complexes. Front. Plant Sci. **3**.

de Graaf, B.H., Cheung, A.Y., Andreyeva, T., Levasseur, K., Kieliszewski, M., and Wu, H.-M.

(2005). Rab11 GTPase-regulated membrane trafficking is crucial for tip-focused pollen tube growth in tobacco. Plant Cell **17,** 2564-2579.

Denninger, P., Bleckmann, A., Lausser, A., Vogler, F., Ott, T., Ehrhardt, D.W., Frommer, W.B., Sprunck, S., Dresselhaus, T., and Grossmann, G. (2014). Male–female communication triggers calcium signatures during fertilization in *Arabidopsis*. Nat. Commun. **5,** 4645.

Dettmer, J., and Friml, J. (2011). Cell polarity in plants: when two do the same, it is not the same. Curr. Opin. Cell Biol. **23,** 686-696.

Dhonukshe, P., Tanaka, H., Goh, T., Ebine, K., Mähönen, A.P., Prasad, K., Blilou, I., Geldner, N., Xu, J., and Uemura, T. (2008). Generation of cell polarity in plants links endocytosis, auxin distribution and cell fate decisions. Nature **456,** 962-966.

Digonnet, C., Aldon, D., Leduc, N., Dumas, C., and Rougier, M. (1997). First evidence of a calcium transient in flowering plants at fertilization. Development **124,** 2867-2874.

Ding, Y., Robinson, D.G., and Jiang, L. (2014). Unconventional protein secretion (UPS) pathways in plants. Curr. Opin. Cell Biol. **29,** 107-115.

Ding, Y., Wang, J., Chun Lai, J.H., Ling Chan, V.H., Wang, X., Cai, Y., Tan, X., Bao, Y., Xia, J., Robinson, D.G., and Jiang, L. (2014). Exo70E2 is essential for exocyst subunit recruitment and EXPO formation in both plants and animals. Mol. Biol. Cell **25,** 412-426.

Dinkel, H., Van Roey, K., Michael, S., Davey, N.E., Weatheritt, R.J., Born, D., Speck, T., Krüger, D., Grebnev, G., Kubań, M., Strumillo, M., Uyar, B., Budd, A., Altenberg, B., Seiler, M., Chemes, L.B., Glavina, J., Sánchez, I.E., Diella, F., and Gibson, T.J. (2013). The eukaryotic linear motif resource ELM: 10 years and counting. Nucleic Acids Res. 1-8.

Dodd, A.N., Kudla, J., and Sanders, D. (2010). The language of calcium signaling. Annu. Rev. Plant Biol. **61,** 593-620.

Dresselhaus, T., and Franklin-Tong, N. (2013). Male–female crosstalk during pollen germination, tube growth and guidance, and double fertilization. Mol. Plant **6,** 1018-1036.

Drews, G.N., and Yadegari, R. (2002). Development and function of the angiosperm female gametophyte. Annu. Rev. Gen.**36,** 99-124.

Drews, G.N., and Koltunow, A.M. (2011). The female gametophyte. The *Arabidopsis* book/American Society of Plant Biologists **9,** e0155.

Dreze, M., Monachello, D., Lurin, C., Cusick, M.E., Hill, D.E., Vidal, M., and Braun, P. (2010). Chapter 12 - High-Quality Binary Interactome Mapping. In Methods in Enzymology, W. Jonathan, G. Christine, and R.F. Gerald, eds (Academic Press), pp. 281-315.

Duan, Q., Kita, D., Li, C., Cheung, A.Y., and Wu, H.-M. (2010). FERONIA receptor-like kinase regulates RHO GTPase signaling of root hair development. Proc. Natl. Acad. Sci. **107,** 17821-17826.

Duan, Q., Kita, D., Johnson, E.A., Aggarwal, M., Gates, L., Wu, H.-M., and Cheung, A.Y. (2014). Reactive oxygen species mediate pollen tube rupture to release sperm for fertilization in *Arabidopsis*. Nat. Com. **5,** 3129.

Durek, P., Schmidt, R., Heazlewood, J.L., Jones, A., MacLean, D., Nagel, A., Kersten, B., and Schulze, W.X. (2010). PhosPhAt: the *Arabidopsis thaliana* phosphorylation site database. An update. Nucleic Acids Res. **38,** D828-D834.

Dyson, H.J., and Wright, P.E. (2005). Intrinsically unstructured proteins and their functions. Nat. Rev.

Mol. Cell Biol. **6,** 197-208.

Ebnet, K. (2015). Cell Polarity 1: Biological Role and Basic Mechanisms. Springer.

Edgar, R.C. (2004). MUSCLE: multiple sequence alignment with high accuracy and high throughput. Nucleic Acids Res. **32,** 1792-1797.

Edlund, A.F., Swanson, R., and Preuss, D. (2004). Pollen and stigma structure and function: the role of diversity in pollination. Plant Cell **16,** 84-97.

Ehrhardt, D.W., Wais, R., and Long, S.R. (1996). Calcium spiking in plant root hairs responding to Rhizobium nodulation signals. Cell **85,** 673-681.

Endo, S., Shinohara, H., Matsubayashi, Y., and Fukuda, H. (2013). A novel pollen-pistil interaction conferring high-temperature tolerance during reproduction via CLE45 signaling. Curr. Biol. **23,** 1670-1676.

Ephritikhine, G., Fellner, M., Vannini, C., Lapous, D., and Barbier-Brygoo, H. (1999). The *sax1* dwarf mutant of *Arabidopsis thaliana* shows altered sensitivity of growth responses to abscisic acid, auxin, gibberellins and ethylene and is partially rescued by exogenous brassinosteroid. Plant J. **18,** 303-314.

Escobar-Restrepo, J.-M., Huck, N., Kessler, S., Gagliardini, V., Gheyselinck, J., Yang, W.-C., and Grossniklaus, U. (2007). The FERONIA receptor-like kinase mediates male-female interactions during pollen tube reception. Science **317,** 656-660.

Fan, L.M., Wang, Y.F., Wang, H., and Wu, W.H. (2001). In vitro *Arabidopsis* pollen germination and characterization of the inward potassium currents in *Arabidopsis* pollen grain protoplasts. J. Exp. Bot. **52,** 1603-1614.

Faure, J.-E., Digonnet, C., and Dumas, C. (1994). An in vitro system for adhesion and fusion of maize gametes. Science **263,** 1598-1600.

Faure, J.E., Rotman, N., Fortuné, P., and Dumas, C. (2002). Fertilization in *Arabidopsis thaliana* wild type: developmental stages and time course. Plant J. **30,** 481-488.

Feijó, J.A., and Moreno, N. (2004). Imaging plant cells by two-photon excitation. Protoplasma **223,** 1-32.

Fletcher, G.C., Lucas, E.P., Brain, R., Tournier, A., and Thompson, B.J. (2012). Positive feedback and mutual antagonism combine to polarize Crumbs in the *Drosophila* follicle cell epithelium. Curr. Biol. **22,** 1116-1122.

Friedman, W.E. (1998). The evolution of double fertilization and endosperm: an "historical" perspective. Sex. Plant Reprod.**11,** 6-16.

Friedman, W.E. (2001). Comparative embryology of basal angiosperms. Curr. Opin. Plant Biol. **4,** 14-20.

Friedrichsen, D.M., Nemhauser, J., Muramitsu, T., Maloof, J.N., Alonso, J., Ecker, J.R., Furuya, M., and Chory, J. (2002). Three redundant brassinosteroid early response genes encode putative bHLH transcription factors required for normal growth. Genetics **162,** 1445-1456.

Friml, J., Vieten, A., Sauer, M., Weijers, D., Schwarz, H., Hamann, T., Offringa, R., and Jürgens, G. (2003). Efflux-dependent auxin gradients establish the apical–basal axis of *Arabidopsis*. Nature **426,** 147-153.

Fujioka, S., and Sakurai, A. (1997). Brassinosteroids. Nat. Prod. Rep. **14,** 1-10.

Fujioka, S., and Yokota, T. (2003). Biosynthesis and metabolism of brassinosteroids. Annu. Rev. Plant Biol. **54,** 137-164.

Galway, M.E., Heckman, J.W., Jr., and Schiefelbein, J.W. (1997). Growth and ultrastructure of *Arabidopsis* root hairs: the *rhd3* mutation alters vacuole enlargement and tip growth. Planta **201,** 209-218.

Ganguly, A., Sasayama, D., and Cho, H.T. (2012). Regulation of the polarity of protein trafficking by phosphorylation. Mol. Cells **33,** 423-430.

Garaschuk, O., Griesbeck, O., and Konnerth, A. (2007). Troponin C-based biosensors: a new family of genetically encoded indicators for in vivo calcium imaging in the nervous system. Cell Calcium **42,** 351-361.

Gebert, M., Dresselhaus, T., and Sprunck, S. (2008). F-Actin organization and pollen tube tip growth in *Arabidopsis* are dependent on the gametophyte-specific Armadillo Repeat Protein ARO1. Plant Cell **20,** 2798-2814.

Geitmann, A. (2010). How to shape a cylinder: pollen tube as a model system for the generation of complex cellular geometry. Sex. Plant Reprod. **23,** 63-71.

Geitmann, A., and Ortega, J.K. (2009). Mechanics and modeling of plant cell growth. Trends Plant Sci. **14,** 467-478.

Geldner, N. (2009). Cell polarity in plants - A PARspective on PINs. Curr. Opin. Plant Biol. **12,** 42-48.

Gervais, C., Simmonds, D.H., and Newcomb, W. (1994). Actin microfilament organization during pollen development of *Brassica napus* cv. Topas. Protoplasma **183,** 67-76.

Gilkey, J.C., Jaffe, L.F., Ridgway, E.B., and Reynolds, G.T. (1978). A free calcium wave traverses the activating egg of the medaka, *Oryzias latipes*. J. Cell Biol.**76,** 448-466.

Goehring, N.W., Trong, P.K., Bois, J.S., Chowdhury, D., Nicola, E.M., Hyman, A.A., and Grill, S.W. (2011). Polarization of PAR proteins by advective triggering of a pattern-forming system. Science **334,** 1137-1141.

Goldman, M., Goldberg, R., and Mariani, C. (1994). Female sterile tobacco plants are produced by stigma-specific cell ablation. EMBO J. **13,** 2976.

Gouy, M., Guindon, S., and Gascuel, O. (2010). SeaView version 4: a multiplatform graphical user interface for sequence alignment and phylogenetic tree building. Mol. Bio. Evol. **27,** 221-224.

Grierson, C., Nielsen, E., Ketelaar, T., and Schiefelbein, J. (2014). Root hairs. The *Arabidopsis* book/American Society of Plant Biologists **12,** e0172.

Groß-Hardt, R., Kägi, C., Baumann, N., Moore, J.M., Baskar, R., Gagliano, W.B., Jürgens, G., and Grossniklaus, U. (2007). *LACHESIS* restricts gametic cell fate in the female gametophyte of *Arabidopsis*. PLoS Biol. **5,** e47.

Grossmann, G., Guo, W.-J., Ehrhardt, D.W., Frommer, W.B., Sit, R.V., Quake, S.R., and Meier, M. (2011). The RootChip: an integrated microfluidic chip for plant science. Plant Cell **23,** 4234-4240.

Grossmann, G., Meier, M., Cartwright, H.N., Sosso, D., Quake, S.R., Ehrhardt, D.W., and Frommer, W.B. (2012). Time-lapse fluorescence imaging of *Arabidopsis* root growth with rapid manipulation of the root environment using the RootChip. J. Vis. Exp. **65**, 4290.

Grote, E. (2010). Secretion is required for late events in the cell-fusion pathway of mating yeast. J. Cell Sci. **123,** 1902-1912.

Grove, M.D., Spencer, G.F., Rohwedder, W.K., Mandava, N., Worley, J.F., Warthen, J.D., Steffens, G.L., Flippen-Anderson, J.L., and Cook, J.C. (1979). Brassinolide, a plant growth-promoting steroid isolated from *Brassica napus* pollen. Nature **281,** 216-217.

Gu, T., Mazzurco, M., Sulaman, W., Matias, D.D., and Goring, D.R. (1998). Binding of an ARM repeat protein to the kinase domain of the S-locus receptor kinase. Proc. Natl. Acad. Sci. **95,** 382-387.

Gu, Y., Fu, Y., Dowd, P., Li, S., Vernoud, V., Gilroy, S., and Yang, Z. (2005). A Rho family GTPase controls actin dynamics and tip growth via two counteracting downstream pathways in pollen tubes. J. Cell Biol.**169,** 127-138.

Guan, Y., Guo, J., Li, H., and Yang, Z. (2013). Signaling in pollen tube growth: crosstalk, feedback, and missing links. Mol. Plant **6,** 1053-1064.

Guan, Y., Lu, J., Xu, J., McClure, B., and Zhang, S. (2014). Two mitogen-activated protein kinases, MPK3 and MPK6, are required for funicular guidance of pollen tubes in *Arabidopsis*. Plant Physiol. **165,** 528-533.

Guignard, M. (1899). Sur les antherozoides et la double copulation sexuelle chez les vegetaux angiosperms. Rev. Gén. Bot. **11,** 129-135.

Haecker, A., Groß-Hardt, R., Geiges, B., Sarkar, A., Breuninger, H., Herrmann, M., and Laux, T. (2004). Expression dynamics of *WOX* genes mark cell fate decisions during early embryonic patterning in *Arabidopsis thaliana*. Development **131,** 657-668.

Hall, A. (2012). Rho family GTPases. Biochem. Soc. Trans. **40,** 1378.

Hamamura, Y., Nagahara, S., and Higashiyama, T. (2012). Double fertilization on the move. Curr. Opin. Plant Biol. **15,** 70-77.

Hamamura, Y., Nishimaki, M., Takeuchi, H., Geitmann, A., Kurihara, D., and Higashiyama, T. (2014). Live imaging of calcium spikes during double fertilization in *Arabidopsis*. Nat. Commun. **5,** 4722.

Hamamura, Y., Saito, C., Awai, C., Kurihara, D., Miyawaki, A., Nakagawa, T., Kanaoka, M.M., Sasaki, N., Nakano, A., and Berger, F. (2011). Live-cell imaging reveals the dynamics of two sperm cells during double fertilization in *Arabidopsis thaliana*. Curr. Biol. **21,** 497-502.

Haruta, M., Sabat, G., Stecker, K., Minkoff, B.B., and Sussman, M.R. (2014). A peptide hormone and its receptor protein kinase regulate plant cell expansion. Science **343,** 408-411.

Haseloff, J., Siemering, K.R., Prasher, D.C., and Hodge, S. (1997). Removal of a cryptic intron and subcellular localization of green fluorescent protein are required to mark transgenic *Arabidopsis* plants brightly. Proc. Natl. Acad. Sci. **94,** 2122-2127.

Hause, G., Hause, B., and Lammeren, A.V. (1992). Microtubular and actin filament configurations during microspore and pollen development in *Brassica napus* cv. Topas. Can. J. Bot. **70,** 1369-1376.

Heider, M.R., and Munson, M. (2012). Exorcising the exocyst complex. Traffic **13,** 898-907.

Heim, N., and Griesbeck, O. (2004). Genetically encoded indicators of cellular calcium dynamics based on troponin C and green fluorescent protein. J. Biol. Chem. **279,** 14280-14286.

Heim, N., Garaschuk, O., Friedrich, M.W., Mank, M., Milos, R.I., Kovalchuk, Y., Konnerth, A., and Griesbeck, O. (2007). Improved calcium imaging in transgenic mice expressing a troponin C–based biosensor. Nat. Methods **4,** 127-129.

Hepler, P.K., and Winship, L.J. (2015). The pollen tube clear zone: clues to the mechanism of polarized growth. J. Integr. Plant Biol. **57,** 79-92.

Hepler, P.K., Vidali, L., and Cheung, A.Y. (2001). Polarized cell growth in higher plants. Annu. Rev. Cell Dev. Bi. **17,** 159-187.

Heslop-Harrison, Y., and Heslop-Harrison, J. (1992). Germination of monocolpate angiosperm pollen: evolution of the actin cytoskeleton and wall during hydration, activation and tube emergence. Ann. Bot. **69,** 385-394.

Hewitt, F.R., Hough, T., O'Neill, P., Sasse, J.M., Williams, E.G., and Rowan, K.S. (1985). Effect of brassinolide and other growth regulators on the germination and growth of pollen tubes of *Prunus avium* using a multiple hanging-drop assay. Aust. J. Plant Physiol. **12,** 201-211.

Higashiyama, T. (2010). Peptide signaling in pollen-pistil interactions. Plant Cell Physiol. **51,** 177-189.

Higashiyama, T., and Takeuchi, H. (2015). The mechanism and key molecules involved in pollen tube guidance. Annu. Rev. Plant Biol. **66,** 393-413

Higashiyama, T., Kuroiwa, H., Kawano, S., and Kuroiwa, T. (1998). Guidance in vitro of the pollen tube to the naked embryo sac of *Torenia fournieri*. Plant Cell **10,** 2019-2031.

Hirohashi, N., Kamei, N., Kubo, H., Sawada, H., Matsumoto, M., and Hoshi, M. (2008). Egg and sperm recognition systems during fertilization. Dev. Growth Differ. **50,** 221-238.

Hoedemaekers, K., Derksen, J., Hoogstrate, S.W., Wolters-Arts, M., Oh, S.-A., Twell, D., Mariani, C., and Rieu, I. (2014). BURSTING POLLEN is required to organize the pollen germination plaque and pollen tube tip in *Arabidopsis thaliana*. New Phytol. **206**, 255-267.

Hofer, R.M. (1991). Root hairs. In: Plant roots: the hidden half, Y. Waisel, A. Eshel, and U. Kafkafi, eds, pp. 129-148. CRC press.

Holdaway-Clarke, T.L., Feijo, J.A., Hackett, G.R., Kunkel, J.G., and Hepler, P.K. (1997). Pollen tube growth and the intracellular cytosolic calcium gradient oscillate in phase while extracellular calcium influx is delayed. Plant Cell **9,** 1999-2010.

Howell, A.S., and Lew, D.J. (2012). Morphogenesis and the cell cycle. Genetics **190,** 51-77.

Hu, Y., Zhong, R., Morrison Iii, W.H., and Ye, Z.-H. (2003). The *Arabidopsis RHD3* gene is required for cell wall biosynthesis and actin organization. Planta **217,** 912-921.

Huang, H.Y., Jiang, W.B., Hu, Y.W., Wu, P., Zhu, J.Y., Liang, W.Q., Wang, Z.Y., and Lin, W.H. (2012). BR signal influences *Arabidopsis* ovule and seed number through regulating related genes expression by *BZR1*. Mol. Plant **6,** 456-469.

Huck, N., Moore, J.M., Federer, M., and Grossniklaus, U. (2003). The *Arabidopsis* mutant *feronia* disrupts the female gametophytic control of pollen tube reception. Development **130,** 2149-2159.

Hughes, H., Lisher, J.P., Hardy, G.G., Kysela, D.T., Arnold, R.J., Giedroc, D.P., and Brun, Y.V. (2013). Co-ordinate synthesis and protein localization in a bacterial organelle by the action of a penicillin-binding-protein. Mol. Microbiol. **90,** 1162-1177.

Hulskamp, M., Schneitz, K., and Pruitt, R.E. (1995). Genetic evidence for a long-range activity that directs pollen tube guidance in *Arabidopsis*. Plant Cell **7,** 57-64.

Hwang, J.-U., Vernoud, V., Szumlanski, A., Nielsen, E., and Yang, Z. (2008). A tip-localized RhoGAP controls cell polarity by globally inhibiting Rho GTPase at the cell apex. Curr. Biol. **18,** 1907-1916.

Iakoucheva, L.M., Radivojac, P., Brown, C.J., O'Connor, T.R., Sikes, J.G., Obradovic, Z., and Dunker, A.K. (2004). The importance of intrinsic disorder for protein phosphorylation. Nucleic Acids Res. **32,** 1037-1049.

Ichikawa, M., Hirano, T., Enami, K., Fuselier, T., Kato, N., Kwon, C., Voigt, B., Schulze-Lefert, P., Baluška, F., and Sato, M.H. (2014). Syntaxin of plant proteins SYP123 and SYP132 mediate root hair tip growth in *Arabidopsis thaliana*. Plant Cell Physiol. **55,** 790-800.

Ingouff, M., Hamamura, Y., Gourgues, M., Higashiyama, T., and Berger, F. (2007). Distinct dynamics of HISTONE3 variants between the two fertilization products in plants. Curr. Biol. **17,** 1032-1037.

Inoue, N., Ikawa, M., and Okabe, M. (2011). The mechanism of sperm-egg interaction and the involvement of IZUMO1 in fusion. Asian J. Androl. **13,** 81-87.

Inoue, N., Ikawa, M., Isotani, A., and Okabe, M. (2005). The immunoglobulin superfamily protein Izumo is required for sperm to fuse with eggs. Nature **434,** 234-238.

Ischebeck, T., Stenzel, I., and Heilmann, I. (2008). Type B Phosphatidylinositol-4-Phosphate 5-Kinases mediate *Arabidopsis* and *Nicotiana tabacum* pollen tube growth by regulating apical pectin secretion. Plant Cell **20,** 3312-3330.

Ishida, T., Kurata, T., Okada, K., and Wada, T. (2008). A genetic regulatory network in the development of trichomes and root hairs. Annu. Rev. Plant Biol. **59,** 365-386.

Iwano, M., Shiba, H., Miwa, T., Che, F.-S., Takayama, S., Nagai, T., Miyawaki, A., and Isogai, A. (2004). Ca^{2+} dynamics in a pollen grain and papilla cell during pollination of *Arabidopsis*. Plant Physiol. **136,** 3562-3571.

Iwano, M., Shiba, H., Miwa, T., Che, F.-S., Takayama, S., Nagai, T., Miyawaki, A., and Isogai, A. (2004). Ca^{2+} dynamics in a pollen grain and papilla cell during pollination of *Arabidopsis*. Plant Physiol. **136,** 3562-3571.

Iwano, M., Ngo, Q.A., Entani, T., Shiba, H., Nagai, T., Miyawaki, A., Isogai, A., Grossniklaus, U., and Takayama, S. (2012). Cytoplasmic Ca^{2+} changes dynamically during the interaction of the pollen tube with synergid cells. Development **139,** 4202-4209.

Iwano, M., Igarashi, M., Tarutani, Y., Kaothien-Nakayama, P., Nakayama, H., Moriyama, H., Yakabe, R., Entani, T., Shimosato-Asano, H., Ueki, M., Tamiya, G., and Takayama, S. (2014). A pollen coat-inducible autoinhibited Ca^{2+}-ATPase expressed in stigmatic papilla cells is required for compatible pollination in the Brassicaceae. Plant Cell **26,** 636-649.

Iwao, Y. (2012). Egg activation in physiological polyspermy. Reproduction **144,** 11-22.

Johnson, M.A., and Preuss, D. (2002). Plotting a course: multiple signals guide pollen tubes to their targets. Dev. Cell **2,** 273-281.

Johnson, C.S., Kolevski, B., and Smyth, D.R. (2002). *TRANSPARENT TESTA GLABRA2*, a trichome and seed coat development gene of *Arabidopsis*, encodes a WRKY transcription factor. Plant Cell **14,** 1359-1375.

Johnson, J.M., Jin, M., and Lew, D.J. (2011). Symmetry breaking and the establishment of cell polarity in budding yeast. Curr. Opin. Gen. Dev. **21,** 740-746.

Johnson, M.A., von Besser, K., Zhou, Q., Smith, E., Aux, G., Patton, D., Levin, J.Z., and Preuss, D. (2004). *Arabidopsis hapless* mutations define essential gametophytic functions. Genetics **168,** 971-982.

Johnson-Brousseau, S.A., and McCormick, S. (2004). A compendium of methods useful for characterizing *Arabidopsis* pollen mutants and gametophytically-expressed genes. Plant J. **39,** 761-775.

Jones, M.A., Shen, J.-J., Fu, Y., Li, H., Yang, Z., and Grierson, C.S. (2002). The *Arabidopsis* Rop2 GTPase is a positive regulator of both root hair initiation and tip growth. Plant Cell **14,** 763-776.

Kaestner, L. (2012). Calcium signalling: approaches and findings in the heart and blood. (Springer Science & Business Media).

Kang, B.-H., Nielsen, E., Preuss, M.L., Mastronarde, D., and Staehelin, L.A. (2011). Electron tomography of RabA4b- and PI-4Kβ1-labeled Trans Golgi Network compartments in *Arabidopsis*. Traffic **12,** 313-329.

Karimi, M., Inzé, D., and Depicker, A. (2002). GATEWAY™ vectors for Agrobacterium-mediated plant transformation. Trends Plant Sci. **7,** 193-195.

Karimi, M., Depicker, A., and Hilson, P. (2007). Recombinational cloning with plant gateway vectors. Plant Physiol. **145,** 1144-1154.

Kasahara, R.D., Portereiko, M.F., Sandaklie-Nikolova, L., Rabiger, D.S., and Drews, G.N. (2005). *MYB98* is required for pollen tube guidance and synergid cell differentiation in *Arabidopsis*. Plant Cell **17,** 2981-2992.

Kasahara, R.D., Maruyama, D., Hamamura, Y., Sakakibara, T., Twell, D., and Higashiyama, T. (2012). Fertilization recovery after defective sperm cell release in *Arabidopsis*. Curr. Biol. **22,** 1084-1089.

Kawashima, T., and Berger, F. (2011). Green love talks; cell-cell communication during double fertilization in flowering plants. AoB Plants **2011,** plr015.

Keilberg, D., and Søgaard-Andersen, L. (2014). Regulation of bacterial cell polarity by small GTPases. Biochemistry **53,** 1899-1907.

Kessler, S.A., and Grossniklaus, U. (2011). She's the boss: signaling in pollen tube reception. Curr. Opin. Plant Biol. **14,** 622-627.

Kessler, S.A., Shimosato-Asano, H., Keinath, N.F., Wuest, S.E., Ingram, G., Panstruga, R., and Grossniklaus, U. (2010). Conserved molecular components for pollen tube reception and fungal invasion. Science **330,** 968-971.

Ketelaar, T. (2013). The actin cytoskeleton in root hairs: all is fine at the tip. Curr. Opin. Plant Biol. **16,** 749-756.

Ketelaar, T., Galway, M.E., Mulder, B.M., and Emons, A.M.C. (2008). Rates of exocytosis and endocytosis in *Arabidopsis* root hairs and pollen tubes. J. Microsc. **231,** 265-273.

Kiegle, E., Moore, C.A., Haseloff, J., Tester, M.A., and Knight, M.R. (2000). Cell-type-specific calcium responses to drought, salt and cold in the *Arabidopsis* root. Plant J. **23,** 267-278.

Kim, S., Mollet, J.-C., Dong, J., Zhang, K., Park, S.-Y., and Lord, E.M. (2003). Chemocyanin, a small basic protein from the lily stigma, induces pollen tube chemotropism. Proc. Natl. Acad. Sci. **100,** 16125-16130.

Kim, T.-W., Hwang, J.-Y., Kim, Y.-S., Joo, S.-H., Chang, S.C., Lee, J.S., Takatsuto, S., and Kim, S.-K. (2005). *Arabidopsis* CYP85A2, a cytochrome P450, mediates the Baeyer-Villiger oxidation of castasterone to brassinolide in brassinosteroid biosynthesis. Plant Cell **17,** 2397-2412.

Kirik, V., Lee, M.M., Wester, K., Herrmann, U., Zheng, Z., Oppenheimer, D., Schiefelbein, J., and Hulskamp, M. (2005). Functional diversification of *MYB23* and *GL1* genes in trichome

morphogenesis and initiation. Development **132,** 1477-1485.

Kleine-Vehn, J., and Friml, J. (2008). Polar targeting and endocytic recycling in auxin-dependent plant development. Annu. Rev. Cell Dev. Bi. **24,** 447-473.

Köhler, C., Hennig, L., Bouveret, R., Gheyselinck, J., Grossniklaus, U., and Gruissem, W. (2003). *Arabidopsis* MSI1 is a component of the MEA/FIE Polycomb group complex and required for seed development. EMBO J. **22,** 4804-4814.

Konrad, S.S., Popp, C., Stratil, T.F., Jarsch, I.K., Thallmair, V., Folgmann, J., Marín, M., and Ott, T. (2014). S-acylation anchors remorin proteins to the plasma membrane but does not primarily determine their localization in membrane microdomains. New Phytol. **203,** 758-769.

Kost, B. (2008). Spatial control of Rho (Rac-Rop) signaling in tip-growing plant cells. Trends Cell Biol. **18,** 119-127.

Kosuta, S., Hazledine, S., Sun, J., Miwa, H., Morris, R.J., Downie, J.A., and Oldroyd, G.E. (2008). Differential and chaotic calcium signatures in the symbiosis signaling pathway of legumes. Proc. Natl. Acad. Sci. **105,** 9823-9828.

Kozubowski, L., Saito, K., Johnson, J.M., Howell, A.S., Zyla, T.R., and Lew, D.J. (2008). Symmetry-breaking polarization driven by a Cdc42p GEF-PAK complex. Curr. Biol. **18,** 1719-1726.

Kranz, E., Wiegen, P., and Lörz, H. (1995). Early cytological events after induction of cell division in egg cells and zygote development following in vitro fertilization with angiosperm gametes. Plant J. **8,** 9-23.

Krebs, M., Held, K., Binder, A., Hashimoto, K., Den Herder, G., Parniske, M., Kudla, J., and Schumacher, K. (2012). FRET-based genetically encoded sensors allow high-resolution live cell imaging of Ca^{2+} dynamics. Plant J. **69,** 181-192.

Krichevsky, A., Kozlovsky, S.V., Tian, G.W., Chen, M.H., Zaltsman, A., and Citovsky, V. (2007). How pollen tubes grow. Dev. Biol. **303,** 405-420.

Kühn, J., Briegel, A., Mörschel, E., Kahnt, J., Leser, K., Wick, S., Jensen, G.J., and Thanbichler, M. (2010). Bactofilins, a ubiquitous class of cytoskeletal proteins mediating polar localization of a cell wall synthase in *Caulobacter crescentus*. EMBO J. **29,** 327-339.

Kulich, I., Vojtíková, Z., Glanc, M., Ortmannová, J., Rasmann, S., and Žárský, V. (2015). Cell wall maturation of *Arabidopsis* trichomes is dependent on exocyst Subunit EXO70H4 and involves callose deposition. Plant Physiol., pp. 00112.02015.

Kwon, M., and Choe, S. (2005). Brassinosteroid biosynthesis and dwarf mutants. J. Plant Biol. **48,** 1-15.

Lai, Y.-S., Stefano, G., and Brandizzi, F. (2014). ER stress signaling requires RHD3, a functionally conserved ER-shaping GTPase. J. Cell Sci. **127,** 3227-3232.

Lalanne, E., and Twell, D. (2002). Genetic control of male germ unit organization in *Arabidopsis*. Plant Physiol. **129,** 865-875.

Lalanne, E., Michaelidis, C., Moore, J.M., Gagliano, W., Johnson, A., Patel, R., Howden, R., Vielle-Calzada, J.P., Grossniklaus, U., and Twell, D. (2004). Analysis of transposon insertion mutants highlights the diversity of mechanisms underlying male progamic development in *Arabidopsis*. Genetics **167,** 1975-1986.

Lau, S., Slane, D., Herud, O., Kong, J., and Jürgens, G. (2012). Early embryogenesis in flowering plants: setting up the basic body pattern. Annu. Rev. Plant Biol. **63,** 483-506.

Lee, Y.J., and Yang, Z. (2008). Tip growth: signaling in the apical dome. Curr. Opin. Plant Biol. **11,**

662-671.

Lee, Y.J., Szumlanski, A., Nielsen, E., and Yang, Z. (2008). Rho-GTPase–dependent filamentous actin dynamics coordinate vesicle targeting and exocytosis during tip growth. J. Cell Biol. **181,** 1155-1168.

Lennon, K.A., Roy, S., Hepler, P.K., and Lord, E.M. (1998). The structure of the transmitting tissue of *Arabidopsis thaliana* (L.) and the path of pollen tube growth. Sex. Plant Reprod. **11,** 49-59.

Leonardy, S., Bulyha, I., and Søgaard-Andersen, L. (2008). Reversing cells and oscillating motility proteins. Mol. Biosyst. **4,** 1009-1014.

Leshem, Y., Johnson, C., and Sundaresan, V. (2013). Pollen tube entry into the synergid cell of *Arabidopsis* is observed at a site distinct from the filiform apparatus. Plant Reprod. **26,** 93-99.

Leydon, A.R., Chaibang, A., and Johnson, M. (2014). Interactions between pollen tube and pistil control pollen tube identity and sperm release in the *Arabidopsis* female gametophyte. Biochem. Soc. Trans. **42,** 340-345.

Leydon, A.R., Beale, K.M., Woroniecka, K., Castner, E., Chen, J., Horgan, C., Palanivelu, R., and Johnson, M.A. (2013). Three MYB transcription factors control pollen tube differentiation required for sperm release. Curr. Biol. **23,** 1209-1214.

Li, H., Lin, Y., Heath, R.M., Zhu, M.X., and Yang, Z. (1999). Control of pollen tube tip growth by a Rop GTPase–dependent pathway that leads to tip-localized calcium influx. Plant Cell **11,** 1731-1742.

Li, S., Gu, Y., Yan, A., Lord, E., and Yang, Z.-B. (2008). RIP1 (ROP Interactive Partner 1)/ICR1 marks pollen germination sites and may act in the ROP1 pathway in the control of polarized pollen growth. Mol. Plant **1,** 1021-1035.

Li, S., van Os, G.M., Ren, S., Yu, D., Ketelaar, T., Emons, A.M.C., and Liu, C.-M. (2010). Expression and functional analyses of *EXO70* genes in *Arabidopsis* implicate their roles in regulating cell type-specific exocytosis. Plant Physiol. **154,** 1819-1830.

Li, H.J., Xue, Y., Jia, D.J., Wang, T., Hi, D.Q., Liu, J., Cui, F., Xie, Q., Ye, D., and Yang, W.C. (2011). *POD1* regulates pollen tube guidance in response to micropylar female signaling and acts in early embryo patterning in *Arabidopsis*. Plant Cell **23,** 3288-3302.

Li, S., Ge, F.R., Xu, M., Zhao, X.Y., Huang, G.Q., Zhou, L.Z., Wang, J.G., Kombrink, A., McCormick, S., Zhang, X.S., and Zhang, Y. (2013). *Arabidopsis* COBRA-LIKE 10, a GPI-anchored protein, mediates directional growth of pollen tubes. Plant J. **74,** 486-497.

Liang, G., He, H., Li, Y., Ai, Q., and Yu, D. (2014). *MYB82* functions in regulation of trichome development in *Arabidopsis*. J. Exp. Bot. **65,** 3215-3223.

Liang, Y., Tan, Z.M., Zhu, L., Niu, Q.K., Zhou, J.J., Li, M., Chen, L.Q., Zhang, X.Q., and Ye, D. (2013). MYB97, MYB101 and MYB120 function as male factors that control pollen tube-synergid interaction in *Arabidopsis thaliana* fertilization. PLoS Genet. **9,** e1003933.

Liu, Y., Tewari, R., Ning, J., Blagborough, A.M., Garbom, S., Pei, J., Grishin, N.V., Steele, R.E., Sinden, R.E., and Snell, W.J. (2008). The conserved plant sterility gene *HAP2* functions after attachment of fusogenic membranes in *Chlamydomonas* and *Plasmodium* gametes. Genes Dev. **22,** 1051-1068.

Liu, J., Zhong, S., Guo, X., Hao, L., Wei, X., Huang, Q., Hou, Y., Shi, J., Wang, C., Gu, H., and Qu, L.J. (2013). Membrane-bound RLCKs LIP1 and LIP2 are essential male factors controlling male-female attraction in *Arabidopsis*. Curr. Biol. **23,** 993-998.

Livak, K.J., and Schmittgen, T.D. (2001). Analysis of relative gene expression data using real-time quantitative PCR and the 2– ΔΔCT method. Methods **25,** 402-408.

Loeb, J. (1906). The dynamics of living matter. Columbia University Press.

Lord, E.M., and Russell, S.D. (2002). The mechanisms of pollination and fertilization in plants. Annu. Rev. Cell Dev. Bi. **18,** 81-105.

Lu, Y., Chanroj, S., Zulkifli, L., Johnson, M.A., Uozumi, N., Cheung, A., and Sze, H. (2011). Pollen tubes lacking a pair of K^+ transporters fail to target ovules in *Arabidopsis*. Plant Cell **23,** 81-93.

Lukowitz, W., Roeder, A., Parmenter, D., and Somerville, C. (2004). A *MAPKK* kinase gene regulates extra-embryonic cell fate in *Arabidopsis*. Cell **116,** 109-119.

Ma, W., and Berkowitz, G.A. (2007). The grateful dead: calcium and cell death in plant innate immunity. Cell. Microbiol. **9,** 2571-2585.

Macara, I.G., and McCaffrey, L. (2013). Cell polarity in morphogenesis and metastasis. Philos. Tr. Soc. Lon. B. **368,** 20130012.

Mandava, N.B. (1988). Plant growth-promoting brassinosteroids. Annu. Rev. Plant Phys. **39,** 23-52.

Marks, M.D. (1997). Molecular genetic analysis of trichome development in *Arabidopsis*. Annu. Rev. Plant Biol. **48,** 137-163.

Márton, M.L., Cordts, S., Broadhvest, J., and Dresselhaus, T. (2005). Micropylar pollen tube guidance by Egg Apparatus 1 of maize. Science **307,** 573-576.

Márton, M.L., Fastner, A., Uebler, S., and Dresselhaus, T. (2012). Overcoming hybridization barriers by the secretion of the maize pollen tube attractant ZmEA1 from *Arabidopsis* ovules. Curr. Biol. **22,** 1194-1198.

Mascarenhas, J.P. (1993). Molecular mechanisms of pollen tube growth and differentiation. Plant Cell **5,** 1303-1314.

Masucci, J.D., and Schiefelbein, J.W. (1994). The *rhd6* mutation of *Arabidopsis thaliana* alters root-hair initiation through an auxin-and ethylene-associated process. Plant Physiol. **106,** 1335-1346.

Mathur, J., Molnár, G., Fujioka, S., Takatsuto, S., Sakurai, A., Yokota, T., Adam, G., Voigt, B., Nagy, F., Maas, C., Schell, J., Koncz, C., and Szekeres, M. (1998). Transcription of the *Arabidopsis CPD* gene, encoding a steroidogenic cytochrome P450, is negatively controlled by brassinosteroids. Plant J. **14,** 593-602.

Mauriello, E.M., Mouhamar, F., Nan, B., Ducret, A., Dai, D., Zusman, D.R., and Mignot, T. (2010). Bacterial motility complexes require the actin-like protein, MreB and the Ras homologue, MglA. EMBO J. **29,** 315-326.

McCaffrey, L.M., and Macara, I.G. (2012). Signaling pathways in cell polarity. Cold Spring Harb. Perspect. Biol. **4**, a009654.

McCormick, S. (2004). Control of male gametophyte development. Plant Cell **16,** 142-153.

McCue, A.D., Cresti, M., Feijó, J.A., and Slotkin, R.K. (2011). Cytoplasmic connection of sperm cells to the pollen vegetative cell nucleus: potential roles of the male germ unit revisited. J. Exp. Bot. **62,** 1621-1631.

Meyer, T., and Stryer, L. (1988). Molecular model for receptor-stimulated calcium spiking. Proc. Natl. Acad. Sci. **85,** 5051-5055.

Miao, Y.-L., Stein, P., Jefferson, W.N., Padilla-Banks, E., and Williams, C.J. (2012). Calcium in-

flux-mediated signaling is required for complete mouse egg activation. Proc. Natl. Acad. Sci. **109,** 4169-4174.

Michard, E., Lima, P.T., Borges, F., Silva, A.C., Portes, M.T., Carvalho, J.E., Gilliham, M., Liu, L.-H., Obermeyer, G., and Feijó, J.A. (2011). Glutamate receptor–like genes form Ca^{2+} channels in pollen tubes and are regulated by pistil D-serine. Science **332,** 434-437.

Miller, Deborah D., De Ruijter, Norbert C.A., Bisseling, T., and Emons, Anne mie C. (1999). The role of actin in root hair morphogenesis: studies with lipochito-oligosaccharide as a growth stimulator and cytochalasin as an actin perturbing drug. Plant J. **17,** 141-154.

Misamore, M.J., Gupta, S., and Snell, W.J. (2003). The *Chlamydomonas* Fus1 protein is present on the mating type plus fusion organelle and required for a critical membrane adhesion event during fusion with minus gametes. Mol. Biol. Cell **14,** 2530-2542.

Miyawaki, A., Llopis, J., Heim, R., McCaffery, J.M., Adams, J.A., Ikura, M., and Tsien, R.Y. (1997). Fluorescent indicators for Ca^{2+} based on green fluorescent proteins and calmodulin. Nature **388,** 882-887.

Miyazaki, S., Murata, T., Sakurai-Ozato, N., Kubo, M., Demura, T., Fukuda, H., and Hasebe, M. (2009). *ANXUR1* and *2*, sister genes to *FERONIA/SIRENE*, are male factors for coordinated fertilization. Curr. Biol. **19,** 1327-1331.

Mo, Y., Nagel, C., and Taylor, L.P. (1992). Biochemical complementation of chalcone synthase mutants defines a role for flavonols in functional pollen. Proc. Natl. Acad. Sci. **89,** 7213-7217.

Moll, C., Von Lyncker, L., Zimmermann, S., Kägi, C., Baumann, N., Twell, D., Grossniklaus, U., and Groß-Hardt, R. (2008). *CLO/GFA1* and *ATO* are novel regulators of gametic cell fate in plants. Plant J. **56,** 913-921.

Monshausen, G.B., Messerli, M.A., and Gilroy, S. (2008). Imaging of the Yellow Cameleon 3.6 indicator reveals that elevations in cytosolic Ca^{2+} follow oscillating increases in growth in root hairs of *Arabidopsis*. Plant Physiol. **147,** 1690-1698.

Monshausen, G.B., Bibikova, T.N., Weisenseel, M.H., and Gilroy, S. (2009). Ca^{2+} regulates reactive oxygen species production and pH during mechanosensing in *Arabidopsis* roots. Plant Cell **21,** 2341-2356.

Morgan, T.H. (1905). "Polarity" considered as a phenomenon of gradation of materials. J. Exp. Zool. **2,** 495-506.

Mori, T., Kuroiwa, H., Higashiyama, T., and Kuroiwa, T. (2006). GENERATIVE CELL SPECIFIC 1 is essential for angiosperm fertilization. Nature Cell Biol. **8,** 64-71.

Mori, T., Igawa, T., Tamiya, G., Miyagishima, S.-y., and Berger, F. (2014). Gamete attachment requires GEX2 for successful fertilization in *Arabidopsis*. Curr. Biol. **24,** 170-175.

Mouline, K., Very, A.A., Gaymard, F., Boucherez, J., Pilot, G., Devic, M., Bouchez, D., Thibaud, J.B., and Sentenac, H. (2002). Pollen tube development and competitive ability are impaired by disruption of a Shaker K^+ channel in *Arabidopsis*. Genes Dev. **16,** 339-350.

Mukhtar, M.S., Carvunis, A.-R., Dreze, M., Epple, P., Steinbrenner, J., Moore, J., Tasan, M., Galli, M., Hao, T., and Nishimura, M.T. (2011). Independently evolved virulence effectors converge onto hubs in a plant immune system network. Science **333,** 596-601.

Müller, M., and Schmidt, W. (2004). Environmentally induced plasticity of root hair development in *Arabidopsis*. Plant Physiol. **134,** 409-419.

Murashige, T., and Skoog, F. (1962). A revised medium for rapid growth and bio assays with tobacco tissue cultures. Physiol. Plantarum **15,** 473-497.

Müssig, C., Shin, G.-H., and Altmann, T. (2003). Brassinosteroids promote root growth in *Arabidopsis*. Plant Physiol. **133,** 1261-1271.

Nagai, T., Yamada, S., Tominaga, T., Ichikawa, M., and Miyawaki, A. (2004). Expanded dynamic range of fluorescent indicators for Ca^{2+} by circularly permuted yellow fluorescent proteins. Proc. Natl. Acad. Sci. **101,** 10554-10559.

Nakagawa, Y., Katagiri, T., Shinozaki, K., Qi, Z., Tatsumi, H., Furuichi, T., Kishigami, A., Sokabe, M., Kojima, I., and Sato, S. (2007). *Arabidopsis* plasma membrane protein crucial for Ca^{2+} influx and touch sensing in roots. Proc. Natl. Acad. Sci. **104,** 3639-3644.

Nawashin, S. (1898). Resultate einer Revision der Befruchtungsvorgange bei *Lilium martagon* und *Fritillaria tenella*. Acad. Imp. Sci. St Pétersbourg **9**, 377-382.

Nebenführ, A., Ritzenthaler, C., and Robinson, D.G. (2002). Brefeldin A: deciphering an enigmatic inhibitor of secretion. Plant Physiol. **130,** 1102-1108.

Neill, A.T., and Vacquier, V.D. (2004). Ligands and receptors mediating signal transduction in sea urchin spermatozoa. Reproduction **127,** 141-149.

Ngo, Q.A., Vogler, H., Lituiev, D.S., Nestorova, A., and Grossniklaus, U. (2014). A calcium dialog mediated by the *FERONIA* signal transduction pathway controls plant sperm delivery. Dev. Cell **29,** 491-500.

Nguema-Ona, E., Coimbra, S., Vicré-Gibouin, M., Mollet, J.-C., and Driouich, A. (2012). Arabinogalactan proteins in root and pollen-tube cells: distribution and functional aspects. Ann. Bot. **110,** 383-404.

Nielsen, E., Cheung, A.Y., and Ueda, T. (2008). The regulatory RAB and ARF GTPases for vesicular trafficking. Plant Phys. **147**, 1516-1526.

Noguchi, T., Fujioka, S., Choe, S., Takatsuto, S., Yoshida, S., Yuan, H., Feldmann, K.A., and Tax, F.E. (1999). Brassinosteroid-insensitive dwarf mutants of *Arabidopsis* accumulate brassinosteroids. Plant Physiol. **121,** 743-752.

Nüsslein-Volhard, C., and Wieschaus, E. (1980). Mutations affecting segment number and polarity in *Drosophila*. Nature **287,** 795-801.

Ohnishi, T., Godza, B., Watanabe, B., Fujioka, S., Hategan, L., Ide, K., Shibata, K., Yokota, T., Szekeres, M., and Mizutani, M. (2012). CYP90A1/CPD, a brassinosteroid biosynthetic cytochrome P450 of *Arabidopsis*, catalyzes C-3 oxidation. J. Biol. Chem. **287,** 31551-31560.

Okabe, M. (2013). The cell biology of mammalian fertilization. Development **140,** 4471-4479.

Okuda, S., Suzuki, T., Kanaoka, M.M., Mori, H., Sasaki, N., and Higashiyama, T. (2013). Acquisition of LURE-binding activity at the pollen tube tip of *Torenia fournieri*. Mol. Plant **6,** 1074-1090.

Okuda, S., Tsutsui, H., Shiina, K., Sprunck, S., Takeuchi, H., Yui, R., Kasahara, R.D., Hamamura, Y., Mizukami, A., Susaki, D., Kawano, N., Sakakibara, T., Namiki, S., Itoh, K., Otsuka, K., Matsuzaki, M., Nozaki, H., Kuroiwa, T., Nakano, A., Kanaoka, M.M., Dresselhaus, T., Sasaki, N., and Higashiyama, T. (2009). Defensin-like polypeptide LUREs are pollen tube attractants secreted from synergid cells. Nature **458,** 357-361.

Oldroyd, G.E., and Downie, J.A. (2008). Coordinating nodule morphogenesis with rhizobial infection

in legumes. Annu. Rev. Plant Biol. **59,** 519-546.

Oldroyd, G.E., Harrison, M.J., and Paszkowski, U. (2009). Reprogramming plant cells for endosymbiosis. Science **324,** 753.

Oppenheimer, D.G., Herman, P.L., Sivakumaran, S., Esch, J., and Marks, M.D. (1991). A *MYB* gene required for leaf trichome differentiation in *Arabidopsis* is expressed in stipules. Cell **67,** 483-493.

Orrenius, S., Zhivotovsky, B., and Nicotera, P. (2003). Regulation of cell death: the calcium–apoptosis link. Nature Rev. Mol. Cell Biol. **4,** 552-565.

Ovečka, M., Lang, I., Baluška, F., Ismail, A., Illeš, P., and Lichtscheidl, I.K. (2005). Endocytosis and vesicle trafficking during tip growth of root hairs. Protoplasma **226,** 39-54.

Pagnussat, G.C., Yu, H.-J., and Sundaresan, V. (2007). Cell-fate switch of synergid to egg cell in *Arabidopsis eostre* mutant embryo sacs arises from misexpression of the *BEL1-like* homeodomain gene *BLH1*. Plant Cell **19,** 3578-3592.

Palanivelu, R., and Preuss, D. (2006). Distinct short-range ovule signals attract or repel *Arabidopsis thaliana* pollen tubes in vitro. BMC Plant Biol. **6,** 7.

Palanivelu, R., and Johnson, M.A. (2010). Functional genomics of pollen tube-pistil interactions in *Arabidopsis*. Biochem. Soc. Trans. **38,** 593-597.

Palanivelu, R., and Tsukamoto, T. (2012). Pathfinding in angiosperm reproduction: pollen tube guidance by pistils ensures successful double fertilization. WIREs Developmental Biology **1,** 96-113.

Palanivelu, R., Brass, L., Edlund, A.F., and Preuss, D. (2003). Pollen tube growth and guidance is regulated by *POP2*, an *Arabidopsis* gene that controls GABA levels. Cell **114,** 47-59.

Pan, J., and Snell, W.J. (2000). Signal transduction during fertilization in the unicellular green alga, C*hlamydomonas*. Curr. Op. Microbiol. **3,** 596-602.

Pang, S.-Z., DeBoer, D.L., Wan, Y., Ye, G., Layton, J.G., Neher, M.K., Armstrong, C.L., Fry, J.E., Hinchee, M.A., and Fromm, M.E. (1996). An improved green fluorescent protein gene as a vital marker in plants. Plant Physiol. **112,** 893-900.

Parker, J.S., Cavell, A.C., Dolan, L., Roberts, K., and Grierson, C.S. (2000). Genetic interactions during root hair morphogenesis in *Arabidopsis*. Plant Cell **12,** 1961-1974.

Parrington, J., Davis, L.C., Galione, A., and Wessel, G. (2007). Flipping the switch: how a sperm activates the egg at fertilization. Dev. Dynam. **236,** 2027-2038.

Pattanaik, S., Patra, B., Singh, S.K., and Yuan, L. (2014). An overview of the gene regulatory network controlling trichome development in the model plant, *Arabidopsis*. Front. Plant Sci. **5,** 259.

Payne, C.T., Zhang, F., and Lloyd, A.M. (2000). *GL3* encodes a bHLH protein that regulates trichome development in *Arabidopsis* through interaction with GL1 and TTG1. Genetics **156,** 1349-1362.

Peifer, M., and Wleschaus, E. (1990). The segment polarity gene *armadillo* encodes a functionally modular protein that is the *Drosophila* homolog of human plakoglobin. Cell **63,** 1167-1178.

Peng, X.B., Sun, M.X., and Yang, H.Y. (2009). Comparative detection of calcium fluctuations in single female sex cells of tobacco to distinguish calcium signals triggered by in vitro fertilization. J. Integr. Plant Biol. **51,** 782-791.

Poppenberger, B., Rozhon, W., Khan, M., Husar, S., Adam, G., Luschnig, C., Fujioka, S., and Sieberer, T. (2011). CESTA, a positive regulator of brassinosteroid biosynthesis. EMBO J. **30,**

1149-1161.

Preuss, M.L., Serna, J., Falbel, T.G., Bednarek, S.Y., and Nielsen, E. (2004). The *Arabidopsis* Rab GTPase RabA4b localizes to the tips of growing root hair cells. Plant Cell **16,** 1589-1603.

Preuss, M.L., Schmitz, A.J., Thole, J.M., Bonner, H.K., Otegui, M.S., and Nielsen, E. (2006). A role for the RabA4b effector protein PI-4Kβ1 in polarized expansion of root hair cells in *Arabidopsis thaliana*. J. Cell Biol.**172,** 991-998.

Primakoff, P., and Myles, D.G. (2007). Cell-cell membrane fusion during mammalian fertilization. FEBS Letters **581,** 2174-2180.

Punwani, J.A., Rabiger, D.S., and Drews, G.N. (2007). *MYB98* positively regulates a battery of synergid-expressed genes encoding filiform apparatus–localized proteins. Plant Cell **19,** 2557-2568.

Qin, Y., and Dong, J. (2015). Focusing on the focus: what else beyond the master switches for polar cell growth? Mol. Plant **8**, 582-594.

Qin, Y., and Yang, Z. (2011). Rapid tip growth: insights from pollen tubes. Semin. Cell Dev. Biol. **22,** 816-824.

Qin, T., Liu, X., Li, J., Sun, J., Song, L., and Mao, T. (2014). *Arabidopsis* Microtubule-Destabilizing Protein 25 functions in pollen tube growth by severing actin filaments. Plant Cell **26,** 325-339.

Qin, Y., Leydon, A.R., Manziello, A., Pandey, R., Mount, D., Denic, S., Vasic, B., Johnson, M.A., and Palanivelu, R. (2009). Penetration of the stigma and style elicits a novel transcriptome in pollen tubes, pointing to genes critical for growth in a pistil. PLoS Genetics **5,** e1000621.

Qin, Y., Wysocki, R.J., Somogyi, A., Feinstein, Y., Franco, J.Y., Tsukamoto, T., Dunatunga, D., Levy, C., Smith, S., Simpson, R., Gang, D., Johnson, M.A., and Palanivelu, R. (2011). Sulfinylated azadecalins act as functional mimics of a pollen germination stimulant in *Arabidopsis* pistils. Plant J. **68,** 800-815.

Qu, X., Jiang, Y., Chang, M., Liu, X., Zhang, R., and Huang, S. (2015). Organization and regulation of the actin cytoskeleton in the pollen tube. Front. Plant Sci. **5,** 786.

Raghavan, V. (1997). Molecular embryology of flowering plants. Camebridge: Cambridge University Press.

Raghavan, V. (2003). Some reflections on double fertilization, from its discovery to the present. New Phytol. **159,** 565-583.

Rerie, W.G., Feldmann, K.A., and Marks, M.D. (1994). The *GLABRA2* gene encodes a homeo domain protein required for normal trichome development in *Arabidopsis*. Genes Dev. **8,** 1388-1399.

Riedl, J., Crevenna, A.H., Kessenbrock, K., Yu, J.H., Neukirchen, D., Bista, M., Bradke, F., Jenne, D., Holak, T.A., Werb, Z., Sixt, M., and Wedlich-Soldner, R. (2008). Lifeact: a versatile marker to visualize F-actin. Nat. Methods **5,** 605-607.

Riggleman, B., Wieschaus, E., and Schedl, P. (1989). Molecular analysis of the armadillo locus: uniformly distributed transcripts and a protein with novel internal repeats are associated with a *Drosophila* segment polarity gene. Genes Dev. **3,** 96-113.

Rodriguez-Enriquez, M.J., Mehdi, S., Dickinson, H.G., and Grant-Downton, R.T. (2013). A novel method for efficient in vitro germination and tube growth of *Arabidopsis thaliana* pollen. New Phytol. **197,** 668-679.

Rosso, M., Li, Y., Strizhov, N., Reiss, B., Dekker, K., and Weisshaar, B. (2003). An *Arabidopsis tha-*

liana T-DNA mutagenized population (GABI-Kat) for flanking sequence tag-based reverse genetics. Plant Mol. Biol. **53,** 247-259.

Rounds, C.M., and Bezanilla, M. (2013). Growth mechanisms in tip-growing plant cells. Annu. Rev. Plant Biol. **64,** 243-265.

Šamaj, J., Muller, J., Beck, M., Bohm, N., and Menzel, D. (2006). Vesicular trafficking, cytoskeleton and signalling in root hairs and pollen tubes. Trends Plant Sci. **11,** 594-600.

Samson, F., Brunaud, V., Duchêne, S., De Oliveira, Y., Caboche, M., Lecharny, A., and Aubourg, S. (2004). FLAGdb^{++}: a database for the functional analysis of the *Arabidopsis* genome. Nucleic Acids Res. **32,** D347-D350.

Samuel, M.A., Salt, J.N., Shiu, S.H., and Goring, D.R. (2006). Multifunctional Arm repeat domains in plants. In: Internat. Rev. Cytol., W.J. Kwang, ed, Academic Press, pp. 1-26.

Sanati Nezhad, A., Packirisamy, M., and Geitmann, A. (2014). Dynamic, high precision targeting of growth modulating agents is able to trigger pollen tube growth reorientation. Plant J. **80,** 185-195.

Schiefelbein, J.W. (2000). Constructing a plant cell. the genetic control of root hair development. Plant Physiol. **124,** 1525-1531.

Schiefelbein, J.W., and Somerville, C. (1990). Genetic control of root hair development in *Arabidopsis thaliana*. Plant Cell **2,** 235-243.

Schiefelbein, J., Galway, M., Masucci, J., and Ford, S. (1993). Pollen tube and root-hair tip growth is disrupted in a mutant of *Arabidopsis thaliana*. Plant Physiol. **103,** 979-985.

Schindelin, J., Arganda-Carreras, I., Frise, E., Kaynig, V., Longair, M., Pietzsch, T., Preibisch, S., Rueden, C., Saalfeld, S., Schmid, B., Tinevez, J.-Y., White, D.J., Hartenstein, V., Eliceiri, K., Tomancak, P., and Cardona, A. (2012). FIJI: an open-source platform for biological-image analysis. Nat. Meth. **9,** 676-682.

Schiøtt, M., Romanowsky, S.M., Bækgaard, L., Jakobsen, M.K., Palmgren, M.G., and Harper, J.F. (2004). A plant plasma membrane Ca^{2+} pump is required for normal pollen tube growth and fertilization. Proc. Natl. Acad. Sci. **101,** 9502-9507.

Schmidt, J., Altmann, T., and Adam, G. (1997). Brassinosteroids from seeds of *Arabidopsis thaliana*. Phytochemistry **45,** 1325-1327.

Schneider, S., Schneidereit, A., Konrad, K.R., Hajirezaei, M.-R., Gramann, M., Hedrich, R., and Sauer, N. (2006). *Arabidopsis* INOSITOL TRANSPORTER 4 mediates high-affinity H^+ symport of myoinositol across the plasma membrane. Plant Physiol. **141,** 565-577.

Scott, R.J., Armstrong, S.J., Doughty, J., and Spielman, M. (2008). Double fertilization in *Arabidopsis thaliana* involves a polyspermy block on the egg but not the central cell. Mol. Plant **1,** 611-619.

Sedgley, M. (1975). Flavanoids in pollen and stigma of *Brassica oleracea* and their effects on pollen germination in vitro. Ann. Bot. **39,** 1091-1095.

Sessions, A., Burke, E., Presting, G., Aux, G., McElver, J., Patton, D., Dietrich, B., Ho, P., Bacwaden, J., and Ko, C. (2002). A high-throughput *Arabidopsis* reverse genetics system. Plant Cell **14,** 2985-2994.

Sfakiotakis, E.M., Simons, D.H., and Dilley, D.R. (1972). Pollen germination and tube growth: dependent on carbon dioxide and independent of ethylene. Plant Physiol. **49,** 963-967.

Shiba, H., Takayama, S., Iwano, M., Shimosato, H., Funato, M., Nakagawa, T., Che, F.-S., Suzu-

ki, G., Watanabe, M., and Hinata, K. (2001). A Pollen Coat Protein, SP11/SCR, determines the pollen S-specificity in the self-incompatibility of *Brassica* species. Plant Physiol. **125,** 2095-2103.

Shimada, Y., Goda, H., Nakamura, A., Takatsuto, S., Fujioka, S., and Yoshida, S. (2003). Organ-specific expression of brassinosteroid-biosynthetic genes and distribution of endogenous brassinosteroids in *Arabidopsis*. Plant Physiol. **131,** 287-297.

Shimizu, K.K., and Okada, K. (2000). Attractive and repulsive interactions between female and male gametophytes in *Arabidopsis* pollen tube guidance. Development **127,** 4511-4518.

Shimizu, K.K., Ito, T., Ishiguro, S., and Okada, K. (2008). *MAA3 (MAGATAMA3)* helicase gene is required for female gametophyte development and pollen tube guidance in *Arabidopsis thaliana*. Plant Cell Physiol. **49,** 1478-1483.

Shinjo, K., Koland, J.G., Hart, M.J., Narasimhan, V., Johnson, D.I., Evans, T., and Cerione, R.A. (1990). Molecular cloning of the gene for the human placental GTP-binding protein Gp (G25K): identification of this GTP-binding protein as the human homolog of the yeast cell-division-cycle protein CDC42. Proc. Natl. Acad. Sci. **87,** 9853-9857.

Sieber, P., Gheyselinck, J., Gross-Hardt, R., Laux, T., Grossniklaus, U., and Schneitz, K. (2004). Pattern formation during early ovule development in *Arabidopsis thaliana*. Dev. Biol. **273,** 321-334.

Silverstein, K.A., Moskal, W.A., Wu, H.C., Underwood, B.A., Graham, M.A., Town, C.D., and VandenBosch, K.A. (2007). Small cysteine-rich peptides resembling antimicrobial peptides have been under-predicted in plants. Plant J. **51,** 262-280.

Singh, I., and Shono, M. (2005). Physiological and molecular effects of 24-epibrassinolide, a brassinosteroid on thermotolerance of tomato. Plant Growth Regul. **47,** 111-119.

Singh, D.P., Jermakow, A.M., and Swain, S.M. (2002). Gibberellins are required for seed development and pollen tube growth in *Arabidopsis*. Plant Cell **14,** 3133-3147.

Sinnott, E.W., and Bloch, R. (1939). Cell polarity and the differentiation of root hairs. Proc. Natl. Acad. Sci. **25,** 248.

Slaughter, B.D., Smith, S.E., and Li, R. (2009). Symmetry breaking in the life cycle of the budding yeast. Cold Spring Harb. Perspect. Biol. **1,** a003384.

Smith, A.G., Eberle, C.A., Moss, N.G., Anderson, N.O., Clasen, B.M., and Hegeman, A.D. (2013). The transmitting tissue of *Nicotiana tabacum* is not essential to pollen tube growth, and its ablation can reverse prezygotic interspecific barriers. Plant Reprod. **26,** 339-350.

Smyth, D.R., Bowman, J.L., and Meyerowitz, E.M. (1990). Early flower development in *Arabidopsis*. Plant Cell **2,** 755-767.

Sommer, J., and Newton, A. (1991). Pseudoreversion analysis indicates a direct role of cell division genes in polar morphogenesis and differentiation in *Caulobacter crescentus*. Genetics **129,** 623-630.

Song, X.-F., Yang, C.-Y., Liu, J., and Yang, W.-C. (2006). RPA, a class II ARFGAP protein, activates ARF1 and U5 and plays a role in root hair development in *Arabidopsis*. Plant Physiol. **141,** 966-976.

Sotomayor, C., Castro, J., Velasco, N., and Toro, R. (2012). Influence of seven growth regulators on fruit set, pollen germination and pollen tube growth of almonds. J. Agric. Sci. Technol. **B,** 1051-1056.

Sousa, E., Kost, B., and Malhó, R. (2008). *Arabidopsis* Phosphatidylinositol-4-Monophosphate 5-Kinase 4 regulates pollen tube growth and polarity by modulating membrane recycling. Plant Cell **20,** 3050-3064.

Sprunck, S. (2010). Let's get physical: gamete interaction in flowering plants. Biochem. Soc. Trans. **38,** 635-640.

Sprunck, S., and Gross-Hardt, R. (2011). Nuclear behavior, cell polarity, and cell specification in the female gametophyte. Sex. Plant Reprod. **24,** 123-136.

Sprunck, S., Hackenberg, T., Englhart, M., and Vogler, F. (2014). Same same but different: sperm-activating EC1 and ECA1 gametogenesis-related family proteins. Biochem. Soc. Trans. **42,** 401-407.

Sprunck, S., Baumann, U., Edwards, K., Langridge, P., and Dresselhaus, T. (2005). The transcript composition of egg cells changes significantly following fertilization in wheat (*Triticum aestivum* L.). Plant J. **41,** 660-672.

Sprunck, S., Rademacher, S., Vogler, F., Gheyselinck, J., Grossniklaus, U., and Dresselhaus, T. (2012). Egg cell–secreted EC1 triggers sperm cell activation during double fertilization. Science **338,** 1093-1097.

Stanley, R., and Liskens, H. (1974). Pollen. Springer.

Steber, C.M., and McCourt, P. (2001). A role for brassinosteroids in germination in *Arabidopsis*. Plant Physiol. **125,** 763-769.

Stefano, G., Renna, L., Moss, T., McNew, J.A., and Brandizzi, F. (2012). In *Arabidopsis*, the spatial and dynamic organization of the endoplasmic reticulum and Golgi apparatus is influenced by the integrity of the C-terminal domain of RHD3, a non-essential GTPase. Plant J. **69,** 957-966.

Steffen, J.G., Kang, I.H., Macfarlane, J., and Drews, G.N. (2007). Identification of genes expressed in the *Arabidopsis* female gametophyte. Plant J. **51,** 281-292.

Steinhorst, L., and Kudla, J. (2013). Calcium - a central regulator of pollen germination and tube growth. BBA-Mol. Cell Res. **1833,** 1573-1581.

Sudbery, P.E. (2011). Growth of *Candida albicans* hyphae. Nat. Rev. Micro. **9,** 737-748.

Swann, K., and Yu, Y. (2008). The dynamics of calcium oscillations that activate mammalian eggs. Int. J. Dev. Biol. **52,** 585.

Synek, L., Schlager, N., Eliáš, M., Quentin, M., Hauser, M.T., and Žárský, V. (2006). AtEXO70A1, a member of a family of putative exocyst subunits specifically expanded in land plants, is important for polar growth and plant development. Plant J. **48,** 54-72.

Szekeres, M., Németh, K., Koncz-Kálmán, Z., Mathur, J., Kauschmann, A., Altmann, T., Rédei, G.P., Nagy, F., Schell, J., and Koncz, C. (1996). Brassinosteroids rescue the deficiency of CYP90, a Cytochrome P450, controlling cell elongation and de-etiolation in *Arabidopsis*. Cell **85,** 171-182.

Sztul, E., and Lupashin, V. (2006). Role of tethering factors in secretory membrane traffic. Am. J. Physiol. Cell Ph. **290**, C11-C26.

Szumlanski, A.L., and Nielsen, E. (2009). The Rab GTPase RabA4d regulates pollen tube tip growth in *Arabidopsis thaliana*. Plant Cell **21,** 526-544.

Takada, S., and Jürgens, G. (2007). Transcriptional regulation of epidermal cell fate in the *Arabidopsis* embryo. Development **134,** 1141-1150.

Takasaki, T., Hatakeyama, K., Suzuki, G., Watanabe, M., Isogai, A., and Hinata, K. (2000). The S receptor kinase determines self-incompatibility in *Brassica* stigma. Nature **403,** 913-916.

Takayama, S., and Isogai, A. (2005). Self-incompatibility in plants. Annu. Rev. Plant Biol. **56,** 467-489.

Takeuchi, H., and Higashiyama, T. (2011). Attraction of tip-growing pollen tubes by the female gametophyte. Curr. Opin. Plant Biol. **14,** 614-621.

Takeuchi, H., and Higashiyama, T. (2012). A species-specific cluster of defensin-like genes encodes diffusible pollen tube attractants in *Arabidopsis*. PLoS Biol. **10,** e1001449.

Tang, W., Kelley, D., Ezcurra, I., Cotter, R., and McCormick, S. (2004). LeSTIG1, an extracellular binding partner for the pollen receptor kinases LePRK1 and LePRK2, promotes pollen tube growth in vitro. Plant J. **39,** 343-353.

Taylor, L.P., and Hepler, P.K. (1997). Pollen germination and tube growth. Ann. Review Plant Physiol. **48,** 461-491.

Taylor, L.P., and Grotewold, E. (2005). Flavonoids as developmental regulators. Curr. Opin. Plant Biol. **8,** 317-323.

Tewari, R., Bailes, E., Bunting, K.A., and Coates, J.C. (2010). Armadillo-repeat protein functions: questions for little creatures. Trends Cell Biol **20,** 470-481.

Thomas, C., Hoffmann, C., Dieterle, M., Van Troys, M., Ampe, C., and Steinmetz, A. (2006). Tobacco WLIM1 is a novel F-actin binding protein involved in actin cytoskeleton remodeling. Plant Cell **18,** 2194-2206.

Thompson, B.J. (2013). Cell polarity: models and mechanisms from yeast, worms and flies. Development **140,** 13-21.

Thussagunpanit, J., Jutamanee, K., Chai-arree, W., and Kaveeta, L. (2012). Increasing photosynthetic efficiency and pollen germination with 24-epibrassinolide in rice (*Oryza sativa* L.) under heat stress. Thai J. Bot. **4,** 135-143.

Tiwari, S.C., and Polito, V.S. (1988). Organization of the cytoskeleton in pollen tubes of *Pyrus communis*: a study employing conventional and freeze-substitution electron microscopy, immunofluorescence, and rhodamine-phalloidin. Protoplasma **147,** 100-112.

Tsokos, C.G., and Laub, M.T. (2012). Polarity and cell fate asymmetry in *Caulobacter crescentus*. Curr. Op. Microbiol. **15,** 744-750.

Tung, C.W., Dwyer, K.G., Nasrallah, M.E., and Nasrallah, J.B. (2005). Genome-wide identification of genes expressed in *Arabidopsis* pistils specifically along the path of pollen tube growth. Plant Physiol. **138,** 977-989.

Twell, D., Yamaguchi, J., and McCormick, S. (1990). Pollen-specific gene expression in transgenic plants: coordinate regulation of two different tomato gene promoters during microsporogenesis. Development **109,** 705-713.

Uhlén, P., and Fritz, N. (2010). Biochemistry of calcium oscillations. Biochem. Biophys. Res. Co. **396,** 28-32.

Vancanneyt, G., Schmidt, R., O'Connor-Sanchez, A., Willmitzer, L., and Rocha-Sosa, M. (1990). Construction of an intron-containing marker gene: splicing of the intron in transgenic plants and its use in monitoring early events in Agrobacterium-mediated plant transformation. Mol. Gen. Genet. **220,** 245-250.

Vetter, I.R., and Wittinghofer, A. (2001). The guanine nucleotide-binding switch in three dimensions.

Science **294,** 1299-1304.

Vielle-Calzada, J.-P., Thomas, J., Spillane, C., Coluccio, A., Hoeppner, M.A., and Grossniklaus, U. (1999). Maintenance of genomic imprinting at the *Arabidopsis medea* locus requires zygotic *DDM1* activity. Genes Dev. **13,** 2971-2982.

Vogler, F., Konrad, S.S.A., and Sprunck, S. (2015). Knockin' on pollen's door: live cell imaging of early polarization events in germinating *Arabidopsis* pollen. Front. Plant Sci. **6**, 246.

Vogler, F., Schmalzl, C., Englhart, M., Bircheneder, M., and Sprunck, S. (2014). Brassinosteroids promote *Arabidopsis* pollen germination and growth. Plant Reprod. **27,** 153-167.

Völz, R., Heydlauff, J., Ripper, D., von Lyncker, L., and Groß-Hardt, R. (2013). Ethylene signaling is required for synergid degeneration and the establishment of a pollen tube block. Dev. Cell **25,** 310-316.

von Besser, K., Frank, A.C., Johnson, M.A., and Preuss, D. (2006). *Arabidopsis HAP2 (GCS1)* is a sperm-specific gene required for pollen tube guidance and fertilization. Development **133,** 4761-4769.

Vriet, C., Russinova, E., and Reuzeau, C. (2013). From squalene to brassinolide: the steroid metabolic and signaling pathways across the plant kingdom. Mol. Plant **6,** 1738-1757.

Wada, Y., Kusano, H., Tsuge, T., and Aoyama, T. (2015). Phosphatidylinositol phosphate 5-kinase genes respond to phosphate deficiency for root hair elongation in *Arabidopsis thaliana*. Plant J. **81,** 426-437.

Walker, A.R., Davison, P.A., Bolognesi-Winfield, A.C., James, C.M., Srinivasan, N., Blundell, T.L., Esch, J.J., Marks, M.D., and Gray, J.C. (1999). The *TRANSPARENT TESTA GLABRA1* locus, which regulates trichome differentiation and anthocyanin biosynthesis in *Arabidopsis*, encodes a WD40 repeat protein. Plant Cell **11,** 1337-1349.

Wang, D.S., and Shaw, G. (1995). The association of the C-terminal region of β1ΣII spectrin to brain membranes is mediated by a pH domain, does not require membrane proteins, and coincides with a inositol-1,4,5 trisphosphate binding site. Biochem. Bioph. Res. Co. **217,** 608-615.

Wang, H., Lockwood, S.K., Hoeltzel, M.F., and Schiefelbein, J.W. (1997). The *ROOT HAIR DEFECTIVE3* gene encodes an evolutionarily conserved protein with GTP-binding motifs and is required for regulated cell enlargement in *Arabidopsis*. Genes Dev. **11,** 799-811.

Wang, X., Teng, Y., Wang, Q., Li, X., Sheng, X., Zheng, M., Šamaj, J., Baluška, F., and Lin, J. (2006). Imaging of dynamic secretory vesicles in living pollen tubes of *Picea meyeri* using evanescent wave microscopy. Plant Physiol. **141,** 1591-1603.

Wang, J., Ding, Y., Wang, J., Hillmer, S., Miao, Y., Lo, S.W., Wang, X., Robinson, D.G., and Jiang, L. (2010). EXPO, an exocyst-positive organelle distinct from multivesicular endosomes and autophagosomes, mediates cytosol to cell wall exocytosis in *Arabidopsis* and tobacco cells. Plant Cell **22,** 4009-4030.

Wedlich-Soldner, R., Wai, S.C., Schmidt, T., and Li, R. (2004). Robust cell polarity is a dynamic state established by coupling transport and GTPase signaling. J. Cell Biol. **166,** 889-900.

Wengier, D.L., Mazzella, M.A., Salem, T.M., McCormick, S., and Muschietti, J.P. (2010). STIL, a peculiar molecule from styles, specifically dephosphorylates the pollen receptor kinase LePRK2 and stimulates pollen tube growth in vitro. BMC Plant Biol. **10,** 33.

Wilkins, K.A., Poulter, N.S., and Franklin-Tong, V.E. (2014). Taking one for the team: self-recognition and cell suicide in pollen. J. Exp. Bot. **65,** 1331-1342.

Wilsen, K., Lovy-Wheeler, A., Voigt, B., Menzel, D., Kunkel, J., and Hepler, P. (2006). Imaging the actin cytoskeleton in growing pollen tubes. Sex. Plant Reprod. **19,** 51-62.

Wittinghofer, A., and Vetter, I.R. (2011). Structure-function relationships of the G domain, a canonical switch motif. Annu. Rev. Biochem. **80,** 943-971.

Wolpert, L. (2013). Cell polarity. Phil. Trans. R. Soc. B. **368,** 20130419.

Wolters-Arts, M., Lush, W.M., and Mariani, C. (1998). Lipids are required for directional pollen-tube growth. Nature **392,** 818-821.

Won, S.-K., Lee, Y.-J., Lee, H.-Y., Heo, Y.-K., Cho, M., and Cho, H.-T. (2009). Cis-element-and transcriptome-based screening of root hair-specific genes and their functional characterization in *Arabidopsis*. Plant Physiol. **150,** 1459-1473.

Wong, J.L., and Johnson, M.A. (2010). Is HAP2-GCS1 an ancestral gamete fusogen? Trends Cell Biol. **20,** 134-141.

Woriedh, M., Wolf, S., Márton, M.L., Hinze, A., Gahrtz, M., Becker, D., and Dresselhaus, T. (2013). External application of gametophyte-specific ZmPMEI1 induces pollen tube burst in maize. Plant Reprod. **26,** 255-266.

Wu, H.-M., Wang, H., and Cheung, A.Y. (1995). A pollen tube growth stimulatory glycoprotein is deglycosylated by pollen tubes and displays a glycosylation gradient in the flower. Cell **82,** 395-403.

Wu, J., Qin, Y., and Zhao, J. (2008a). Pollen tube growth is affected by exogenous hormones and correlated with hormone changes in styles in *Torenia fournieri* L. Plant Growth Regul. **55,** 137-148.

Wu, J.Z., Lin, Y., Zhang, X.L., Pang, D.W., and Zhao, J. (2008b). IAA stimulates pollen tube growth and mediates the modification of its wall composition and structure in *Torenia fournieri*. J. Exp. Bot. **59,** 2529-2543.

Wu, J., Qin, X., Tao, S., Jiang, X., Liang, Y.K., and Zhang, S. (2014). Long-chain base phosphates modulate pollen tube growth via channel-mediated influx of calcium. Plant J. **79,** 507-516.

Wu, J., Shang, Z., Wu, J., Jiang, X., Moschou, P.N., Sun, W., Roubelakis-Angelakis, K.A., and Zhang, S. (2010). Spermidine oxidase-derived H_2O_2 regulates pollen plasma membrane hyperpolarization-activated Ca^{2+}-permeable channels and pollen tube growth. Plant J. **63,** 1042-1053.

Xu, J., and Scheres, B. (2005). Dissection of *Arabidopsis* ADP-RIBOSYLATION FACTOR 1 function in epidermal cell polarity. Plant Cell **17,** 525-536.

Xu, T., Wen, M., Nagawa, S., Fu, Y., Chen, J.G., Wu, M.J., Perrot-Rechenmann, C., Friml, J., Jones, A.M., and Yang, Z. (2010). Cell surface- and rho GTPase-based auxin signaling controls cellular interdigitation in *Arabidopsis*. Cell **143,** 99-110.

Yang, Z. (2008). Cell polarity signaling in *Arabidopsis*. Annu. Rev. Cell Dev. Bi. **24,** 551-575.

Yang, Z., and Lavagi, I. (2012). Spatial control of plasma membrane domains: ROP GTPase-based symmetry breaking. Curr. Opin. Plant Biol. **15,** 601-607.

Yang, X.-H., Xu, Z.-H., and Xue, H.-W. (2005). *Arabidopsis* Membrane Steroid Binding Protein 1 is involved in inhibition of cell elongation. Plant Cell **17,** 116-131.

Ye, Q., Zhu, W., Li, L., Zhang, S., Yin, Y., Ma, H., and Wang, X. (2010). Brassinosteroids control male fertility by regulating the expression of key genes involved in *Arabidopsis* anther and pollen development. Proc. Natl. Acad. Sci. **107,** 6100-6105.

Yetisen, A., Jiang, L., Cooper, J., Qin, Y., Palanivelu, R., and Zohar, Y. (2011). A microsystem-based assay for studying pollen tube guidance in plant reproduction. J. Micromech. Microeng. **21,** 054018.

Ylstra, B., Touraev, A., Brinkmann, A.O., Heberle-Bors, E., and Tunen, A. (1995). Steroid hormones stimulate germination and tube growth of in vitro matured tobacco pollen. Plant Physiol. **107,** 639-643.

Ylstra, B., Touraev, A., Moreno, R.M.B., Stöger, E., van Tunen, A.J., Vicente, O., Mol, J.N.M., and Heberle-Bors, E. (1992). Flavonols stimulate development, germination, and tube growth of tobacco pollen. Plant Physiol. **100,** 902-907.

Yu, R., and Kaiser, D. (2007). Gliding motility and polarized slime secretion. Mol. Microbiol. **63,** 454-467.

Yu, N., Cai, W.-J., Wang, S., Shan, C.-M., Wang, L.-J., and Chen, X.-Y. (2010). Temporal control of trichome distribution by microRNA156-targeted *SPL* genes in *Arabidopsis thaliana*. Plant Cell **22,** 2322-2335.

Yu, D., Yu, F., Du, C., Li, X., Zhao, X., and Liu, X. (2015). RPN1a, a subunit of the 26S proteasome, controls trichome development in *Arabidopsis*. Plant Physiol. Bioch. **88,** 82-88.

Yu, G.-H., Zou, J., Feng, J., Peng, X.-B., Wu, J.-Y., Wu, Y.-L., Palanivelu, R., and Sun, M.-X. (2014). Exogenous γ-aminobutyric acid (GABA) affects pollen tube growth via modulating putative Ca^{2+}-permeable membrane channels and is coupled to negative regulation on glutamate decarboxylase. J. Exp. Bot. **65,** 3235-3248.

Žárský, V., Kulich, I., Fendrych, M., and Pecenkova, T. (2013). Exocyst complexes multiple functions in plant cells secretory pathways. Curr. Opin. Plant Biol. **16,** 726-733.

Žárský, V., Cvrčková, F., Potocký, M., and Hála, M. (2009). Exocytosis and cell polarity in plants – exocyst and recycling domains. New Phytol. **183,** 255-272.

Zhang, Y., and McCormick, S. (2009). AGCVIII kinases: at the crossroads of cellular signaling. Trends Plant Sci. **14,** 689-695.

Zhang, Z., and Laux, T. (2011). The asymmetric division of the *Arabidopsis* zygote: from cell polarity to an embryo axis. Sex. Plant Reprod. **24,** 161-169.

Zhang, Y., He, J., and McCormick, S. (2009). Two *Arabidopsis* AGC kinases are critical for the polarized growth of pollen tubes. Plant J. **58,** 474-484.

Zhang, F., Gonzalez, A., Zhao, M., Payne, C.T., and Lloyd, A. (2003). A network of redundant bHLH proteins functions in all TTG1-dependent pathways of *Arabidopsis*. Development **130,** 4859-4869.

Zhang, M., Wu, F., Shi, J., Zhu, Y., Zhu, Z., Gong, Q., and Hu, J. (2013). ROOT HAIR DEFECTIVE3 family of dynamin-like GTPases mediates homotypic endoplasmic reticulum fusion and is essential for *Arabidopsis* development. Plant Physiol. **163,** 713-720.

Zhao, J., Yang, H.-Y., and Lord, E.M. (2004). Calcium levels increase in the lily stylar transmitting tract after pollination. Sex. Plant Reprod. **16,** 259-263.

Zheng, H., and Chen, J. (2011). Emerging aspects of ER organization in root hair tip growth: Lessons from RHD3 and atlastin. Plant Signal. Behav. **6,** 1710-1713.

Zheng, B., Chen, X., and McCormick, S. (2011). The Anaphase-Promoting Complex is a dual integrator that regulates both MicroRNA-mediated transcriptional regulation of *Cyclin B1* and degrada-

tion of Cyclin B1 during *Arabidopsis* male gametophyte development. Plant Cell **23,** 1033-1046.

Zhou, X., and Meier, I. (2014). Efficient plant male fertility depends on vegetative nuclear movement mediated by two families of plant outer nuclear membrane proteins. Proc. Natl. Acad. Sci. **111,** 11900-11905.

Zhou, Z., Shi, H., Chen, B., Zhang, R., Huang, S., and Fu, Y. (2015). *Arabidopsis* RIC1 severs actin filaments at the apex to regulate pollen tube growth. Plant Cell, *published online before print.*

Zhu, L., Zhang, Y., Kang, E., Xu, Q., Wang, M., Rui, Y., Liu, B., Yuan, M., and Fu, Y. (2013). MAP18 regulates the direction of pollen tube growth in *Arabidopsis* by modulating F-actin organization. Plant Cell **25,** 851-867.

Zimmermann, P., Hirsch-Hoffmann, M., Hennig, L., and Gruissem, W. (2004). GENEVESTIGATOR. *Arabidopsis* microarray database and analysis toolbox. Plant Physiol. **136,** 2621-2632.

Acknowledgements

I thank my supervisor Dr. Stefanie Sprunck for offering me an interesting project and giving me the opportunities to develop own ideas and follow up interesting side-projects.

Many thanks go to Dr. Stefanie Sprunck, Prof. Dr. Thomas Dresselhaus and the SFB924 to render possible to participate in international courses and conferences and to support collaborations.

I am very grateful to Dr. Stefanie Sprunck and my mentors Prof. Dr. Thomas Dresselhaus and Prof. Dr. Benedikt Kost for open ears, fruitful discussions, great ideas and all general support.

Also many thanks go to the RIGeL graduate school and the Graduate Research Academy that offered an excellent PhD program, professional courses, interesting excursions and funding of a student helper. Sanna and Kinga, you really significantly contributed to improve our PhD program at the UR!

All collaborators are acknowledged for contributing to my projects. In particular I thank Prof. Dr. Frank Sprenger for his support with Spinning Disc microscopy and ImageJ, Prof. Dr. Rainer Merkl for answering bioinformatic questions, Prof. Dr. Benedikt Kost and Dr. Aude LeBaile for performing expression analysis in *Physcomitrella patens* (data not shown), Dr. Pascal Braun, Angela Alkofer and Quirin Ranftl for support during yeast 2-hybrid screening, Sebastian Konrad for performing TIRF microscopy, Dr. Jens Steinbrenner for sharing yeast 2-hybrid data and performing pathogen infections (data not shown), Dr. Ivan Kulich and Zdeňka Vojtíková for yeast 2-hybrid interaction verification, Dr. Ivan Kulich for trichome phenotyping (data not shown) and Dr. Hiromasa Shikata for kinase assays (data not shown).

During the time of my PhD I had the luck to be part of a great work group. I am very grateful to all undergraduate students that I was allowed to supervise during my time. Especially I want to thank my long-lasting colleagues and friends Ingrid, Kinga, Marc, Maria, Monika, Phil, Sanna and Tom for contributing to a great work atmosphere! Many thanks for ongoing help with graphical and text editing issues go to Maria.

I want to thank my whole family, especially my parents, for everything they did and do for me. Finally I want to thank the person that helped me the most of all – my wife Daniela. I thank you for your infinite support, for strengthening my back and for your great job with our daughter Felizia!

Author Contributions Statement

Herewith I confirm the accuracy of the statements by Frank Vogler regarding his contributions to publications as stated at the beginning of each chapter.

_____

Dr. Stefanie Sprunck, Supervisor